METABOLIC ANALYSIS OF CAROTENOID DYNAMICS AND GLOBAL METABOLISM IN CAROTENOID MUTANTS OF *RHODOSPIRILLUM RUBRUM* USING HPLC/MS METHODOLOGY

Von der Fakultät Energie-, Verfahrenstechnik- und Biotechnik der Universität Stuttgart zur Erlangung der Würde einer Doktorin der Naturwissenschaften (Dr.rer.nat.) genehmigte Abhandlung

Vorgelegt von

Judit Bóna-Lovász,
aus Pécs (Ungarn)

Hauptberichter: Prof. Dr. Robin Ghosh

Mitberichter: Prof. Dr. Oliver Sawodny

Tag der mündlichen Prüfung: 16. Dezember 2013

Biologisches Institut der Universität Stuttgart

Abteilung Bioenergetik

Pfaffenwaldring 57, 70569 Stuttgart

und

Institut für Systemdynamik

Pfaffenwaldring 9, 70569 Stuttgart

2013

Declaration

I hereby declare that this PhD thesis has been compiled by me under the supervision of Professor Robin Ghosh, Institute of Biology, Department of Bioenergetics, University of Stuttgart.

Erklärung

Hiermit versichere ich, dass ich die vorliegende Arbeit selbstständig und nur unter Verwendung der angegebenen Hilfsmittel und Quellen angefertigt habe.

Stuttgart, den 12.10.2013

Judit Bóna-Lovász

Declaration

The carotenoid mutants were provided by Prof. Dr. Robin Ghosh.

My thesis contains some data, which were obtained from fermentations performed by Dr. Ronny Feuer (ISYS).

Acknowledgments

Foremost, I would like to express my sincere gratitude to my supervisor Professor Robin Ghosh for the continuous support and encouragement during my PhD study. I am very thankful to him for the collaboration and his personal attention, especially in the last year.

I would like to express my deep gratitude and respect to Professor Oliver Sawodny, who gave me the opportunity for my PhD providing the necessary resources to accomplish my research work.

I gratefully acknowledge Michael Ederer for his valuable suggestions and encouragement at the critical stage of my Ph.D.

I take the opportunity to sincerely acknowledge Marion Fleischer for her understanding and encouragement. The results described in this work would not have been obtained without her excellent and generous assistance.

I would also like to thank Ronny Feuer for the extensive discussions and the constructive criticism. I expand my thanks to the entire “Biogruppe” for the extensive discussions. My special thanks to my roommates (Samantha and Joachim) for providing a fun-filled environment.

I am also grateful to Gerlind Preisenhammer and Corinna Hommel for their support during my Ph.D. years.

Last but certainly not least, I would like to pay high regards to my parents, sisters and brother and my closest friends Reni and Gabi who have never given up on me.

I am most indebted to my family, who supported me in every possible way. Special thanks to my daughters for their patience and encouragement.

The final but the most heartful thanks to Aron, I owe everything to him.

I want to open my thesis with my favourite quote of Louis Pasteur:

"The more I study nature, the more I stand amazed at the work of the Creator... There is something in the depths of our souls which tells us that the world may be more than a mere combination of events."

Contents

Abbreviations

αKGDH	α-ketoglutarate dehydrogenase
Δp	proton chemical gradient
APCI	Atmospheric-pressure chemical ionization
BChl*a*	Bacteriochlorophyll *a*
BPh*a*	Bacteriopheophytin *a*
CID	Collision induced dissociation
DAG	Diglyceride
Dhspx	3,4-dihydrospirilloxanthin
DOPG	Dioleoyl- phosphatidylglycerol
dX5P	1-deoxy-D-xylulose 5-phosphate
DXR	dX5P reductoisomerase
DXS	1-deoxy-D-xylulose-5-phosphate synthase
EMP	Embden–Meyerhof–Parnas
ESI	Electrospray ionization
ETC	Electron transport chain
ETF	Electron transport flavoprotein
FA	Fatty acid
Fnor	Ferredoxin:NADPH oxidoreductase
FRD	Fumarate reductase
GGPP	Geranylgeranyl-pyrophosphate
HPLC	High pressure liquid chromatography
ICM	Intracellular membrane
LH1	Light-harvesting complex
MEP	2C-methyl-D-erythritol-4-phosphate
MS	Mass spectrometer
NADHdH	NADH dehydrogenase
NADH TH	NADH/NADPH transhydrogenase
PC	Phosphatidylcholine
PdH	Pyruvate dehydrogenase
PE	Phosphatidylethanolamine
Pfor	Pyruvate:ferredoxin oxidoreductase
PG	Phosphatidylglycerol

Pfl	Pyruvate-formate lyase
PHB	Polyhydroxybutyrate
PoOPG	Palmitoleyl-oleoyl-phosphatidylglycerol
POPG	Palmitoyl-oleoyl-phosphatidylglycerol
PLs	Phospholipids
PM	Photosynthetic membrane
PPoPG	Palmitoyl-palmitoleyl-phosphatidylglycerol
PSU	Photosynthetic unit
PSY	Phytoene synthase
RC	Reaction centre
RQ	Rhodoquinone
SdH	Succinate dehydrogenase
SIM	Selected Ion Monitoring
spx	Spirilloxanthin
TCA	Tricarboxylic acid cycle
thspx	3,4,3',4'-tetrahydrospirilloxanthin
TIC	Total ion count
UQ	Ubiquinone

Summary

In this study, *Rhodospirillum rubrum*, a photosynthetic, facultative anaerobic bacterium was investigated in detail, as a potentially good candidate for industrial carotenoid production. Due to its high amounts of intracellular membrane (ICM), it provides more possibilities for the storage of carotenoids than *E. coli*, where only the cytoplasmic membrane is available for sequestration. Since *R. rubrum* is an anoxygenic phototrophic bacterium, all photosynthetic operators are consequently regulated by oxygen in contrast to aerobic phototrophic microorganisms. The photosynthetic membrane (PM) and carotenoid biosynthesis can only be induced at low (pO_2<0.5%) oxygen concentrations. Despite the detailed characterization of the PM there is a paucity of information regarding the biosynthesis and the assembly of the photosynthetic system. Therefore, the wild-type, ST4 (Δ*crtD*) and SLYC18 (Δ*crtC*Δ*crtD*) carotenoid mutants were studied by rapid sampled anaerobic and microaerophilic, dark fed-batch fermentations using fructose-succinate medium. The roles of the regulatory signals - O_2 and ubiquinone (UQ) pool - mediating the metabolic pattern and the induction of PM biosynthesis were also investigated in this study.

The metabolic pattern showed that strong oxygen and CO_2 limitation occurred during the experiments, which resulted in extremely slow growth (G_t=60h). High-level organic acid excretion and polyhydroxybutyrate (PHB) biosynthesis were observed, reflecting the fully reduced state of the cell. The metabolic profile, induced by the high intracellular acetate concentrations occurring in the initial phase of the growth curve, indicates that the citramalate and the ethylmalonyl pathways were active under anaerobic conditions. Succinate production, presumably via the methylmalonyl pathway, was also observed in absence of oxygen.

SLYC18 was found to grow twice as fast as the wild-type under CO_2- and oxygen-limited conditions. Furthermore, under anaerobic conditions SLYC18 contained a two fold high level of rhodoquinone-10 (RQ-10) and PHB than the wild-type. Since the high RQ level and the enhanced PHB production show a strong correlation, it is proposed here that the RQ-mediated production of NADPH occurs via a putative NADPH dehydrogenase.

In order to investigate the biosynthesis of the PM, it was necessary to measure the major lipid fractions (fatty acids, phospholipids), as well as carotenoids, isoprenoid quinones and bacteriochlorophyll *a* (BChl*a*) simultaneously during the fermentation process. Therefore, a single-step extraction with a ternary hexane/methanol/water mixture followed by HPLC with mass spectrometric detection has been developed for determination of carotenoids and other non-polar compounds present in phototrophic bacteria. The method is suitable for extracting

large numbers of samples, which is common in systems biology studies. The procedure was able to determine 18 carotenoids, 4 isoprenoid-quinones, BChl*a* and bacteriopheophytin *a* as well as four different phosphatidylglycerol species of different acyl chain compositions.

The high-resolution time courses of the carotenoid biosynthesis allowed us to investigate the conversion rate of each carotenogenic reaction. A strong bottleneck was observed at the reactions of CrtD. Furthermore, the second reactions of all enzymes are significantly slower than the first one. Analysis of the carotenoid dynamics indicated that several parallel carotenoid pathways can be linked at common connection points (hydroxylated carotenoids).

The carotenoid biosynthesis was more strongly affected by the low oxygen concentration than the central metabolic pattern. The carotenoid mutants were the most sensitive to oxygen, which resulted in inhibited growth and 33% decrease of anaerobic carotenoid concentration in SLYC18. The carotenogenic reaction sequence was blocked in the wild-type in the presence of oxygen, which resulted in the accumulation of anhydrorhodovibrin instead of the normal major carotenoid, spirilloxanthin. The presence of oxygen clearly affected the activity of CrtD which resulted in the opening of two new side-pathways, which do not use this enzyme: the alternative spheroidene pathway (4%) in the wild-type and ST4 and the 3,4-didehydrolycopene pathway (6%) in ST4. The existence of the 3,4-didehydrolycopene pathway, which has never been observed in *R. rubrum* earlier, indicated the ability of CrtI in catalyzing five desaturation steps in the presence of oxygen in the ST4 mutant.

The PM biosynthesis showed a strong dependence on the changes of the [UQ]/[UQH_2] ratio. Under anaerobic conditions, the metabolism is very sensitive to oxygen, and after applying an oxygen pulse, the oxidative tricarboxylic acid cycle and the electron transport chain can become temporarily active, inducing changes in the UQ pool redox state. After rapidly consuming the oxygen, the UQ pool becomes reduced again, thereby inducing the PM biosynthesis again. This oscillation pattern was analyzed by system biological methods.

To investigate and understand the dynamics of the PM compound production, a dynamic model containing carotenoid biosynthetic reactions described by mass action kinetics was developed. Different regulatory schemes were tested and studied in detail based on the carotenoid production time courses. The results reaffirmed the hypothesis that the oscillation of the PM compounds - particularly the carotenoids - is not a result of an endogenous regulation; rather the isoprenoids are regulated together via MEP pathway flux through an exogenous signal. Considering the metabolic observations in the experiments, the regulatory signal might possibly be the [UQH_2]/[UQ] ratio.

Zusammenfassung

Im Zuge dieser Arbeit wurde *Rhodospirillum rubrum*, ein photosynthetisches, fakultativ anaerobes Bakterium, als potentiell guter Kandidat für industrielle Carotinoid-Produktion detailliert untersucht. Seine Fähigkeit große Mengen intrazellulärer Membranen (ICM) auszubilden, ermöglicht es *R. rubrum* mehr Carotinoide zu speichern als *E. coli*, bei dem nur die Cytoplasmatische Membran zur Einlagerung von Carotinoiden zur Verfügung steht. Da *R. rubrum* ein anoxygenes phototrophes Bakterium ist, werden, im Gegensatz zu den aeroben, phototrophen Mikroorganismen, alle photosynthetischen Gene durch den Sauerstoff-Partialdruck (pO_2) reguliert. Nur bei niedrigen Sauerstoffkonzentrationen (pO_2<0,5 %) kann die Biosynthese der photosynthetischen Membran (PM) und der Carotinoide induziert werden. Obwohl die PM detailliert untersucht wurde, gibt es wenig Information über die Biosynthese und die Assemblierung des Photosynthetischen Systems. Daher wurden in dieser Arbeit sowohl der Wildtyp als auch die Carotinoidmutanten ST4 (Δ*crtD*) und SLYC18 (Δ*crtC*Δ*crtD*) genauer untersucht. Hierbei wurden anaerobe und microaerophile Kulturen aus Fed-Batch Fermentationen im Dunkeln in einem Fructose-Succinat Medium durch schnelles *Sampling* gewonnen und die Rolle der regulatorischen Signale - O_2 und Ubichinon (UQ) Pool, die das Stoffwechselprofil und die Induktion der PM Biosynthese vermitteln - genauer untersucht.

Das Stoffwechselprofil zeigte, dass eine große O_2 und CO_2 Limitierung während der Experimente vorlag, was ein extrem langsames Wachstum zur Folge hatte (G_t=60h). Es konnte eine Ausscheidung von organischen Säuren in höheren Mengen und eine erhöhte Polyhydroxybutyrat (PHB) Biosynthese beobachtet werden, was den voll reduzierten Zustand der Zelle reflektierte. Das Stoffwechselprofil, das durch die hohen intrazellulären Acetat-Konzentrationen, die in der Anfangsphase der Wachstumskurve auftraten, induziert wurde, deutete darauf hin, dass der Citramalat und der Ethylmalonyl Stoffwechselweg unter anaeroben Bedingungen aktiv waren. Auch Succinatproduktion, wahrscheinlich durch den Methylmalonyl Stoffwechselweg, wurde in Abwesenheit von Sauerstoff beobachtet.

SLYC18 wuchs doppelt so schnell wie der Wildtyp. Außerdem enthielt SLYC18 unter anaeroben Bedingungen doppelt so viel Rhodochinon-10 (RQ-10) und PHB wie der Wildtyp. Da der hohe RQ Level und die erhöhte PHB Produktion stark korrelierten, wird hier vorgeschlagen, dass die RQ vermittelte NADPH Produktion über eine putative NADPH Dehydrogenase abläuft.

Um die Biosynthese der PM zu untersuchen war es notwendig, die Haupt-Lipidfraktionen (Fettsäuren, Phospholipide), sowie die Carotinoide, Isoprenoid-Chinone und

Bakteriochlorophyll *a* (BChl*a*) simultan während des Fermentationsprozesses zu messen. Hierfür wurde eine Ein-Schritt-Extraktionsmethode mit einem ternären Hexan/Methanol/Wasser-Gemisch, gefolgt von HPLC mit Massenspektrometrie-Detektion, entwickelt, um Carotinoide und andere nicht-polare Substanzen in phototrophen Bakterien bestimmen zu können. Diese Methode ist geeignet für die Extraktion einer großen Anzahl von Proben, wie es in systembiologischen Studien üblich ist. Mit der Methode konnten 18 Carotinoide, 4 Isoprenoid-Chinone, BChl*a* und Bakteriophäophytin *a*, sowie 4 verschiedene Phosphatidylglycerol Spezies mit unterschiedlicher Acyl-Ketten Zusammensetzung nachgewiesen werden.

Die hoch-aufgelösten *Time Course* Messungen der Carotinoid Biosynthese erlaubten uns die Umwandlungsrate jeder carotinogenen Reaktion zu untersuchen. Ein starker Flaschenhalseffekt wurde bei den CrtD vermittelten Reaktionen beobachtet. Außerdem sind die zweiten Reaktionen aller Enzyme signifikant langsamer als ihre ersten. Die Analyse der Carotinoid-Dynamik deutete darauf hin, dass verschiedene parallele Carotinoid *Pathways* an gemeinsamen Verbindungspunkten (hydroxylierte Carotinoide) miteinander verlinkt werden können. Durch die niedrige Sauerstoffkonzentration wurde die Carotinoid Biosynthese stärker beeinflusst als das Profil des Zentralstoffwechsels. Die Carotinoidmutanten waren sehr sauerstoffempfindlich, was in SLYC18 zu gehemmtem Wachstum und einem 33 %igem Rückgang der anaeroben Carotinoidproduktion führte. Im Wildtyp wurde in Anwesenheit von Sauerstoff die carotinogene Reaktionssequenz blockiert, was zur Akkumulation von Anhydrorhodovibrin, anstelle des normalen Hauptcarotinoids Spirilloxanthin, führte. Die Anwesenheit von Sauerstoff beeinflusste die CrtD Aktivität deutlich, was zum Auftreten zweier neuer Seitenwege, die dieses Enzym nicht verwenden, führte: der alternative Spheroiden Stoffwechselweg (4%) im Wildtyp und ST4 und der 3,4-Didehydrolycopin Stoffwechselweg (6%) in ST4. Die Existenz des 3,4-Didehydrolycopin Weges, der bislang in *R. rubrum* nie beobachtet worden ist, zeigte die Fähigkeit von CrtI zur Katalyse von fünf Desaturierungsschritten in der ST4 Mutante in Anwesenheit von Sauerstoff.

Die PM Biosynthese zeigte eine starke Abhängigkeit von den Änderungen des [UQ]/[UQH_2] Verhältnisses. Unter anaeroben Bedingungen ist der Stoffwechsel sehr empfindlich gegenüber Sauerstoff, und, nach Einbringen eines Sauerstoff-Pulses, können der oxidative Tricarboxylsäure-Zyklus und die Elektronentransportkette temporär aktiv werden, was zu Änderungen im UQ Pool Redoxzustand führt. Nachdem der Sauerstoff schnell verbraucht worden ist, wird der UQ Pool wieder reduziert, und somit wird die PM Biosynthese wieder induziert. Dieses Oszillationsmuster wurde mit Hilfe systembiologischer Methoden analysiert.

Um die Dynamik der Produktion der PM Bestandteile zu untersuchen und genauer zu verstehen, wurde ein dynamisches Modell entwickelt, das die Carotinoid Biosynthesereaktionen, beschrieben durch Massenwirkungskinetiken, enthielt. Verschiedene Regulationsschemata wurden getestet und auf Basis der Carotinoidproduktion *Time Courses* detailliert untersucht. Die Ergebnisse bestärkten die Hypothese, dass die Oszillation der PM Komponenten - vor allem der Carotinoide - nicht ein Ergebnis endogener Regulation ist, sondern dass die Isoprenoide vielmehr zusammen durch ein exogenes Signal, via des MEP *Pathway* Fluxes reguliert werden. Wenn man die experimentellen Beobachtungen des Stoffwechsels in Betracht zieht, so könnte es sich bei diesem regulatorischen Signal eventuell um das $[UQ]/[UQH_2]$ Verhältnis handeln.

1 Introduction

Carotenoids are natural pigments occurring in higher plants, bacteria and fungi (Ernst, 2002). They have widespread functions: energy collection in photosynthesis, photoprotection of bacteriochlorophyll *a* (BChl*a*) and influence of the cell membrane fluidity. In addition, carotenoids are highly valuable, because of their antioxidant properties (Stahl and Sies, 2003) and their colour (Mortensen, 2006). They are used as colour additives in the food industry and in dietary supplements (Ausich, 1997, Mortensen, 2006).

Carotenoids can be synthesized chemically but also by biotechnological processes. Chemical synthesis is cheap, but results in racemic mixtures. In contrast, the carotenoids produced by microorganisms, are stereospecific products. In the last decades, different bacteria, fungi and algae were screened and optimized metabolically for carotenoid production (reviewed by Das et al, 2007; Ye at al., 2012).

In this study*, Rhodospirillum rubrum*, a photosynthetic, facultative anaerobic bacterium was investigated in detail, as a potentially good candidate for industrial carotenoid production since it is able to biosynthesize carotenoids at a high level. Due to the high amounts of intracellular membrane (ICM), it provides more possibilities for the storage of carotenoids than *E. coli*, where only the cytoplasmic membrane is available for sequestration.

Since *R. rubrum* is an anoxygenic phototrophic bacterium, the primary environmental signal is oxygen. In addition, all photosynthetic genes are consequently regulated by oxygen in contrast to aerobic phototrophic microorganisms. This metabolic attribution opens up numerous questions and optimization tasks relevant to biotechnological application. At high oxygen concentrations, high growth rates occur but no carotenoids are produced. Carotenoid biosynthesis can be induced only at low oxygen concentration. Furthermore, there are some industrially relevant xanthophylls, such as astaxanthin, bearing oxo-, hydroxyl-, or keto-groups, where the oxygen concentration is critical for the biosynthesis. In recent years, carotenoid production has been observed in *R. rubrum* under semiaerobic conditions (Wang *et al.*, 2012).

Therefore, this study examines the possibilities of the microaerobic carotenoid production by considering the active metabolic pattern of the cell and the dynamics of the carotenoid biosynthesis at low oxygen availability. The double role of the oxygen, as a repressing agent of the photosynthetic membrane biosynthesis and as a substrate for cell growth, is discussed in detail. In order to achieve high resolution data for the carotenoid time courses, a robust

extraction and a reliable chemical analysis method for carotenoid determination has been developed.

1.1 Carotenoids and their relevance

Isoprenoids are an extensive class of extraordinarily diverse natural products (>35,000). They fulfill different functions in living cells: electron transport, hormone-based signalling, regulation of transcription and posttranslational processes, meiosis, apoptosis, glycoprotein biosynthesis, and protein degradation. Isoprenoids are formed by sequential condensation of five-carbon isoprenoid units. Depending on the number of isoprenoid units, these compounds can be grouped into six classes: mono-, sesqui-, di-, tri-, tetra-, and polyterpenes. Carotenoids are one subclass of isoprenoids.

The most characteristic members of the groups and their functions are listed in Table 1.

Class	Carbon Nr.	Function
Monoterpenes	C10	essence of flower, herb and spices
Sesquiterpenes	C15	antimicrobial phytoalexins in essential oils
Diterpenes	C20	Phytol, geraniol, side chain of chlorophyll, phylloquinones, tocopherol, gibberellins
Triterpenes	C30	phytosterols, brassinosteroids, toxins and waxes
Tetraterpenes	C40	**carotenoids**, pigments for light harvesting in plants, bacteria, fungi
Polyterpenes	C>40	side chain of ubiquinone and plastoquinone, rubber

Table 1. Isoprenoid classification based on isoprenoid units and their properties (Rodri *et al.*, 2002)

1.1.1 Chemical structure and properties of carotenoids, BChls and isoprenoid-quinones

Carotenoids consist of 40 carbon atoms with additional hydrogen atoms and optionally oxygen atoms. Originally, the name carotenoid was used for tetraterpenes that consist of only hydrogen and carbon atoms (Fig. 1). Oxygenated carotenoids are called xanthophylls. Xanthophylls can be substituted with hydroxyl groups (astaxanthin), epoxy groups (violaxanthin), oxo-groups (cantaxanthin) or ether groups (spirilloxanthin (spx)) (Fig. 2).

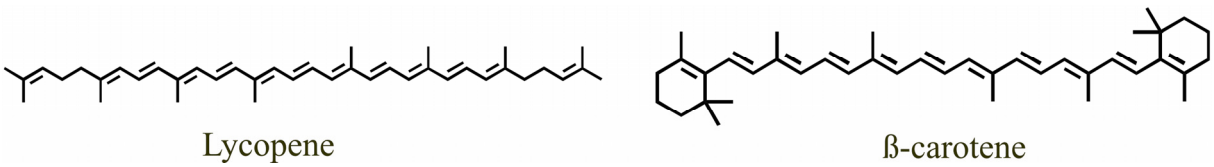

Fig. 1. Chemical structure of some industrial relevant carbohydrate carotenoids

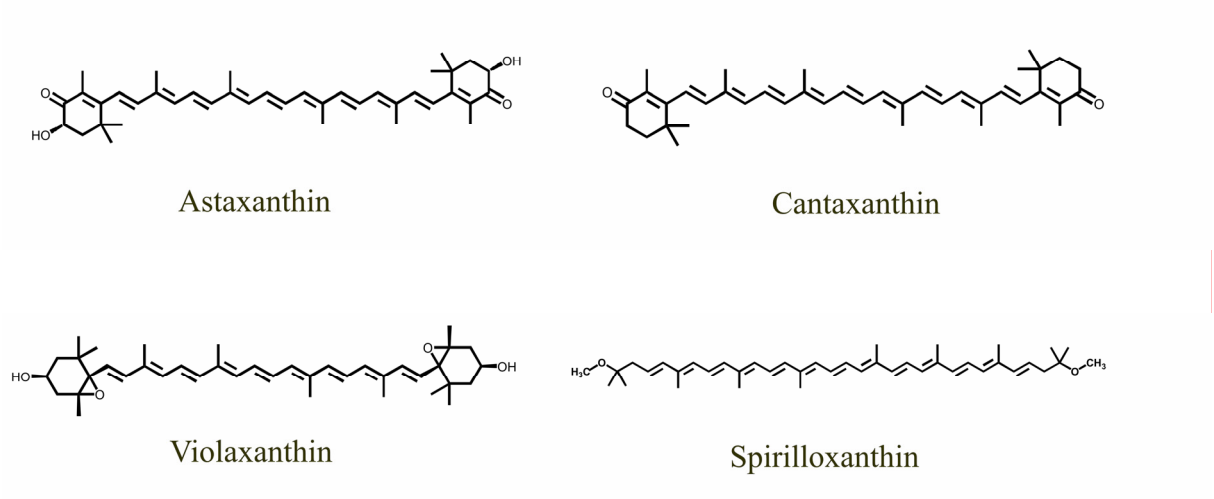

Fig. 2. Chemical structure of some industrial relevant xanthophylls

Carotenoids can be fully or partially conjugated. The partially conjugated carotenoids, such as phytoene, neurosporene or lycopene, are precursors of the fully conjugated carotenoids, such as spx (Amaya and Kimura, 2004).

The π electrons of the conjugated double-bond system are highly delocalized, which allows photoexcitation from the ground state (S_0) to the second singlet excited state (S_2) by low energy photons. This results in the characteristic three-peak absorption spectrum (Fig. 3), which is caused by the three different vibrational levels of the S_2 state (Pan *et al.*, 2008, Polivka and Sundström, 2004).

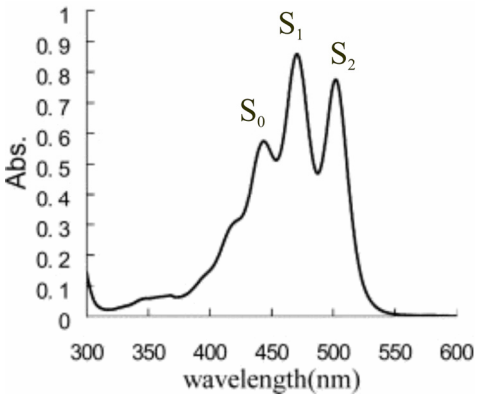

Fig. 3. Visible absorption spectrum of lycopene showing the typical three maxima of the carotenoids in the 350-550 nm region

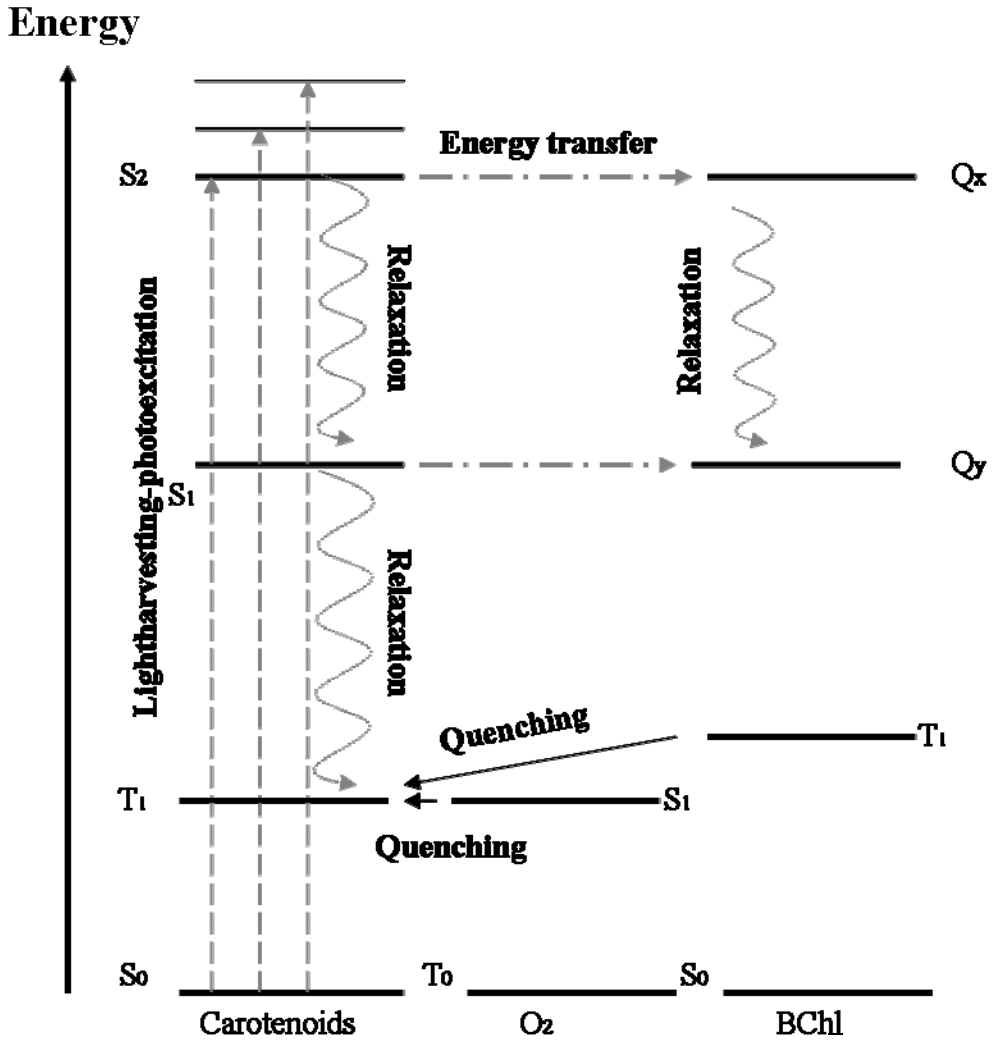

Fig. 4. Jablonsky diagram of the reactions of carotenoids

The wavelengths of the maximal absorption values (λ_{max}) are a characteristic for the chromophore but can alter with solvent polarity.

Due to their conjugated double bond systems, carotenoids are highly reactive molecules. They react rapidly with free radicals via different reaction mechanisms:

1 Adduct formation, for example in the case of peroxyl radical (ROO●), which can bind to the polyene-chain (ROO-Car):

$$ROO\bullet + Car \rightarrow ROO\text{-}Car\bullet$$

2 Electron transfer is the reaction which produces carotenoid cation and anion radicals and alkyl radicals (Truscott *et al.*, 1990, Koyama *et al.*, 1991, Truscott *et al.*1997, Krinsky *et al.*, 2003).

$$Car + NO_2\bullet \rightarrow Car^+ + NO_2^-$$

3 Allylic hydrogen abstraction (Krinsky *et al.*, 2003)

$$ROO\bullet + Car \rightarrow ROOH + Car\bullet$$

4 Triplet quenching

In this reaction the energy from the singlet state oxygen is transferred to the carotenoids (Fig. 4) leading to the photoprotection of BChl*a* during photosynthesis (Koyama *et al.*, 1991).

$$^1Car + ^1O_2\bullet \rightarrow ^3Car + ^1O_2$$

5 Photoprotective function

Carotenoids also serve as photoprotective agents against photooxidative damage of the biomembrane and BChl*a* (Woodall *et al.*, 1997). In the presence of excess light, BChl*a* is photoactivated, and its spin state changes from the singlet to the triplet state. Triplet BChl*a* reacts easily with triplet molecular oxygen, forming highly reactive singlet oxygen, which can damage proteins and the DNA. In order to avoid this damage, carotenoids efficiently quench the triplet state of BChl*a* via electron-exchange mechanism, since they are usually present in close vicinity to BChl*a*. The excited carotenoid emits the extra energy by heat (Koyama *et al.*, 1991).

$$^3BChl + ^1Car \rightarrow ^1BChl + ^3Car$$

$$^3Car \rightarrow ^1Car + heat$$

6 Photoinduced energy transfer-light harvesting reaction

The light-harvesting reactions at the level of carotenoids start with the absorption of light energy (hν), which generates excited singlet states ($^1Car^*$). The energy is transferred to a singlet state BChl*a* (Fig. 4).

$$^1Car + h\nu \rightarrow ^1Car^*$$

$$^1Car^* + ^1BChl \rightarrow ^1Car + ^1BChl$$

Carotenoids also have a membrane fluidity-stabilizing function, which modifies the dynamics and structural properties of the membrane (Reviewed by Gruszeczky and Strzalka, 2005). In isolated membrane model systems, the carotenoids are located in the hydrophobic core of the membrane. The hydrophilic groups are located at the two opposite polar zones of the membrane in xanthophylls which have *trans* conformation. If the xanthophylls occur in a *cis* conformation, the two end groups are anchored at the same polar zone of the membrane, and the chromophore occurs in the hydrophobic core of the membrane. The presence of carotenoids modulates the membrane fluidity and the penetration barrier of small molecules, such as glucose, oxygen, proton and water (Gruszeczky and Strzalka, 2005).

BChl*a* is a porphyrin molecule with a long side chain, with a magnesium ion in the middle of the ring. A long terpenoid alcohol such as phytol or geraniol can occur as side chain, which is

connected to the ring with a condensation reaction. The more reduced porphyrin ring results in a characteristic spectrum.

There are different types of BChl-s: a, b, c, d, e, f. depending on the type of the short carbon chains on the porphyrin molecule (Fig. 5).

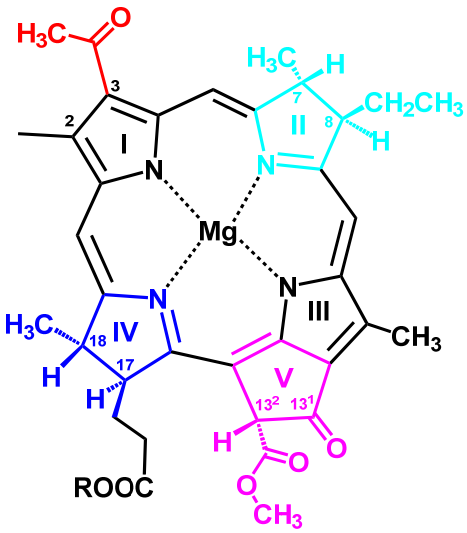

Fig. 5. Chemical structure of BChl*a* (R = geranylgeranyl in *R. rubrum*)

Isoprenoid-quinones are composed of a hydrophilic head group and an apolar isoprenoid side chain. Several classes of quinones can be defined based on the hydrophilic head group: ubiquinones (UQ), rhodoquinones (RQs), menaquinones and plastoquinones. The members of each quinone class differ only in the number of isoprene units occurring in the side chain. Ubiquinone-10 (UQ-10) is a well-known member of this molecule-family consisting of a quinone head group and a side chain containing 10 isoprene units (Fig. 6). It functions as electron carrier from NADH dehydrogenase (NADH dH) and succinate dehydrogenase (SdH) towards cytochrome bc_1. UQ has high redox potential, but in some organisms low redox potential quinones exist: menaquinone in *E. coli* and RQ in *R. rubrum*.

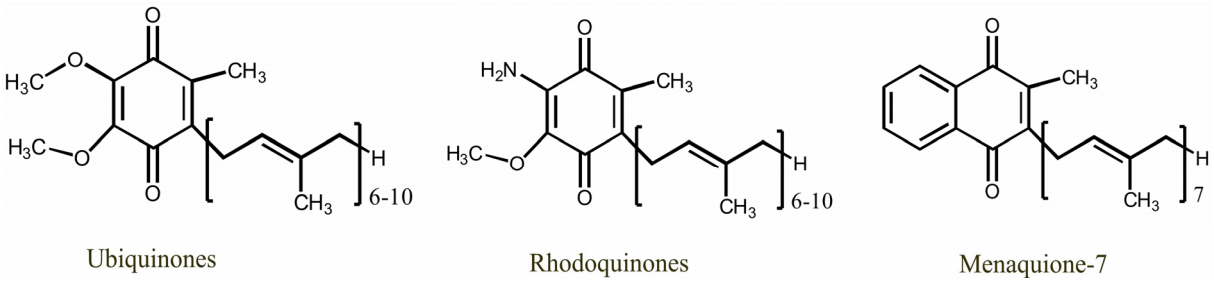

Fig. 6. Chemical structures of selected isoprenoid-quinones

1.1.2 Utility of isoprenoids

Chlorophylls and carotenoids are commonly used colour additives in the food industry due to their intensive colours. They are also applied as animal feed additives e.g.: for chicken (ß-carotene), for salmons and shrimps (astaxanthin) (Ernst, 2002; Mortensen, 2006). UQs and carotenoids are also used as neutraceuticals and pharmaceuticals due to their antioxidant effects (Das *et al.*, 2007). The medical opinion of the effect of carotenoids is not consistent. There are several studies where enhanced serum levels of carotenoids are correlated with a reduced risk of some cancers, cardiovascular diseases, but there are also contradictory studies in this area (Woodall *et al.,* 1997; Mayne, 1996). The antioxidant activity of carotenoids is reviewed by Stahl *et al.* (2003), Paiva *et al.* (1999) and Edge *et al.* (1997). In any case, there is a high demand for carotenoids and the global market of carotenoids is growing continuously. In 2010, the global market value of commercially used carotenoids was estimated to be about $1.2 billion and is expected to grow to $1.4 billion in 2018 (Global market of Carotenoid, BCC Research).

Even though more than 600 carotenoids are known (Amaya and Kimura, 2004), only five carotenoids are synthesized chemically at an industrial scale: astaxanthin, ß-carotene, zeaxanthin, cantaxanthin and lycopene (Fig. 7). The chemical synthesis of carotenoids is carried out with a double Wittig condensation of a symmetrical C_{10}-dialdehyde with two equivalents of an appropriate C_{15}-phosphonium salt (Ernst, 2002).

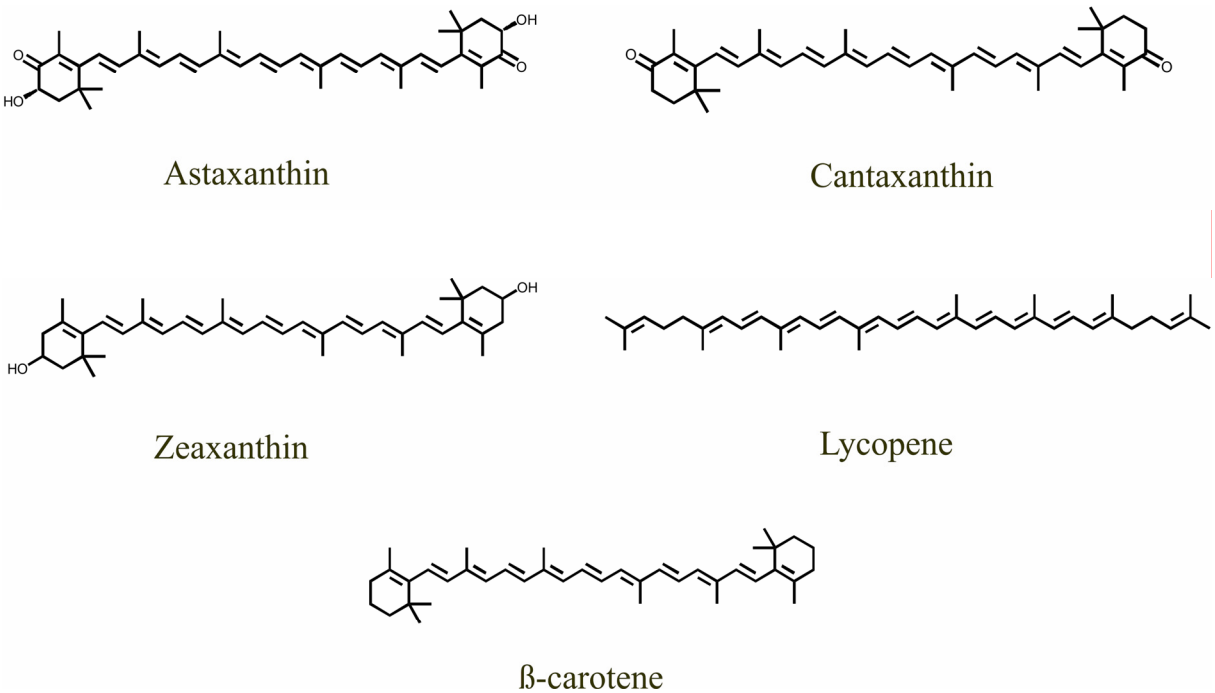

Fig. 7. Industrially produced carotenoids

The first relevant effort for the microbial production of ß-carotene was carried out with the unicellular algae *Dunaliella salina*. These algae produce large amounts of ß-carotene under high salt concentrations and light intensity (Ausich, 1997).

Although fungi do not produce carotenoids naturally, 103 µg/g β-carotene can be achieved by overexpression of the carotenogenic genes (Yamano *et al.* 1994).

In order to raise the precursor supply for the carotenoid production, the optimization of the central metabolism was investigated. The first precursors of the isoprenoid backbone pathway originating from glycolysis are pyruvate and glyceraldehyde 3-phosphate (G3P) (Fig. 8). The knock-out of the pathways competing for these precursors enhances the lycopene yield in *E. coli* (Farmer and Liao, 2001; Vadali *et al.*, 2005).

Alper *et al.*, (2005) used the first systematic approach to optimize *E. coli* metabolism for carotenoid production. They used a genome wide flux balance analysis to find an active genome expression scenario resulting in a good growth rate and an improved lycopene production. The knock-outs of three genes of the central metabolism (formate dehydrogenase, pyruvate dehydrogenase, glutamine dehydrogenase resulted in 6 mg/g lycopene (Alper *et al.*, 2005).

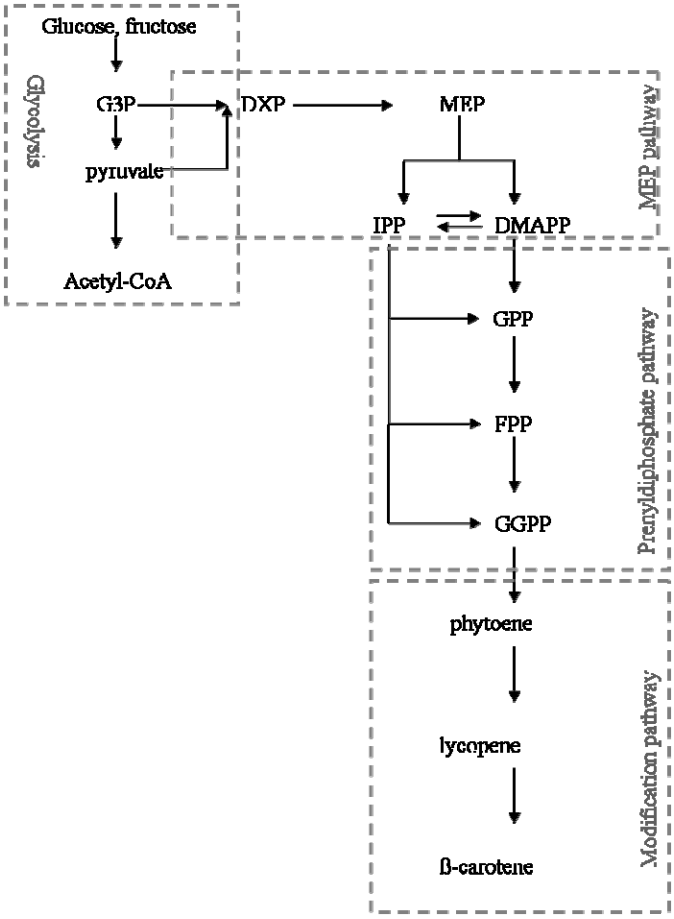

Fig. 8. Carotenoid biosynthesis block diagram

The MEP pathway directs the input flux towards carotenoids production (for detailed description of the biosynthetic pathways see below). Metabolic engineering of the MEP pathway was very successful and yielded 6 mg/g ß-carotene in *E. coli* (Yuan *et al.*, 2006). Overexpression of the bottleneck enzymes of the MEP pathway resulted in a 4.5 fold increase in the ß-carotene production in *E. coli* (Suh, 2012), enhanced chlorophyll and carotenoid levels in tomato (Estevez *et al.*, 2001, Lois *et al.*, 2000), enhanced carotenoid and UQ8 levels in *E. coli* (Matthews *et al.*, 2000, Harker *et al.*, 1999), and also enhanced taxol levels in *E. coli* (Ajikumar *et al.*, 2010).

Overexpression of the modification pathway genes (see Fig. 8) enhances the carotenoid production (820 µg/g DCW, (Nishizaki *et al.*, 2007)) but engineering of the MEP and prenyldiphosphate pathways (Harada and Misawa, 2012, Matthews et al, 2000, Wang *et al.*, 2000) is the most efficient way to reach higher carotenoid yields.

The fermentation techniques have been optimized for the industrial production of carotenoids. In order to develop an industrial carotenoid production the following parameters must be considered (Ausich, 1997):

1 the cost of the biomass production
2 the intracellular carotenoid concentration
3 the carotenoid biosynthetic rate.

The optimization of high cell density fermentation by *E. coli* also resulted in a high yield, 220mg/l of lycopene (Alper *et al.*, 2006). In *E. coli*, the addition of glycerol resulted in 32 mg/g lycopene (Kim *et al.*, 2011).

1.2 Physiological properties of *R. rubrum*

R. rubrum is a gram-negative, facultative anaerobic, non-sulphur purple spiral bacterium. It has a width of 0.8-1.0 µm and a length of 3-10 µm depending on the growth phase. It is flagellated, and therefore motile. It occurs naturally in the deeper layers of high mountain lakes (Schlegel, 1992) but is also found in mud (Brock, 2000). Due to the phototactic mobility *R. rubrum* can move between the upper and the lower layers of the lake. In order to adapt to a changing environment, *R. rubrum* uses different metabolic pathways. This metabolically versatile microorganism can grow in the light under anaerobic conditions using anoxygenic photosynthesis, under fermentative conditions and under also aerobic conditions with O_2 as terminal electron acceptor. *R. rubrum* is also capable of anaerobic respiration using DMSO or TMAO as electron acceptor with substrates such as succinate, malate or acetate (Schultz and

Weaver, 1982). It has been observed that the biomass composition also alters with changes of the environment (Cohen-Bazire and Kunisawa, 1963).

Under fermentative conditions (in absence of non-oxygenic terminal electron acceptors) chemical energy is produced via glycolysis and fermentative processes such as ethanol and organic acid (acetate, formate, lactate, malate, and propionate) production. If the cell is in an over-reduced state, the hydrogenases can use the reduced redox equivalents and produce hydrogen. *R. rubrum* has several different hydrogenases, demonstrating the importance of this system (Maness and Weaver, 2001). The uptake hydrogenase, which is a membrane-bound nickel-iron protein, allows the cell to use hydrogen as an energy source. They are in connection with the UQ pool and with the anaerobic electron acceptors (SO_4^-, NO_3^-). It can work in two directions (consuming or producing hydrogen) depending on the redox state of the cell (Vignais *et al.*, 2004). The formate-hydrogen lyase is a Fe-only, membrane-bound hydrogenase, which splits formate into carbon dioxide and hydrogen (Gorrell *et al.*, 1977). *R. rubrum* is also able to produce hydrogen from carbon monoxide (CO) gas (Bonam *et al.*, 1989). The CO-induced enzymes dehydrogenase and hydrogenase allow *R. rubrum* to grow in the dark on CO as only carbon source (Kerby *et al.*, 1995). The peripheral CO dehydrogenase enzyme oxidizes CO to CO_2 and passes the electrons to a ferredoxin. From the ferredoxin, the electrons flow to a membrane-bound Ni-Fe hydrogenase, which is thereby reduced, resulting in hydrogen (Fox *et al.*, 1995; Ensign and Ludden, 1991).

The main system producing hydrogen, under phototrophic conditions, in the absence of NH_4^+ as nitrogen source, is the nitrogen-fixing system.

$$N_2 + 8H^+ + 8e^- + 16\,ATP = 2NH_3 + H_2 + 16ADP + 16\,P_i$$

In the nitrogen-fixing reaction, hydrogen is produced as side-product via the iron protein (Brostedt and Nordlund, 1991). The major nitrogenase enzyme consists of two components: a small iron protein, which is the ATP-dependent electron donor for the larger molybdenum-iron protein, which contains the catalytic site (Dixon and Kahn, 2004). *R. rubrum* also contains an alternative nitrogenase system.

R. rubrum performs photosynthesis in the presence of light and absence of oxygen. In this reaction chain, in contrast to that of photosynthesis in plants, H_2O is not the final electron donator and oxygen gas is not produced. The oxygen is potentially poisonous for the whole photosynthetic system; therefore the photosystem is expressed only at low levels of oxygen tension. For the related bacteria, such as *Rhodobacter sphaeroides,* the repressing limit is defined by $pO_2 < 2.5$ % (Kiley and Kaplan, 1988).

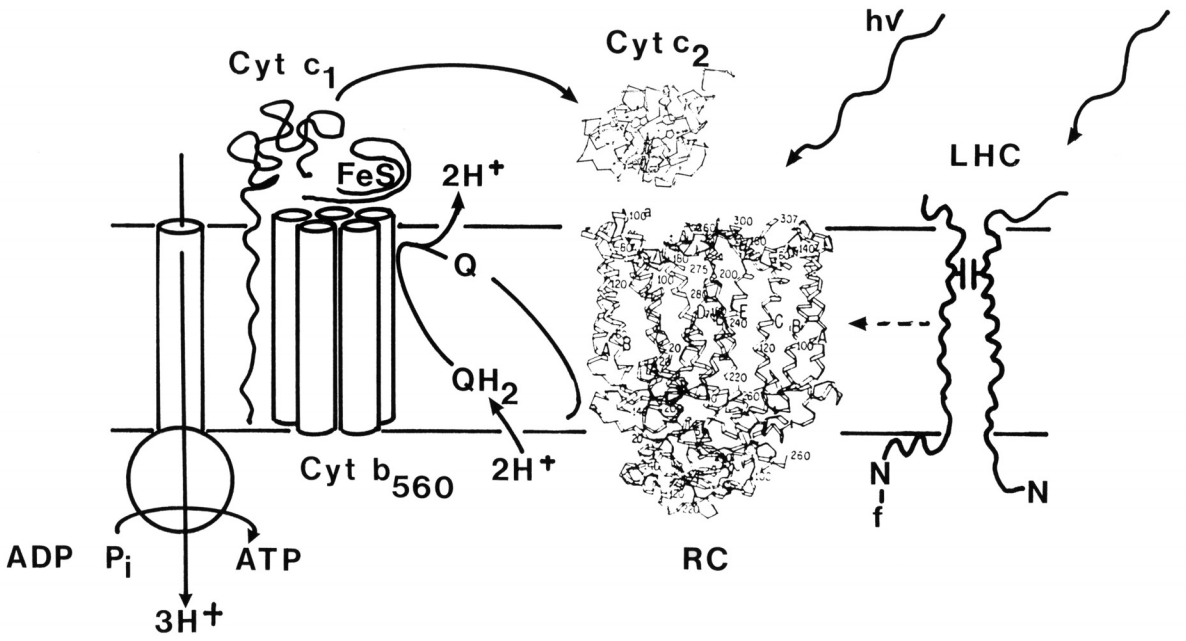

Fig. 9. Anoxygenic photosynthesis and cyclic electron flow (Ghosh and Bachofen, 1989**)**

Under phototrophic conditions purple bacteria produce photosynthetic units (PSU), which consists of a reaction centre (RC) and a light-harvesting complex (LH1). The RC consists of 3 protein subunits: H, M, L and 10 co-factors, e.g.: BChl*a.* The light-harvesting system forms a ring around the RC, and consists of 16 protein-cofactor components. Each component contains two polypeptide chains, α and ß and as cofactors BChl*a,* bacteriopheophytin *a* (BPh*a*), UQ and carotenoids.

The bacterial photosynthesis is a cycling electron flow due to absence of a final electron acceptor (Fig. 9). The LH1 collects the light and the energy is transferred to the RC, where the "special pair" BChl*a*-s are excited, and one electron of the delocalized electron system is sent to outer accessory BChl*a*, further to a BPh*a* and finally to the UQ-10. UQ-10 is oxidized by the cytochrome bc_1 oxidase. In this reaction, the protons are pumped into the periplasm, thus generating proton motive force, and the electrons flow first onto cytochrome c_2 and finally back to the RC. Under phototrophic conditions the cell's carbon source is CO_2, which is fixed via the Calvin cycle.

1.1.3 Regulation of the metabolism in anoxygenic phototrophic bacteria

The primary environmental signal and the main metabolic regulator is oxygen (Kiley and Kaplan, 1988). The two-component oxygen-dependent regulatory system, controlling anaerobic and aerobic gene expression, is present in all photosynthetic bacteria. The PrrB/PrrA and RegB/RegA systems in *Rb. sphaeroides* and *Rhodobacter capsulatus*,

respectively, have been investigated in detail (Oh and Kaplan, 2000; Elsen et al, 2004; Dubbs and Tabita, 2004). The oxygen sensor is the cbb_3-type cytochrome c oxidase (Oh and Kaplan, 1999), which is the final oxidase enzyme in the electron transport chain transferring electrons to oxygen. The flux through cbb_3 is "sensed" by the protein PrrC/SenC (Eraso and Kaplan, 2000). In the presence of oxygen, a high electron flux occurs and a lot of SenC is produced, which inhibits the autophosphorylation of Prr/RegB, a membrane-bound histidine kinase. If the oxygen concentration drops below 2.5% pO_2 the inhibition disappears and RegB autophosphorylates, and phosphorylates the water-soluble RegA (Oh and Kaplan, 2000). The phosphorylated RegA-P activates the transcription of the following operons:

- *puf, puc puh* (LH and RC protein units) (Sganga *et al.*, 1992, Mosley *et al.*, 1994),
- *bch* (BChl*a* biosynthesis),
- *crt* (carotenoid biosynthesis; Willett *et al.*, 2007).
- *cbb* (carbon fixation; Qian *et al.*,1996),
- *nif* (nitrogen fixing gene; Joshi and Tabita,1996),
- *dor* (DMSO respiration; Kappler *et al.*, 2002),
- *cyc* (cytochromes bc and c) (Swem *et al.*, 2001) and
- *hup* (uptake hydrogenase biosynthesis) (Elsen *et al.*, 2000).

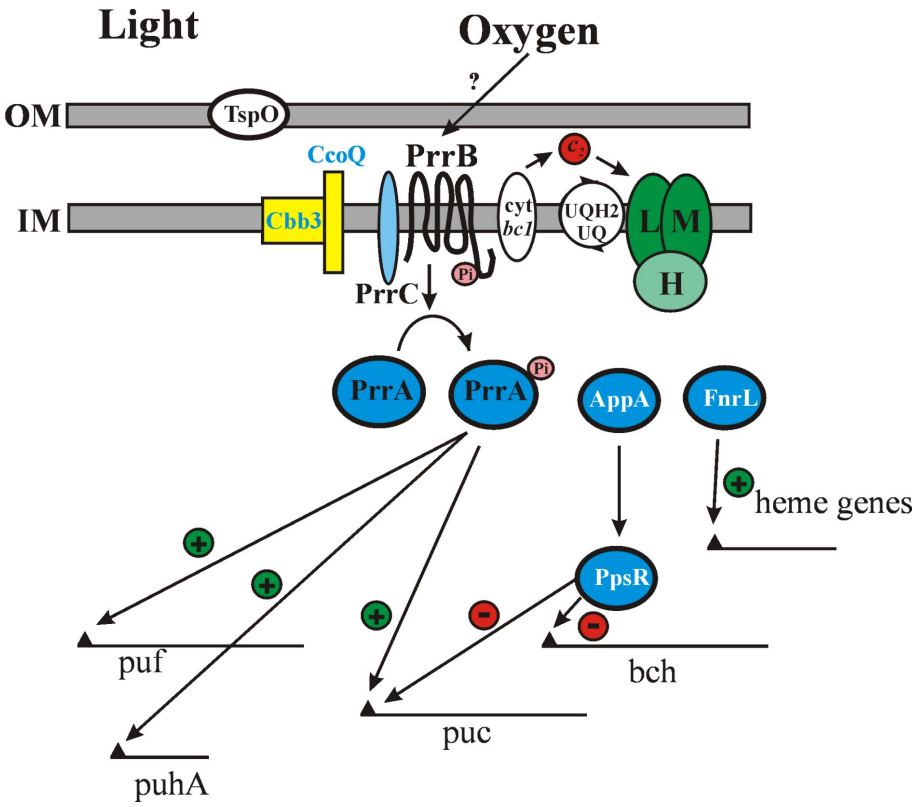

Fig. 10. Regulation of the photosynthetic genes according to the oxygen availability and the light intensity in *Rb. sphaeroides* (Ghosh, unpublished)

As determined in *Rb. sphaeroides* the activity level of the RegAB system depends also on the light intensity sensed by the AppA-PpsR system (Braatsch *et al.*, 2002). Under high oxygen concentrations and high light conditions, AppA occurs in an oxidized form and cannot act with PpsR, which binds the DNA, thereby repressing the transcription of the photosynthetic genes. Under low light conditions and in absence of oxygen, the active AppA can reduce PpsR releasing the repression. At high light conditions, AppA oxidizes PpsR, which binds the DNA again repressing photosynthetic gene expression (Braatsch *et al.*, 2002). PpsR can also be oxidized or reduced depending on the redox state of UQ pool (Kovacs *et al.*, 2005). Light signalling can be achieved via reduced UQ-pool or by a light intensity sensor HvrA protein which was observed in *Rb. capsulatus* (Buggy *et al.*, 1994). It was also shown in *Rb. sphaeroides*, that AppA is a blue light repressor for photosynthetic gene expression (Masuda and Bauer, 2002).

1.1.4 Metabolic pattern in *R. rubrum* under microaerophilic conditions

The metabolism of *R. rubrum* was investigated also under microaerophilic conditions. Apart from aerobic (oxygen not limited) and anaerobic (oxygen excluded) conditions, a microaerobic condition can be defined, where the oxygen occurs in limiting concentrations. Under these conditions, anaerobic genes such as photosynthetic genes are expressed with modified activity and the central metabolism is also distinguishable from the anaerobic one.
Grammel *et al.* (2003) showed in *R. rubrum* that at a pO_2 = 0.5% the cooperation of the reductive and oxidative pathways allows maximal photosynthetic membrane production. These authors have also shown that growing the cells on medium containing fructose and succinate (Ghosh *et al.*, 1994; Grammel *et al.*, 2003) under microaerobic conditions results in a unique metabolic profile (Fig. 11). *R. rubrum* can grow on succinate only under aerobic conditions and the succinate is utilized via succinate-dehydrogenase (SdH), producing fumarate. The uptake of succinate is carried out via a succinate transporter (DCT) as the protonated form (succinic acid). The counterion (Na^+ or NH_4^+) is not transported equally rapidly, thus causing the medium to become alkaline. The reduced redox equivalents are produced via the oxidative tricarboxylic acid cycle (TCA) and oxidized in the electron transport chain. Since succinate is also necessary for porphyrin biosynthesis, it must also be made available under anaerobic conditions. Succinate can be produced under anaerobic conditions via fumarate reductase (FRD). In *R. rubrum*, FRD and SdH is the same enzyme (since only one succinate:quinone oxidoreductase has been annoted in the genome), which is able to catalyze the forward and reverse reactions depending on the redox state of the cell.

The FRD activity has been found to be dependent on the RQ in *R. rubrum* (Haraishi, 1988). Succinate can be produced also via the methylmalonyl pathway in an ATP-consuming reaction: propionyl-CoA reacts with bicarbonate (CO_2 dependency) using ATP and yielding methylmalonyl-CoA as a product. Then, methylmalonyl-CoA is converted into succinyl-CoA.

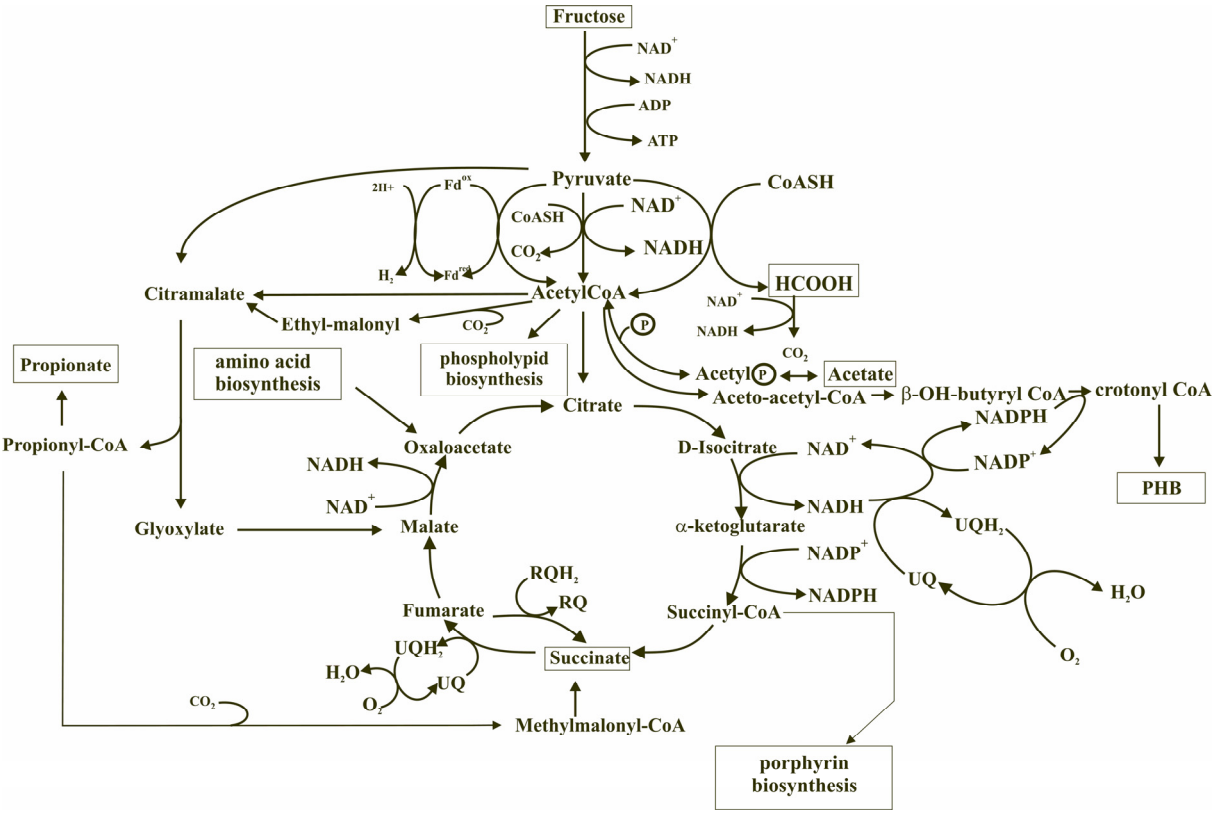

Fig. 11. Potential metabolic pathways under microaerophilic conditions according to Grammel *et al.* (2003) and Ivanovsky *et al.* (1997).

The TCA cycle enzyme profile shows significant differences in *R. rubrum* to that of *E. coli*. In contrast to that in *E. coli*, the presence of SDH and α-ketoglutarate dehydrogenase (αKGDH) at low activity levels under anaerobic conditions allows the TCA cycle to leak intermediates also in the absence of oxygen. Under microaerophilic conditions, the activities of SDH and αKGDH are more significant, which means, the oxidative TCA cycle contributes to the metabolic profile (Grammel *et al.*, 2003). The activities from FRD, SDH and αKGDH unambiguously show that the metabolic pattern of the microaerobic state consists of both anaerobic and aerobic pathways in cooperation (Grammel *et al.*, 2003).

Oxalacetate is a necessary metabolite for amino acid biosynthesis, therefore it must also be produced in alternative pathways in case of slow oxidative TCA cycle operation. Oxaloacetate can be produced from pyruvate and form acetyl-CoA via the enzyme pyruvate carboxylase and via ethyl-malonyl pathway, respectively.

Under anaerobic conditions the high activity of FRD has been measured. The reduction of fumarate is probably carried out by the oxidation of RQH_2.

Fructose can be utilized in the absence as well as in the presence of oxygen, although the aerobic growth on fructose is rather slow. The fructose breakdown occurs exclusively via the Embden–Meyerhof–Parnas (EMP) pathway, whereas the Entner–Doudoroff pathway was found to be inactive in *R. rubrum* under all growth conditions (Grammel *et al.*, 2003). Pyruvate, obtained from the EMP pathway, is decarboxylated by pyruvate dehydrogenase (PdH) to yield acetyl-CoA, which is fed into the TCA cycle. In contrast to *E. coli*, where PdH activity was significantly lower under limiting oxygen concentration than that under aerobic conditions, the activity of PdH in *R. rubrum* was found at highest under oxygen limiting conditions (Grammel *et al.*, 2003),

The decarboxylation of pyruvate can also be catalysed by pyruvate:ferredoxin oxidoreductase (Pfor) yielding acetyl-CoA and reduced ferredoxin. The reduced ferredoxin can transfer the electrons to the ferredoxin-hydrogenase, thus producing hydrogen.

Pyruvate can also be converted into acetyl-CoA via pyruvate formate lyase (Pfl) producing formate. Formate can be excreted or can be utilized for hydrogen production via formate dehydrogenase.

The absence of oxygen results in an acidic pH of the medium due to the production of fermentative organic acids. The excretion of acetate is the most significant, which is produced when acetyl-CoA is converted by phosphate acetyltransferase to acetyl–phosphate , which is then dephosphorylated by acetyl kinase to yield acetate. Large amounts of acetyl-CoA are also necessary for the lipid biosynthesis.

Excretion of propionate has also been observed under microaerophilic conditions (Grammel *et al.*, 2003). In several microorganisms (e.g. *E. coli*), propionyl-CoA can be produced via the glyoxylate pathway. Since *R. rubrum* lacks isocitrate lyase, propionate must arise from other pathways. Propionate production has been observed to occur via the citramalate and ethylmalonyl pathway as the lytic product of citramalate (Ivanovsky *et al.*, 1997). These pathways were observed simultaneously in *R. rubrum* under phototrophic conditions, growing on acetate (Berg and Ivanovsky, 2009). The ethymalonyl pathway is also the entrance to the biosynthetic pathway of polyhydroxybutyrate (PHB). Significant production of PHB occurs under oxygen, nitrogen or sulphur limitation (Henderson and Jones, 1997). PHB stores energy and carbon, furthermore it also serves as a sink for redox equivalents due to the reduction step

with NADPH. NADPH was found to be produced by the enzymes ICDH and NADH TH under microaerophilic conditions (Grammel *et al.*, 2003).

Grammel and Ghosh (2008) showed that the $[UQH_2]/[UQ]$ ratio is the same in the fructose-succinate medium as in the succinate medium under aerobic conditions and that it is two fold higher in the former medium under microaerophilic conditions. Under microaerophilic conditions, the role of $[UQH_2/UQ]$ ratio is a regulatory factor in the induction of the photosynthetic membrane (PM) biosynthesis (Grammel and Ghosh, 2008). At low oxygen availability, the electrons cannot flow via the electron transport chain (ETC) due to the absence of flux on cbb_3, which leads to a reduced state of the UQ pool and the accumulation of the reduced redox equivalents. The reduced UQ pool mediates the light-induced signal triggering the PM biosynthesis (Grammel and Ghosh, 2008).

The PM forms vesicles (chromatophores) in the cell. Each chromatophore contains the PSUs and the enzymes of the ETC: NADH dehydrogenase (NADHdH), the cytochrome bc_1 complex, SDH and the cbb_3 cytochrome c oxidase. Furthermore, the PM also contains NADH/NADPH transhydrogenase (NADH TH) and electron transfer species such as RQ and UQ (Fig. 12).

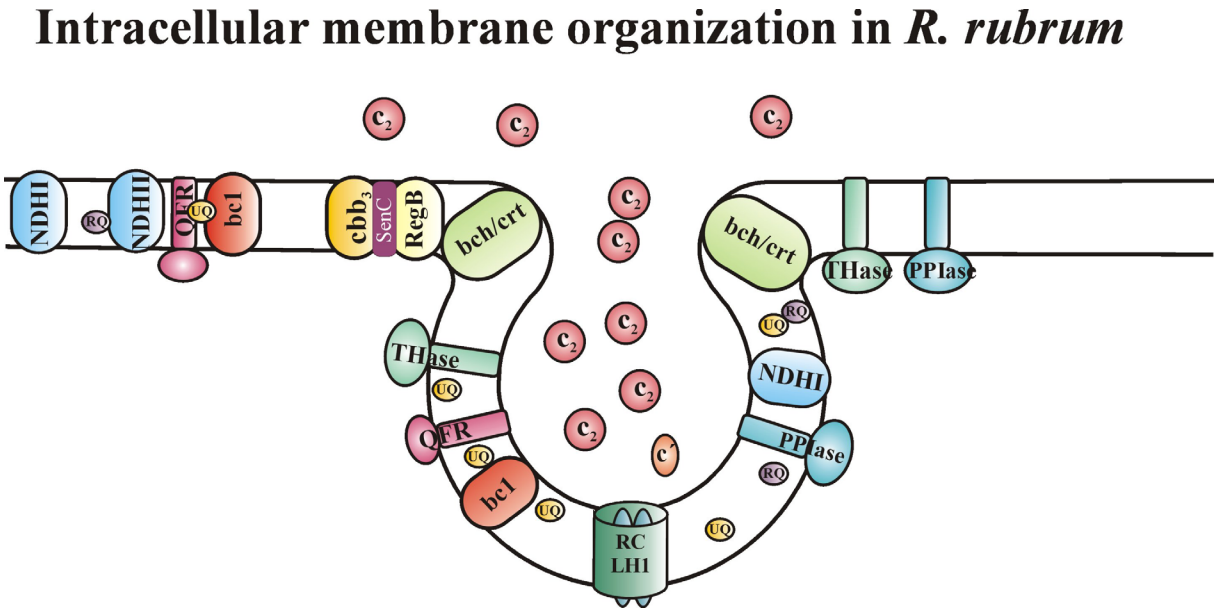

Fig. 12. PM membrane forms vesicles containing the PSU and the ETC enzymes and cofactors (R. Ghosh, unpublished)

It is commonly thought that NADH TH operates in the direction of producing NADPH, consuming proton chemical gradient (Δp).

$$NADH + NADP^+ + xH^+_{out} \Leftrightarrow NAD^+ + NADPH + xH^+_{in}$$

It can also work in the reverse direction, producing NADH and generating Δp. However, this has not yet been shown experimentally (Kaister and Yike, 1967).

At present, the major source of NADPH under anaerobic conditions is unclear. A possibility, analogous to the enzyme function in spinach, is that NADPH may be produced via a ferredoxin:NADPH oxidoreductase (Fnor).

The redox potential of UQ-10 (+90mV) has been determined in *Rb. sphaeroides* (Takamiya and Dutton, 1979). In contrast to the former bacterium, *R. rubrum* has a lower potential quinone, RQ, with a redox potential of -30 mV in the chromatophores (Erabi *et al.,* 1975). In the presence of RQ, ATP generation has been observed in the dark using PMS as an electron donor. This process does not use the cytochrome bc_1 complex, since the reaction is not sensitive to antimycin, which is a specific inhibitor for bc_1 complex.(Yamamoto *et al.*,1970) RQ has an essential role in the photosynthesis, which was shown with the RQ^- (F11) mutant which is unable to grow under phototrophic conditions (Lonjers *et al.*, 2011; Gimenez-Gallego *et al*., 1981). In the F11 mutant, the lack of RQ also resulted in reduced fumarate reductase activity, therefore an important role of RQ in this reaction has been postulated (see Ferguson *et al.*, 1987).

SDH and FRD is single enzyme in *R. rubrum*, which is dependent on the redox state of the cell (Ferguson *et al*., 1987; Hiraishi, 1988; Munk *et al.,* 2011). SDH is a flavoprotein (Davis *et al.,* 1977; Hatefi *et al.,* 1972) which contains four subunits: two hydrophilic (SdhA, SdhB) and two hydrophobic (SdhB, SdhC). The SdhA subunit is a flavoprotein which contains covalently bound FAD and the succinate binding site. SdhB is an iron-sulphur protein with three [2Fe-2S] clusters. In *R. rubrum*, the SdhB and SdhC form a cytochrome b complex with six transmembrane helices with a heme b group and at least one UQ binding site. The SDH activity was 7-fold higher under aerobic conditions than under phototrophic conditions (Collins and Hughes, 1983). Kaister and Yike (1967) observed succinate-linked NADH production driven by light and ATP in chromatophores of *R. rubrum*. Furthermore, $FMNH_2$-dependent FRD activity was observed in *R. rubrum* due to its RQ content. The FRD activity was diminished after the treatment of Triton X-100 (Hiraishi, 1988). An NADH-dependent FRD has also been observed in *R. rubrum* (Hiraishi, 1988).

The enhanced RQ biosynthesis under anaerobic/microaerophilic conditions has been observed in mitochondrion of the worm, *Ascaric suum* and the protist*, Euglena gracilis.* In *E. gracilis* Castro-Guerrero *et al.* (2005) have shown that RQ has a role in the anaerobic metabolism, especially in the fumarate reduction. Furthermore, these authors have shown that RQH_2 is able to transfer electrons to the bc_1 complex, a cytochrome bc_1-like complex, and to an

alternative oxidase. In *A. suum,* RQH_2 is also used as electron donor in fumarate reduction (Yamashita *et al.*, 2004). Furthermore, it is able to pass electrons to the NADH dehydrogenase under anaerobic conditions (Ma *et al.*, 1993). An electron transport flavoprotein (ETF) has been characterized in *A. suum*, which accepts the electrons from RQH_2 and transfers them to the NADH-dependent acyl-desaturase. This allows reversed ß-oxidation, resulting in short branched-chain fatty acids (Komuniecky *et al.*, 1989). The characterisation of the ETF:RO oxidoreductase showed that the reduction of flavin occurred in two steps and an RQ semiquinone radical has been determined as an intermediate (Ma *et al.*, 1993).

1.3 Microbial biosynthesis of isoprenoids

After giving an overview of the molecules of interest and the metabolism of *R. rubrum*, we look at the special biosynthetic pathway for the carotenoids and for its two competing pathways: the isoprenoid-quinone and BChl*a* biosynthesis pathways. These pathways originate from the MEP pathway, which was first discovered in 1993 in higher plants by Rohmer, Arigoni and their colleagues (Eisenreich *et al.*, 2004; Kuzuyama *et al.*, 2003; Rohmer *et al.*, 1999; Rohmer *et al.*, 1993; Rohmer *et al.*, 1996).

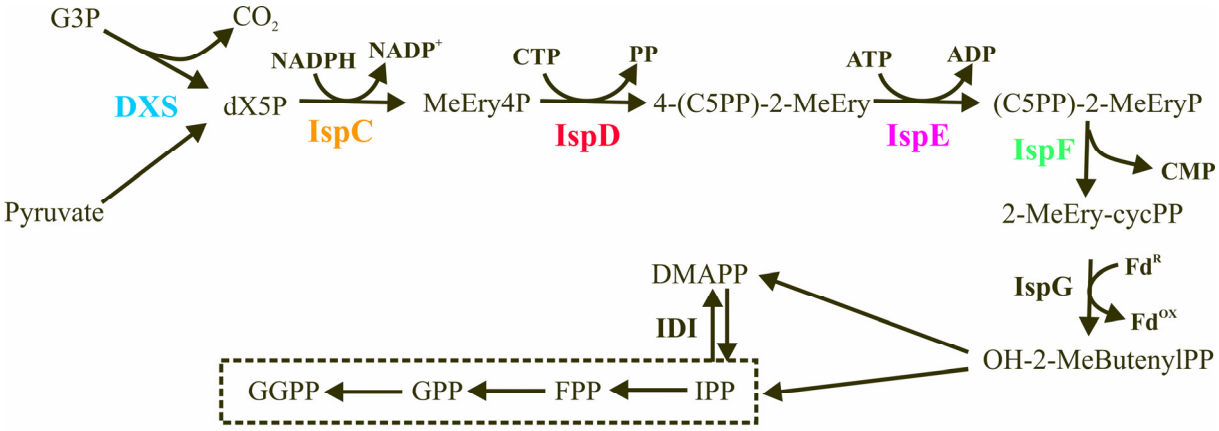

Fig. 13. Terpenoid backbone biosynthesis (R. Ghosh, unpublished)

Earlier, only a mevalonate-dependent isoprenoid pathway was known in higher plants, but Rohmer *et al.* (1993) showed that another pathway, producing isoprenoids, exists. They examined the ^{13}C pattern of the produced isoprenoids, which showed no accordance with the expected mevalonate pathway prediction (Rohmer *et al.*, 1993; Rohmer *et al.*, 1996). During the past decade, much new information of this novel pathway was discovered. The MEP

pathway consists of eight reactions (Fig. 13). The first metabolite, 1-deoxy-D-xylulose 5-phosphate (dX5P), is obtained by a transketolase condensation of pyruvate and D-glyceraldehyde 3-phosphate catalyzed by 1-deoxy-D-xylulose-5-phosphate synthase (DXS) using Mg^{+} and thiamine pyrophosphate as cofactors. The catalytic activity of DXS is relatively high compared to the enzymes downstream on the pathway (Xiang *et al.*, 2007; Eubanks and Poulter, 2003). The dX5P is reduced by the enzyme dX5P reductoisomerase (IspC (DXR in Fig. 13)) resulting in 2C-methyl-D-erythritol 4-phosphate (MEP), which is the metabolite giving the pathway its name. In the next step, a nucleotide derivative, CMP, binds to MEP resulting in 4-diphosphocytidyl-2-C-methylerythritol (4-(C5PP)-2-MeEry in Fig. 13). This molecule is phosphorylated by IspE. In the next step, CMP leaves the molecule, which closes into a ring resulting in the molecule 2-C-methyl-D-erythritol 2,4-cyclopyrophosphate (2-MeEry-cycPP). This molecule is reduced with the help of ferredoxin converting it into 1-hydroxy-2-methyl-2-(E)-butenyl 4-diphosphate (OH-2-MeButenylPP). The last step is carried out by IspH using NADPH leading the end products of the pathway: DMAPP and IPP. These molecules can be interconverted by the enzyme IDI (isopentenyl diphosphate isomerase).

1.3.1 Regulation of the MEP pathway in microorganisms and higher plants

DXS of *E. coli* was first characterized by Sprenger and coworkers (Sprenger *et al.*, 1997, Lois *et al.*, 1998, Lange *et al.*, 1998). The compound dX5P is a branch point for isoprenoid, thiamine and pyridoxal biosynthesis (Cordoba *et al.*, 2009), therefore it is also a control point of the system. So far, most investigations on the enzyme DXS have been carried out in plants. For instance, the addition of DXS via plasmid transfer resulted in higher levels of chlorophylls, tocopherols, carotenoids, abscisic acid, and gibberellins in plants. The amounts of these compounds correlates with changes in DXS levels. Therefore, it can be concluded that in plants, DXS is one of the bottleneck enzymes of the MEP pathway (Estevez *et al.*, 2001). Similar results have been obtained in other plants including tomato (Lois *et al.*, 2000; Enfissi *et al.*, 2005). A transgenic tomato containing bacterial DXS produced an increased carotenoid content (Enfissi *et al.*, 2005). Product inhibition of DXS was observed by adding exogenous labelled dX5P to the system resulting in very little change of isoprene emission. The activity of DXS was nearly zero as long as exogenous dX5P was available, indicating strong inhibition of dX5P on DXS (Wolfertz *et al.*, 2004).

High levels of DXS, DXR proteins were observed in *ispH*$^{-}$ and *ispD*$^{-}$ MEP pathway mutants, which suggests a feedback from the downstream products on the MEP pathway (Cordoba *et al.*, 2009). Furthermore, the transcript level of DXS was significantly reduced, indicating a

post-translational regulatory mechanism. The same phenomenon was observed by applying fosmidomycin, a specific inhibitor of the MEP pathway. This molecule inhibits the second enzymatic step of the pathway, which results in accumulation of dX5P. Due to the treatment with fosmidomycin, high level of the DXS protein could be measured. These results hint a translational and/or posttranslational feedback regulation of DXS in plants in response to the MEP pathway flux rate (Roma *et al.*, 2005).

Taken together, all studies carried out on MEP pathways so far have confirmed the main controlling role of DXS, whereas the role of DXR and IspH is minor (Rodri *et al.*, 2002). Under certain circumstances IspH and DXR can become also rate-limiting enzymes for isoprene synthesis (Botella-Pavia *et al.*, 2004; Carretero-Paulet *et al.*, 2006).

As we have seen, the levels of some isoprenoids change according to the level of DXS, but there are also various isoprenoids, which do not follow the changing pattern of DXS. This phenomenon suggests further downstream regulation on the post-IPP biosynthetic pathways. Clearly, each post-IPP biosynthetic pathway might have its own regulatory system (Estevez *et al.*, 2001) which cooperates with the MEP pathway in order to make sure that the required precursor will be supplied. Lois *et al.* (2000) reported about downstream product feedback regulation of the carotenoid pathway on DXS. They demonstrated that quantitative and qualitative composition of carotenoid changes due to the increase the mRNA level of DXS. This suggests that the downregulation of DXS is dependent on the end product of the pathway. Furthermore, the pattern of the accumulation of the DXS mRNA is similar to the pattern of expression of phytoene synthase (PSY) in dark. This is a downstream enzyme from DXS, and it is the first enzyme in the carotenoid production. Interestingly, PSY can be induced earlier than DXS, and the activation of PSY increased the expression of DXS. It is likely, that PSY and DXS cooperate to fine-tune the regulation of the carotenoid biosynthesis. DXS is probably the first regulatory step, and PSY (sitting at the branch point to BChl*a*, carotenoids and isoprenoid-quinones) is the second one. It assumes that geranylgeranyl-pyrophosphate (GGPP) (substrate for PSY, see below) does not occur at a limiting level. In *Arabidopsis thaliana* it was also shown that PSY has a feedback effect on DXS in order to ensure the optimal precursor supply (Rodriguez-Villallón *et al.*, 2009).

The MEP pathway genes in plants (*e.g. A. thaliana*) show high sequence similarity to the bacterial MEP pathway genes (Rodriguez-Concepcion and Boronat, 2002).

In *E. coli*, overexpression of DXS resulted also in increased carotenoid levels (Matthews *et al.*, 2000; Yuan *et al.*, 2006). *E. coli* containing overexpressed DXS showed not only increased lycopene levels, but also elevated levels of UQ-8. The level of these end products

corresponded with enhanced DXS activity, showing that enhancement of DXS activity affects all isoprenoid pathways downstream (Harker *et al.*, 1999).

1.3.2 Reactions downstream from the MEP pathway

The MEP pathway ends up with two products: dimethylallyl-pyrophosphate (DMAPP) and isopentenyldiphosphate (IPP). The consecutive condensation of these molecules is carried out downstream from the MEP pathway. These steps are catalyzed by the prenyltranferases resulting prenyl diphosphates with various chain lengths (Fig. 14). Geranyl-diphosphate synthase catalyzes the condensations of IPP with DMAPP resulting in geranyl-diphosphate (GPP). Farnesyl-diphosphate synthase (FDP synthase, IspA), is a prenyltransferase, which catalyzes a single transfer of IPP to GPP, yielding farnesyl-diphosphate (FPP). GGPP synthase (CrtE) catalyzes the condensation of FDP and IPP yielding geranylgeranyl-diphosphate (GGPP), which serves as an important branching point for carotenoid, isoprenoid-quinone and chlorophyll synthesis pathways (Ohnuma *et al.*, 1996; Burke *et al.*, 1999).

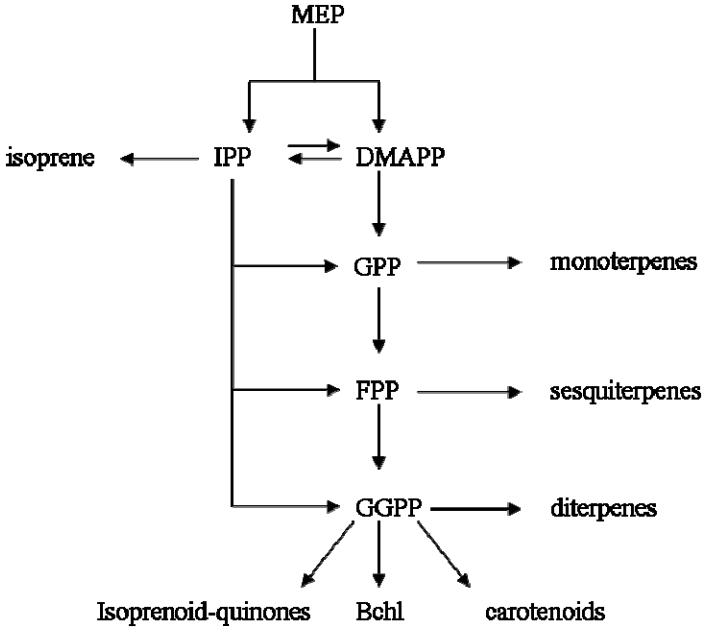

Fig. 14. Isoprenoid pathways arising from the MEP pathway

As can be seen in Fig. 14, the BChl*a* and isoprenoid- quinone biosynthesis arise from the metabolite GGPP, thus competing with the carotenoid pathway. Isoprenoid quinones as well as BChl*a*-s both have polar head groups which are biosynthesized via different pathways. BChl*a* and isoprenoid-quinone biosynthesis are regulated by oxygen and light. Furthermore, BChl*a* biosynthesis is also regulated by heme (which is a product of the pathway) and

cytochrome c as well (Biel *et al*., 2004). The BChl*a* pathway starts with protoporphyrin IX. This is a branching point for the biosynthesis of the heme, cytochrome as well as BChl*a*. The first well-regulated step is the insertion of Mg^{2+} into the porphyrin IX.
UQ biosynthesis starts from tyrosine. In *E. coli*, the biosynthesis of UQ is catabolite repressed by fructose and glucose (Sippel *et al.*, 1983).

1.3.3 Discovery of carotenoid pathways in phototrophic bacteria

Spx was first isolated from *R. rubrum* by van Niel and Smith in 1935 as the major carotenoid. Spx was examined spectroscopically and stereochemically by Polgar *et al.* (1944). The absorption properties of the purple bacteria pigments were resumed by van Niel in 1946. The first time courses of Spx biosynthesis were recorded by Goodwin and Osman in 1953 (Goodwin and Osman, 1953). In this work, the effect of diphenylamine (DPA), an inhibitor for CrtI, on the concentration of spx was introduced. They found that the spx concentration decreased after the addition of DPA. The resolution of the carotenoid composition was investigated by van Niel *et al.* (1956) in *R. rubrum*. He showed that initially many different carotenoids are observable and that they disappear during the growth curve. They also showed how the relative amount of spx rises with the cultivation time.
Rb. sphaeroides, which is closely relatived to *R. rubrum*, was also investigated regarding the carotenoid production by van Niel (1947) and Goodwin *et al.* (1955). Goodwin *et al. (1945)* performed the same investigation procedure, as with *R. rubrum* in 1953, analyzing the composition of the carotenoids as well as the effect of DPA in the bacteria *Rb. sphaeroides*.

1.3.4 Identification of the metabolites of the carotenoid pathways

After it became clear that the carotenoid biosynthesis is a maturation process, which ends up in spx in the wild-type, carotenoid mutants were also investigated. In 1956, Griffith and Stanier carried out a large investigation on pigment mutants of *Rb. sphaeroides*. They isolated different UV radiation-induced mutants with different colours, and analyzed them spectroscopically. They found that the different colour was due to the changes in the carotenoid composition. The colourless mutants had lost both BChl and carotenoids. They found phytoene to be the end product in the blue-green mutant, and neurosporene (and dihydroxy-neurosporene) in the green mutant. In the brown mutant, several end products could be identified, for example lycopene. In 1962, Griffith analyzed the BChl biosynthesis in mutants showing changes in the chlorophyll composition. He showed that certain precursors of BChl must be available for carotenoid production.

The effect of DPA inhibition on *R. rubrum* cultures was studied extensively by Jensen, which was a milestone in carotenoid research (Jensen *et al.*, 1958). They separated the carotenoids chromatographically and determined the extinction coefficients for the *R. rubrum* pigments. They found more than 20 carotenoids in the DPA-inhibited cultures. The identification of the carotenoids was based on the UV-VIS spectrum. They also recorded the dynamics of the carotenoid biosynthesis after DPA addition. They found, that in the presence of DPA, the lycopene concentration decreased rapidly and the more saturated carotenoids accumulated. They also recorded the time courses of the carotenoids after removal of the inhibitor. Based on the dynamics recorded by applying and removing DPA, they proposed a desaturation reaction sequence from phytoene to lycopene, which is catalyzed by the enzyme CrtI (see below). Jensen *et al.* (1961) introduced a new member of the pathway, 3,4-didehydrorhodopin. They showed the reaction sequence from 3,4- didehydrorhodopin to rhodovibrin. They also showed that under normal growth unsaturated carotenoids are produced and DPA inhibits the desaturation of phytoene leading to unnatural carotenoid products. They also show that anhydrorhodovibrin is a precursor to spx, and that they differ only in the number of methoxy groups.

With these results the linear reaction sequence from phytoene to spx was established (Fig. 15). Jackman and Jensen (1964) revealed a proposal for the spheroidene pathway for *Rb. sphaeroides*.

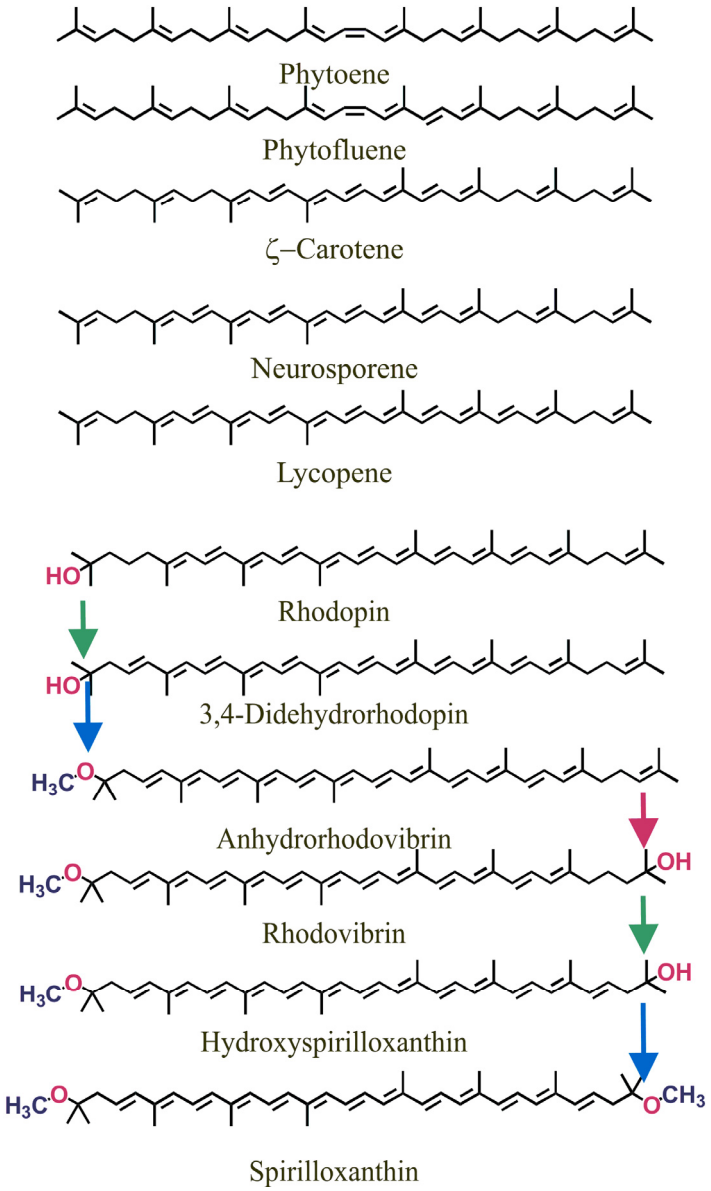

Fig. 15. Linear reaction sequence starting with phytoene, ending with spx (Jensen *et al.*, 1961)

The next milestone was the studies of DPA inhibition experiments made by Davies in 1970 due to which the pathway in *R. rubrum* was unambiguously identified. He was the first researcher studying *R. rubrum* carotenoids with mass spectrometric detection. He applied the knowledge of the pathways, which were determined by Jensen and his coworkers (Jensen *et al.*, 1961; Jensen *et al.*, 1963; Eimhjellen and Jensen, 1964) in *Rb. sphaeroides*, *R. rubrum* and in *Rvi. gelatinosus*. Davies separated the carotenoids with thin-layer chromatography and measured them spectrophotometrically and mass spectrometrically. He also found the 1-hydroxy-1,2-dihydro derivatives of the normal carotenoids as has been described by Jensen *et al.* (1958). He also determined the spheroidene pathway observed in *Rb. sphaeroides* (Jensen *et al.*, 1963). The simultaneous occurrence of the spx pathway and spheroidene pathway suggests, that the two pathways are interconnected, as in the case of *Rps. gelatinosus*. Based

on the known pathways and the measured carotenoids in DPA-inhibited cultures, he created a map (see Fig. 16) for the possible carotenoid biosynthetic pathways in *R. rubrum*. This map shows that there are several pathways leading to the end product, spx. According to Davies, these pathways must be connected, and the metabolites of one pathway can be converted to those of another pathway (Fig16).

Jensen reviewed all the significant information about the carotenoid pathways and chemical considerations of the carotenoid properties in photosynthetic bacteria (Jensen and Andrewes, 1972).

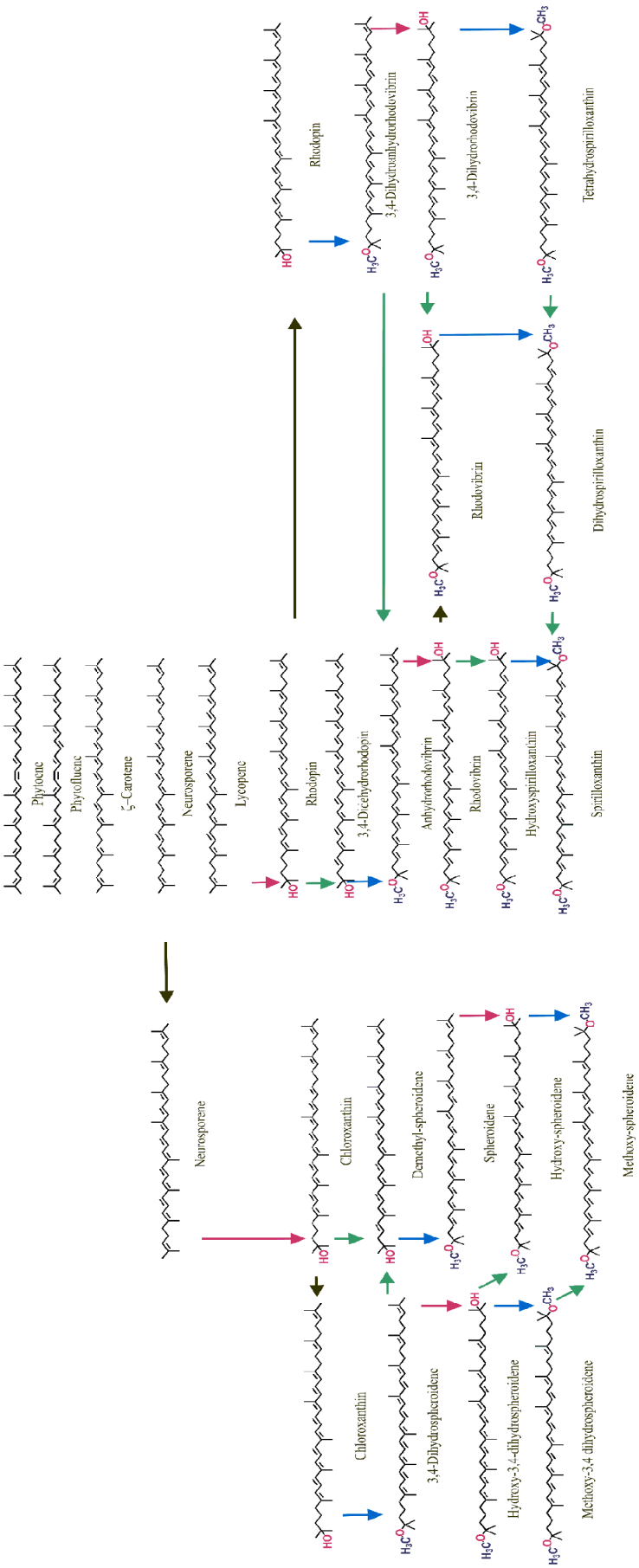

Fig. 16. Combinatorial carotenogenic pathways according to Davies (1970)

1.3.5 Identification of carotenogenic enzymes

In 1974 Barry Marrs presented a tool for gene transfer in *Rb. capsulatus*, the mechanism of capsduction (Marrs, 1974). The name originated from the transduction phrase, where bacteriophages are the DNA transfer agents. In capsduction in contrast, there are phage-like particles (electron microphages) as gene transfer agents (GTA). Applying this gene transfer system, the photopigment region was mapped in *Rb. capsulatus,* (Yen and Marrs, 1976; Scolnik and Marrs, 1980), in which they showed, that *bch* genes and the *crt* genes are linked in the chromosome. They identified the genes *crtA crtB, crtC, crtD, crtE* and the *bchc*, *bchD*, *bchG* genes (Table 2.).

Gene	Function of the product
crtA	oxydation of spheroidene to spheroidene
crtB	early step of carotenoid biosynthesis
crtC	hydration of neurosporene to hydroxy neurosporene
crtD	dehydrogenation of methoxyneurosporene to spheroidene dehydrogenation of hydroxyneurosporene to demethylspheroidene
crtE	early step of carotenoid biosynthesis
crtF	methylation of hydroxyneurosporene to methoxyneurosporene methylation of demethylspheroidene to spheroidene

Table 2. Actual knowledge of the carotenoid biosynthetic enzymes in 1980

Marrs isolated the R´ plasmid in 1981, which contained all genes for the core bacterial photosystem. In 1983, the genes of the photopigment system were identified from the R´-plasmid with restriction mapping with marker rescue/complementation analysis. Four new *bch* genes and two genes for the light harvesting system were found (Taylor *et al.*, 1983). The partial genetic physical map of the photopigment system was available.

The Hearst group extended this knowledge by transposon mapping of the photosynthesis genes of the R` plasmid by simultaneous use of Tn5 and Tn7 (Zsebo *et al.* 1984). The *crt*I was identified, and a more precise genetic and physical map was created (Zsebo *et al.*, 1984).

After the map of the photopigment genes became known, the period of sequencing began. The complete sequence analysis of the photosynthesis gene cluster was obtained by the Hearst group (Youvan *et al.*, 1984; Armstrong *et al.*, 1989; Armstrong *et al.*, 1990; Burke *et al.*, 1993). The structural genes for the RC and for LHI were sequenced in 1984 (Youvan *et al.*, 1984). The sequence and analysis of the carotenoid biosynthetic gene cluster were carried out in 1989 (Armstrong *et al.*, 1989; Armstrong *et al.*, 1990). The BChl*a* biosynthetic gene cluster

was sequenced and studied by Burke *et al*. (1993). Interposon mapping was used in order to uncover the organization and regulation of the carotenogenic genes (Giuliano *et al*., 1988). They showed, that with the exception of *crtB* and *crtI*, all *crt* genes are one transcriptional unit and observed oxygen-sensitive transcription of the *crt* gene cluster. After these results, the investigations of the regulation of the photopigment system gene clusters using mRNA hybridization began (Zhu and Hearst, 1986; Zhu *et al.,* 1986; Kiley and Kaplan, 1987). They found that the shift from aerobic-to-anaerobic conditions activates the expression of the investigated genes. Furthermore, they established the dependence of the photosynthetic gene expression in response to light intensity. In *Rb. capsulatus*, the BChl*a* genes are present at a single chromosomal locus and are comprised of several operons expressed under low oxygen concentrations (Biel and Marrs, 1983; Biel and Marrs, 1985; Mosley and Bauer, 1994). The *puf* operon was identified, which encodes the proteins for RC and LHI and *pufQ* of the regulatory protein (Clark *et al.*, 1984; Bauer *et al.*, 1988; Bauer and Marrs, 1988). The *puc* operon was investigated and found to be coding the LHII polypeptide genes (Youvan and Ismail, 1985; Nickens and Bauer, 1998). The superoperon behaviour of the photosystem operons was proven in 1989 (Young *et al.*, 1989).

Rb. sphaeroides were investigated in detail by Scolnik and Marrs (1987); initial genetic mapping was performed using chromosome transfer (Sistrom, 1977; Pemberton and Bowen, 1981; Bowen and Pemberton, 1985). Applying this method, a genetic map of carotenogenic genes was created (Pemberton and Harding, 1986). Southern hybridization as well as gene sequencing showed a high degree of homology between the photosynthetic genes of *Rb. capsulatus* and *Rb. sphaeroides* (Beatty and Cohen, 1983; De Bont *et al.*, 1981). The conservative behaviour of the carotenoid genes was also shown elsewhere (Armstrong *et al.*, 1990). Regulation of these genes is also similar to the regulation with light and oxygen in *Rb. capsulatus* (Cohen-Bazire *et al.*, 1957; Gomelsky and Kaplan, 1995 a,b; Penfold and Pemberton, 1994). The final genetic map of the carotenoid genes was completed in 1995 and the gene functions were identified in *Rb. capsulatus* (Lang *et al.*, 1995). The information about the photosynthetic gene cluster of *Rb. sphaeroides* was summarized by Naylor *et al.* (1999).

The whole genome of the wild-type of *R. rubrum* (S1) was sequenced in 2011 (Munk *et al.*, 2011). At present, all of the *crt* genes in *R. rubrum* have been identified functionally (Sagaesser, 1992; Komori *et al.*, 1998; Wang *et al.*, 2012, Autenrieth and Ghosh unpublished).

1.3.6 Introduction of the carotenogenic enzymes

Phytoene synthase (CrtB, PSY) is a peripheral transferase and is the first pathway-specific step in carotenoid biosynthesis. It connects two GGPP molecules to each other in a condensation step which requires a Mn^{2+} as a cofactor (Fig. 17). Numerous different PSYs have been identified from different microorganisms. Initially, this reaction was thought to be carried out by two enzymes, in *Rb. capsulatus*, but in 1991 it has been shown, that phytoene is produced via a single enzyme, CrtB (Sandmann and Misawa, 1991). Considerable homology was found in the amino acid sequences of some carotenogenic gene products from the anoxygenic photosynthetic and non-photosynthetic prokaryotes *Erwinia uredovora* and *Erwinia herbicola* (Misawa *et al.*, 1990; Armstrong *et al.*, 1990). In aerobic photosynthetic microorganisms, such as cyanobacteria, the PSY was characterized and also found to be a single enzyme which catalyzes this 2-step reaction. This enzyme shows also high homology with the cDNA from tomato (Chamowitz *et al.*, 1992). The first bacterial PSY was purified from *E. uredovora* in 1998. It was biochemically characterized including kinetic studies (K_m determination for GGPP, inhibition by phosphate) by Neudert *et al.* (1998).

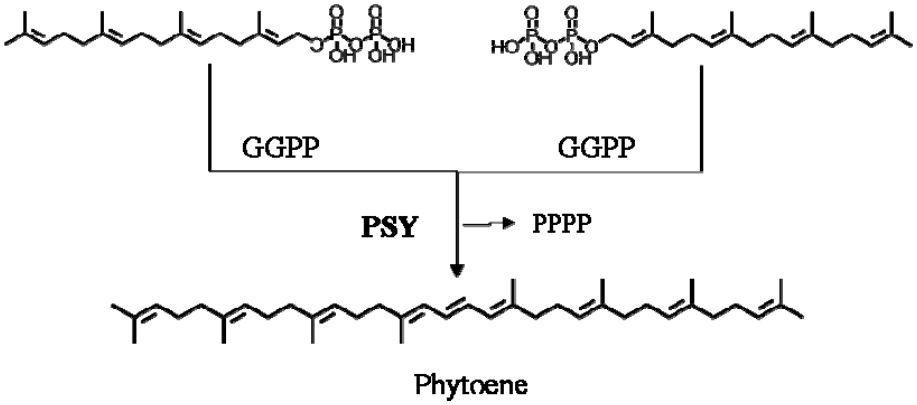

Fig. 17. The condensation step of two GGPPs results in phytoene. The reaction is catalyzed by the enzyme, PSY

Since PSY is the initial enzyme of the carotenoid biosynthesis, it is potentially a perfect regulation point. In the case of higher plants, several regulatory mechanisms in connection to PSY were observed. In *A. thaliana*, PSY was shown to be active in the dark, but mediated positive responses to light induction (Welsch *et al.*, 2003). PSY was also found to be regulated with direct light regulation via a phytochrome-interacting transcription factor, which represses the PSY transcription (Toledo-Ortiz *et al.*, 2010). Negative feedback regulation due to the disruption of the carotenoid pathway was also observed (Kachanovsky *et al.*, 2012). The collective regulation of the carotenoid pathway of DXS and PSY was

demonstrated in *A. thaliana*. In the dark, an increased amount of carotenoid was measured, which correlated with enhanced PSY and DXS transcript levels. This is contrary to the mechanism found in light, where the enhanced DXS expression does not lead to enhanced carotenoid production. Interestingly, in the dark, first PSY is induced and DXS is expressed only thereafter. These results suggest a feedback regulation of PSY on DXS in order to achieve optimal precursor input under the actual conditions (Rodriguez-Villalón *et al.*, 2009, Schofield and Paliyath, 2005).

Phytoene desaturase (CrtI) is a transmembrane protein and the second enzyme in the pathway. CrtI catalyzes a three- and/or four-step desaturation of phytoene producing both neurosporene and lycopene in *Rb. gelatinosus* depending on the kinetic conditions. It was proven by a knockout of CrtI that only phytoene is available, indicating that this organism has only one phytoene desaturase (Stickforth and Sandmann 2007; Stickforth and Sandmann 2011; Harada *et al.*, 2001). The ratio of neurosporene to lycopene depends on the kinetic conditions. It has been shown *in vitro*, that high enzyme concentrations and low precursor (phytoene) concentration favour lycopene production. This observation shows a competition for the substrate binding site between neurosporene and lycopene. In *E. uredovora*, CrtI can produce lycopene or 3,4-didehydrolycopene. In this bacterium, CrtI was found to be a flavoprotein, which is inhibited by $NADP^+$ and NAD^+ (Fraser *et al.*, 1992). Carotenoid desaturases (CrtI and CrtD see below) in *Rb. capsulatus* and *Neurospora crassa* were found to be structurally and functionally conserved flavoproteins. Due to its flavin cluster it is assumed to be extremely oxygen-sensitive (Bartley *et al.*, 1990). The number of the desaturation steps catalyzed can vary among bacterial species. In *R. rubrum* it can catalyze 4 steps resulting in lycopene. In the case of *Rb. sphaeroides* and *Rb. capsulatus* only three desaturation steps are carried out. In *E. uredovora* there are six desaturation steps resulting in 3,4,3´,4´- tetradehydrolycopene (Fig. 18).

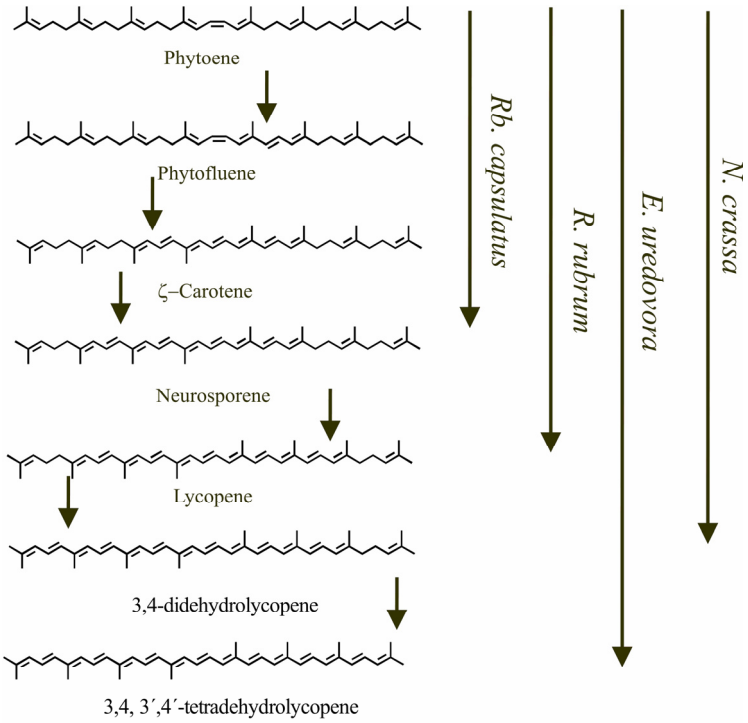

Fig. 18. Characteristics of CrtI from different microorganisms (according to Stickforth and Sandmann, 2007)

Acyclic carotenoid 1,2-hydratase (CrtC) is a lyase and it can catalyze the addition of water only in the case of acyclic carotenoids (Fig. 19). Enzymatic characterization of the purified protein showed, that water is the source of hydration in *Rb. sphaeroides* (Steiger *et al.*, 2003; Hiseni *et al.*, 2011; Yeliseev and Kaplan, 1997). The catalytic properties of CrtC in *Rb. capsulatus* and in *Rvi. gelatinosus* are different. CrtC catalyzes the water addition step in both the spheroidene and spx pathways, but with different kinetics (Steiger *et al.*, 2003). The different kinetics depend on the respective substrate and result in different end products. In *Rb. capsulatus*, the only end product is spheroidene, which is an asymmetrical carotenoid (one water addition). The CrtC of *Rb.capsulatus* is capable of producing only monohydroxylated carotenoids. Bearing one hydroxyl group, the carotenoids do not match the active site of the enzyme CrtC in *Rb. capsulatus* (Steiger *et al.*, 2003).

In the case of *Rvi. gelatinosus*, there are two end products: the primary end product is spheroidene, and the secondary is spx with two water addition steps. The kinetics of the enzyme CrtC are crucial in the reaction sequence between the spx pathway and the spheroidene pathway. The CrtC of *Rvi. gelatinosus* has a broad substrate specificity; apart from the conversion of neurosporene and lycopene, further substrates with alternative double bond systems were tested such as 3,4-didehydrolycopene, 3,4,3′,4′-tetradehydrolycopene with a successful conversion. Monohydroxylated carotenoids such as 1-OH-lycopene, 1-OH neurosporene, 1-OH-3,4-didehydrolycopene were also taken as substrates by CrtC (Steiger *et*

al., 2002). Furthermore, the monomethoxylated carotenoids can also be successfully hydrated. This low substrate specificity of CrtC makes the branching of the carotenoid pathway possible. The substrate preference can be calculated as the ratio of V_{max} and K_m values which correspond to k_{cat}. According to this value the substrates can be ranked. The substrate preference list for CrtC is the following: spheroidene, neurosporene, 1-OH- neurosporene and lycopene in the case of *Rvi. gelatinosus* (Steiger *et al.*, 2002).

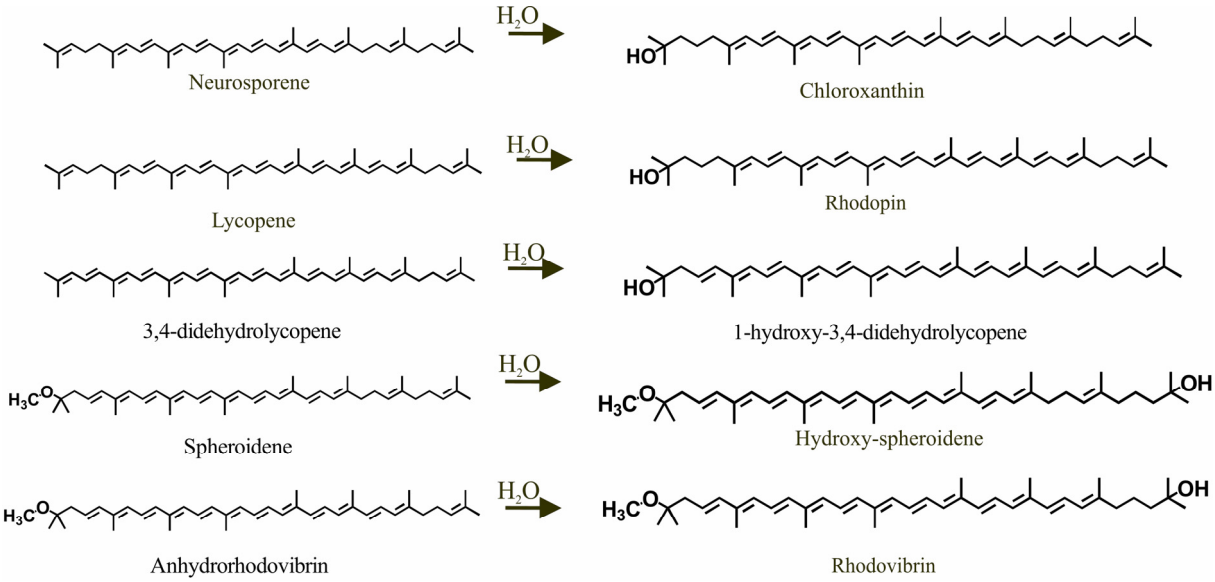

Fig. 19. Examples for the water addition steps biosynthesis catalyzed by CrtC.

Hydration of carotenoids is followed by the 3,4-desaturation carried out by **3,4-carotenoid desaturases (CrtD)**. These enzymes are flavoproteins, which catalyze the desaturation of the hydroxylated carotenoids (Steiger *et al.*, 2000, Albrecht *et al.*, 1997) In the case of *Rvi. gelatinosus,* CrtD has a broad substrate specificity and successfully converts 1-OH-lycopene, 1-OH-neurosporene, but not 1,1-dihydroxy neurosporene (Fig. 20). Substrates for CrtD can also be dihydroxylated or methoxylated molecules, but only if a double bond is available on the 3,4 position. Therefore, CrtD might dehydrate the mono and dihydroxylated and the methoxylated form of 3,4-didehydrolycopene and 3,4,3´4´- tetradehydrolycopene. In order to identify the substrate specificity, several hydroxylated carotenoids as substrates were tested. There was a high conversion rate for 1-hydroxylycopene and 1-hydroxyneurosporene. The conversion of 1,1-dihydroxylycopene was not so effective and the conversion of 1´hydroxy-3,4-didehydrolycopene took place only in traces. Also non-hydroxy carotenoids as substrates were tested, but showed no conversions (Steiger *et al.*, 2000). In *Rb.sphaeroides*, CrtD catalyzes the desaturation of 1-OH lycopene and 1-OH-neurosporene.

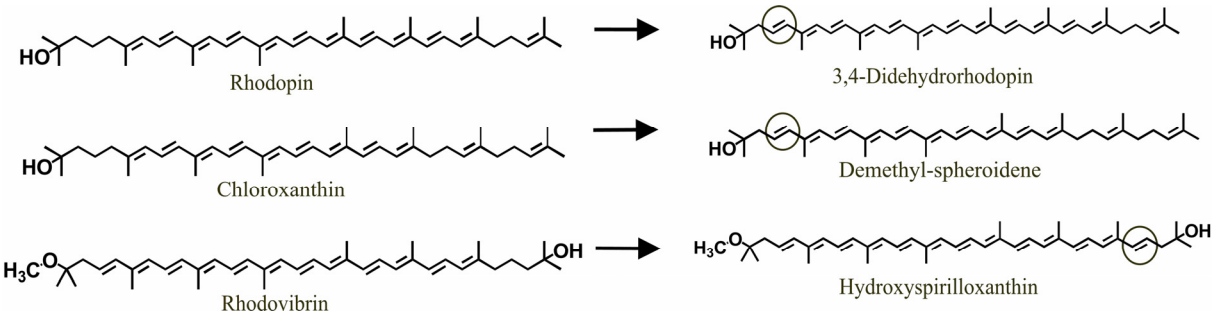

Fig. 20. Examples for desaturation steps carried out by CrtD.

1-OH-carotenoid methylase (CrtF) is the last enzyme in the carotenoid pathway and belongs to the transferases. It catalyzes the *O*-methylation of the 1-hydroxyl group (Fig. 21). The source of the methyl group and the only cofactor of the enzyme is the S-adenosylmethionine (SAM) which is converted to S-adenosylhomocysteine (SAH) during the reaction in both *Rb. sphaeroides* and *Rb. capsulatus* (Singh *et al.*, 1973; Scolnik *et al.*, 1980). CrtF was found to have very low substrate specificity (Badenhop *et al.*, 2003). In *Rb. capsulatus,* CrtF can convert carotenoids without sensing the length of the conjugative double bond system (downstream of neurosporene). Therefore, the mono and dihydroxylated form of lycopene, neurosporene, 3,4-didehydrolycopene, 3,4,3′,4′-tetradehydrolycopene can be methylated by CrtF, with the exception of the 1-OH-didehydrolycopene (Badenhop *et al.*, 2003). These results indicate that CrtF reacts with acyclic molecules, where there is a double bond on position 5,6 in the conjugative system. The double bond on position 3,4 is not a requirement and the end group at the other end of the molecule does not inhibit the methylation. Similar substrate specificity was observed in *Rvi.gelatinosus* (Takaichi and Shimada, 1999; Pinta *et al.*, 2003).

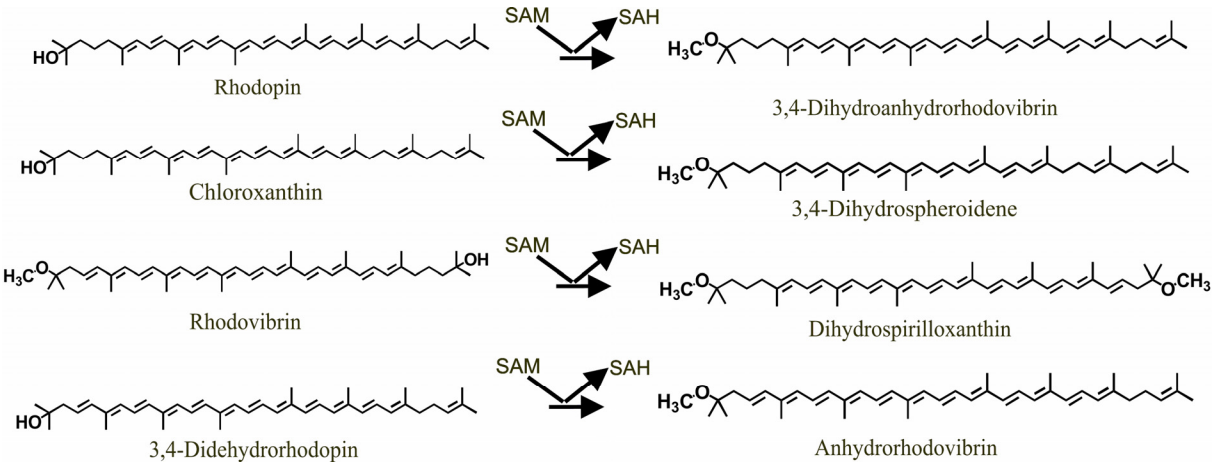

Fig. 21. Methylation reaction catalyzed by the enzyme CrtF using the cofactor S-adenosylmethionine (SAM)

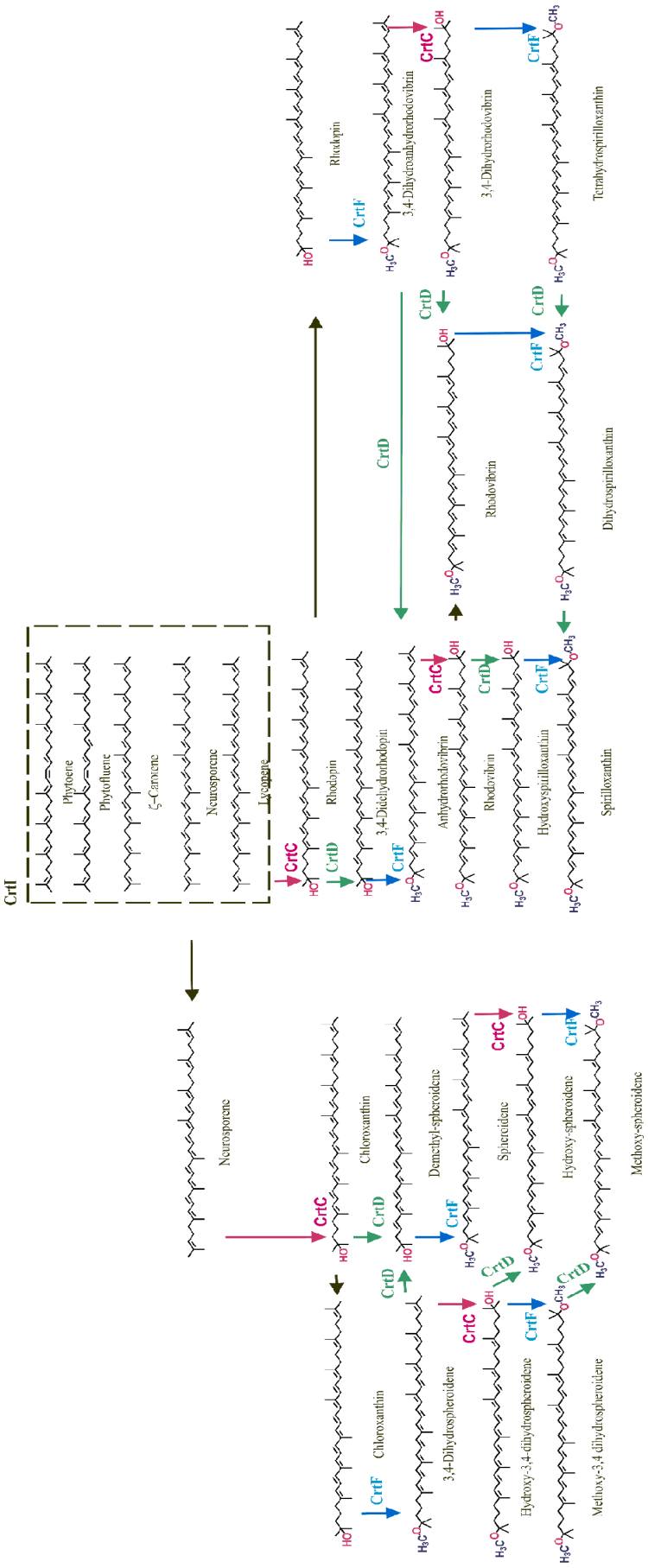

Fig. 22. Combinatorial carotenoid biosynthetic pathways including the catalyzing enzyme

1.4 R. rubrum strains containing mutations in carotenoid biosynthesis

It is now well-established that the carotenoid biosynthesis pathway in the wild-type strain S1 shows a linear reaction sequence, whereby lycopene is produced via 4 sequential dehydrogenation steps from phytoene by a single enzyme CrtI, und thereafter, hydration (catalyzed by CrtC), 3,4-/3´-4´-dehydrogenation (catalyzed by CrtD) and methylation (catalyzed by CrtF) are performed sequentially on both ends of the carotenoid molecule, to yield the final product, spx (Jensen *et al.* 1958; Davies, 1970; Schwerzmann and Bachofen, 1989). This pathway is designated as normal spx pathway (Takaichi, 2008).

However, as first demonstrated by Komori *et al*. (1998), deletion of *crtD* leads to the appearance of alternative side pathways, due to the lack of absolute substrate specificity of the carotenoid biosynthetic enzymes. Thus, as indicated in Fig. 70, in the absence CrtD (which normally dehydrogenates rhodopin, and rhodovibrin, leading to 3,4-didehydrorhodopin and monomethylated spx, respectively), the enzyme CrtF is able to methylate rhodopin, yielding the non-natural carotenoid 3,4-dihydroanhydrorhodovibrin. The latter can also act as a non-natural substrate for CrtC which yields 3,4-dihydrorhodovibrin, which in turn acts as a non-natural substrate for CrtF, to yield the final product, 3,4,3’,4’-tetrahydrospirilloxanthin (thspx) (Fig. 23). This pathway has been designated as “unusual spx” pathway (Takaichi, 2008). In the late exponential phase, ST4 cells grown either phototrophically or semiaerobically, thspx is the predominant (about 80% of the total) carotenoid produced in the photosynthetic membrane (Komori *et al.,* 1998). The observation of the non-natural thspx pathway, which arises solely due to the deletion of *crtD*, unambiguously confirmed that the substrate specificity of the carotenoid biosynthesis enzymes is broad, and that they can act combinatorially upon available substrates. In recent years, the broad substrate specificity, which allows "sequential" reactions to occur combinatorially (provided that the chemistry of the reactions remains unchanged), has been used for the biotechnological production of non-natural carotenoids (Schmidt-Dannert *et al.* 2000; Albrecht *et al.* 2000).

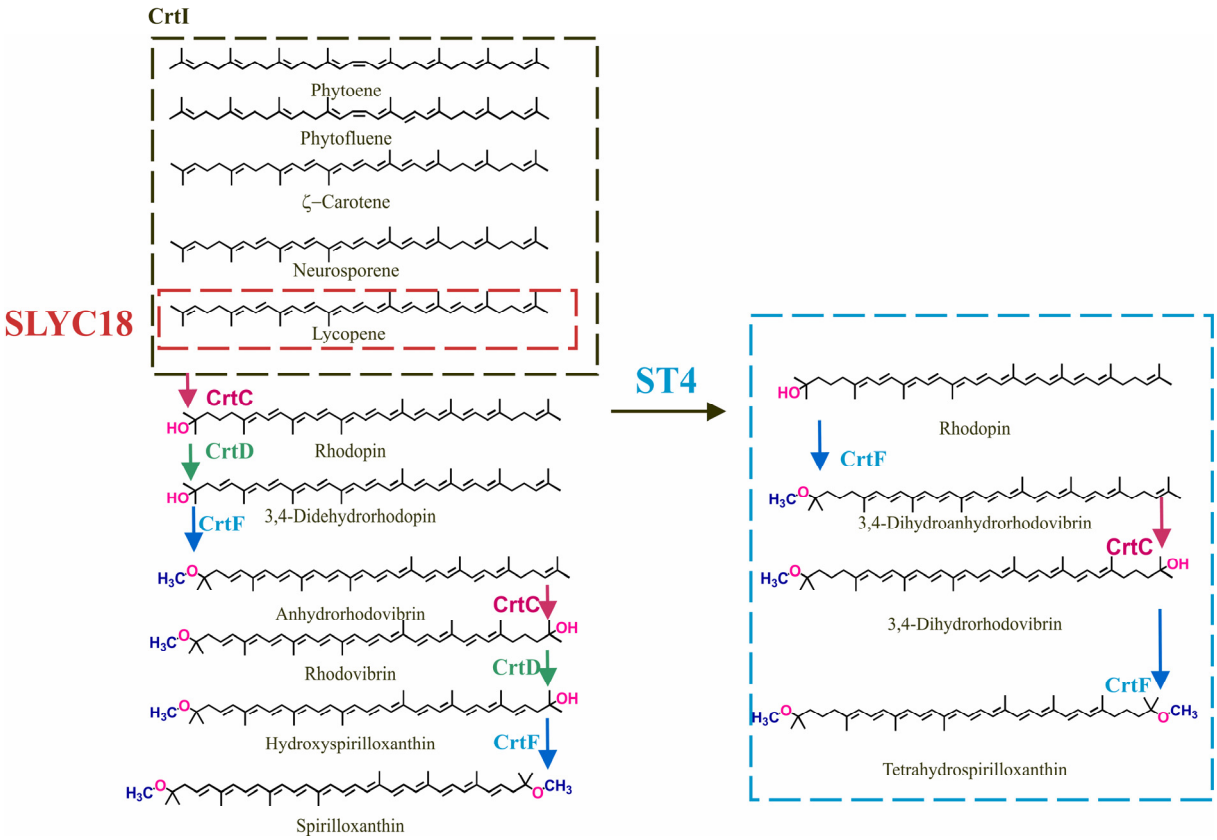

Fig. 23. The "normal" spx pathway and the "unusual" spirilloxanthin pathway (Takaichi, 2008) in *R. rubrum* observed in wild-type and ST4 (Komori *et al.*, 1998) respectively

Recently, a *crtC-crtD* deletion mutant of *R. rubrum* has been published, SLYC18. The double mutant produces only lycopene as carotenoid under phototrophic and semiaerobic conditions, since only the reaction of CrtI can be carried out (Wang *et al.,* 2012). SLYC18 yielded 2 mg/g lycopene and the spectral analysis showed that lycopene was incorporated into the LH1 complex despite the fact that the methoxy groups are missing. SLYC18 showed similar growth physiology as the wild-type, only the lycopene producing mutant had a significantly longer lag phase under microaerobic conditions. The long lag phase occurs probably due to the higher sensitivity of the strain to oxygen concentrations.

Regarding the low substrate specificity and the actual knowledge of the enzymes, the combinatorial map proposed by Davies (1970) can be extended with the carotenogenic enzymes (Fig. 22).

1.5 The focus of the thesis

Despite the detailed characterisation of the PM there is a paucity of information regarding the biosynthesis and the assembly of the pigments into the photosynthetic unit. Therefore, the role of the regulatory signals (O_2 and UQ pool) in PM biosynthesis was investigated. Furthermore, the existence of a competition among the isoprenoid pathways during PM induction has also been studied due to the simultaneous measurement of different isoprenoids. In addition, the combinatorial behaviour of the carotenogenic enzymes, originally proposed by Davies (1970), was investigated in detail using new and defined carotenoid mutants of *R. rubrum*. Here, the effect of the oxygen upon dynamics of carotenoid biosynthesis has been examined applying oxygen pulses during active growth. Finally, the effect of carotenoid lesions upon global metabolism has also been examined.

2 Material and methods

2.1 Chemicals

In general chemicals were obtained from Carl Roth GmbH, Merck and Fluka.

HPLC standards lycopene, ß-carotene, UQ-10, soybean lecithin, BChl*a*, dioleylphosphatidylcholine (dioleyl-PC) were obtained from Sigma Aldrich.

UQH_2-10 standard was prepared by the reduction of UQ-10 with BH_4. The oversaturated BH_4 solution was prepared with approximately 20 mg BH_4 in 0.5 ml. Then, 3µl BH_4 solution was added to 2.5 ml 0.1 g/l UQ-10 solution. The standard was measured with HPLC-MS method (description in 2.4.7). Furthermore, the spectrum of the standard was also measured directly after the BH_4 solution addition.

2.2 Culture conditions

All the strains used in the experiments are listed in Table 3.

R. rubrum	*Genotype*	*Reference*
S1	wild-type	Cohen-Bazire *et al.*, 1956
SLYC18	*ΔcrtC⁻, ΔcrtD⁻*	Wang *et al.*, 2012
ST4	Δ*CrtD⁻*	Komori *et al.*, 1998

Table 3. Employed *R. rubrum* strains

2.2.1 Inocula

Inocula for our experiments were obtained from cultures in the exponential phase growing on M2SF medium (Table 4) aerobically, in the dark. In the case of the strains SLYC18 and ST4 kanamycin-sulphate were added to the medium reaching the final concentration of 20 µg/ml (Kan_{20}). The cells were grown in Erlenmeyer flasks containing 500 ml medium and a stainless steel spiral, and agitated mechanically at 120 rpm (2.5cm throw) in a controlled environment incubator shaker (New Brunswick Scientific Co. Inc. Edison, N.J, USA) with a seed of 120 and throw 2.5 cm to provide the necessary aeration. The incubation temperature was 30°C.

Cultures for long term (up to six months) storage were grown in M-medium (Table 4) 4 days long in dark and 7 days with light at 30°C in stirred closed bottle.

2.2.2 **Growth medium** (according to Sistrom (1960); Ghosh *et al.* (1994)

Stock solution	Content	concentration [g/l]	Per liter M medium	per liter M2S medium	per liter M2SF/M2S2F medium
M1	KH_2PO_4 K_2HPO_4* 3 H_2O with KOH tablets pH 6.8	148 222	10 ml	20 ml	20 ml
M2	Succinic acid KOH tablets (pH 6.8)	236 224	10 ml	---	---
NH_4-succinate	Succinic acid pH6.8 with 25% NH_4OH	236	---	20 ml	20 ml
M3	NH_4Cl	214	2 ml	---	---
M4	nitrilotriaceticacid KOH L-glutamic acid L-aspartic acid $MgSO_4$* 7 H_2O FeSO4 x 7 H_2O Nicotinic acid Thiamine Biotin $CaCl_2$ x 2 H_2O (dissolve separately) Trace elements according to Hutner (Table 5)	20 22 10 4 28,8 0,2 0,1 0,05 0,002 6,6 20 ml	10 ml	10 ml	10 ml
HEPES	2M HEPES soluted in water, containing 12.9 ml 25% NH4OH (pH 6,8 with NH_4OH)	---	---	20 ml	20 ml
M5	NaCl	120	1 ml	1 ml	1 ml
M6	p-aminobenzoic acid	2,85	1 ml	1 ml	1 ml
Fructose	addition with a sterile filter after autoclave	300	---	---	10 ml/20 ml

Table 4. Medium according to Sistrom (1960) and Ghosh *et al.* (1994)

The M4 stock solution must be prepared following the order in the protocol. Adjust pH to 6.85 with KOH prior to autoclave. Kanamycin-sulphate stock solution (50mg/ml H_2O) was added after autoclave.

Chemicals	Concentration [g/l]
EDTA	50
$ZnSO_4$ x 7 H_2O	22
H_3BO_3	11.4
$MnCl_3$ x 4 H_2O	5.1
$FeSO_4$ x 7 H_2O	5
$CoCl_2$ x 6 H_2O	1.6
$CuSO_4$ x 5 H_2O	1.1
$2(NH_4)_6Mo_7O_{24}$ x 4 H_2O	1.1

Table 5.Trace element solution according to Hutner (1944), pH 6.8 (KOH)

2.3 Introduction of the bioreactor and the fermentation conditions

2.3.1 Fermentation conditions

The following parameters were recorded online: temperature, pH, pO_2, pressure, bioreactor weight, H_2 and CO_2. The control of the pH and pO_2 value was carried out with a process control system of Siemens by the use of 1M NaOH and by the adjustment of the flow rate of the input sterile air, respectively. The fermentation parameters are summarized in Table 6.

Fermentation parameters	value
Working volume	10-13 l
Temperature	30 °C
pH	6,5-6.85
stirring	200 rpm
pO_2	<0.05 %
Inocula	6-8 %
Medium	M2SF/M2S2F

Table 6. Fermentation parameters

2.3.2 Bioreactor NLF 22

The fed batch fermentations of the several *R. rubrum* strains were performed in the bioreactor Type NLF 22 (Bioengineering, Wald Switzerland) at 30 °C (Fig.24). The stirred-tank bioreactor is equipped with a double-wall water jacket heater and circulation loop for temperature control. To ensure good mixing, the reactor is equipped with a Rushton-style impeller. The features of the bioreactor are listed in Table 7.

Type	NLF 22
Vessel/tank	stainless steel with double-wall jacket and inspection glass
Working volume	12-14 l
Stirring	three adjustable Rushton-style impellers, drive from the bottom
Aeration	compressed air, pressure reducing station with flow meter, ceramic sterile filter, HPLC gas filter, waste gases with cooling system and sterile filter.
Plugs on the top	Manometer, safety valve, inoculation flask, substrate, waste gas (H_2 (ExTox) and CO_2 (Siemens Ultramat Oxymate) sensors, lamp, sterile filter for extra input gas(N_2 or waste gas dilution)
Plugs on the side	Temperature sensor (PT100), pO_2 electrode (Ingold), pH electrode (Ingold), sampling valve, presence pO_2 sensor (Precision Sensing GmbH)
Plugs on the bottom	Pneumatic draining valve
Sterilisation	In situ
Bioreactor weight	electronic balance (Sartorius)
Feedings weight	electronic balance (Sartorius)
Feeding	Pump(Watson-Marlow)

Table 7. Equipment of the bioreactor NLF22

2.3.3 Bioreactor and medium sterilisation

All the externally connected solutions e.g. fructose were sterile filtered with a Millipore Express PLUS-Membrane vacuum-filtration system, pore size 0.22 µm. For the addition of fructose during the fermentation, a Millidisk10 (pore size 0.22 µm) filter was used for sterile filtration. All plugs, air cartridges and vessels were sterilised by autoclaving. The bioreactor was sterilised by heating at 121 °C for 40 min. At 104 °C the aeration station was connected to the bioreactor. At a temperature of 30 °C the pO_2 sensor (Ingold) was calibrated.

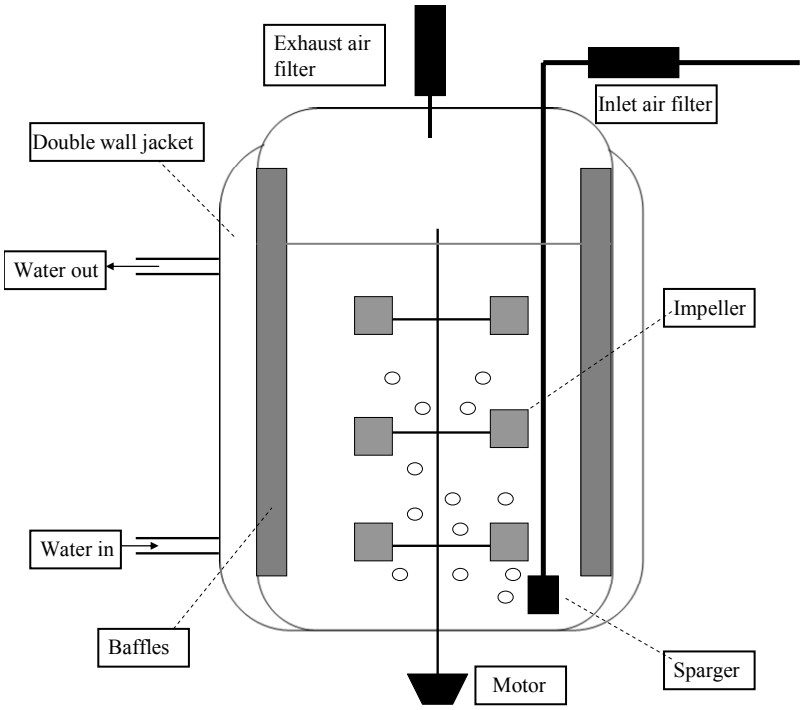

Fig. 24. Bioreactor NLF22

2.3.4 Fermentation in stirred bottles

The stirred bottle fermentations were carried out in closed Pyrex flasks with magnetic stirring. The bottles were filled leaving only a small gas area (1 cm) in order to exclude oxygen. The cells were grown in the dark, in M2SF medium at 30 °C. The amount of inocula was different by each strain due to different growth of the strains. Initially and during sampling, argon was flushed into the bottle. The sampling followed every 3-4 hours.

2.3.5 Sampling and sample preparation

The pO_2 and pH values were measured online, and other parameters, such as optical density, polyhydroxybutyrate (PHB), carotenoids, external acids, and fructose were measured off-line. The sampling was carried out on the side-sampling valve of the bioreactor every 3-4 hours. For routine sampling, the sampling capillary was sterilized with the disinfectant, Meliseptol. The sampling metal capillary was cooled during the sampling with an icy water cooled jacket. An aliquot of the sample was used for optical density measurements at different wavelengths, and for the determination of dry weight. The rest was centrifuged in 12 ml glass centrifugation tubes at 1800xg (Biofuge Stratos) for 10 minutes and the pellets were frozen (-18 °C). 2 ml supernatant was put into Eppendorf tubes was also frozen (-18 °C). The whole procedure of the sample treatment is summarized in Fig. 25.

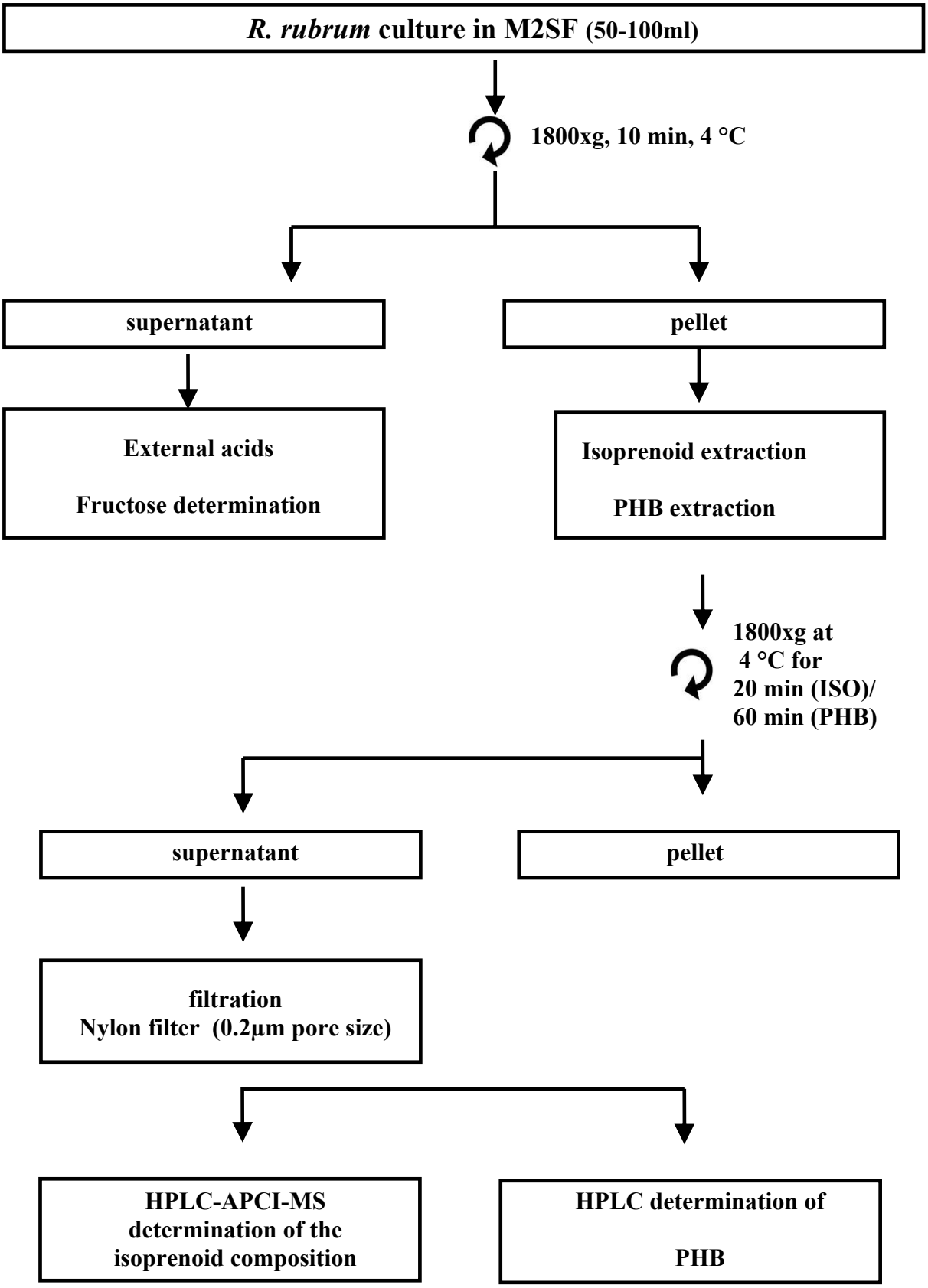

Fig. 25. Sample preparation procedure

2.4 Analytical methods

2.4.1 Growth curve parameters

The parameters of growth curve were measured at the following wavelengths: 511 nm, 660 nm, 750 nm, 880 nm, 882 nm using a Kontron T80 UV/VIS Spectrophotometer. A 1cm path-length cuvette was employed for the measurement. Starting at the value A_{660} = 0.35, the samples had to be diluted.

2.4.2 Dry cell weight measurement

10-40 ml (depending on A_{660}) samples were filtered under vacuum onto pre-weighed and dried cellulose acetate filters (0.45 µm pore size, 47 mm diameter (Sartorius)) and washed twice with 3-5 ml water. The filter with the sample was heated overnight at 110 °C and on the following day they were placed for at least 30 min into a dessicator and then weighed. The dry cell weight value was obtained as the difference between initial and final weight values. Control values were determined with the same filter washed with water as above.

2.4.3 Fructose determination

The D-glucose/D-fructose enzymatic test from Roche Diagnostics/ R-BIOPHARM was used for fructose determination with addition of PGI (1µl/cuvette). During the measurement, fructose was phosphorylated to fructose-6-phosphate (1) then converted to glucose-6 phosphate (2). In the next step glucose-6 phosphate was oxidized to D-gluconate-6-phosphate using the electron acceptor, $NADP^+$. (3) In the assay, the amount of NADPH was measured at the wavelength 365 nm and converted to µmol using the extinction coefficient of 3500 $M^{-1} \cdot cm^{-1}$, which was equal to the fructose concentration. Glucose-6 phosphate isomerase was obtained from Sigma Aldrich.

D-Fructose + ATP $\xrightarrow{\text{Hexokinase}}$ F-6-P + ADP (1)

F-6-P $\xrightarrow{\text{Fructose-6P isomerase}}$ G-6-P (2)

G-6-P + $NADP^+$ $\xrightarrow{\text{G-6P dehydrogenase}}$ D-gluconate-6-phosphate + NADPH + H^+ (3)

2.4.4 **PHB determination** (Laboratory Methods/C. Del Don and H. Brand)

In the first step the PHB was degraded to crotonic acid by the incubation of the pellets with 1 ml 2 N NaOH in a boiling water bath for 30 min. After cooling in iced water, 1 ml 2 N HCl was added and the samples were centrifuged for 1 hour at 1800 rpm. The supernatant was analyzed by HPLC using a Sykam S1121 HPLC. As a stationary phase Inertsil ODS-3 5 µm 4,6 * 250 mm (GL Sciences Inc) column was used with the guard column Partisil ODS-3 5 µm at a flow rate of 1 ml/min (pressure ca 10 MPa). The mobile phase consisted of 50 mM $(NH_4)_2HPO_4$ with 0.8% acetonitrile at pH 2.26 (adjusted with H_3PO_4). The analysis took 45 min and the injection volume was 20 µl. The detection was performed at 210 nm.

2.4.5 Ion chromatographic determination of organic acids

The ion chromatographic method was adapted from Ritter *et al.* (2006) and was optimized for the following organic acids: lactate, formate, acetate, propionate, pyruvate, succinate, malate, and fumarate. The ion chromatographic determination of organic acids was carried out on an ICS-3000 (Thermo Fisher Scientific Inc., Sunnyvale, USA) instrument with conductivity detection (ICS-3000 Conductivity Detector, Thermo Fisher Scientific Inc, Sunnyvale, USA). The suppressor (2-mm ASRS, Thermo Fisher Scientific Inc., Sunnyvale, USA) showed 63 mA. The stationary phase consisted of coupled IonPac AS11 analytical columns (Thermo Fisher Scientific Inc., Sunnyvale, USA) with an IonPac AS11 guard column (Thermo Fisher Scientific Inc., Sunnyvale, USA). The run time was 60 min and the injection volume was 20 µl. The flow rate was 0.25 ml/min. The applied KOH gradient was the following:

Time (min)	KOH concentration (mM)	Curve
-15	1	5
8	1	5
28	30	5
38	60	5
40	100	5
45	60	5

2.4.6 Isoprenoid extraction

Several extraction methods were tested and compared with the self-developed extraction for rapid sampling. The procedures of the different extractions can be seen in Fig. 26

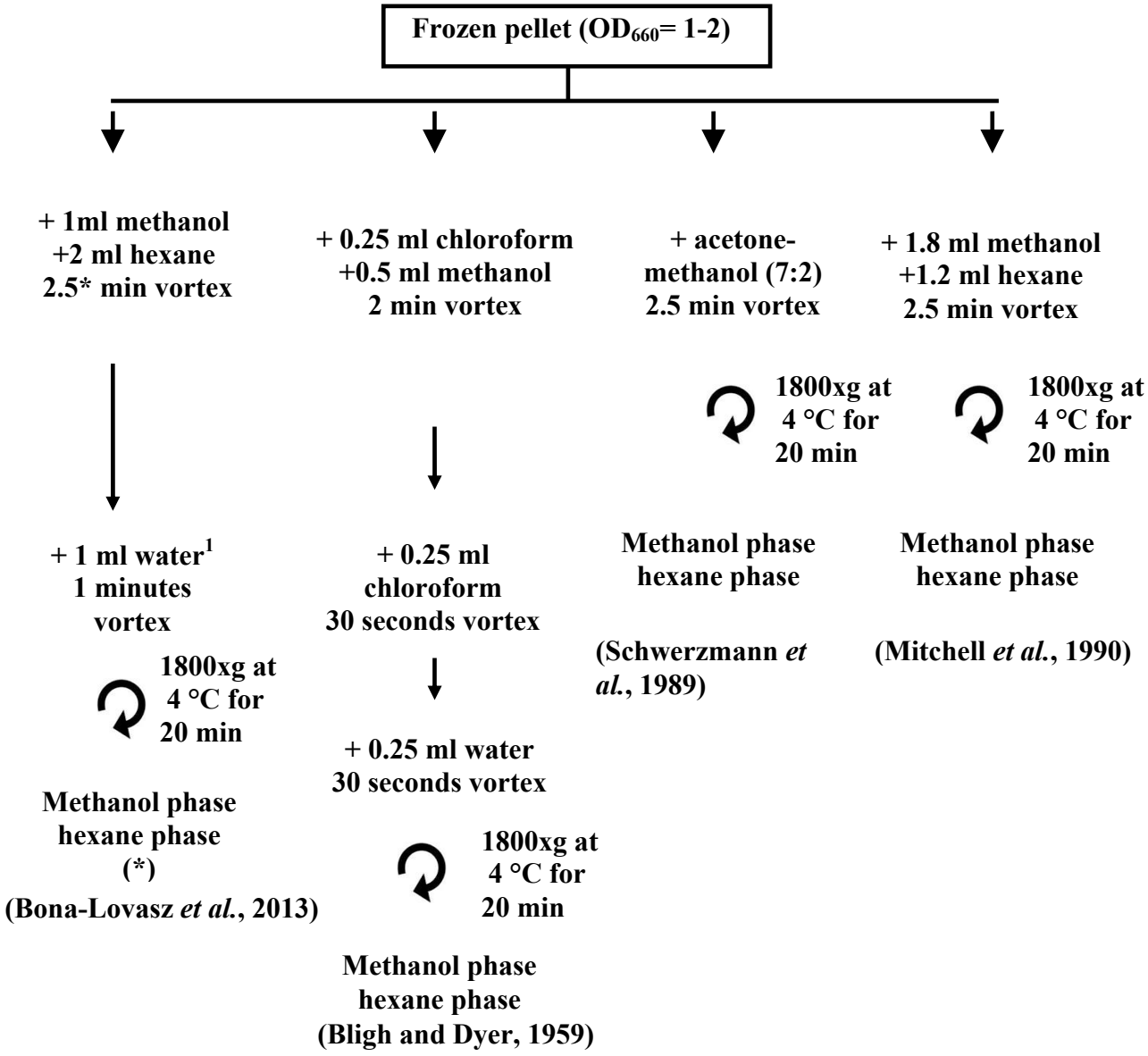

Fig. 26. Applied methods for extraction of hydrophobic membrane compounds from *R. rubrum* cells. All centrifugation steps were carried out at 4 °C, 1800g for 10 min.
* The extracts were directly measured by HPLC-MS method. The samples cannot be frozen, because BChl*a* precipitates at low temperature.

2.4.7 HPLC-APCI-MS analysis of the isoprenoid components

HPLC analyses were performed on a ThermoFisher (Dionex) Ultimate 3000 (Dionex Corp., Sunnyvale, CA, USA) separation module equipped with a Dionex Ultimate (Dionex Corp.,

Sunnyvale, CA, USA) column oven, and VWD-3000 UV-VIS (Dionex Corp., Sunnyvale, CA, USA) detector controlled by a UCI-1500 Universal chromatography interface (Dionex Corp., Sunnyvale, CA, USA). The analytical scale Spherisorb C18 reversed-phase column (VDS Optilab, 250mm x 4.6 mm i.d., 5 µm particle size) used was operated at 25 °C. The mobile phase consisted of acetone/water (50:50 (v/v)) as a starting composition using a flow rate of 1 ml/min. A non-linear gradient used, which was set using the software Chromeleon™ 6.8, is shown in Fig. 27. The total run time was 45 min and the injection volume was 20 µl. UV-VIS detection was performed at 475 nm.

The HPLC system was coupled on-line to a ThermoFisher (Dionex) (Sunnyvale, CA, USA) model MSQ™ single quadrupole mass spectrometer fitted with an APCI ion source. MS control was performed using Excalibur software. The instrument was operating in positive ion mode at a fragmentor voltage of 75V. The mass spectra of the column eluates were recorded in the range of *m/z* = 250-1000 with a dwell time of 0.3 s. Nitrogen was used as the nebulising gas at a pressure of 100 psi. The vaporizer temperature was set at 450 °C. Corona current was set at 7.5 µA. All data were acquired in centroid mode and processed using Chromeleon™ 6.8 software.

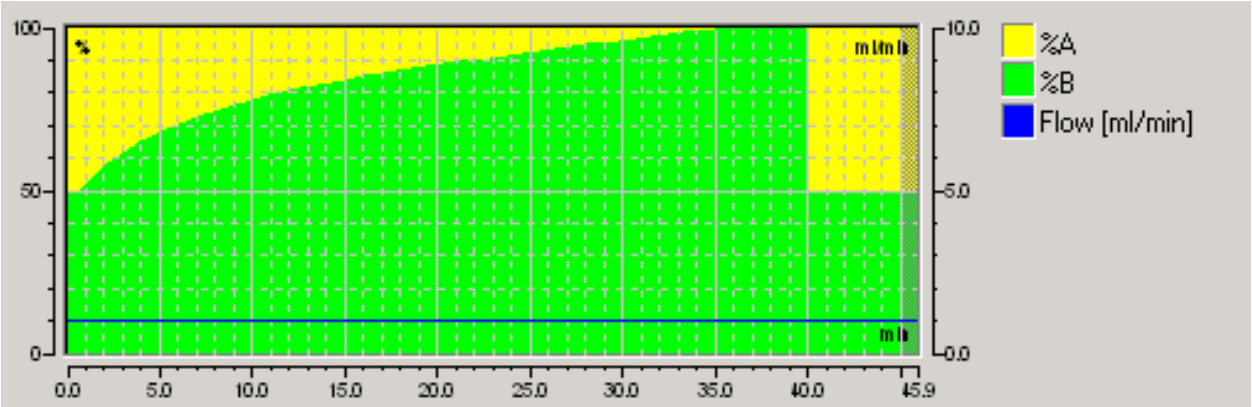

Fig. 27. Nonlinear acetone (B)-water (A) gradient applied in HPLC analysis

2.5 Preliminary considerations

2.5.1 The absorption spectrum of *R. rubrum*

The absorption spectrum of *R. rubrum* can be seen in Fig. 28. At the wavelength of 660 nm, the pigment absorption does not contribute to the spectrum. Therefore, this wavelength can be used for the measurement of the cell density. BChl*a* built in the LH1 complex absorbs at the wavelength 880 nm. Since LH1 occurs only in the intracellular membrane, the ICM content is proportional to the A_{880} value. (The protein and phospholipid level in the cell is constant

during the whole cell growth.) With the use of the normalized value (A_{880}/A_{660}) the ICM level of the cells can be described.

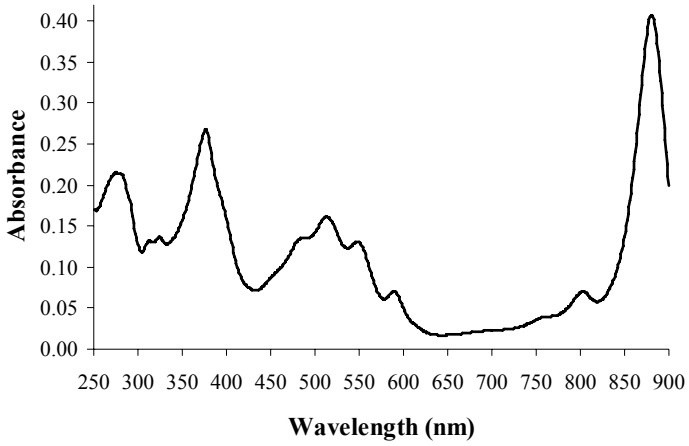

Fig. 28. Absorption spectrum of *R. rubrum* cells

2.5.2 Introduction of the detector MSQ Plus

The mass spectrometric detection measures the mass charge ratio (*m/z*). The separation of the matrix components is carried out on the chromatographic module (LC). Then, the eluent leaves the LC area and flows into the ion source, which is the first important unit of the mass spectrometer. In the case of atmospheric-pressure chemical ionization (APCI) the ion source consists of a capillary which is flushed with nitrogen and a corona discharged electrode (corona pin). Due to the heat and the nebulising gas flow, the eluent form an aerosol, this evaporates rapidly, resulting in desolvated neutral molecules. The neutral molecules become ions by passing by the corona pin held at a high potential (5 kV) The APCI ion source and the mechanism of the ionization can be seen in Fig. 29.

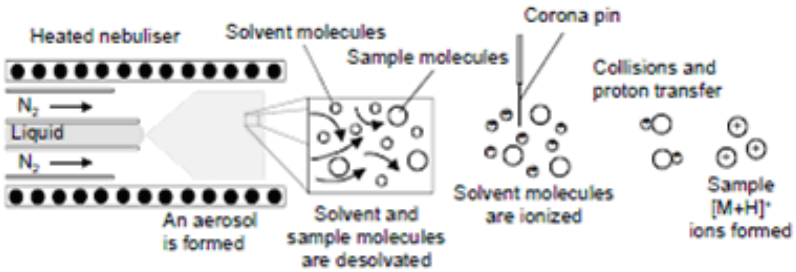

Fig. 29. Ionization in the APCI ion source (ThermoFisher Corp. MSQ Manual)

These ions enter through the entrance cone into the Collision Induced Dissociation (CID) region due to the great vacuum and the opposite charge. Due to the "Z" form of the channel between the entrance and exit cones (Fig. 30) the ionized molecules collide with the

nebulising gas molecules and with each other and this kinetic energy of the collision is sufficient to cause bond breakage, resulting fragmentation of the molecular ions.

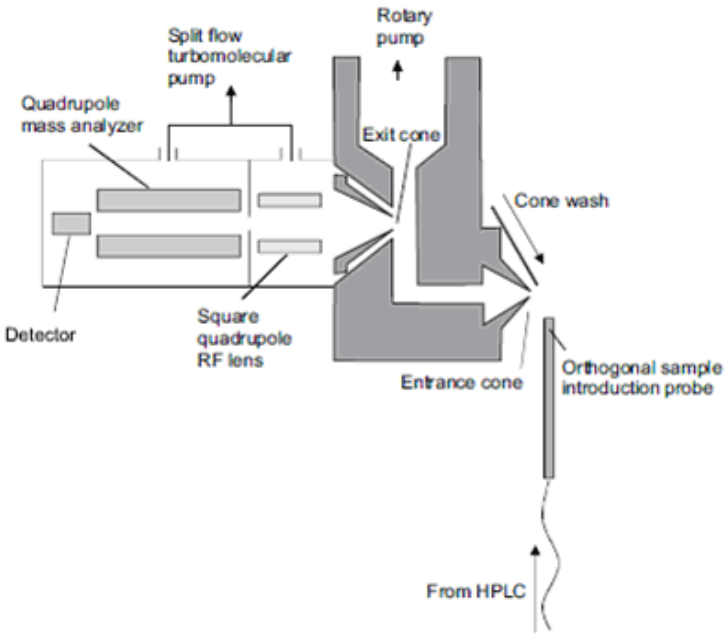

Fig. 30. Assembly of the MSQPlus mass spectrometer (ThermoFisher Corp. MSQ Manual)

After the CID region, the ions flow through the second cone (exit cone) and enter into the analyzer, in this case a single quadrupole mass analyzer. The square quadrupole RF lens (Fig. 30) help in focusing the ions before they enter the quadrupole analyzer. The quadrupole detector consists of four parallel metal rods and uses an alternating electric field to separate ions. The voltage applied to each rod is the summation of a constant DC voltage and a varying radio frequency.

The opposite rods have the same potentials: one pair is positive the other pair is negative. The applied potential can be described as the sum of the DC voltage (U_{DC}) and the AC voltage ($V\cos(\omega t)$): $U_r = +U_{DC}+V\cos(\omega t)$

The actual voltage affects the flight path of the ions. Due to the oscillating electromagnetic force, the ions either fly out of the area to the wall or to flow toward to the rods. A unique radio frequency for each ion (*m/z*) exists, where only this ion can oscillate through the 4 rods reaching the detector.

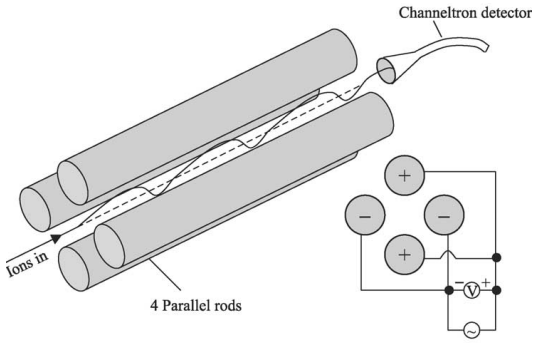

Fig. 31. Linear quadrupole analyzer (Baldwin, 2005)

The detector is a Channeltron electron multiplier, which is the "eye" of the mass spectrometer. The detector uses the principle of secondary electron emission. When a charged or neutral particle hits a surface it releases electrons associated with the outer layers of atoms. Due to the applied voltage the electrons are accelerated and collide with the opposite wall of the channel setting more. The efficiency of this process depends on the type of primer particle, its energy and the geometrics of the surface.

The output of the mass spectrometric detection is the mass spectrum. The signal is distinct and looks like a narrow spike. The *m/z* ratio is on the X axis and the ion counts (intensity) on the Y axis. The ion with the highest intensity (base peak) is assigned an abundance of 100. The time integral of these spike signals is a Gaussian peak, whose area is proportional to the concentration of the molecule.

3 A rapid method for the extraction and analysis of isoprenoids

The primary motivation for introducing a new carotenoid extraction and analysis procedure is the interest in monitoring the dynamics of terpenoid metabolism for subjection to system biology analysis. Therefore, a reliable, widely applicable and inexpensive HPLC-VIS-APCI-MS method has been developed for the characterization and quantification of the several PM compounds. This analytical method will be introduced in this chapter.

3.1 Overview of existing lipid analysis methods

In order to investigate the biosynthesis of the PM, it is necessary to measure the major lipid fractions (fatty acids, phospholipids), as well as carotenoids, isoprenoid-quinones and BChl*a* simultaneously during fermentation. Lipidomics is a broad autonomic discipline, which involves the analysis of cellular lipids in biological systems such as triglycerides, phospholipids (PLs) and carotenoids. There are several methods, which are capable of determining one type of substance (fatty acids, PLs, carotenoids, BChls and isoprenoid-quinones) accurately, but provide no information about the others. For metabolic studies, in particular ones employed in system biological approaches; there is a need for a method, in which all these compounds can be measured simultaneously.

Several HPLC separations of carotenoids have been reported in the literature using a wide variety of mobile phases, typically consisting of complex binary or ternary solvent mixtures of methyl tert-butyl ether, acetone, acetonitrile, methanol, ethyl acetate, hexane, tetrahydrofuran (Mercadante *et al.*, 1997; Careri *et al.*, 1999; Weber *et al.*, 2007; Stöggl *et al.*, 2007; Inbaraj *et al.*, 2008; Kurz *et al.*, 2008; Mizoguchi *et al.*, 2008; Breithaupt, 2004). Carotenoid analysis is sometimes difficult with soft ionization techniques such as fast atom bombardment (FAB) or electrospray (ESI); therefore, atmospheric pressure chemical ionization (APCI) has become the most widely used ionization technique for carotenoids, and shows high sensitivity for their analysis. (R.B. van Breemen *et al.*, 1996) There are also several methods for chromatographic separation and for mass spectrometric detection of PLs. The common ion source is ESI, but also APCI is available. These ion sources combined with MS/MS provide structural information for the intact molecule as well as the possibility of obtaining molecule-related fragment ions by in-source fragmentation or by collision-induced dissociation (CID). (Tolonen *et al.*, 2005; Sommer *et al.*, 2005; Karlsson *et al.*, 1996) Many analytical methods have been reported for the analysis of isoprenoid-quinones. The detection

of isoprenoid-quinones is usually based on HPLC analysis with UV, electrochemical (ED) or MS detection, of which MS is the most superb regarding its sensitivity and selectivity particularly with the use of tandem mass spectrometry (Mahendra *et al.*, 2011; Mitchell *et al.*,.1990; Lang *et al.*, 1986; Ruiz-Jimenez *et al.*, 2007; Lytle *et al.*, 2001).

Airs *et al.* (2001; 2002; 2003) have contributed significantly to the development for HPLC based BChl*a* analysis, in particular developing chromatographic separation and recording characteristic fragmentation patterns.

All these methods mentioned above are accurate, but we need a simple, cheap, and one with a wide range polarity method, which gives all the qualitative and quantitative information of all PM non-polar molecules in one run.

Recently, general methods for the extraction of carotenoids and quinones which are also compatible with HPLC-MS analysis have been presented (Kaiser *et al.*, 2007; Kaiser *et al.*, 2012). These methods have been shown to be highly efficient and can be used for the extraction of terpenoids form a wide variety of cellular sources. Unfortunately, these latter methods have significant disadvantages for some applications. In particular, they require a many steps of extraction, including a cell breakage step, which becomes prohibitive for the large number of samples which are often required in systems biology studies of metabolism.

For this reason, a very simple one-step procedure has been developed, which is capable of extracting terpenoids as well as most other hydrophobic cellular substances present in bacteria efficiently, using a ternary solvent system (hexane/methanol/water) compatible with modern HPLC-MS analytical procedures. This method is closely related to the hexane-isopropanol (Hara and Radin, 1978; Kolarovic and Fournier, 1986; Guckert and White, 1988;) and hexane-ethanol (Takada *et al.* 1982; Cabrini *et al.* 1992) solvent systems, which are effective extraction methods without halogen-containing solutes, but is more efficient for the extraction of the special combination of hydrophobic compounds (in particular pigments) present in photosynthetic bacteria.

3.2 Development of a method for the extraction and analysis of carotenoids and other hydrophobic substances

The ideal mobile phase has the following properties: a wide polarity spectrum, ionizable, cheap, harmless and easy to prepare. An acetone-water mixture meets all of the requirements described above. Furthermore, acetone has its UV cut-off far from the absorption maxima of the carotenoids. The use of hexane led to a very poor separation and to a very low ionization

of the compounds in the MS detector, also by the addition of tetrahydrofuran or methanol. Methyl tert-butyl ether and acetonitrile were excluded based on environmental considerations. The optimization of the gradient was done first and foremost for the carotenoids and BChls.

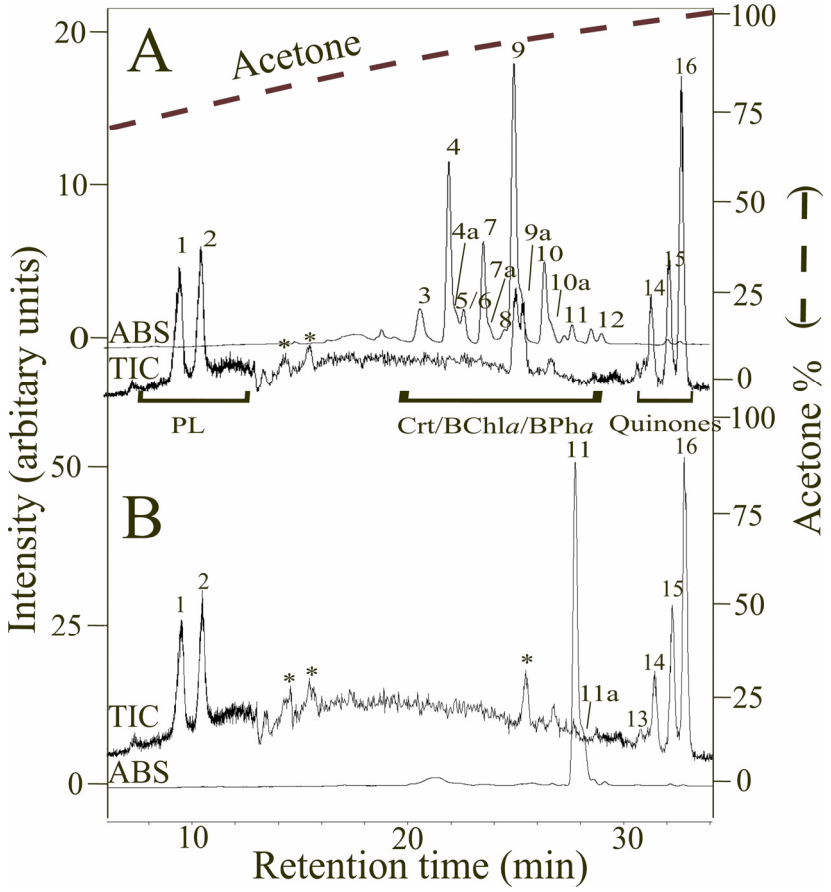

Fig. 32. HPLC profile of carotenoid mutants: ST4 (A) and SLYC18 (B)

Typical HPLC-MS chromatograms of *R. rubrum* mutant strains: (A) the crtD$^-$ strain ST4; and (B) the (crtCD)$^-$ strain SLYC18. The chromatogram shows three separation regions, corresponding to phospholipids (PLs), photosynthetic pigments (BChla, BPha, crt), and quinones, respectively. Peak identifications (1) PPoPG and PoOPG; (2) POPG and DOPG; (3) 1-methoxy-1´-OH-3,4-didehydrolycopene; (4) trans-3,4-dihydrorhodovibrin; (4a) cis-3,4-dihydrorhodovibrin; (5) 1-OH-3,4-didehydrolycopene; (6) 1´-OH-3,4-dihydrospheroidene; (7) trans-rhodopin; (7a) cis-rhodopin; (8) 1´-OH-neurosporene (chloroxanthin); (9) trans-tetrahydrospirilloxanthin (thspx); (9a) cis-thspx; (10) trans-3,4-dihydroanhydrorhodvibrin; (10a) cis-3,4-dihydroanhydrorhodovibrin; (11) trans-lycopene; (11a) cis-lycopene; (12) neurosporene; (13) RQ-9; (14) UQ-9; (15) RQ-10; (16) UQ-10. The absorption at 475 nm (ABS) and total ion counts (TIC) channels between *m/z* 350-1000 are indicated. The CID fragmentation patterns of PL peaks (1) and (2) at 75 fragmentor voltage are shown in (C) and (D), respectively. Base peaks are the DAG_{MS} fragments (549.4/575.4). A fatty acid fragment

with its glycerol backbone is also observable in the extended MS profile with lower intensities. $[M+74]^+$: 339 = oleic acid, 311 = palmiteolic acid (data not shown). Peaks marked by asterisks are due to three minor contaminants present in the elution solvent. For the SLYC18 profile, the third minor contaminant coelutes with lycopene.

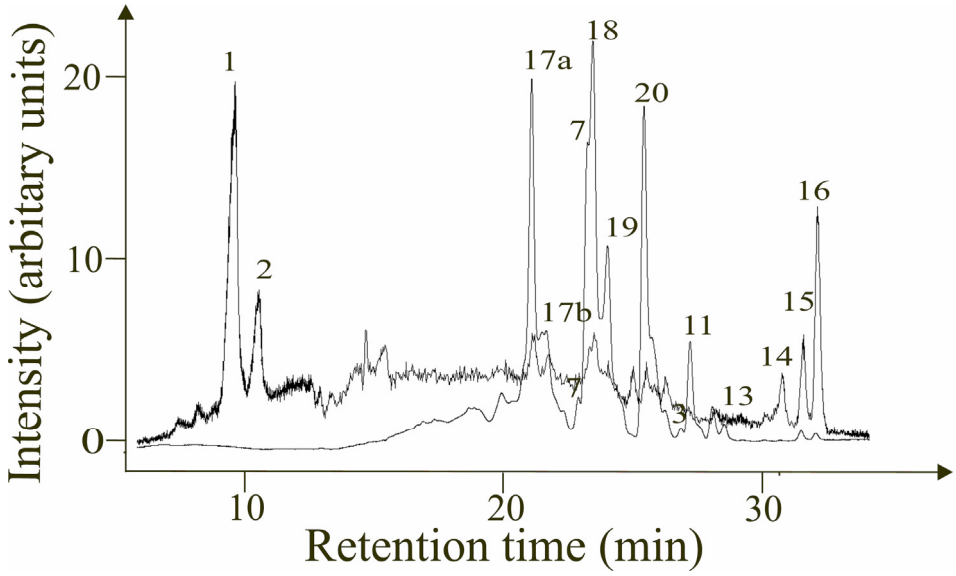

Fig. 33. Typical HPLC-MS chromatograms of *R. rubrum* wild-type: (1) PPoPG and PoOPG; (2) POPG and DOPG; (7) *trans*-rhodopin; (11) *trans*-lycopene; (13) RQ-9; (14) UQ-9; (15) RQ-10; (16) UQ-10; (17a) *trans*-rhodovibrin; (17b) *cis*-rhodovibrin; (18) spx; (19) 3,4-dihydrospx (dhspx); (20) andhydrorhodovibrin

Due to the optimization of the non-linear gradient, an efficient separation has been achieved which has only two coelutions among 18 investigated carotenoids. In the carotenoid region the gradient was adjusted to be flatter, since carotenoids have a wide range of components and are difficult to separate.

In order to identify compound-specific mass spectrometer parameters, the ionization of the compounds was optimized. Carotenoids give an appropriate signal only over 60 V, but the best signal at 75 V. UQ-10 and PLs are easier to ionize and provide a sensitive response at 75 V. This voltage is not enough for the fragmentation of carotenoids or isoprenoid-quinones, but cleaves the PL molecules. The same phenomenon is described by Karlsson *et al.*, 1996. The fragmentation of phosphatidylglycerols results in diacylglycerides, which are the characteristic fragment ions for PLs with CID. The optimized mass spectrometric parameters are described in the Material and Methods section.

3.3 Optimization of the PM compound extraction

Since the final goal was to develop a method for the manual extraction of hydrophobic compounds from a large numbers of samples, we avoided halogen-containing solvents which - though efficient - are usually toxic and not environmentally friendly. Our initial extraction trials with the commonly used solvents such as acetone, methanol or hexane alone proved unsatisfactory. Acetone-methanol and hexane-ethanol mixtures showed low efficiencies of extraction for many hydrophobic but non-terpenoid molecules of interest (e.g. carotenoids). Hexane, which is a good solvent for terpenoids, was inefficient for the co-extraction of PLs, as well as BChl*a* and BPh*a*. After various trials, we discovered that the ternary solvent MeOH/hexane/H_2O was extremely efficient for one-step extraction of carotenoids and quinones as well as other hydrophobic substances of interest in phototrophic bacteria e.g. BChl*a*, BPh*a* as well as the major PLs. This method is closely related to hexane-isopropanol (Hara and Radin, 1978; Guckert and White, 1988; Koralovic and Fournier, 1986) and hexane-ethanol (Takada *et al.*; 1982; Cabrini *et al.*, 1992) solvent systems, which are effective extraction methods without halogen containing solutes. We modified the extraction method to obtain a more rapid and reproducible analysis method for the downstream analysis of *R. rubrum* fermentations. The one-step methanol-water-hexane extraction enables the rapid sampling of the bioreactor in order to record the dynamics of the carotenoid production. The following extraction parameters were optimized: extracting water amount, the pellet size and the effect of lyophilisation, which is a recommended sample preparation method (Fig. 34).

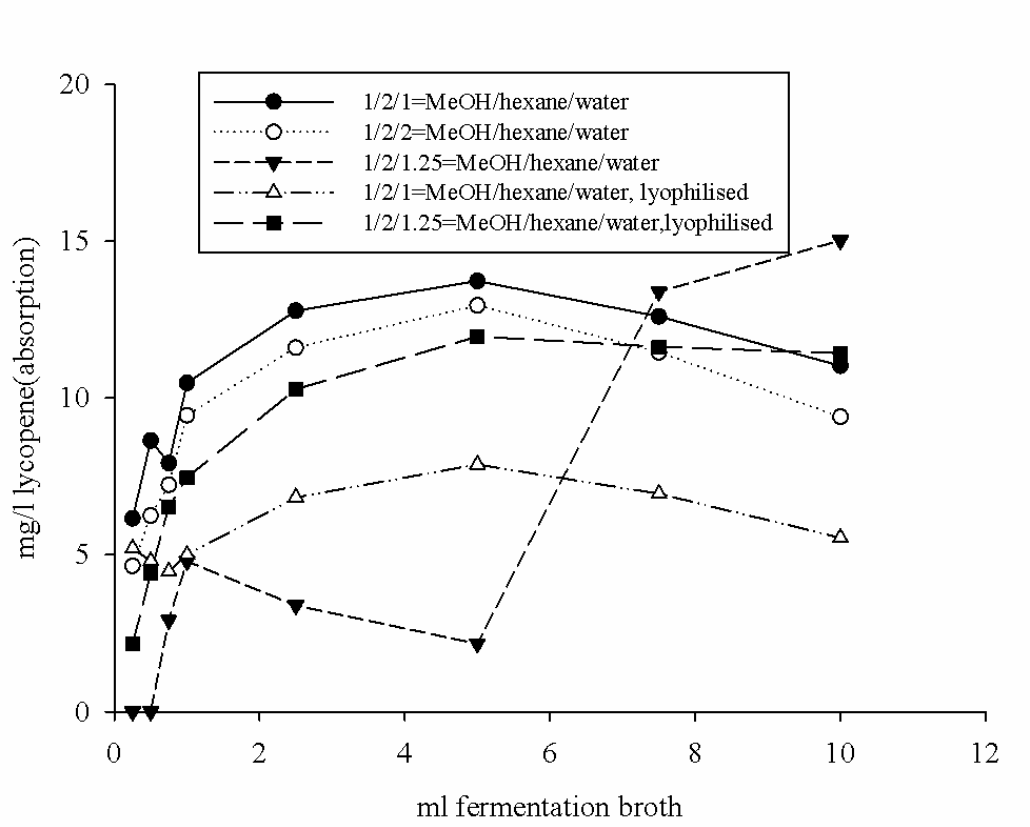

Fig. 34. Optimization of the extraction parameters

The extraction did not become more effective through the lyophilisation step but the varying water amount causes large differences in the yield of the extraction. The optimal pellet size can be defined which is centrifuged from 5 ml fermentation broth at the cell density of A_{660}=10.

The one-step hexane-methanol-water extraction method was compared to three other PM compound extraction methods found in the literature (Bligh and Dyer, 1959; Mitchell *et al.*, 1990; Schwerzmann *et al.*, 1989.) We found, that our yield for carotenoids is close to the yield of the Bligh method which is a standard method for lipid extraction applying halogenated solvent. The reproducibility of our method was as high as that of the Bligh and Dyer (1959) method, but we do not apply halogenated solvents, which makes our method more suitable for industrial applications. (Fig. 35) The Bligh and Dyer method was more successful for extracting BChl*a* and PL but weaker for isoprenoid-quinones extraction. Our extraction can be easily optimized for PL and BChl*a* extraction by omitting the water addition. The methanol phase contains the whole BChl*a* fraction, but leads to a significant loss of carotenoids, since a part of carotenoids occur in the methanol phase if water is not present.

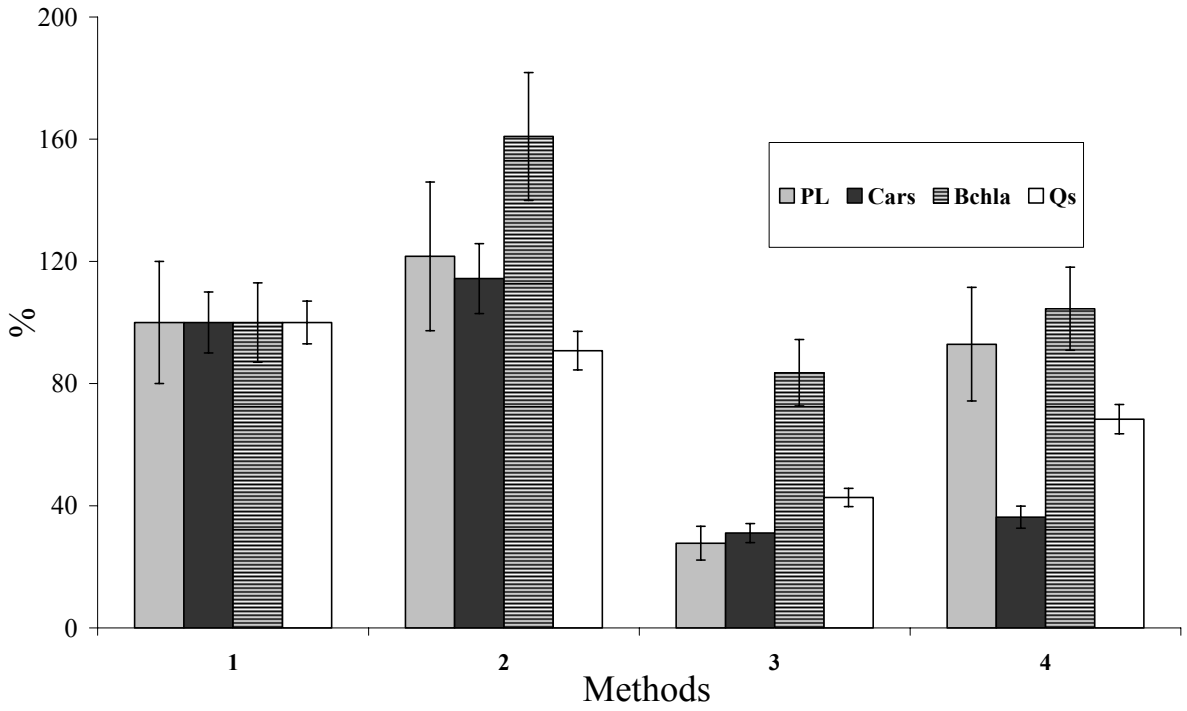

Fig. 35. Relative yield comparison of the extraction methods **1** = Bona-Lovasz *et al.* (2013) (100%, reference); **2**= Bligh and Dyer (1959); **3**=Mitchell *et al.* (1990); **4**= Schwerzmann *et al.* (1989)

3.4 Characterization of the PM compounds in R. rubrum

The characterization of PLs was carried out with the help of phosphatidylglycerol (PG) fragmentation patterns determined by Karlsson *et al.* (1996) and using the membrane composition of *R. rubrum* found in the literature (Snozzi and Bachofen, 1979; Schröder and Drews, 1968; Wood *et al.*, 1965; Hirayama, 1968; Russell and Harwood, 1979; Oelze *et al.*, 1975; Collins and Niedermann, 1976). The PL molecular ions ($[M+H]^+$) were present in the chromatogram with a low intensity. The molecular ion zone is the *m/z* interval of 700-800 in the mass spectrum. Due to the CID zone fragmentation voltage the $[M+H]^+$ ions were fragmented into three fragment categories.

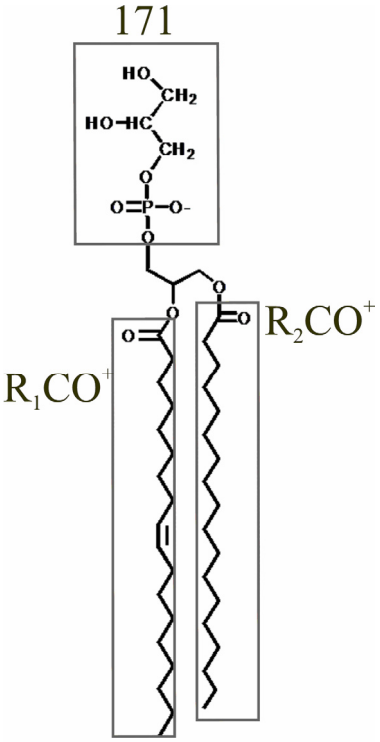

Fig. 36. The structure of POPG and the fragmentation spots

- **Fragment 1** $[M+H-172]^+$: The fragmentation of PGs in positive mode led to a $[M+H-172]^+$ ion as base peak obtained from the neutral loss of the PG head group (Fig. 37), resulting in a detection of diglycerides (DAGs) as diglycerol-like (DAG_{MS}) fragments. (Karlsson *et al.*,1996). The fragment structure can be seen in Fig. 36.

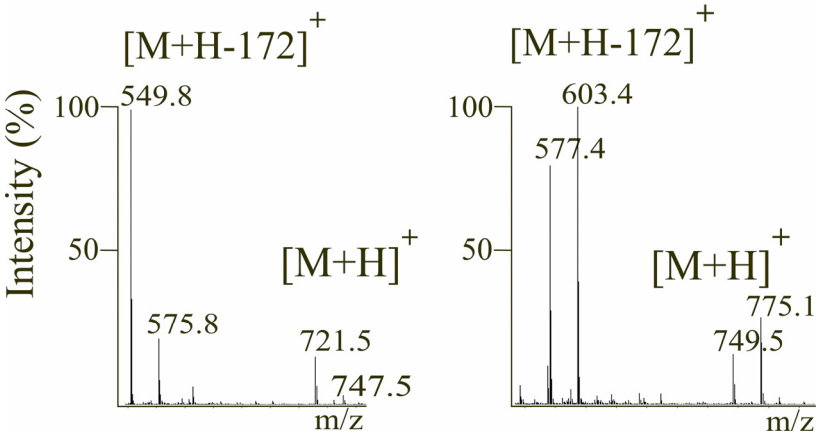

Fig. 37. Diglyceride fragmentation and molecular ion region $[M+H]^+$ of PG in positive mode

- **Fragment 2** $[RCO]^+$: are the free fatty acid (FA) fragments. This fragment could be detected only in traces.
- **Fragment 3** $[RCOO+58]^+$: are the FA fragments with glycerine backbone. The fatty acids could be detected via these fragments at low intensity. Although the characterization of PGs is carried out based on the DG fragments, the affirmation for the FA composition was carried out with these fragments. Fatty acid related fragment

region occurs in the *m/z* = 250-370 interval. The fragments of different FAs are listed in
Table 8. In the case of C16:1 and C18:1 equals *m/z* = 311.3 and *m/z* = 339.3, respectively (Fig. 38).

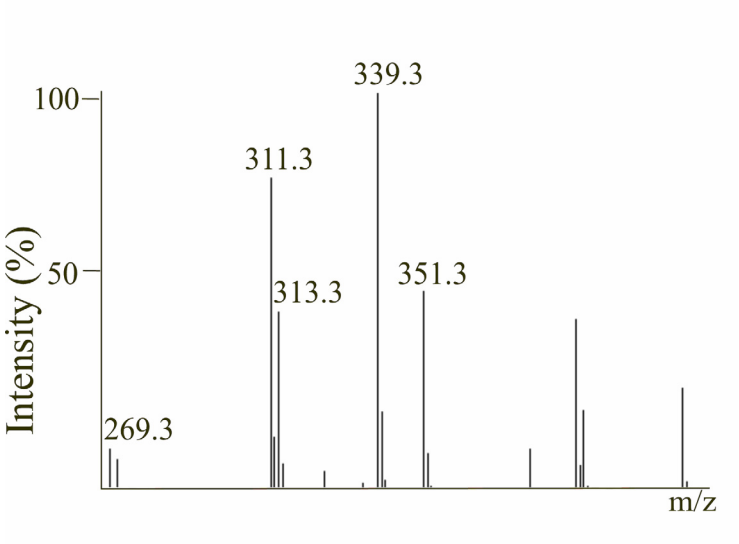

Fig. 38. Free fatty acids associated with acetone $[M+57]^+$

Fatty acids	Exact mass	$[RCOO+58]^+$
C13:1	212.5	269.5
C14:0	228.5	285.5
C14:1	226.5	283.5
C15:0	242.5	299.5
C16:0	256.5	313.5
C16:1	254.5	311.5
C17:1	268.5	325.5
C18:0	284.5	341.5
C18:1	282.5	339.5
C19:0	298.5	355.5
C19:1	296.5	353.5
C20:0	312.5	369.5

Table 8. Fatty acids attached to the glyceride backbone

The PGs occur in TIC chromatogram of the cell extracts at about the 9 min in these peaks and in the region PEs could be detected with very low intensity. The PEs are eluted from the stationary phase in a sharp peak but are dissolved slowly, creating a rather broad peak (15 min) (Fig. 39). The fragmentation of PEs follows the pattern described by Karlsson *et al.*, 1996 and can be determined as diglycerol-like fragments losing the ethanolamine and phosphate group.

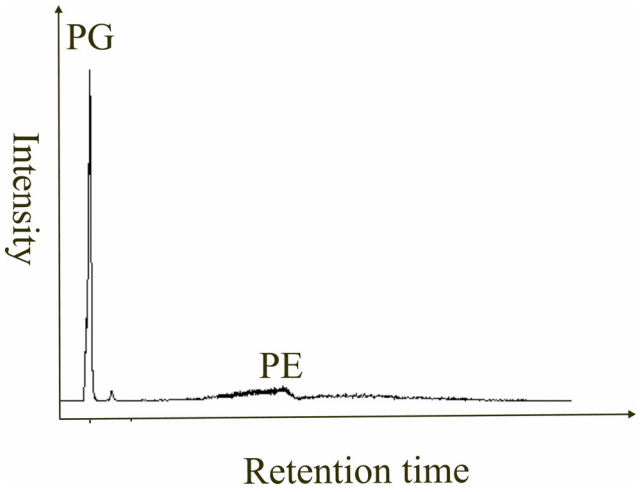

Fig. 39. HPLC profile of PG and PE by extraction of the DAG_{MS} 575.5 *m/z*. The sample obtained from wild-type and was extracted according to Bligh and Dyer (1959).

Carotenoids and isoprenoid-quinones are not fragmented at the fragmentor voltage of 75 V, instead they form the molecular ion by accepting a proton. (Fig. 40 and Fig. 41)

All major terpenoid quinones, such as RQ-9, RQ-10, UQ-9, UQ-10 and UQH_2-10 have been found at the end of the chromatogram (t_{ret}= 30-33.5 min). Although ubiquinol-10 co-eluates with RQ-9, the molecular ions are different, therefore quantitative analysis is feasible. The characteristic 197 fragment of UQ-10 was measured, but the intensity of the molecular ions is higher, therefore the molecular ion was used for quantification.

The molecular ion $[M+H]^+$ of BChl*a* (904.4) occurs with very low intensity in the sample, because BChl*a* loses its magnesium ion at a fragmentor voltage of 75 V and can be detected as protonated geranylgeranyl-BPh *(m/z = 883.5),* but still at very low intensity. We also found the fragment ion *m/z* = 889.4, that corresponds to the mass of protonated BPh*a*. Geranylgeranyl-BPh*a* has been also detected at low intensity with the base beak 883.5 (Fig. 42). The identified PM compounds in *R. rubrum* are summarized in Table 9.

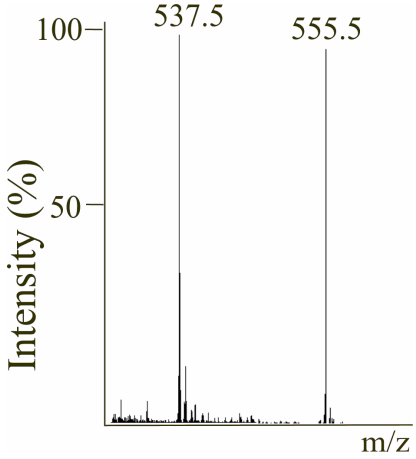

Fig. 40. Lycopene (537.5) and rhodopin (555.5) signal in mass spectrometer

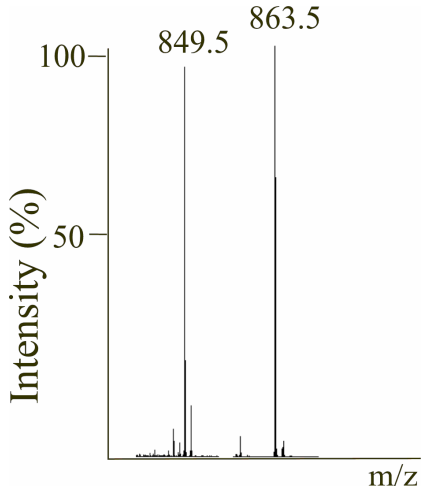

Fig. 41. RQ-10 (948.5) and UQ-10 (862.5) molecular ions $[M+H]^+$ in positive ion mode

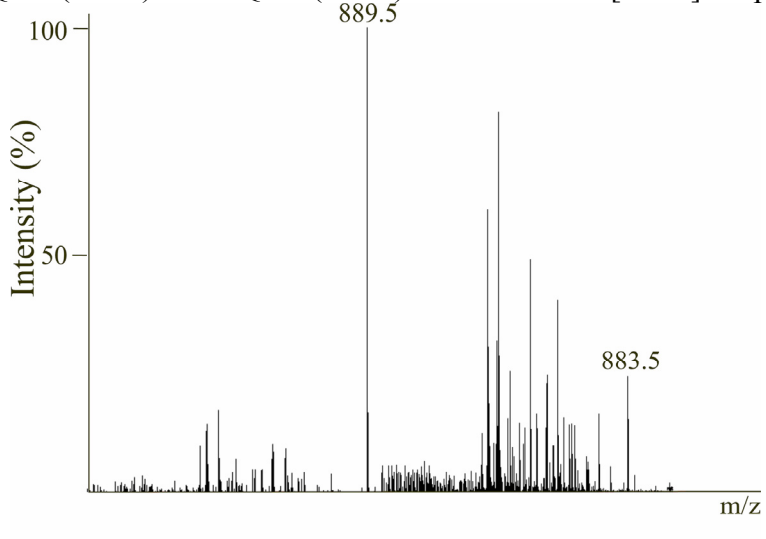

Fig. 42. BChl*a* and BPh*a* molecular ion in positive mode

	Compound	Retention time (min)	Exact Mass (g)	Molecular ion	Molec. ion/ fragment[a]
Phospholipids	Palmitoyl-palmitoleyl-PG(C16:0/C16:1)(PPoPG)	9.14	720.5	$[M+H-172]^+$	549.4
	Palmitoleyl-oleoyl-PG (C16:1/C18:1) (PoOPG)	9.14	746.5	$[M+H-172]^+$	575.4
	Palmitoyl-oleoyl-PG (C16:0/C18:1) (POPG)	9.95	748.5	$[M+H-172]^+$	577.4
	Pentadecicloyl-oleoyl-PG(C15:0/C18:1)	9.95	734.5	$[M+H-172]^+$	563.4
	Myristoyl-palmitoyl-PG (C14:0/C16:0)	9.95	694.5	$[M+H-172]^+$	523.4
	Margaroleyl-oleoyl-PG(C17:1/C18:1)	9.95	760.5	$[M+H-172]^+$	589.4
	Oleoyl-nondecycoleyl-PG (C18:1/C19:1)	9.95	788.5	$[M+H-172]^+$	617.4
	Tridecyloyl-oleoyl-PG(C13:0/C18:1)	9.95	706.5	$[M+H-172]^+$	535.4
	Distearoyl-PG (C18:0/C18:0)	9.95	778.5	$[M+H-172]^+$	607.4
	Stearoyl-nondecycloyl-PG (C18:0/C19:0)	9.95	792.5	$[M+H-172]^+$	621.4
	Dioleoyl-PG (C18:1/C18:1) (DOPG)	9.95	774.5	$[M+H-172]^+$	603.4
Carotenoids/BChla/ BPha	BChl*a* (geranylgeranyl)	19.06	904.5	$[M+H]^+$	905.5
	Rhodovibrin	21.43	584.5	$[M+H]^+$	585.5
	1,1´-Dihydroxy-3,4-didehydrolycopene	21.43	570.5	$[M+H]^+$	571.5
	1´-Hydroxyspirilloxanthin	20.85	582.5	$[M+H]^+$	583.5
	1-Methoxy-1´-OH-3,4-didehydrolycopene	20.67	584.5	$[M+H]^+$	585.5
	3,4-Dihydrorhodovibrin	22.07	586.5	$[M+H]^+$	587.5
	1-Hydroxy-3,4-didehydrolycopene	22.24	552.5	$[M+H]^+$	553.5
	3,4-Didehydrorhodopin	22.07	552.5	$[M+H]^+$	553.4
	Chloroxanthin (1-OH-neurosporene))	24.61	556.5	$[M+H]^+$	557.5
	BPha (geranylgeranyl)	23.60	882.5	$[M+H]^+$	883.5
	Rhodopin	23.63	554.4	$[M+H]^+$	555.4
	Spirilloxanthin	23.87	596.4	$[M+H]^+$	597.4
	3,4-Dihydrospirilloxanthin	24.46	598.5	$[M+H]^+$	599.5
	3,4,3´,4´-Tetrahydrospirilloxanthin	25.05	601.4	$[M+H]^+$	602.4
	BPh*a* (phytyl)	26.75	888.5	$[M+H]^+$	889.5
	1´-Hydroxy-3,4-dihydrospheroidene	22.72	588.5	$[M+H]^+$	589.5
	Anhydrorhodovibrin	25.91	566.5	$[M+H]^+$	567.5
	3,4-Dihydroanhydrorhodovibrin	26.74	568.5	$[M+H]^+$	569.5
	Phytoene	31.25	544.5	$[M+H]^+$	545.5
	Lycopene	27.75	536.5	$[M+H]^+$	537.5
	Neurosporene	29.11	538.5	$[M+H]^+$	539.5
Quinones	Rhodoquinone-9 (RQ-9)	30.77	779.6	$[M+H]^+$	780.6
	Ubiquinol-10 (UQH_2-10)	31.08	864.7	$[M+H]^+$	865.7
	Ubiquinone-9 (UQ-9)	31.43	794.6	$[M+H]^+$	795.6
	Rhodoquinone-10 (RQ-10)	32.24	847.7	$[M+H]^+$	848.7
	Ubiquinone-10 (UQ-10)	32.81	862.7	$[M+H]^+$	863.7

Table 9. List of identified compounds in *R. rubrum.*

[a] the molecular ion fragments arising from the PGs corresponds to the calculated mass of the diglyceride-like (DAG_{MS}) species (Karlsson *et al*.,1996). Species shown in italics were only detected in trace amounts.

3.4.1 The application of the HPLC-MS method for apo-carotenoid characterization

The cleavage products of canthaxanthin and apo-8´-carotenal were investigated applying the analytical method described above. (Hoffmann *et al.*, 2012) The cleavage products carbon chains vary C_{20}-C_{30}. Due to the shorter non-polar hydrocarbon chain and the oxygen, apocarotenoids are more polar than normal carotenoids and occur earlier in the chromatogram.

Cleavage products	$[M+H]^+$
apo-8´-carotenal	417.7
apo-10´-carotenal	377.2
apo-12´-carotenal	351.1
apo-13`-canthaxanthinone	273.2
apo-14´-canthaxanthinal	325.2
apo-12´-canthaxanthinal	365.2

Table 10. Canthaxanthin and apo-8´-carotenal cleavage products

3.4.2 Calibration and quantification considering reduction of standards

The pellet extracts contain many unique products, which are characteristic for purple bacteria. Therefore, standards for some materials cannot be commercially obtained, or they are exceedingly expensive. Thus, it is reasonable to limit the number of standards for the calibration.

In order to validate our method, we completed the calibration for one representative from each molecule group: carotenoids, PLs, BChl and terpenoid-quinones. As we show below, this enables us to quantify many related molecules as well.

Concentrations of lycopene stock solutions were determined spectrophotometrically using its molar absorption coefficient at 502 nm in hexane (1.72×10^5 $M^{-1}.cm^{-1}$). The plot of the selected ion monitoring (SIM) [total of *m/z* 537.5 $(M+H)^+$] integrated chromatographic peak area versus lycopene absorption at 502 nm is linear. The molar absorption coefficient of carotenoids is mainly dependent upon their conjugation length (Britton *et al.*, 2004), which means that the calibration curve of lycopene can be utilized for rhodopin as well. For all the other carotenoids (anhydrorhodovibrin, rhodovibrin, spx, thspx, etc.) the extinction coefficients can be calculated from the extinction coefficients described by Jensen *et al.*, 1958. For quantification, the absorbance signal is recommended to use, because of the higher sensitivity and the drift of the MS detector.

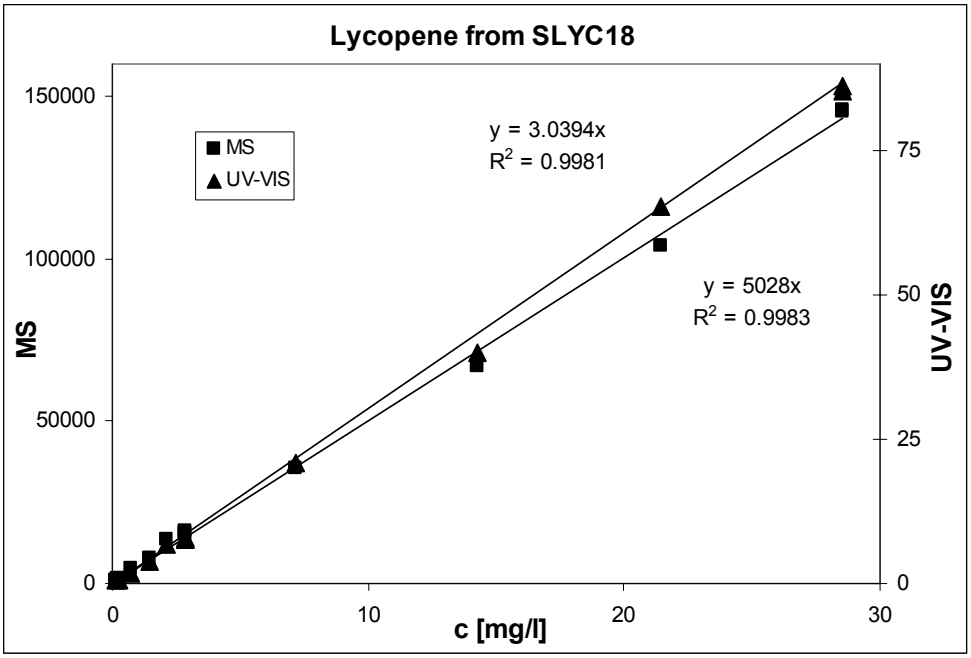

Fig. 43. Lycopene calibration curves with absorbance and mass spectrometric detection

Isoprenoid-quinone calibration was done by using UQ-10, and showed a linear response. This was also true for the calibration for UQ-9, since it only differs in the length of its isoprenoid chain; therefore its molar ionization rate is the same (Callender *et al.*, 2007). RQs need to be calibrated separately, since they differ from UQs in the hydrophilic head group. UQ-10 and UQH_2-10 have different ionization rates (Muraca *et al.*, 1967), consequently the calibration curve of UQ-10 cannot be utilized for the alcohol. Therefore, UQH_2-10 was calibrated separately by reduction of UQ-10 with H_4B (detailed description in Material methods chapter). The calibration showed that the ionisation rate of UQH_2-10 is two fold lower than that is of UQ-10 (Fig. 45).

.

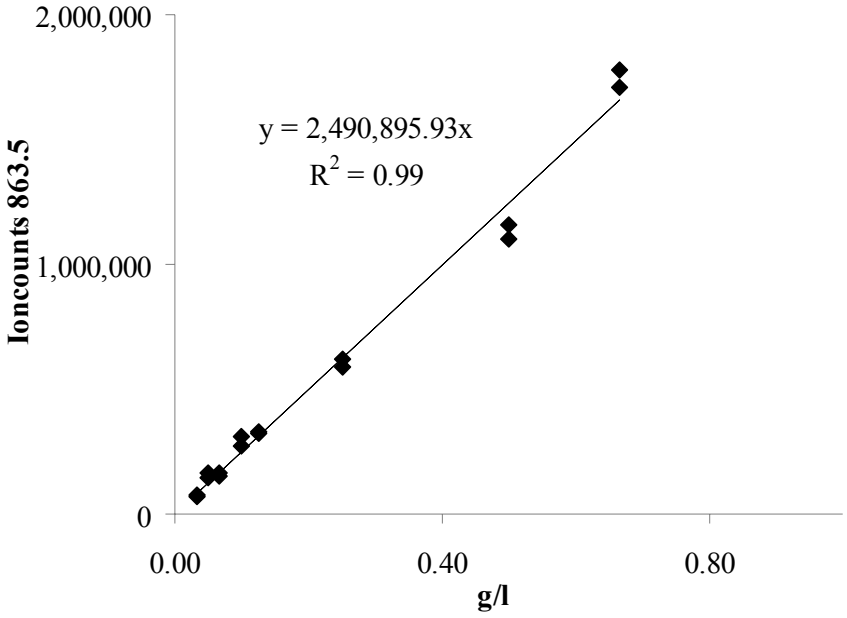

Fig. 44. UQ-10 calibration curve with mass spectrometric detection

BChl*a* was calibrated with the methanol extracts of the wild-type of *R. rubrum*. The chromatogram of the extract had only one absorption peak at the wavelength, and the concentration was determined spectrophotometrically at 772 nm using its specific absorption coefficient (6 x 10^4 $M^{-1}cm^{-1}$ in methanol at 772 nm) (Olson *et al.*, 2007). Since we could not achieve a good ionization, we used the signal at 772 nm for quantification.

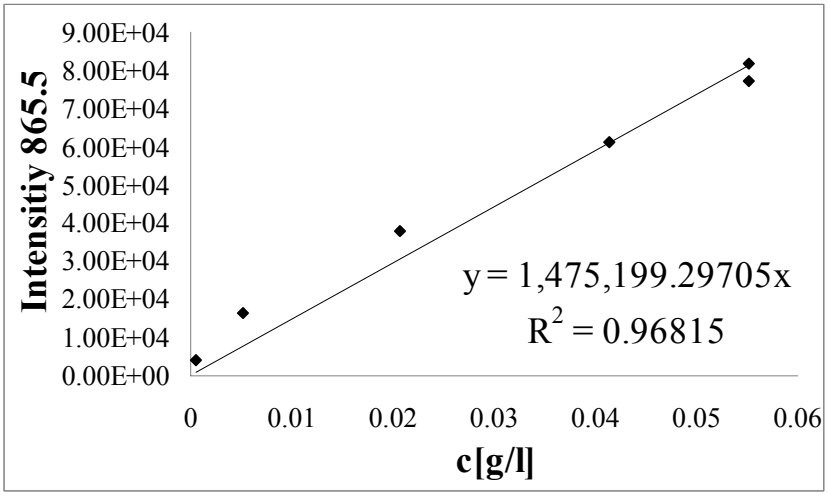

Fig. 45. Calibration curve of UQH_2-10 using the channel intensity of 865.5 *m/z*

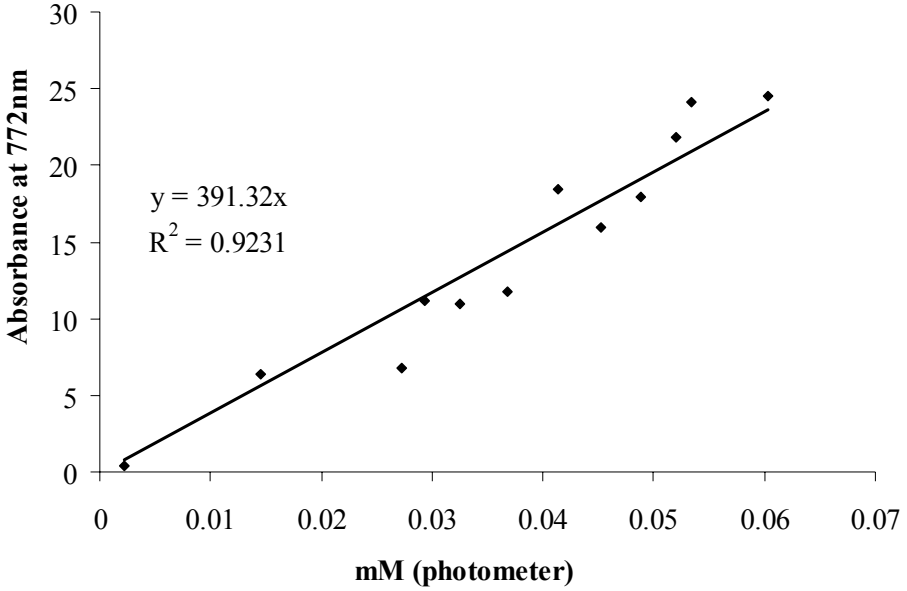

Fig. 46. BChl*a* calibration and UV-VIS spectrum of the methanol extract of *R. rubrum*

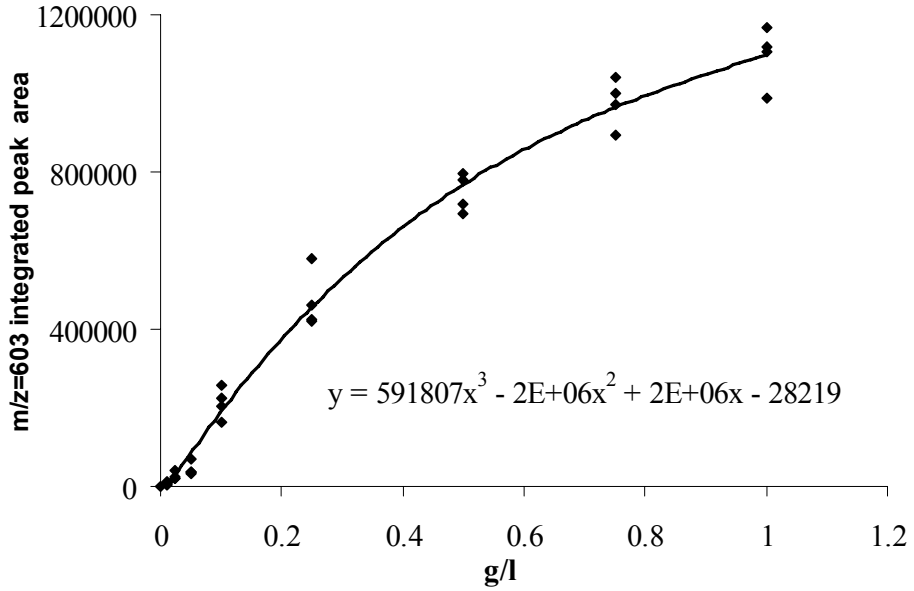

Fig. 47. PG calibration curve with the base peak *m/z* = 603

In the case of PLs, the ionization rate does not depend on the type of the fatty acids (Callender *et al.*, 2007). Furthermore, PEs, PCs and PGs appear as diacylglycerides. Therefore, PLs can be calibrated with a PC standard. We used the extracted mass signal between *m/z* 540-610 to obtain the cumulative PL level in the cell.

The validation of the extraction and the analysis was performed with three fold measurements at different cell densities. The standard deviation of PL was performed from 6x3 measurements and the standard deviation of carotenoids, quinones and BChl from 13x3 measurements. The accuracy and precision of the HPLC-APCI/MS method were determined

from many independent repeated analyses. The coefficient of variation (CV) is about 10 % for all compounds (except PLs at small cell densities CV ~17 %). The calibration and validation data are shown in Table 11.

Compound	Range of linearity (mg/l)	measurements	CV % average (mg/l)
UQ-10	3.3-700	39	11.7
POPC	5.8-1000	18	16.9
Lycopene	0.14-30	39	8.0
Bpha	0.2-30	39	9.7

Table 11. Validation of the HPLC-MS method

3.5 Fatty acid composition of R. rubrum

The first detailed investigation of the fatty acid and PL composition was carried out by Wood *et al.* (1965). They showed that the PLs of *R. rubrum* consist of PG, phosphatidylethanolamine (PE) and cardiolipin. Furthermore, they have found, that stearic, palmitic and oleic acids are the major components of the PLs under aerobic as well as anaerobic conditions. Hirayama (1968) performed a more detailed investigation on the PL composition of *R. rubrum*. He determined the fatty acid composition in each subclass of PLs respectively under phototrophic conditions. Russell and Harwood (1978) have shown that the PG fraction of the chromatophore membranes is higher, than the PG fraction of the total lipid extract. Therefore, the PG fraction is higher under phototrophic conditions compared to non-photosynthetic conditions. This might be the result of the fact that under the transition into phototrophic conditions only PGs are produced, since they are the metabolically most active PLs according to the ^{32}P experiments made by Lascelles and Szilagyi (1965). Klein and Mindich (1976) have also shown that the PL biosynthesis and the pigment synthesis are associated.

The fatty acid analysis of the PGs in Fig. 49 is consistent with those observed using classical extraction procedures in the literature (Snozzi *et al.*,1979; Wood *et al.*,1968; Schröder *et al.,*1968; Oelze *et al,* 1975; Collins *et al.,*1976; Russell *et al.*,1979). The two peaks appearing at about 10 min in the HPLC profile of the different *R. rubrum* strains (Fig. 32A,B) are each comprised of two PLs, which were identified unambiguously in the mass profile as PGs. Peak 1 contained palmitoleyl (C16:1)-oleoyl (C18:1)-phosphatidylglycerol ((PoOPG, *m/z* = 747.5) and palmitoyl (C16:0)-palmitoleyl-PG (PPoPG, *m/z* = 721.5), where PPoPG was the predominating phospholipid. The fatty acid residues were thus identified as their DAG_{MS} fragments (*m/z* (C18:1/C16:1) = 575.4; *m/z* (C16:1/C16:0) = 549.4). Peak 2 contained dioleoyl-PG (DOPG, *m/z* = 775.1) and palmitoyl-oleoyl-PG (POPG, *m/z* = 749.5), which also yielded the corresponding DAG_{MS} fragments (*m/z* (C18:1/C18:1) = 603.4; *m/z* (C16:0/C18:1) = 577.4), respectively, in the MS profile. Phosphatidylethanolamine, which is the major phospholipid in *R. rubrum*, comprising about 80% of the total phospholipid (Hirayama, 1968 and Snozzi *et al*., 1979), can be detected as a broad peak of low intensity, eluting between 10-25 min (Fig. 39). According to our measurments the PE:PG ratio under dark and microaerobic conditions is 3:1. The high fraction of PG supports the hypothesis of Lascelles and Szilagyi (1965) that the anaerobic environment induces the biosynthesis of PGs

in contrast to the PE. The higher PGs fraction is also a result of the high level of chromatophores in the cell.

PG comprises about 17% of the total phospholipid under both phototrophic as well as dark, semi-aerobic conditions (Hirayama, 1968 and Snozzi *et al*., 1979). In all of the aforementioned studies, the predominant fatty acids in *R. rubrum* under all growth conditions are C16:0, C16:1, and C18:1, with the latter comprising about 10% more than either C16:0 or C16:1 (although the absolute values vary somewhat depending upon the growth conditions as well as the extraction procedure used). If we assume that all the PG fatty acids are observable in the MS profiles, a preliminary calculation indicates that the PG produced under the dark, semi-aerobic conditions employed here, is principally constituted from C16:0, C16:1, and C18:1 fatty acids in the ratio 32.8%, 25.0%, and 42.4% by weight, respectively. These ratios are very similar to those observed by Russell and Harwood (1979) for *R. rubrum* growing under dark, semi-aerobic conditions.

The PG compositions were determined in hexane, methanol and chloroform extracts providing the same results. In aforementioned studies the fatty acid compositions of the PGs were determined. Applying the HPLC-MS method described above, not only the fatty acid composition, but the fatty acid pairs belonging to the same PG molecule, can be determined (Fig. 48). According to DAG_{MS} fragments, 12 different PGs could be determined in *R. rubrum* (Table 12).

Nr.	Fragment	Exact mass	Molecular ion	Name	Structure
1	523	689.0	723	myristroyl-palmitoyl-	C14:0+C16:0
2	535	673.0	707	tridecycloyl-oleyl-	C13:0+C18:0
3	**549**	**687.0**	**721**	**palmitoleyl-palmitoyl-**	**C16:0+C16:1**
4	563	701.0	735	pentadecicloyl-oleoyl-	C15:0+C18:1
5	**575**	**713.0**	**747**	**palmitoleyl-oleoyl**	**C16:1+C18:1**
6	**577**	**715.0**	**749**	**palmitoyl-oleoyl**	**C16:0+C18:1**
7	589	727.0	761	margaroleyl-oleyl-	C17:1+C18:1
8	**603**	**741.0**	**775**	**dioleoyl-**	**C18:1+C18:1**
9	607	745.0	779	distearoyl-	C18:0+C18:0
10	617	755.0	789	oleyl-nondecyloeyl-	C18:1+C19:1
11	621	759.0	793	stearoyl-nondecyloyl-	C18:0+C19:0
12	633	771.0	805	oleyl-arachidic-	C18:1+C20:0

Table 12. The list of PGs occurring in *R. rubrum* strains. The major PLs are shown in bold.

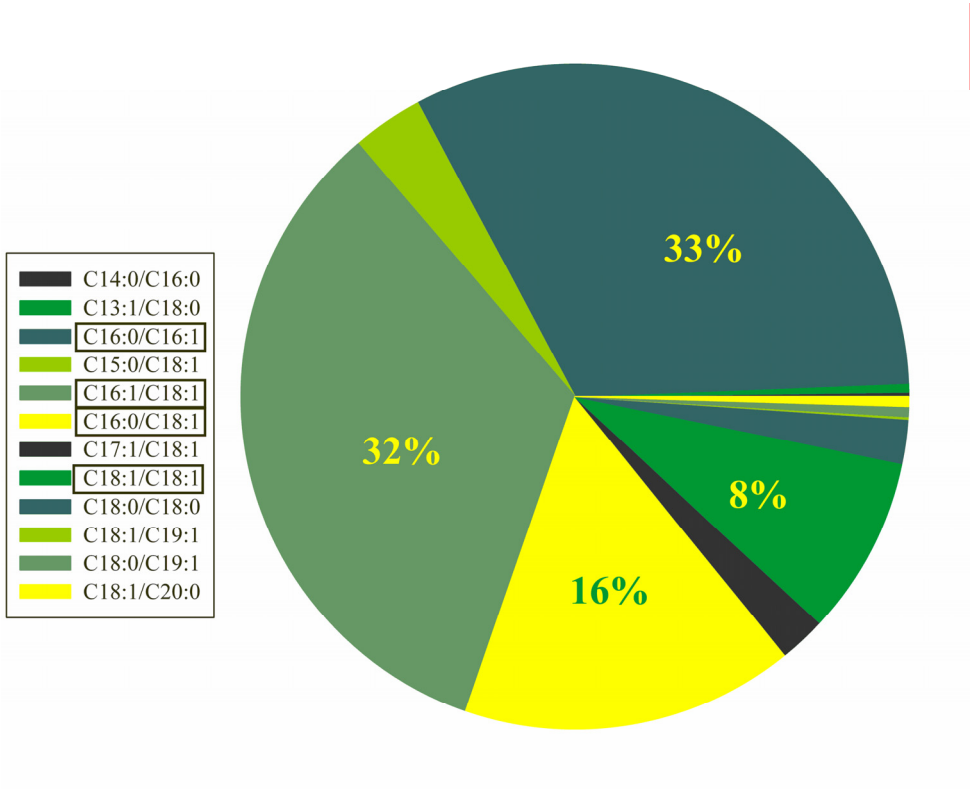

Fig. 48. PG composition (%) of *R. rubrum*. The two greatest PG fractions are C16:1/C18:1 and C16:1/C16:0 fatty acid containing PGs. The third relevant PG consists of the fatty acids C16:0/C18:1.

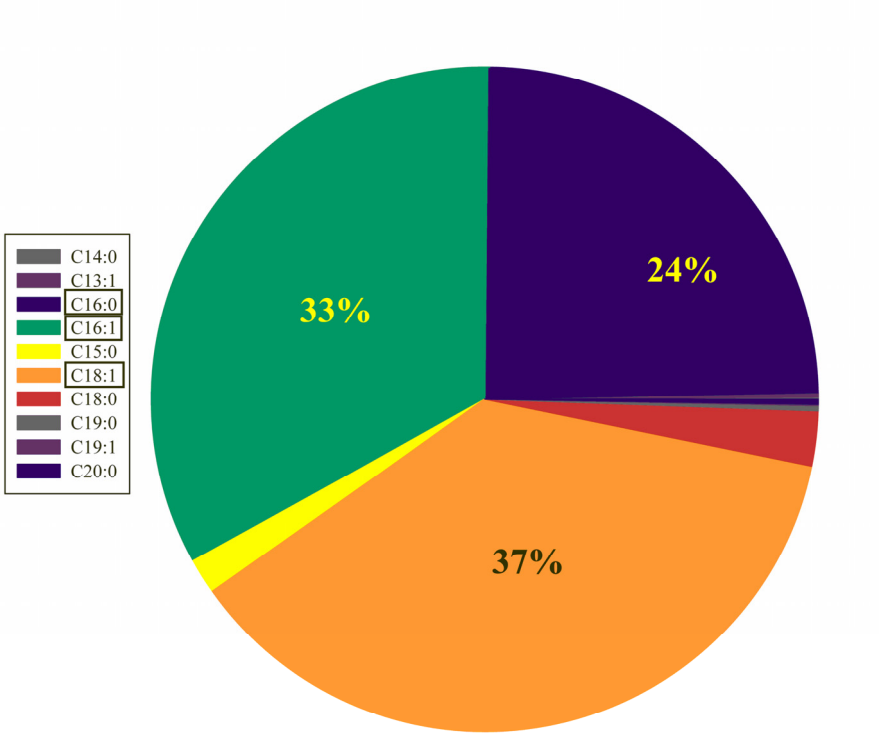

Fig. 49. FA composition of PGs under microaerophilic conditions in M2SF medium

4 Growth kinetics under microaerophilic and anaerobic conditions in medium M2SF

4.1 Preliminary considerations

Initially, we intended to investigate the dependence of the metabolic profile upon oxygen, but during the analysis of the fermentation data, it became clear that strong oxygen limitation occurred in all of the experiments independent of the adjusted pO_2 values. The complete exclusion of oxygen is difficult to achieve. Therefore a very small amount of residual oxygen may be present under these conditions. During the fermentation, the initial growth phase is aerobic, which utilizes residual O_2 in the medium, as well as in the initial inoculum. Fructose is only poorly metabolized under aerobic conditions. This aerobic metabolism is the only source of CO_2 in the initial phase, thereafter, only small amounts of CO_2 are produced via fermentative metabolism.

Since all fermentations were carried out under similar conditions, the all of the cultures studied were both in oxygen as well as CO_2 limitation during the whole growth curve. The limitation of these two substrates is a unique growth condition, which can be designated as "stress conditions".

Regarding the oxygen availability, a unique oxygen limitation occurs, which is here designated as "**semiaerobic-turnover**" conditions. Thus, the terms "anaerobic" and "semiaerobic" in this study do not correspond to the common usage in the literature. Under these conditions, the oxygen dissolved in the medium is consumed immediately. This extreme oxygen limitation causes an extremely low flux of the oxidative TCA cycle, which leaks only with the turnover speed. Under semiaerobic-turnover conditions the fermentative pathways are dominant and this anaerobic metabolism, which yields low amount of ATP, results in an extremely slow growth. The simultaneous limitation of oxygen and CO_2 do not allow the investigation of the oxygen dependence of metabolism but makes it possible to determine the metabolic pathways occurring under such stress conditions.

4.2 Fed-batch anaerobic fermentation of the wild-type

In order to investigate the PM production of *R. rubrum*, the dark, fed-batch cultivation of the wild-type was carried out in M2SF medium under "anaerobic" conditions (no aeration was used). The growth of wild-type in the absence of oxygen was used as a reference point for further comparison of other strains or other conditions. The growth curve of the wild-type obtained from the "anaerobic" bioreactor fermentation is shown in Fig. 50A. Due to the

absence of oxygen, the cells showed no lag phase, in contrast to the lag phase observed by Grammel *et al.* (2003), under microaerobic conditions. During the whole experiment, the cells are continuously growing and do not reach the stationary phase. Therefore, all the biosynthetic processes (e.g. lipid, amino acid and porphyrin biosynthesis) are active during the whole fermentation process. An extremely long generation time (60 h) can be observed which probably arises from the double substrate limitation. The stress conditions explain both the long generation times, and the apparent strong overreduction of the redox pool, reflected in the large amount of PHB production starting at timepoint 50 h.

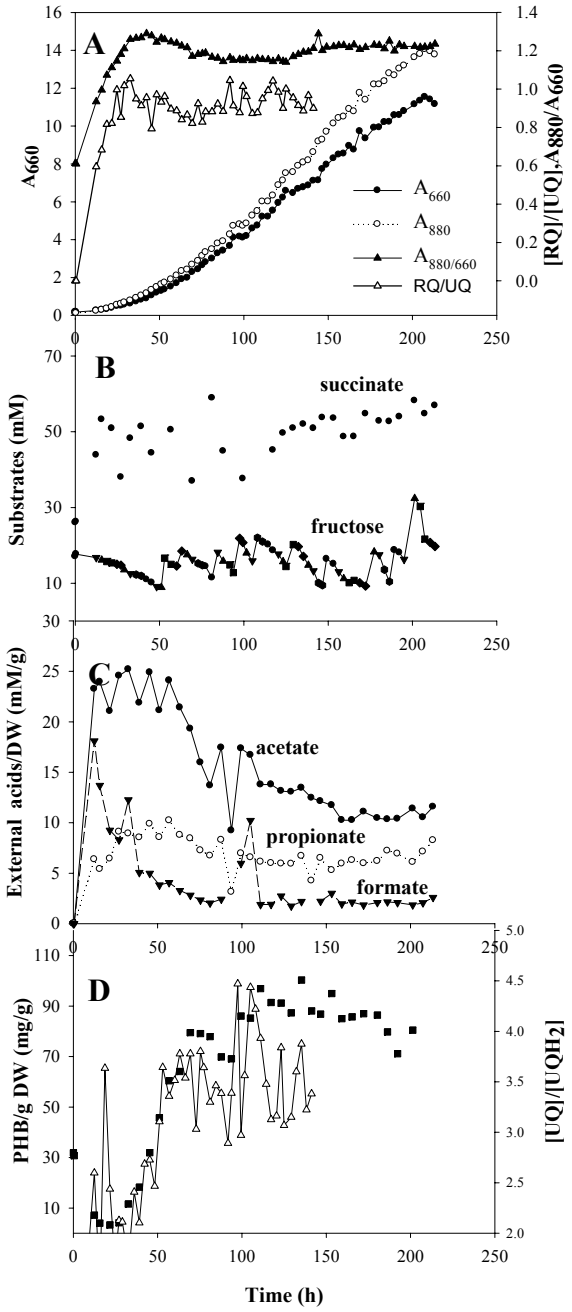

Fig. 50. Anaerobic fermentation of the wild-type in nitrogen flushed bioreactor- small fructose pulses were added (B) in order to avoid fructose limitation

The inoculum was obtained from dark, aerobic cultures. The aerobic inoculum (grown aerobically with M2SF) utilized succinate via the TCA oxidative cycle and the fructose was utilized via glycolysis. The acetyl-CoA was formed principally by the PdH reaction, which also produces CO_2. Furthermore, CO_2 can be produced by the αKGDH reaction of the TCA cycle. CO_2 is utilized via the Calvin cycle which during fructose/succinate growth has the principal function as a sink of reducing equivalents. The citramalate enzymes, necessary for acetate utilization, are acetate-inducible and are therefore probably negligible for the initial inoculum. The Pfl pathway is probably also inactive for the initial inoculum and even for normal semi-aerobic M2SF cultures is only of minor significance, since only small amounts of H_2 are produced. The low level of PHB in the initial growth phase again suggests that the oxidative TCA pathway, via PdH, is the principal mode of metabolism.

In absence of oxygen, the PM biosynthesis starts immediately after inoculation, which can be followed by the ratio A_{880}/A_{660}. In the early growth phase, the PM biosynthesis reaches a peak A_{880}/A_{660} of 1.3 about 30 h and then decreases to 1.2 (Fig. 50 A). The spillover in the PM biosynthesis arises from the sharp transition from fully aerobic-to-anaerobic conditions. The cells present in the aerobic inoculum contain a high level of oxygenases, which become inactive under anaerobic conditions, resulting in an overreduced UQ pool and excess of other redox equivalents such as NADH and NADPH. Under these circumstances the PM biosynthesis serves partly as a sink for redox equivalents resulting higher PM level than under microaerobic conditions (Grammel *et al.*, 2003).

Fructose was utilized as substrate. Thus, small fructose pulses were fed into the fermenter every 12 h in order to avoid fructose limitation, which affects PM biosynthesis. The anaerobic breakdown of fructose resulted in an excretion of organic acid. The most relevant excreted acids are acetate, propionate and formate, although pyruvate, lactate, malate and fumarate were also detected at low concentration.

The acetate production is induced immediately due to the activation of the anaerobic metabolism and the intracellular concentration of acetate increases up to a maximum of 25 mM/g at the 50 h time point (Fig. 50 C). At the same timepoint, PHB biosynthesis initiates, the intracellular acetate concentration decreases (Fig. 50 B, D). We deduce, that the decrease of the acetate concentration occurs due to the demand for PHB biosynthesis, which requires large amounts of acetyl-CoA as well as an excess of redox equivalents in the form NADPH. The intracellular PHB level reaches a saturation concentration at 90 mg/g. The large amount of PHB unambiguously indicates that the glycolytic flux reaches acetyl-CoA and subsequently the majority of the carbon and redox equivalent flux is directed into the

production of PHB. The residual lower flux is ultimately appears as excreted acids (see below).

The production of formate is known to be activated by the absence of oxygen and the intracellular formate concentration reaches a peak value of 18 mM/g at about 20h and then its value decreases (Fig. 50C). The rapid decrease might occur due to the activation of the Pfl, which consumes formate and produces hydrogen. Unfortunately, the hydrogen production was not measured during these series of experiments.

The production of propionate was also observed under anaerobic conditions (Fig. 50C). The dynamics of propionate closely resembled that of acetate. Interestingly, at all time points, the excretion of propionate is linearly proportional to that of acetate (Fig. 51). This is not only consistent with the common origin at acetyl-CoA, but also indicates that the flux regulation is completely linear at this level.

However, two phases can be distinguished. Initially, the correlation between acetate and propionate is strongly linear (R^2=0.97). At higher concentrations, the linear correlation shows higher slope (0.82). The absolute concentrations are indirectly proportional to the fermentation time, since no utilization of acetate or propionate occurs under anaerobic conditions in the presence of fructose. Therefore, the acetate-propionate correlation indicates that initially the propionate production is strongly coupled with acetate, and in the latter growth phase an additional contribution to propionate appears.

In principle, propionate can arise from the contributions of the citramalate and the ethylmalonyl pathway. The latter is branched by 3-hydroxy-butanoyl-CoA from the PHB biosynthetic pathway. However, since ethylmalonyl pathway requires CO_2, which is limiting, this pathway does not contribute significantly in the propionate production.

Consequently, propionate could be initially produced via citramalate pathway, resulting in the strongly linear correlation between acetate and propionate. As growth converges on the stationary phase of the growth, the level of porphyrin biosynthesis decreases and succinyl-CoA becomes available for the conversion into propionate. Thus, propionate is produced from two sources, and one of them is not proportional to acetate, the linear correlation changes, since more propionate is produced pro acetate (Fig. 51).

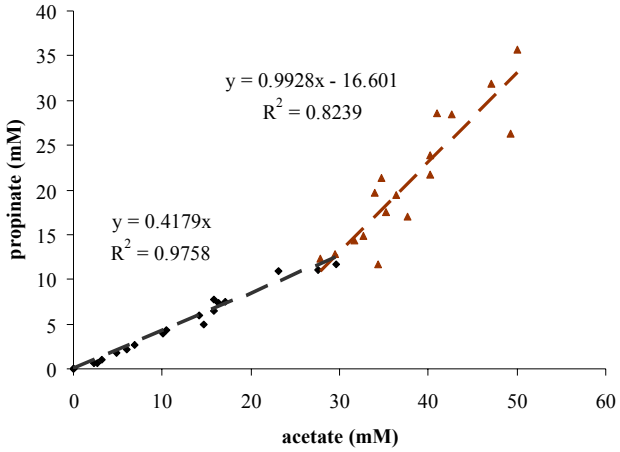

Fig. 51. Changes of propionate and acetate concentration in the wild-type under anaerobic conditions. The linear relationship indicates that propionate is produced via the citramalate pathway.

The ion chromatographic measurement of the medium shows, that the succinate concentration is approximately constant during the whole fermentation (Fig. 50 B). Succinate is essential for porphyrin biosynthesis and cannot be produced efficiently via the oxidative TCA cycle in absence of oxygen. Therefore, succinate must be utilized from the medium. However, since no decrease in succinate concentration can be observed, the production and consumption of succinate must be approximately equal.

The RQ level of the cells was significantly higher ([RQ]/[UQ] = 1) under anaerobic conditions, than in aerobic cells ([RQ]/[UQ]=0.5, (Grammel and Ghosh, 2008)).

The redox state of the UQ pool was found to be in oxidized state ([UQ]/[UQH_2] =6), which is unlikely under anaerobic conditions (Fig. 50D). Thus, the [UQ]/[UQH_2] values probably cannot describe the redox state of the UQ pool, possibly because the sample preparation was not optimal for retain the physiological redox state (data not shown). Since the oxidation level of UQH_2-10 probably rises systematically, the [UQ]/[UQH_2] values can still be used to empirically compare the UQ state among the different fermentations.

4.2.1 Fed-batch anaerobic fermentation of SLYC18

The growth curves of the anaerobic bioreactor fermentation of SLYC18 are shown in Fig. 52. Initially, the cells were held under aerobic conditions in the bioreactor, and the aeration was switched off at the time point of 18 h. The repression of oxygen was abolished very quickly (2 hours) due to the initial high cell density. Since the oxygen concentration is consumed rapidly no lag phase occurs, as in contrast to that observed under microaerobic conditions by Wang *et al.,*(2012). During the experiment the cells were continuously growing up to the late exponential phase.

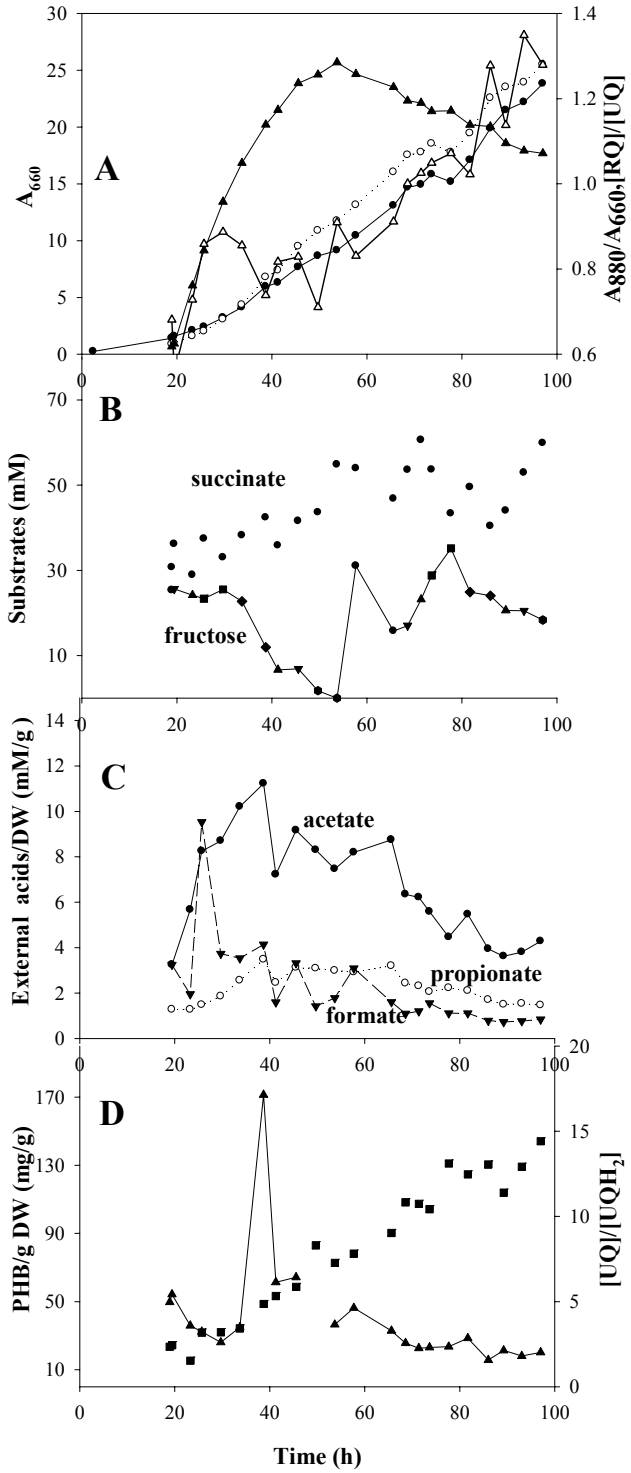

Fig. 52. Anaerobic fermentation in the bioreactor with the strain SLYC18. During the fermentation two fructose pulses were added (B) in order to avoid fructose limitation.

Although, the G_t of SLYC18 is significantly shorter (30h) than that of the wild-type (60h) under anaerobic conditions (Fig. 60), it still shown very slow growth due to the semiaerobic-turnover conditions and the CO_2 limitation. The induction of the PM biosynthesis was

identical with the observations obtained from the wild-type in absence of oxygen: "spillover" PM production due to the sharp transition from aerobic-to-anaerobic conditions (Fig. 52A).

The metabolic pattern of SLYC18 is very similar to that of the wild-type: the fermentative pathways are activated immediately in absence of oxygen, which resulted in a high level of PHB and organic acid excretion. There are three important differences between the anaerobic metabolic pattern of S1 and SLYC18:

1.) In SLYC18 the amount of succinate produced showed a weak positive slope which was not the case in the wild-type. The succinate concentration in the medium increased from 30mM to 50 mM (Fig. 52B). The production of succinate can indicate flux of the reductive TCA pathway via the enzyme FRD enzyme (as well as) the activity of the methylmalonyl pathway. The correlation between succinate and acetate was also found to be strongly linear suggesting that the biosynthesis of the organic acids was coupled (Fig. 53). The linear correlation suggests that succinate production is coupled to the citramalate/ethylmalonyl pathway. In order to produce succinate from propionate, CO_2 is essential. In the anaerobic fermentation of the wild-type CO_2 was limiting, since in the fully anaerobic fermenter the cells grew very slowly. In contrast, in the SLYC18 fermentation, the cells were initially aerobic during 16 hours and they could produce significant amounts of CO_2 which could be utilized subsequently for succinate production.

Interestingly, the slope of the acetate vs. propionate plot is identical to that of the wild-type up to the concentration of (over 40 mM). This is consistent with the observation that SLYC18 fermentation data was delayed (18 h) in PM biosynthesis, so that the region corresponding to the high slope in the S1 data was outside of the measurements region (Fig. 54).

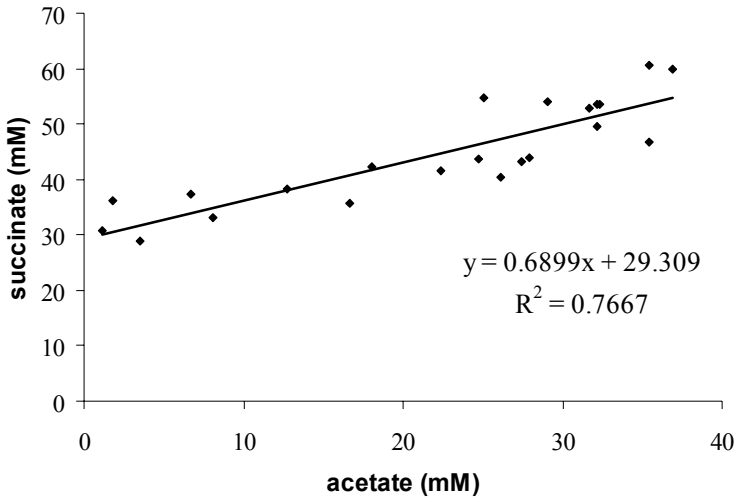

Fig. 53. Correlation between acetate and succinate in SLYC18 under anaerobic conditions. This indicates that succinate is produced via the methylmalonyl pathway in the presence of carbon-dioxide.

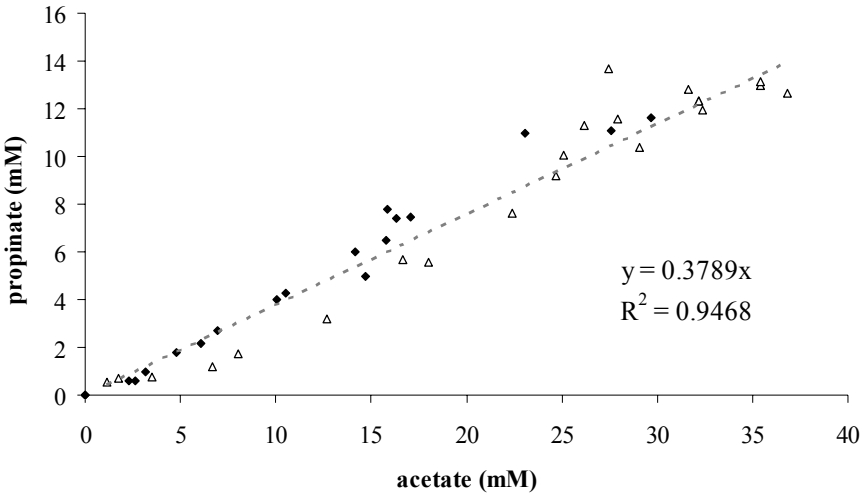

Fig. 54. Propionate production shows linear correlation with acetate in wild-type as well as in SLYC18. Δ- SLYC18 anaerobic, ■ -wild-type anaerobic.

2.) A higher PHB level was achieved in SLYC18 (150 mg/g) than in the wild-type (90 mg/g) (Fig. 52D).These results indicate that SLYC18 cells are more reduced and have higher excess of NADPH compared to the wild-type. It is surprisingly, since SLYC18 has less redox equivalents due to the missing desaturation steps. Since in this experiment PHB biosynthesis occurs simultaneously with the production of organic acids; these pathways probably compete for acetyl-CoA. Thus, due to the higher PHB production rate less organic acids are excreted.
3.) Significantly more RQ accumulated in SLYC18 ([RQ]/[UQ] = 1.3) than in the wild-type ([RQ]/[UQ] = 1), (Fig. 50A and Fig. 52A).

4.2.2 Fed-batch microaerophilic fermentation of the wild-type and SLYC18

During the "microaerobic" experiments different initial pO_2 values were adjusted. The analysis of the data showed, that these pO_2 values did not affect the metabolic profile of the cells, since the oxygen was consumed rapidly, and the cells became essentially anaerobic (semiaerobic turnover conditions). In these experiments, it takes approximately 12 hours depending on the cell growth to consume the oxygen below the repressing pO_2 = 0.3 %.
The growth dynamics under microaerophilic conditions were identical to the anaerobic growth in the wild-type (Fig. 55A, Fig. 56A). In case of SLYC18, a longer lag phase was observed under microaerobic conditions, which is consistent with the observation of Wang *et al.* (2012) (Fig. 59A, Fig. 58A).

4.2.2.1 Microaerobic fermentations obtained from the wild-type

The wild-type was investigated under two different "microaerophilic" conditions.

In experiment 1, the pO_2 was about 0.05%, the "spillover" of the PM biosynthesis (a maximal value of 1.3 in the A_{880}/A_{660} time course) could not occur due to the smoother transition of the metabolism from aerobic-to-microaerophilic conditions. The metabolic pattern of the wild-type in experiment1 is very similar to that determined in the absence of oxygen. Thus, high fluxes in the fermentative pathways are present, resulting in PHB biosynthesis and excretion of organic acids. However, the level of PHB (Fig. 55C, D) is slightly lower (70 mg/g). Furthermore, the [RQ]/[UQ] ratios were also lower (0.9) than under anaerobic conditions (Fig. 55A).

In experiment 2 no aeration was applied in the bioreactor. The growth curve of experiment 2 followed the anaerobic one with a delay of 12 h due to the initial oxygen repression. The "spillover" of the PM biosynthesis was also observed as in anaerobic case (Fig. 56A). The fermentative pathways showed similar activities as those observed in complete absence of oxygen. The production of PHB and the organic acid was induced after the PM biosynthesis rate reached the maximum value, indicating once again competition for the acetyl-CoA pool (Fig. 56A, D). As expected from the above discussion, the cessation of PM biosynthesis is correlated to a high availability of acetyl-CoA and the simultaneous production of PHB and organic acids. (Fig. 56C, D).

In experiment 1, the succinate concentration was constant, in contrast to experiment 2, where a net production of succinate was observed (Fig. 55B and Fig. 56B). The different succinate profiles occur probably due to the variation of CO_2 availability during the experiments. In the case of experiment 1, the cells were inoculated into a rather anaerobic bioreactor. Furthermore, the reactor was also aerated at a low rate, which further depleted CO_2. Therefore, no accumulation of CO_2 could occur prohibiting the succinate production. In experiment 2, the cells were grown initially in an aerobic, then in a microaerobic environment, which resulted in relative large amounts of CO_2. Since no significant aeration was used during the fermentation, significant amount of CO_2 was available, and it could be used for succinate productions. Succinate production also correlates linear with acetate in this case (Fig. 57).

The dynamics of the $[UQ]/[UQH_2]$ ratio are different in the two experiments. In experiment1 the $[UQ]/[UQH_2]$ ratio shows a large perturbation at the time point of the fructose pulse (66 h).

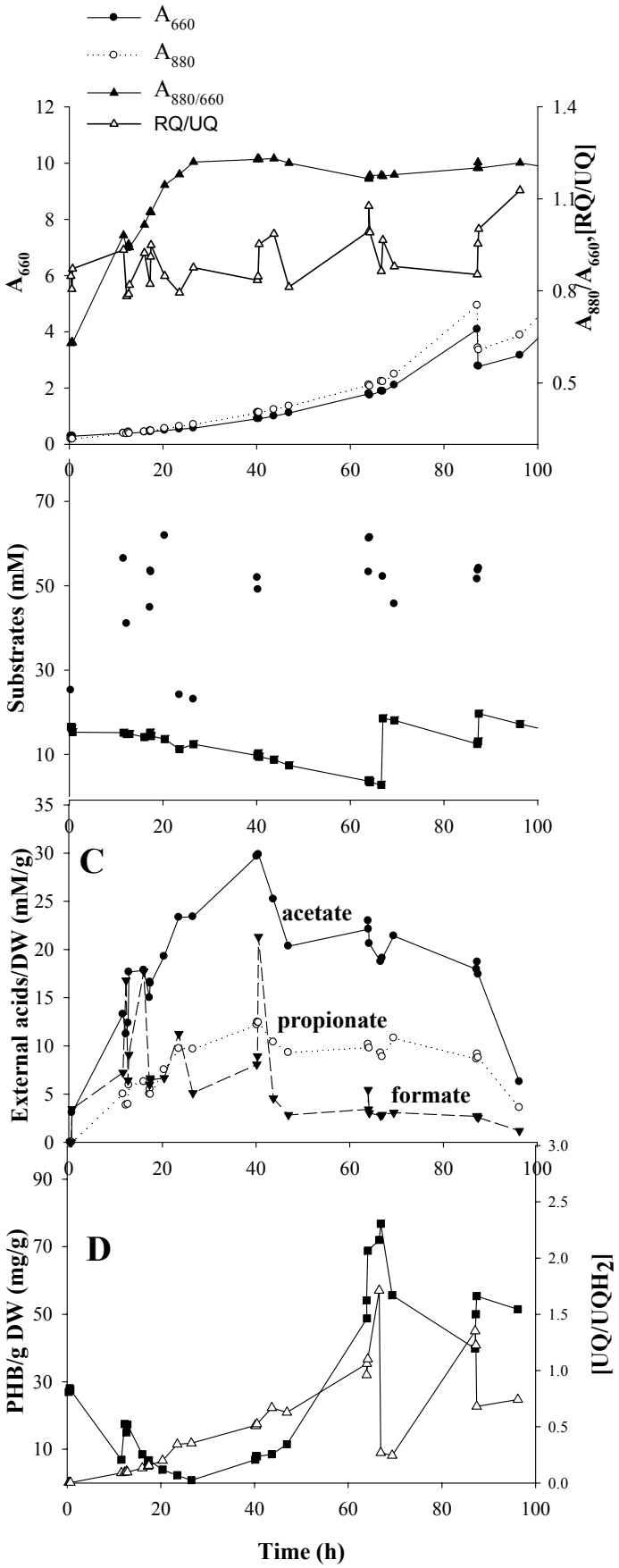

Fig. 55. "Microaerobic" fermentation of the wild-type applying two fructose pulses (Experiment1)

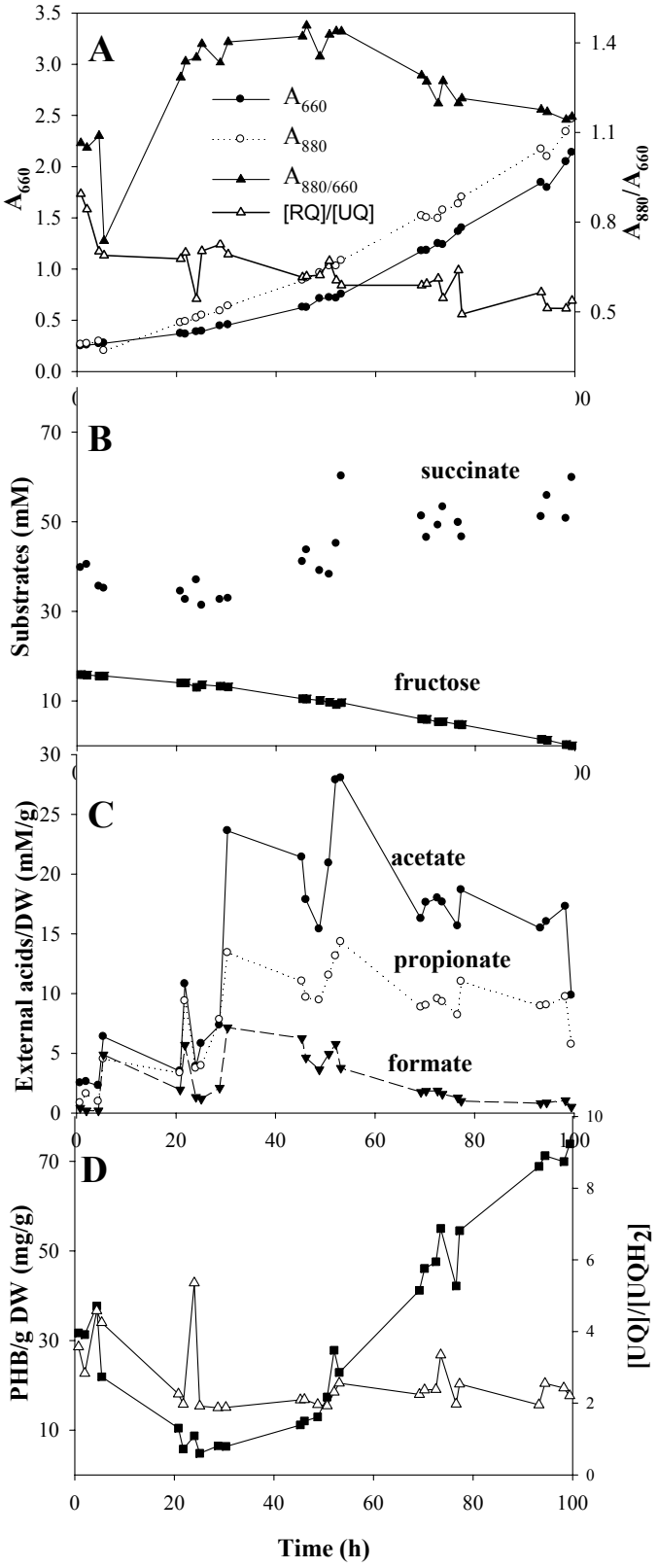

Fig. 56. "Microaerobic" fermentation of the wild-type without a fructose pulse. (Experiment 2)

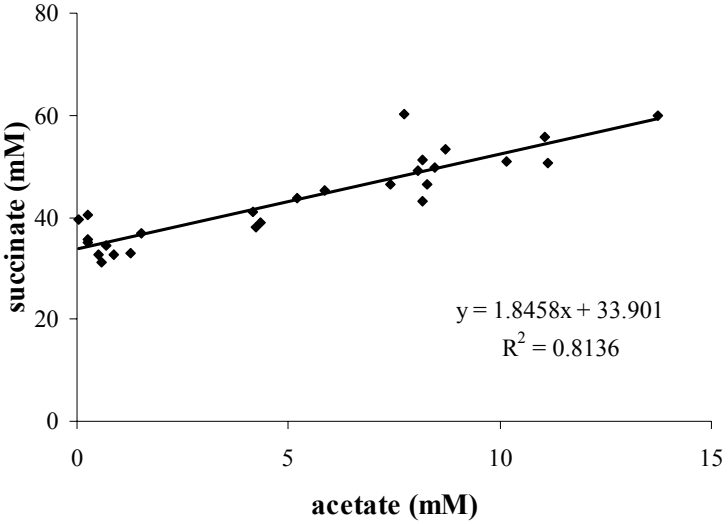

Fig. 57. Correlation between acetate and succinate, which indicates, that succinate is produced via methylmalonyl pathway in the wild-type in the presence of carbon dioxide.

4.2.2.2 "Microaerobic" fermentations obtained from SLYC18

The strain, SLYC18 was fermented under four different initial pO_2 adjustments: 0.45%, 0.3% and 0.6%, 0.25%.

Under these conditions, the PM "spillover" biosynthesis does not occur due to the initial relative high oxygen concentration in the fermenter. Nevertheless, the growth curves are consistent with the anaerobic growth curve.

The experiments at pO_2 = 0 45% and 0.3% showed essentially identical results and in general agree with the observations of Grammel *et al*. (2003):

- In the case of higher oxygen availability, the simultaneous utilization of succinate and fructose occurs.
- Acetate is utilized as a substrate before fructose become limiting.

In these experiments, higher production of PHB (170 mg/g) could be observed than in absence of oxygen (Fig. 58D). The RQ/UQ ratio is also significantly higher (1.2-1.6) than under anaerobic conditions (Fig. 58A).

During the third SLYC18 experiment two different pO_2-s were applied. Initially, the cells were grown at pO_2= 0.6% and in the 49 h time point the pO_2 was adjusted to 0.25 %.The metabolic profile in the third experiment is similar to that of the former two SLYC18 experiments, although the adjustment of oxygen induced the following transient changes in the metabolic profiles:

1.) The induction of the PM biosynthesis occurs for a short period triggering a significant decrease in the PHB production. The induction of PM biosynthesis resulted in lower flux into the PHB biosynthesis, but after the cessate of PM biosynthesis cessates, the PHB production appeared again. (Fig. 59D).
2.) After the oxygen adjustment, production of succinate occurred. The lower oxygen concentration and the CO_2, accumulated during the first 49 hours, activated the succinate production via the methylmalonyl pathway (Fig. 59B, C).

The growth curves obtained from bioreactor fermentations of the wild-type and SLYC18 can be seen in Fig. 60. Although the generation times are extremely long, a significantly higher growth rate (0.02) can be observed in the case of SLYC18 at low/zero oxygen than in the wild-type (0.01).
The correlation between the dry cell weight (DCW) and A_{660} in SLYC18 and the wild-type was measured and found to be strongly linear with similar correlation factors: 0.389 and 0.3904 in wild-type and SLYC18, respectively (Fig. 61). This indicates that in these experiments no large, global physiological transition (e.g. cell lengthening in the stationary phase) has occurred.

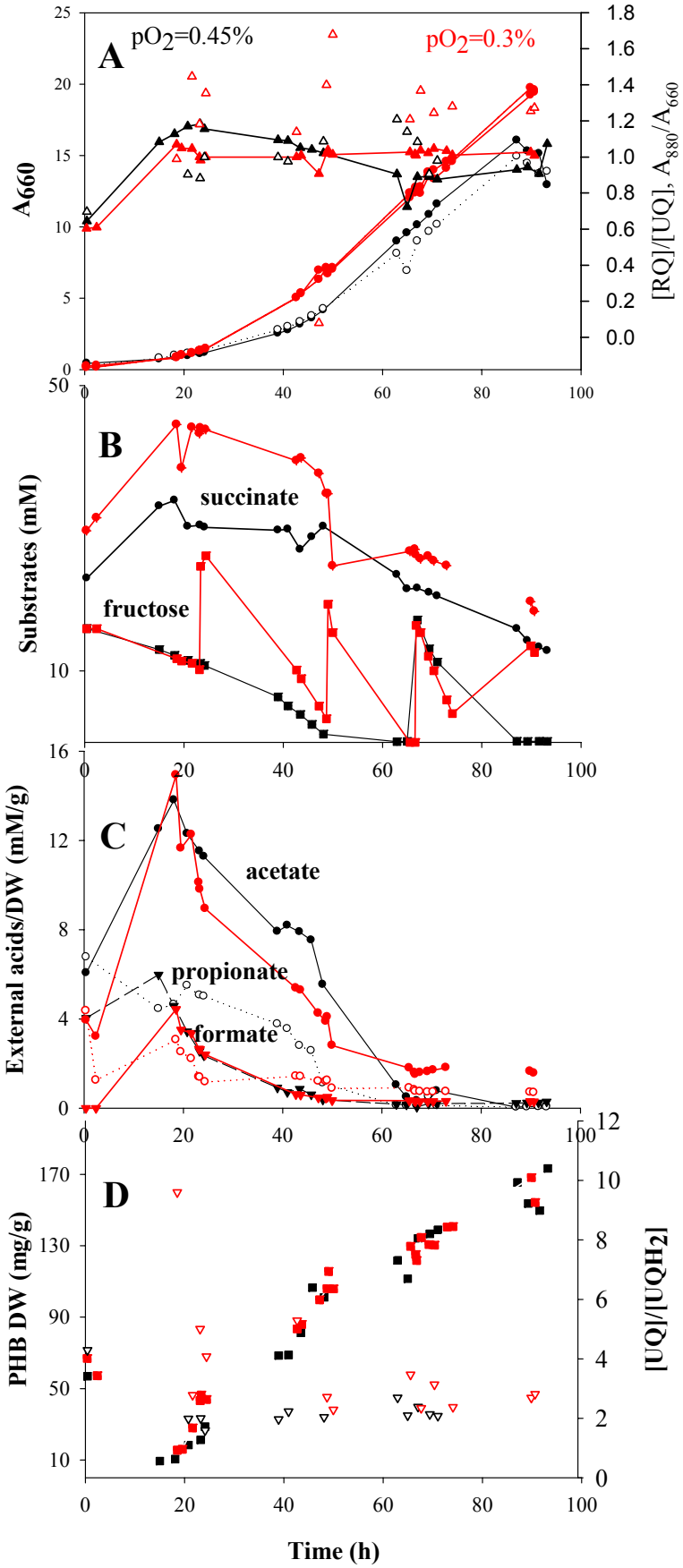

Fig. 58. "Microaerobic" fermentation of SLYC18 at pO_2=0.3% and pO_2=0.45%.

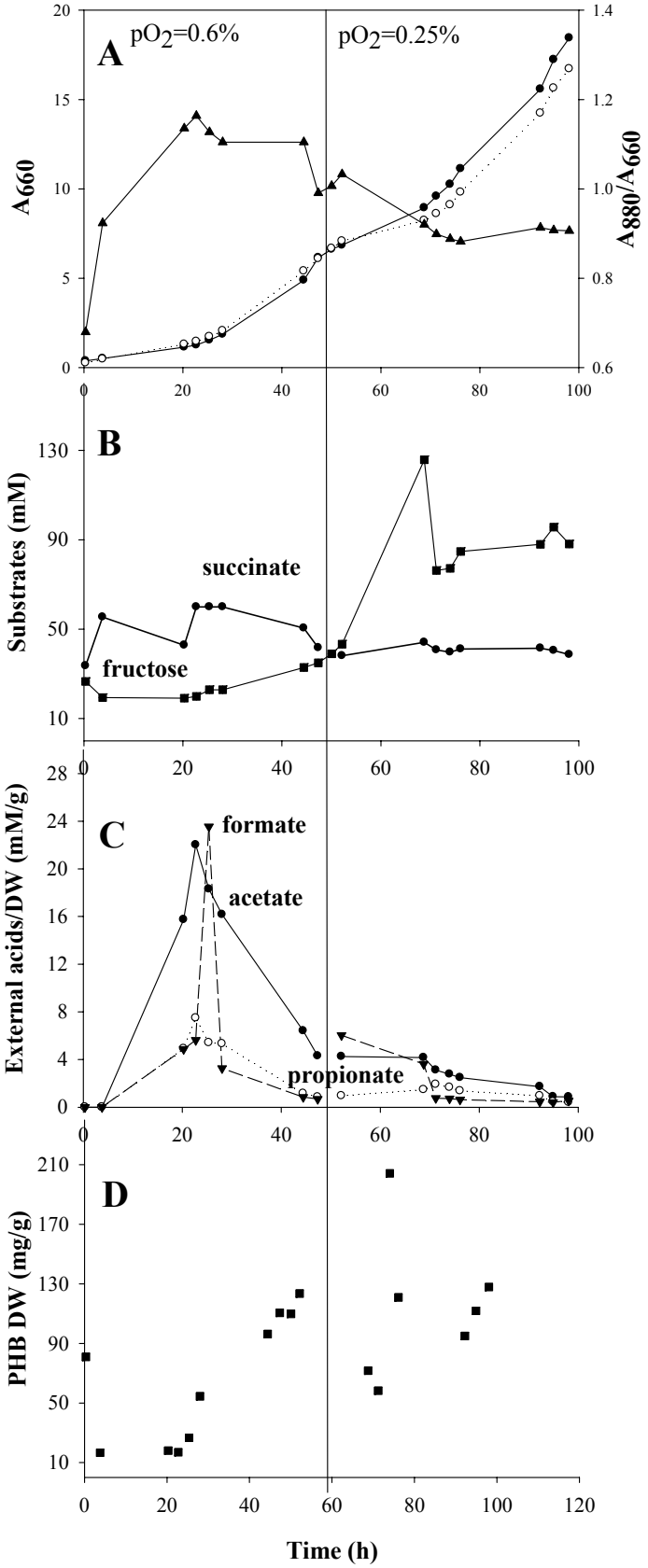

Fig. 59. "Microaerobic" fermentation of SLYC18 pO_2=0.6% and 0.25% with fructose feeding.

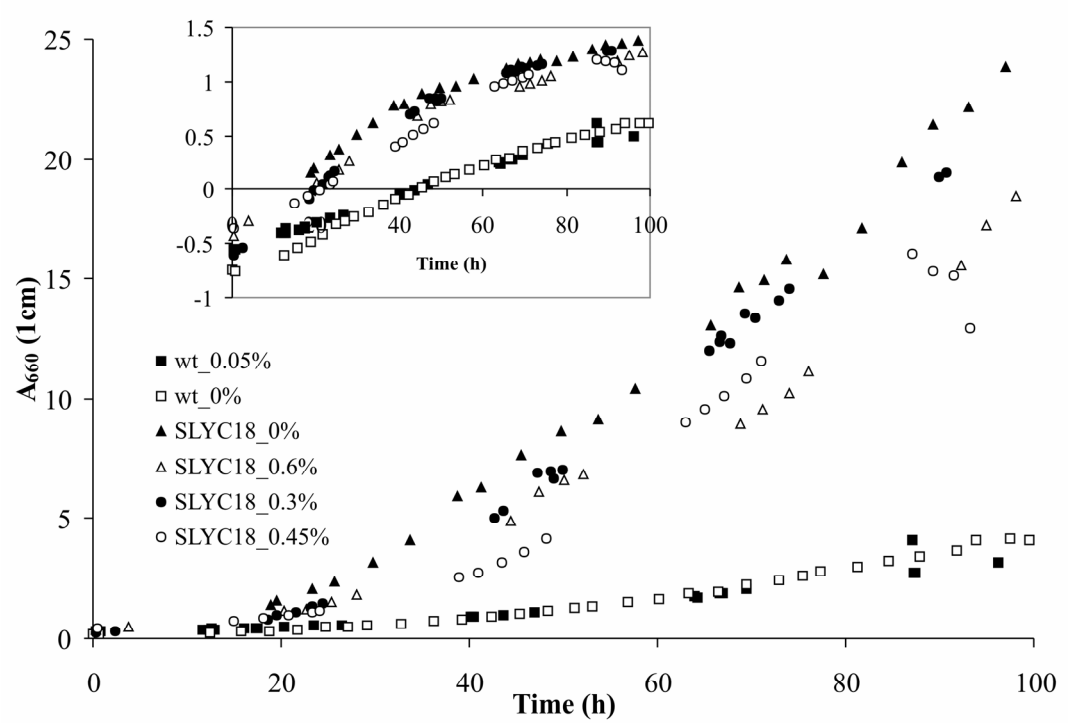

Fig. 60. Growth curves of SLYC18 and the wild-type under different oxygen availabilities. These results show that under limiting oxygen concentration SLYC18 grow faster than the wild-type.

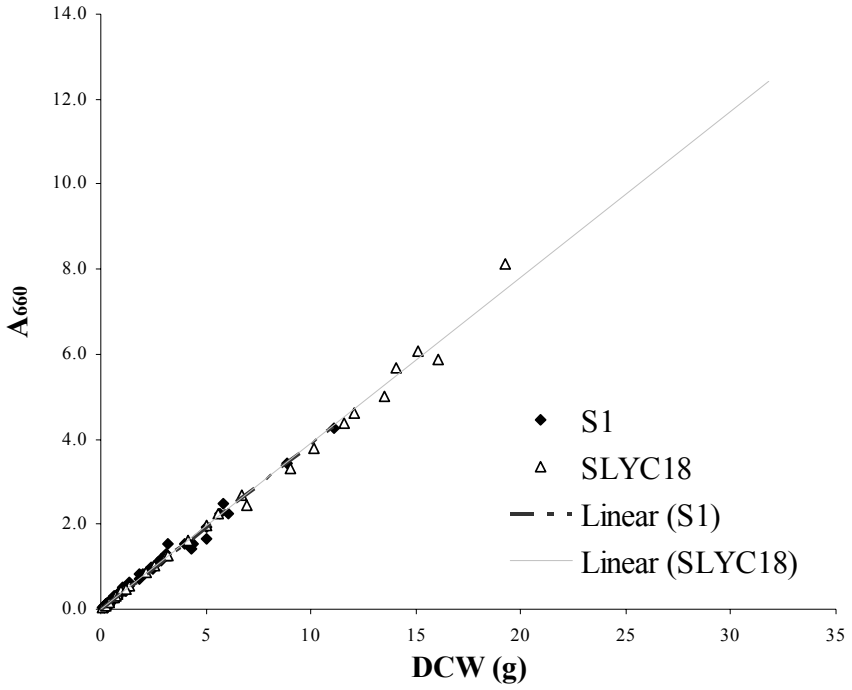

Fig. 61. Linear correlation between DCW and A_{660} (in 1 cm cuvette) resulting in the slopes 0.389 and 0.3904 in the wild-type and SLYC18, respectively.

4.2.3 Growth curves in stirred bottle

In order to investigate the PM biosynthesis of the wild-type and both carotenoid mutants simultaneously, the cells were grown in stirred bottles under semiaerobic conditions. Slower growth of SLYC18 was observed in the presence of oxygen during both experiments. During the first stirred bottle experiment two large oxygen pulses were applied, which are observable also as rapid changes of the [UQ]/[UQH_2] ratio (Fig. 62A). The oxygen concentration affected the PM biosynthesis significantly in the carotenoid mutants, as indicated by the A_{880}/A_{660} ratio, which is significantly lower in the mutants compared to the wild-type (Fig. 62 A, B).

4.2.4 Discussion

The fermentative pathways were dominant in the metabolic profile under semaerobic-turnover conditions and CO_2 limitation.

The production of propionate indicates that citramalate/ethylmalonyl pathways are active under all the growth conditions studied here. In the case of CO_2 availability, succinate production from propionate, probably via the methylmalonyl pathway, was observed. Since all the significant fluxes start from pyruvate and acetyl-CoA, these metabolites and the pyruvate conversion reactions to acetyl-CoA are probably major control points of the cell under low oxygen availability.

SLYC18 produces significantly more PHB than the wild-type indicating a high availability of NADPH. The PHB production reflects the reduced state of the cell, where the redox equivalents are directed into the storage materials. The reduced state cannot be confirmed with the UQ pool, which was found in an oxidized state in every experiment. The higher PHB production in SLYC18 indicates that this mutant is more reduced than the wild-type, even though the lack of CrtD-mediated desaturation steps should lead to a more oxidized redox state. The significantly higher [RQ]/[UQ] ratio for SLYC18 indicates that a correlation between the quinone composition and the direction of the redox equivalents to PHB may exist. This phenomenon is discussed in details in Chapter 7.

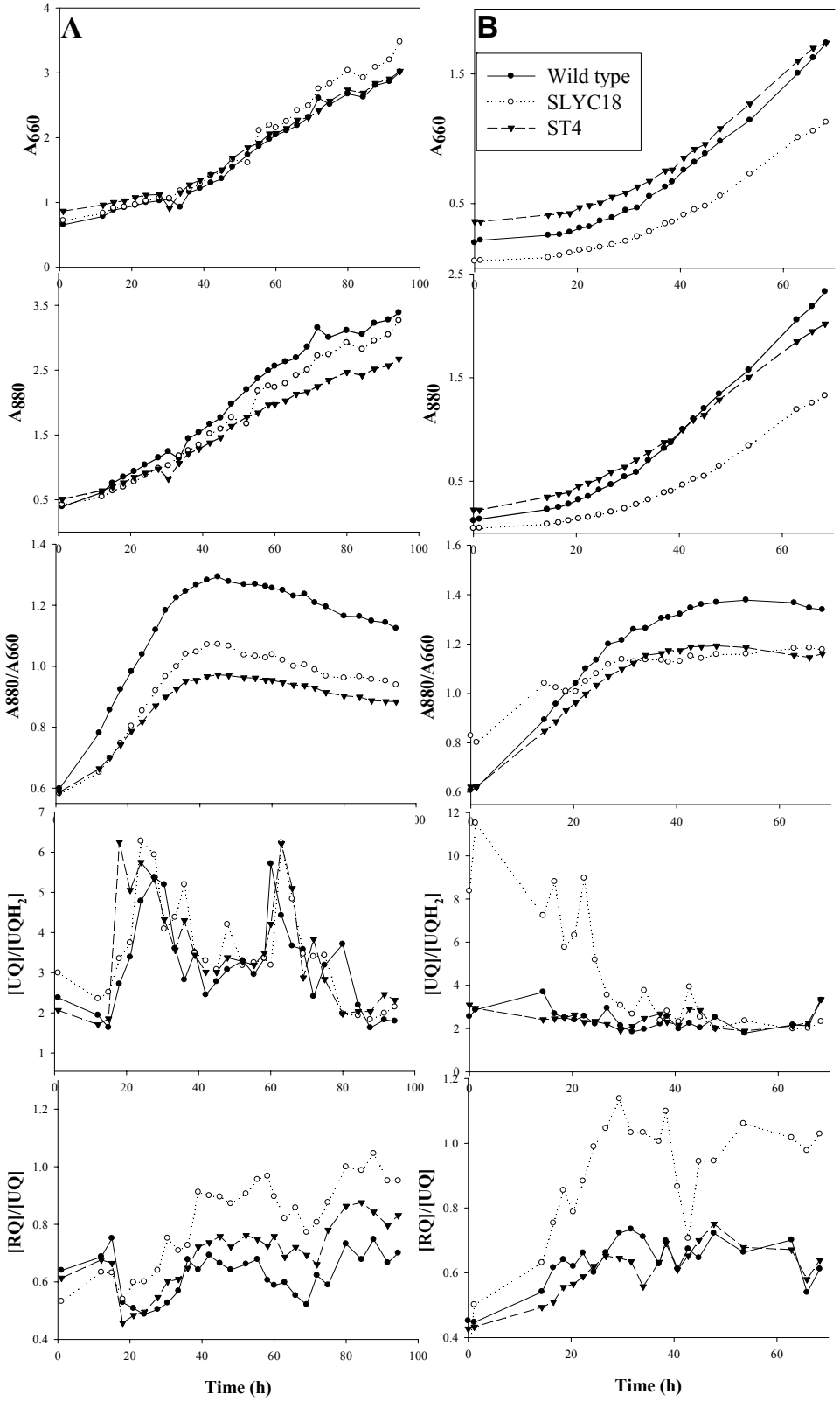

Fig. 62. Growth curves obtained from stirred bottle fermentations: wild-type (●). SLYC18 (○), ST4 (▼).

5 Dynamics of the carotenoid biosynthesis

The dynamics of the PM biosynthesis following the aerobic-to-anaerobic transition were investigated in detail by measuring several compounds of the PM. The aerobic-microaerobic transition allows us to study the effect of oxygen on the PM biosynthesis at both the gene and the enzyme level. According to Jensen *et al.* (1958) and Schwerzmann *et al.* (1989), during carotenoid biosynthesis all the intermediates of the normal spx pathway are converted consecutively to spx under phototrophic conditions (Jensen *et al.,* 1958; Schwerzmann *et al.,* 1989). In order to characterize the carotenoid production in the dark, anaerobic bioreactor fermentations were carried out in M2SF medium on the wild-type and SLYC18.

In order to study the sensitivity of the carotenogenic enzymes to oxygen, the wild-type, SLYC18 and ST4 were fermented in bioreactor and stirred bottle under microaerobic conditions (applying a direct oxygen pulse after anaerobic induction). During the stirred bottle experiments, a special regime of oxygen-limitation occurs during the fermentation, which was achieved with alternating small oxygen and argon pulses. The largest oxygen pulses occurred between the 18-21 h time points resulting in an almost repressing oxygen concentration, which is reflected in the changes of the [UQ]/[UQH_2] ratio (Fig. 65D). The oxygen effect appears first in ST4, then in SLYC18 and finally in S1 according to the different cell density. Although the three experiments were independent from each other, the oxygen concentration changed very reproducibly in all three bottles (Fig. 63.).

The dynamics of the carotenoid time courses were essentially identical in all experiments, starting with an induction phase, where the absence of oxygen induces anaerobic gene expression (Fig. 65A, B). During the induction phase, the intermediate carotenoids and the end product (spx) occur at approximately the same concentrations. The total carotenoid level reaches a peak concentration at the 24 h time point of the fermentation. After reaching the peak concentration, a strong decrease of the intracellular carotenoid level occurs. The rapid sampling of the fermenter allows us to follow the dynamics of the system with a resolution which has never been presented before in *R. rubrum*.

In all experiments the methoxylated carotenoids, such as anhydrorhodovibrin, spx, dhspx, and thspx were the major carotenoids found, although their fractions were strongly affected by oxygen.

The dynamics of the carotenoid biosynthetic pathway can be visualized more effectively by calculating the "fraction carotenoid" from the raw data as:

$$\text{fraction carotenoid i} = \frac{[\text{carotenoid}]_i}{\sum_j [\text{carotenoid}]_j} \qquad (1)$$

where [carotenoid] is the concentration of a given carotenoid species i at time point t, and the sum $\sum_j$ is the total concentration (total carotenoid) of all carotenoid species found at time point t.

For the purpose of visualizing the dynamics of carotenoid biosynthesis, the calculation of the fraction carotenoid has a great advantage over the direct visualization of the primary data. Namely, the systematic sampling errors are largely "cancelled out", thereby causing a smoothing of the data. Secondly, whereas the primary data value “µmol carotenoid/g DW” is essential for calculating the yield of carotenoid produced, it also contains contributions from extraneous factors (e.g. systematic sampling errors, changes of cell morphology or composition during growth), which make intuitive evaluation of the dynamics difficult. For instance, in Fig. 69A, the thspx level seems to decrease at the end of the growth curve, whereas in Fig. 71A the thspx level rises continuously to an asymptotic value. The reason for this discrepancy is probably due to the fact that *R. rubrum* cells show significant lengthening in the late exponential phase, probably associated with substrate limitation, with a non-proportional increase in the biomass (G.-S. Wang and R. Ghosh, unpublished data), thus causing the amount of carotenoid/g DW cell to decrease. However, the data in Fig. 71 A shows that the relative amount of carotenoid with respect to the total remains unchanged within the lengthening phase.

5.1 Anaerobic carotenoid production in the wild-type

In absence of oxygen the “normal spx” pathway was found to be active with the extension of the step from rhodovibrin to dhspx. The extended “normal spx” pathway is shown on Fig. 64. All the carotenoid intermediates were converted into spx, which occurs as the only carotenoid at the latter growth curve. The peak concentrations of the total carotenoid and spx were 3.6 and 1.3 µmol/g, respectively.

The recalculation of the raw data of the anaerobic wild-type experiment according to equation (1) is shown in Fig. 65B. As we can see, the fraction spx continuously increases during the fermentation and finally it is the only carotenoid which can be observed. Analysis of the data in Fig. 65B allows the temporal behaviour of the end product (spx) and the intermediates to be assessed visually. For instance, at early times, the spx level (initially due to the inoculum)

drops continuously until about 18 h, after which it rises continuously. Comparison of the position of the trough for spx (at 12 h) and the appearance of the carotenoid intermediates shows that the first and second highest intermediates of the pathway correspond to anhydrorhodovibrin and rhodovibrin, respectively (Fig. 65B). Dhspx, rhodopin and lycopene occur at significantly lower concentration levels.

At the 70 h timepoint a second induction (smaller than the first induction) can be observed. The difference between the first and the second induction is the concentration of the intermediates. During the second induction the intermediate concentrations only slightly increases in contrary to the spx concentration.

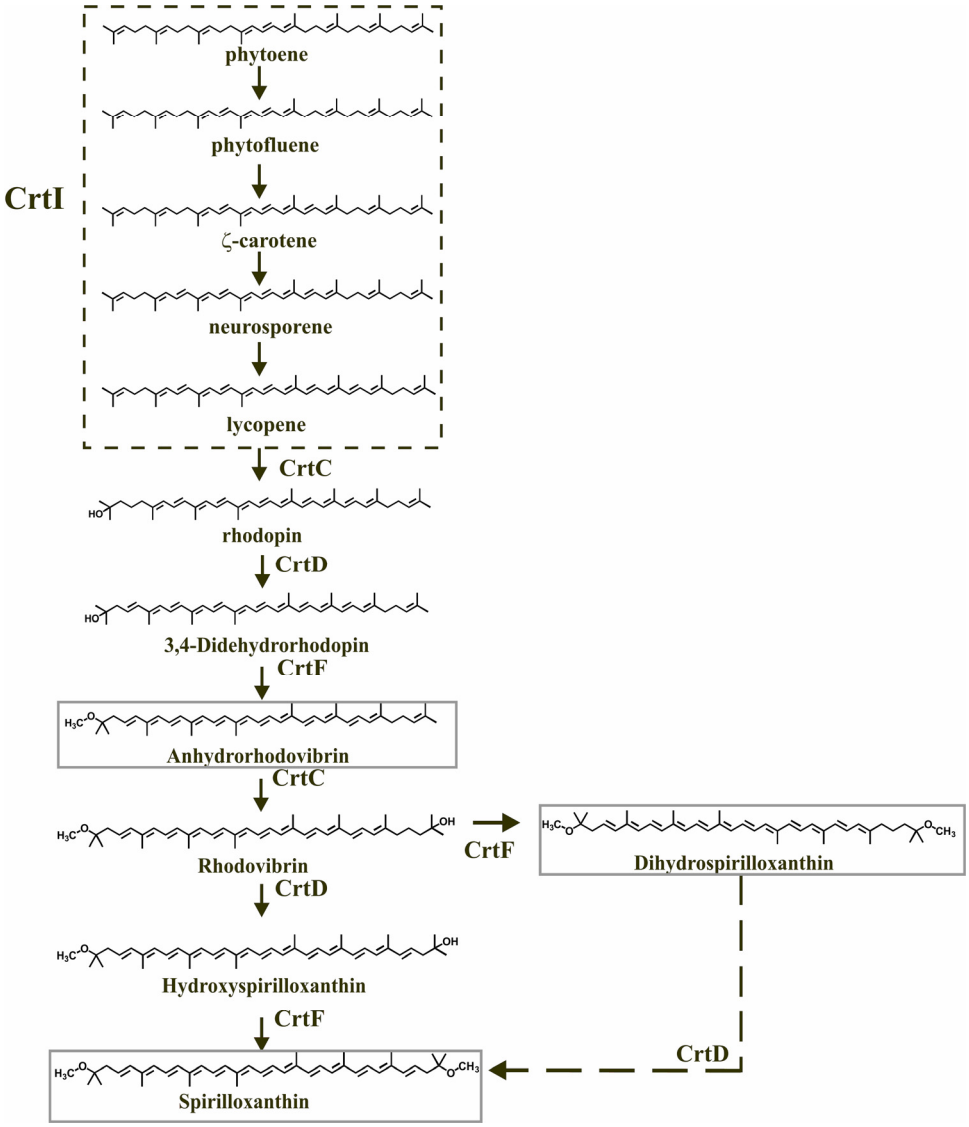

Fig. 64. Carotenoid biosynthesis in the wild-type under anaerobic conditions in dark (extended normal spx pathway)

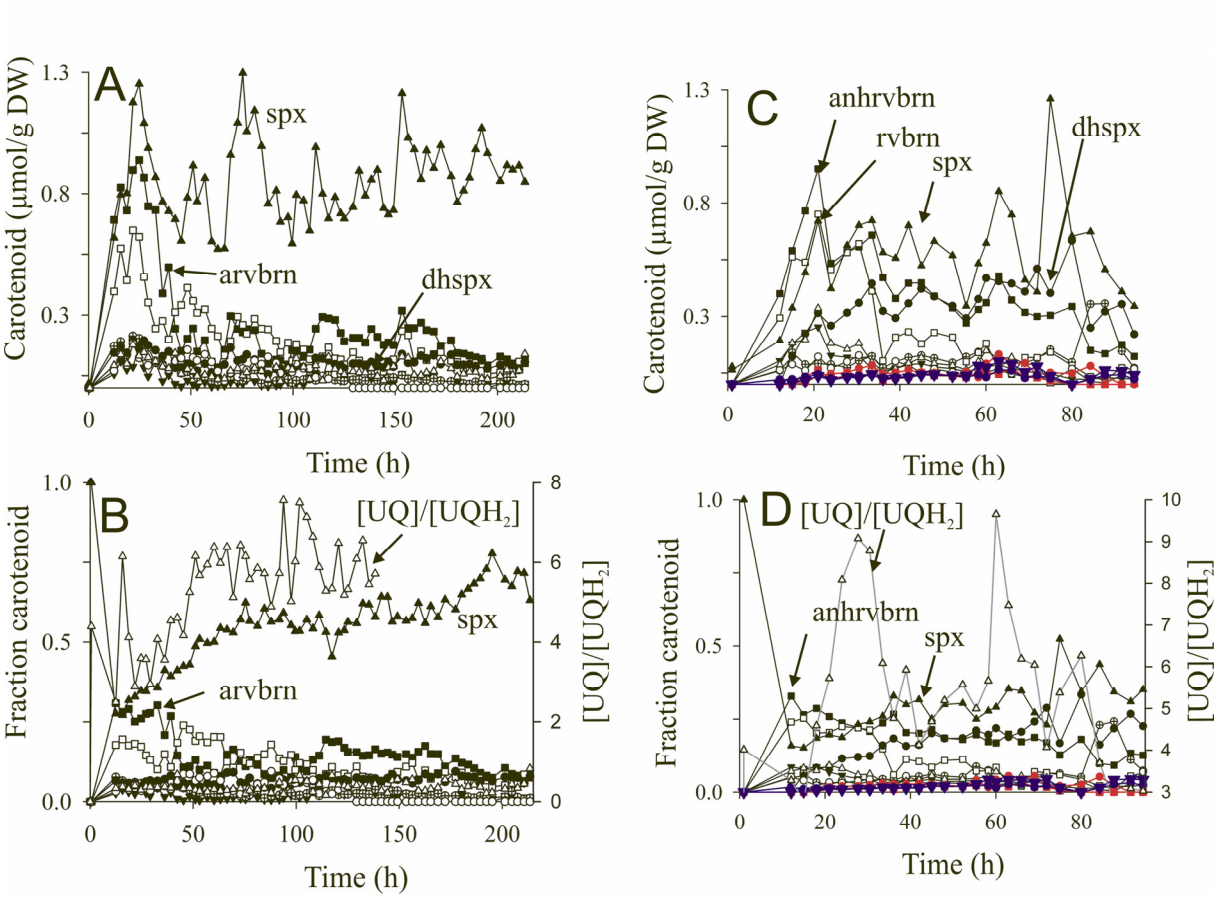

Fig. 65. (A) Primary data of carotenoid profile and (B) fraction carotenoid obtained from anaerobic fermentation. (C) Primary data of carotenoid profile and (D) fraction carotenoid obtained from microaerobic stirred bottle fermentation of the wild-type. spx (▲), rhodovibrin (■), rhodopin (ɵ), anhydrorhodovibrin (anhrvbrn) (□), dhspx (●), OH-spx (○), 3,4-didedyhrorhodopin (Δ), lycopene (▼), [UQ]/[UQH_2] (Δ), thspx (▼), 3,4-dihydroanhydrorhodovibrin(●), OH-dhspheroidene (■), chloroxanthin (●)

5.2 Carotenoid production in the wild-type applying an oxygen pulse

The carotenoid time courses of the wild-type obtained from the stirred bottle experiments can be seen on Fig. 65C, D. The abrupt breaks of the carotenoid profiles are partly due to the technical difficulties of sampling a liquid shake culture under argon. In our manual sampling procedure, it is very difficult to avoid the introduction of a small pulse of oxygen during sampling, which causes a rapid, though transient, slowing of carotenoid biosynthesis subsequent to the sampling event.

Regarding the intracellular total carotenoid levels, there were no notable differences between the anaerobic bioreactor and the stirred bottle fermentation. In contrast, the carotenoid composition showed large deviations from the anaerobic one.

First of all, the normal maturation process producing spx cannot take place in the presence of a significant oxygen level. Spx is not the only product as in absence of oxygen, but occurs at the same concentration level as anhydrorhodovibrin and dhspx. (Fig. 65C, D). Under microaerobic conditions the lycopene concentration is significantly higher and the rhodopin concentration is considerable lower than in anaerobic case, which indicates activity loss of CrtC.

In the presence of oxygen, numerous carotenoids were identified which were found earlier only in DPA-inhibited cultures. Since the oxygen pulse occurred after the induction of the carotenoid biosynthesis, the enzyme expression level was not affected by oxygen, only their activity. The oxygen pulses allow us to characterize the enzyme activity changes under microaerophilic conditions. The active pathways found in the wild-type in the presence of oxygen are shown in Fig. 66.

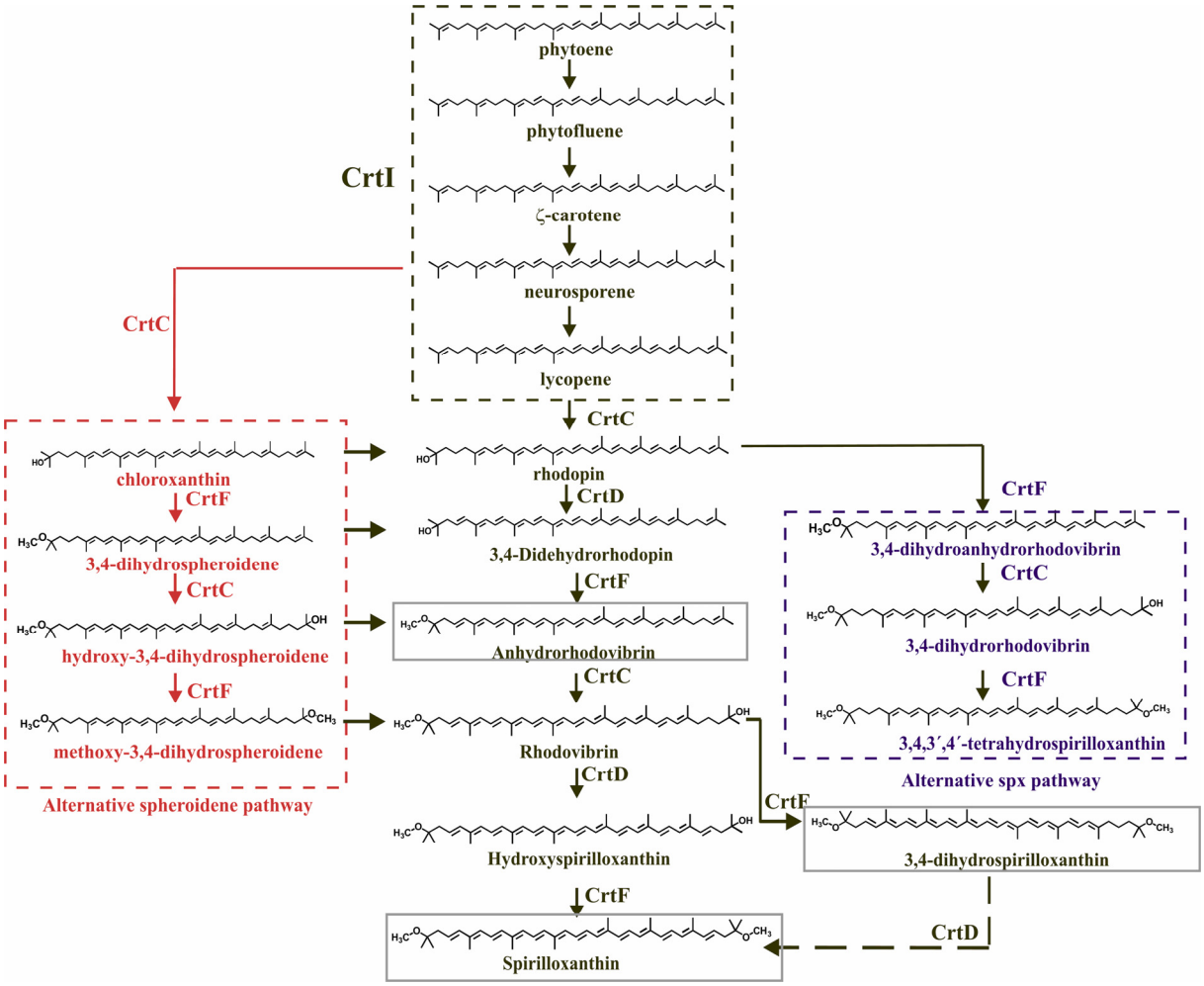

Fig. 66. Active carotenoid pathways in the wild-type after an oxygen pulse. Apart from the normal spx pathway two alternative pathways appear due to the effect of oxygen: the alternative spheroidene pathway and the alternative spx pathway.

Two new pathways opened up beside the usual "normal spx" pathway: the "alternative spheroidene" (Fig. 66 red) and the "alternative spx" (Fig. 66 viola) pathway. Remarkably, these two pathways do not use the enzyme CrtD. The alternative spx pathway corresponds to the one determined by Komori *et al.* (1998) starting with rhodopin and ending up with thspx. (Thspx was found only in traces in absence of oxygen.) The "alternative" spheroidene pathway origins from neurosporene, which is a substrate for hydroxylation by CrtC producing chloroxanthin (1-OH-neurosporene, Fig. 32 A, peak 8). Chloroxanthin can clearly act as a non-natural substrate for CrtF, evidenced by the appearance of 1′-OH-3,4-dihydrospheroidene (Fig. 32A). The latter product arises from the action of CrtC upon 3,4-dihydrospheroidene. However, 3,4-dihydrospheroidene was not observed, presumably because the CrtC-mediated reaction is much more efficient than that of CrtF under O_2-limiting conditions. A further

possible intermediate, 1´-methoxy-3,4-dihydrosperoidene, which could arise by the action of CrtF upon the last product, was not observed in this experiment.

The opening of the side pathways corresponds to the first oxygen pulse time. 3,4-dihydroanhydrorhodovibrin can be observed first as alternative carotenoid about 12 h (Fig. 67). The complete alternative pathways are observable starting from the 18 h time point according to the oxygen pulse.

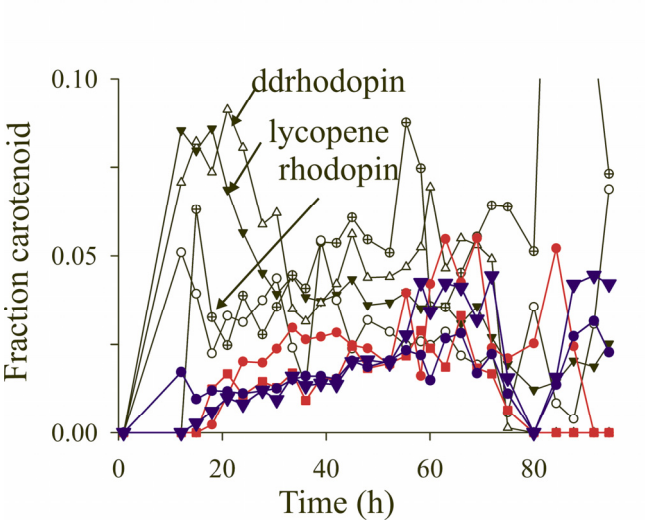

Fig. 67. Fraction carotenoid obtained from microaerobic wild-type fermentation: 3,4-didehydrorhodopin (ddrhodopin) (Δ), lycopene(▼), thspx (▼), 3,4-dihydroanhydrorhodovibrin(●), OH-dhspheroidene (■), chloroxanthin (●).

5.2.1 "Microaerobic" fermentation in the bioreactor applying a fructose pulse

The microaerobic carotenoid biosynthesis of the wild-type was also investigated in bioreactor experiments under different initially adjusted pO_2 values. The time courses of these fermentations are essential identical with the observations described in chapter 5.1.

The microaerobic biosynthesis of carotenoid was also investigated by applying fructose pulse in order to avoid oxygen limitation. During the fructose pulse oxygen cannot be excluded, therefore the oxygen availability increased temporarily, which could be observed also on the $[UQ]/[UQH_2]$ ratio (Fig. 68B). The changes in the UQ pool induced the carotenoid production at 65 h time point, resulting in a strong oscillation of the intracellular carotenoid concentration (Fig. 68A).

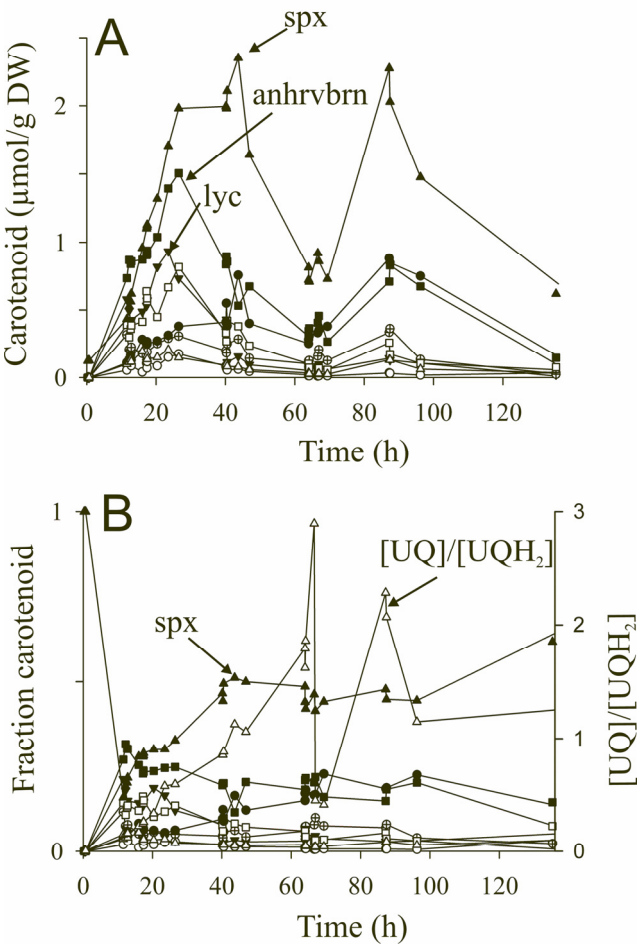

Fig. 68. (A) Primary data of carotenoid profile and (B) fraction carotenoid obtained from microaerobic fermentation (pO_2=0.05%) of the wild-type: spx (▲),rvbn (■),rhodopin (ɵ),anhrvbrn (□), dhspx (●),OH-spx(○), 3,4-ddhrhodopin (Δ), lycopene(lyc)(▼), $[UQ]/[UQH_2]$ (Δ)

5.3 Carotenoid production in ST4 following an oxygen pulse

The carotenoid production is also strongly inhibited in ST4 in the presence of oxygen, which can be seen in the low production rate, 0.033 µmol/g*h, during the whole experiment whereas the initial carotenoid production rate in the wild-type was 0.2 µmol/g*h. The carotenoid mutants struggle in the presence of oxygen, which can be seen not only in the carotenoid production but also in the slower cell growth of both, ST4 and SLYC18 (Fig. 62A).

The oxygen affected significantly the carotenoid composition of ST4. Fig. 32A shows a typical HPLC profile of extracted carotenoids present in ST4 cells growing exponentially under dark, semi-aerobic conditions. Three active pathways were identified in ST4 in the presence of oxygen. Nevertheless, consistent with the results of Komori *et al.* (1998), who extracted carotenoids from phototrophically-grown stationary-state cells, thspx is the major carotenoid at the end of the growth phase. Thus, under our growth conditions, we can detect clear evidence for two alternative pathways in addition to the major linear reaction sequence produced by the sequential action of the enzymes CrtC and CrtF upon lycopene (shown as the central block in Fig. 70).

The observation of the carotenoids 1-OH-3,4-didehydrolycopene (Fig. 32A, peak 5) and 1-methoxy-1´-OH-didehydrolycopene (Fig. 32A peak 3) indicates that an minor pathway (here designated the 3,4-didehydrolycopene pathway (Fig. 70, pathway in green)) is also operative under oxygen- limiting conditions. 1-methoxy-1´-OH-didehydrolycopene can be produced via three potential routes, two of which occur via a CrtI-mediated side reaction and one of which is due to the action of CrtF and CrtC on the CrtI-mediated intermediate 1-OH-3,4-didehydrolycopene (Fig. 70). The CrtI-mediated reactions are probably minor (as the main thspx pathway is predominant), so we propose that the concerted action of CrtF and CrtC on 1-OH-3,4-didehydrolycopene is the principle pathway. The latter product was substrate for CrtC and CrtF as well resulting 1,1´-dihydroxy-3,4-didehydrolycopene and 1-methoxy-3,4-didehydrolycopene, respectively. Finally, 1,1´-dihydroxy-3,4-didehydrolycopene was converted by CrtF to the last member of the pathway, 1´-hydroxy-1-methoxy-3,4-didehydrolycopene. The presence of these metabolites is the new proofs for the low substrate specificity and the combinatorial behaviour of the carotenogenic enzymes (Fig. 70).

However, the obligatory intermediate of this latter pathway, 1-methoxy-3,4-didehydrolycopene, was not detected, presumably because the CrtC-mediated reaction is faster than the CrtF reaction under oxygen-limited conditions (see below). In contrast, Komori *et al.* (1998) detected only 1,1´-diOH-lycopene as a minor component in the carotenoid

extracts from anaerobic, phototrophically-grown ST4 cells. However, in our experiments (using semi-aerobically-grown ST4 cells) this latter intermediate was not observed. We hypothesize that this difference is due to the different growth conditions employed in the study of Komori *et al.* (1998) and those reported here.

We deduce that the 3,4-dehydrogenation step, in the absence of CrtD, which normally catalyzes this reaction *in vivo*, is due to the action of CrtI, since this is the only carotenoid desaturase present in the strain ST4. In fact, several groups (Schwerzmann and Bachofen, 1989; Albrecht *et al.,* 2000) have shown that fungal CrtI overexpressed in *E. coli* can catalyze a 3,4- as well as 3´,4´-desaturation step, though very inefficiently. Although the desaturation of a lycopene derivative containing a 1- or 1´-tetrahedral substituent (e.g. rhodopin, which possesses a 1-hydroxy-substituent) has to our knowledge not been reported so far, the observation of 1-OH-3,4-didehydrolycopene is evidence that the *R. rubrum* CrtI can perform this reaction, albeit at very low levels. The absence of 3,4-didehydrolycopene in both ST4 and the lycopene-producing mutant SLYC18, suggests that, under our growth conditions, the direct dehydrogenation of lycopene by CrtI does not occur. Nevertheless, it seems also likely that the methoxy-derivatives of rhodopin can also be dehydrogenated by CrtI. We therefore have indicated putative CrtI-mediated branch points connecting the major pathway to the minor 3,4-didehydrolycopene pathway in Fig. 70.

The HPLC profile of cell extracts of the lycopene-producing mutant SLYC18 (Fig. 32B) provides an interesting control experiment. Since this mutant lacks both CrtC and CrtD, none of the carotenoids beyond lycopene can be present. The HPLC profile indeed shows lycopene as the only major carotenoid present (Fig. 32B, peak 11), although very low amounts of neurosporene are also observable (very minor peak situated to the right of peak 11 in Fig. 32B). It has been shown recently that lycopene in SLYC18 is sequestered exclusively in the LH1 complexes immediately following its production by CrtI and does not accumulate on the carotenoid biosynthetic complex (Wang *et al.,* 2012). Thus, the presence of the alternative spheroidene pathway in ST4 is presumably due to the accumulation of lycopene on CrtI during oxygen-limiting conditions, which is due to product inhibition of the enzyme, and causes a small amount of neurosporene to be released for further biosynthetic processing.

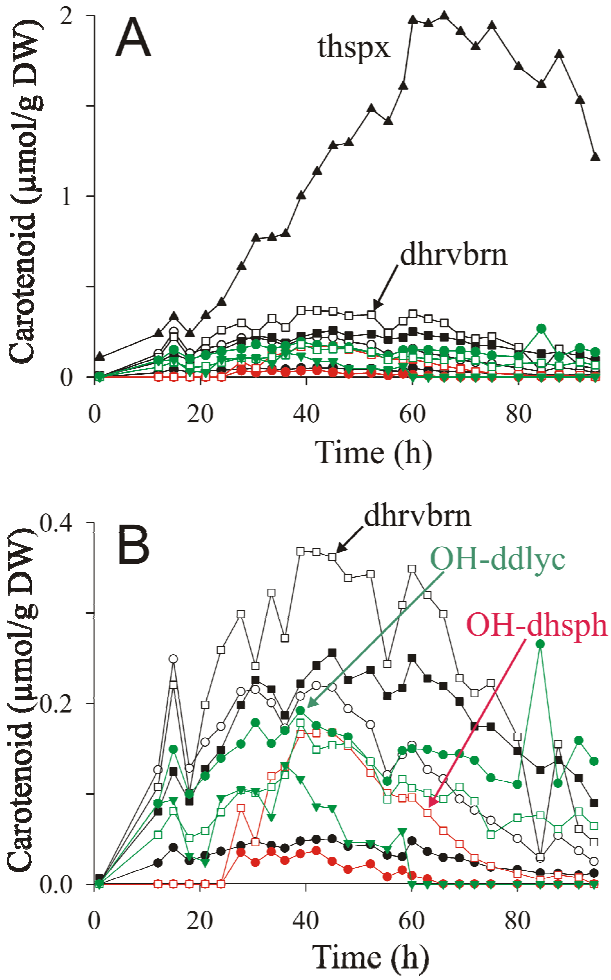

Fig. 69. Primary data for dynamic changes of various carotenoid species as derived from LC-MS data from extracts of ST4 obtained at various at time points of a semi-aerobic growth curve performed under an argon atmosphere: thspx (▲); 3,4-dihydrorhodovibrin (dhrvbn) (□); rhodopin (○); 3,4-dihydroanhydrorhodovibrin (■); lycopene (●); chloroxanthin (●); 1´-OH-3,4-dihydrospheroidene (OH-dhsph) (□); 1 -OH-3,4-didehydrolycopene (OH-ddlyc) (●); 1-methoxy-1´-OH-didehydrolycopene (□); 1,1´-diOH-3,4- didehydrolycopene (▼).

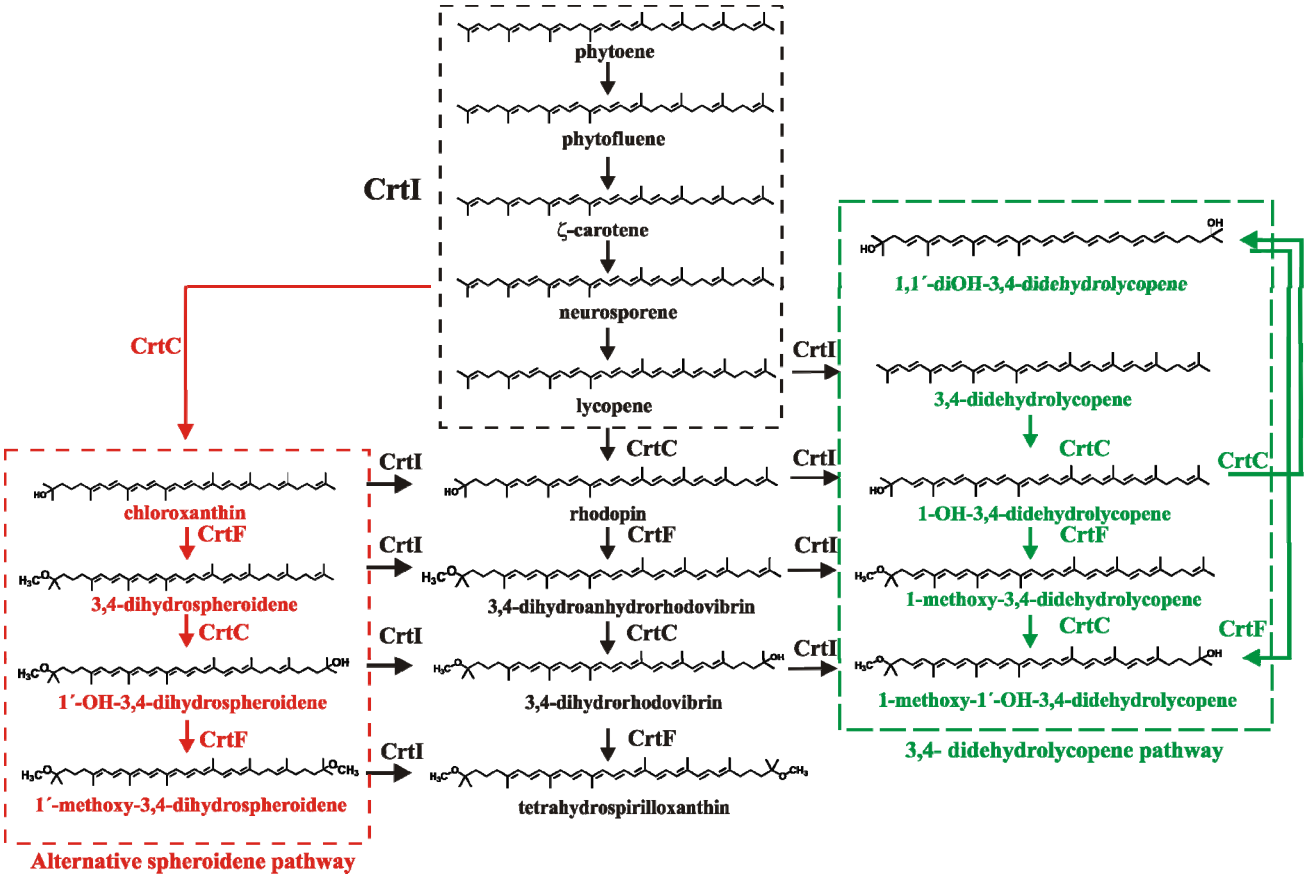

Fig. 70. Active carotenoid biosynthetic pathway in mutant ST4 under microaerobic conditions

Comparison of the position of the trough for thspx (at 18 h) and the appearance of the carotenoid intermediates in Fig. 71A,B shows that the highest intermediate of the main thspx pathway at 18 h corresponds to rhodopin (the third intermediate prior to thspx), followed closely by 3,4-dihydrorhodovibrin (the first intermediate prior to thspx), whereas the second intermediate prior to thspx, 3,4-dihydroanhydrorhodovibrin, is somewhat lower in fractional concentration at this time point. This apparently contradictory appearance of intermediates in a linear pathway indicates that the CrtF-mediated reactions are limiting compared to the CrtC-mediated reactions, thus causing a build-up (at early times) of the appropriate intermediates. This hypothesis is also consistent with the low concentration of lycopene, which is rapidly converted to rhodopin by an efficient CrtC-mediated reaction (Fig. 71B).

The accumulation of the 3,4-dihydroanhydrorhodovibrin and 3,4-dihydrorhodovibrin on the main pathway would explain the "spillover" into the minor 3,4-didehydrolycopene pathway, presumably due to the action of CrtI upon these intermediates. Although the role of CrtI in this context has not been demonstrated unambiguously, in the absence of CrtD, CrtI is the only carotenoid desaturase present in the genome which might catalyze the cross-over reactions to the side pathway.

At the 18 h time point, the fractional levels of 1,1´-diOH-3,4-didehydrolycopene and 1-OH-3,4,-didehydrolycopene are closely similar, which again suggests that the CrtF-mediated reaction (here leading to 1-methoxy-3,4-didehydrolycopene) is rate limiting. However, at late times, the intermediate 1,1´-diOH-3,4-didehydrolycopene falls to undetectable levels, presumably due to CrtF-mediated methylation to form 1-methoxy-1´-OH-3,4-didehydrolycopene (Fig. 70). The latter intermediate remains at low but significant levels until the end of the growth curve, as does the first minor pathway intermediate, 1-OH-3,4-didehydrolycopene. In contrast, the CrtF-mediated intermediate, 1-methoxy-3,4-didehydrolycopene was not detected, presumably because low levels of this carotenoid are rapidly removed by the efficient CrtC-mediated reaction step (Fig. 70). In summary, these observations indicate that CrtF possesses “end" specificity, as is also indicated by the analysis of the thspx major pathway, even though the enzyme can act combinatorially.

The alternative spheroidene pathway was found to be also active after the oxygen pulse. The appearance of the alternative spheroidene pathway (Fig. 70, pathway in red), implies that most or all of the intermediates are still possible substrates for CrtI, since thspx is still produced as the major carotenoid in the late phase of growth (see below for a description of the dynamics of the system).

Interestingly, the minor alternative spheroidene pathway (Fig. 70, red) in ST4 as well as in the wild-type appears only after the other pathways are decaying. In this context, it is significant that neurosporene was hardly detected, despite the fact that this intermediate is an obligatory precursor for the alternative spheroidene pathway. The experiments here with ST4 indicated that lycopene begins to accumulate at about 18 h, and thus may also act as the product inhibitor of CrtI, thereby leading to the release of small amounts of neurosporene, which is immediately converted (via CrtC) to chloroxanthin. This low level channelling initiates the alternative spheroidene pathway, which ultimately is rechannelled into the thspx pathway via CrtI at the level of 1' -OH-3,4-dihydrospheroidene (as indicated by its accumulation with respect to chloroxanthin) (Fig. 71B). A further possible intermediate, 1´-methoxy-3,4-dihydrospheroidene was not found, which would be consistent with the higher "end specificity" of CrtF in comparison to CrtC.

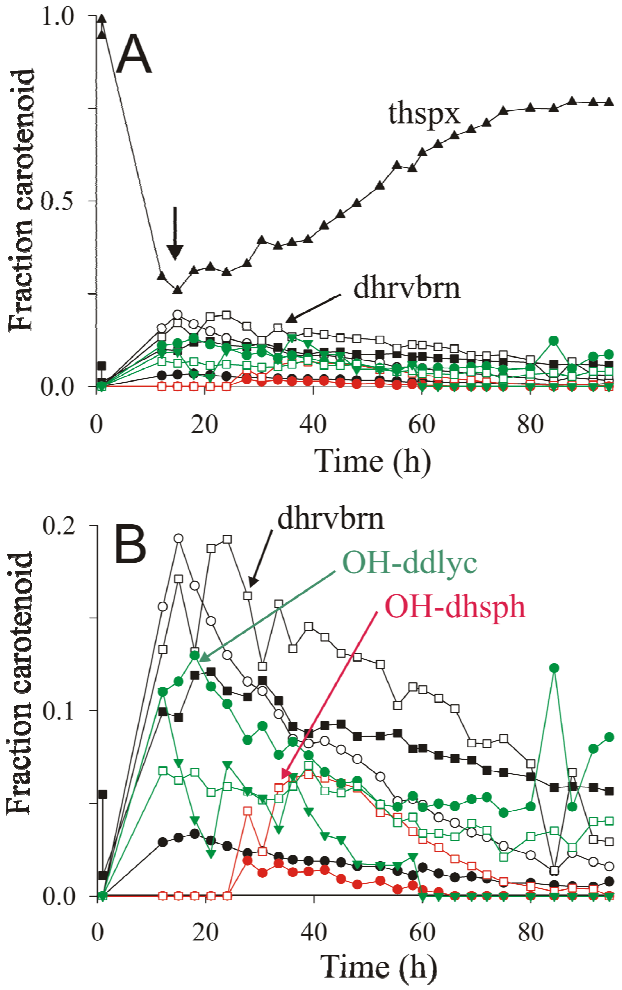

Fig. 71. The fractional profiles of carotenoid dynamics calculated from the primary dynamic data thspx (▲); 3,4-dihydrorhodovibrin (dhrvbn) (□); rhodopin (○); 3,4-dihydroanhydrorhodovibrin (■); lycopene (●); chloroxanthin (●); 1´-OH-3,4-dihydrospheroidene (OH-dhsph) (□); 1 -OH-3,4-didehydrolycopene (OH-ddlyc) (●); 1-methoxy-1´-OH-didehydrolycopene (□); 1,1´-diOH-3,4- didehydrolycopene (▼)

5.4 SLYC18, lycopene production applying an oxygen pulse

The strain SLYC18 was fermented in the bioreactor under different oxygen concentrations. The lycopene time course under anaerobic conditions was similar to the one measured also under anaerobic conditions in the wild-type (Fig. 72). The carotenoid production under "microaerobic" conditions in all SLYC18 fermentation resulted in 33-50 % loss of carotenoid compared to the anaerobic fermentation (Table 13**)**. The peak lycopene concentration (7 µmol/g) was almost two times higher under anaerobic conditions than in the presence of oxygen (4 µmol/g).

The carotenoid production of SLYC18 under microaerobic conditions can be seen in Fig. 72B. The lycopene concentration shows a small oscillation. Since the second induction of the carotenoid biosynthesis occurs directly after the adjustment of the pO_2 to 0.25% (49 hours), the oscillation occurs probably due to varied oxygen availability.

After applying an oxygen pulse to the stirred bottle, the lycopene concentration drops from 3 to 2 µmol/g directly after the oxygen pulse and stays constant until the oxygen is consumed and accordingly the $[UQ]/[UQH_2]$ ratio is low. In the absence of the repressing oxygen SLYC18 is able to start the carotenoid production again and reaches the "microaerobic" lycopene saturation at 4µmol/g (Fig. 72C).

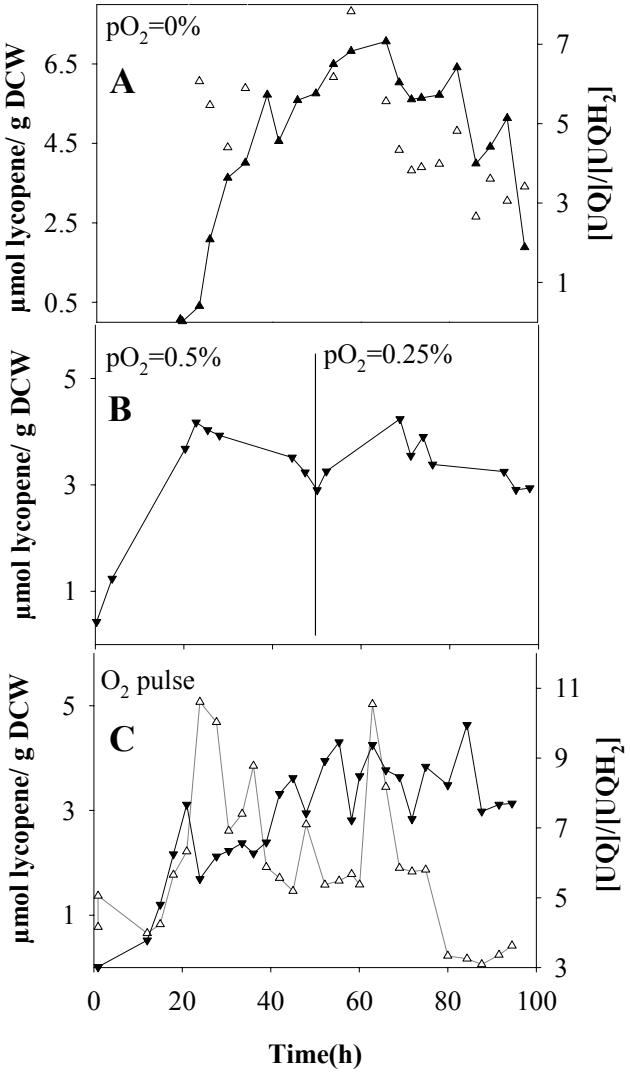

Fig. 72. Lycopene time courses at several oxygen concentrations in the bioreactor obtained from the strain, SLYC18: lycopene (▲), $[UQ]/[UQH_2]$ (Δ).

5.5 Competitive isoprenoid pathways

As described in chapter 1.3.2, a branch point occurs downstream from the MEP pathway at the metabolite GGPP (Fig. 14). The branch point opens up several pathways, such as carotenoid, isoprenoid-quinone and BChl biosynthesis. In order to investigate whether the isoprenoids are regulated together (e.g. regulated input flux from the MEP pathway) the concentration changes of the isoprenoids should be analyzed. The applied HPLC-MS method provided information about the other metabolites (beside carotenoids) occurring in the competitive pathways.

Four different isoprenoid-quinones (UQ-10, UQ-9, RQ-10, RQ-9) were measured in order to quantify the activity of the isoprenoid biosynthesis. In order to follow the activity of the BChl biosynthesis A_{880} and BPh*a* concentrations were measured.

Under anaerobic conditions the time courses of the isoprenoids follow the carotenoid time course in the wild-type as well as in SYLC18 (Fig. 73). The time courses of the isoprenoid pathways obtained from microaerobic fermentation showed also common dynamics for all isoprenoids (data not shown). These results suggest a common regulation for the biosynthesis of these PM compounds under semiaerobic-turnover conditions.

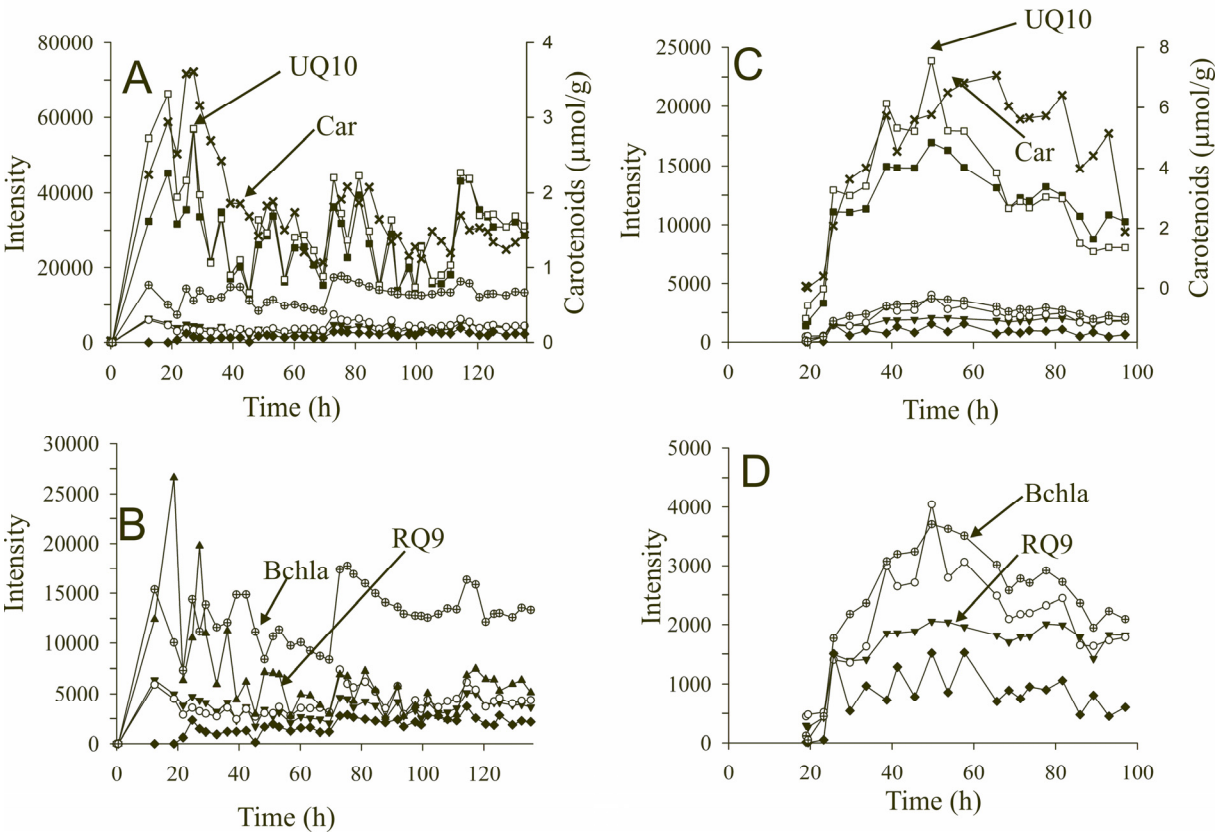

Fig. 73. Time courses of competitive isoprenoids in the wild-type under anaerobic conditions (pO_2=0.05%) of the wild-type: UQH_2-10 (▲), RQ-10 (■), BChl*a* (ɵ), Carotenoids (Car) (**X**), BPh*a* (●), UQ-9 (○), RQ-9 (▼).

5.6 Discussion

The characterization of the carotenoid biosynthesis in *R. rubrum* strains was investigated in M2SF medium, in the dark. The induction of the carotenoid biosynthesis showed essentially identical dynamics in all strains. The high resolution time courses allowed the characterization of the dynamics of the carotenoid biosynthesis during the induction phase and led to the determination of a strong bottleneck at the reactions of CrtD. Furthermore, the second reactions of the enzymes seem also to be significantly slower than the first ones.

The [UQ]/[UQH_2] ratios were the same in all experiments, only the oxygen pulse induced temporary changes in the UQ pool due the oxydases. After consuming oxygen rapidly, the UQ pool became reduced again inducing again the carotenoid biosynthesis.

Oxygen inhibited CrtD, which resulted in side pathways lacking double-bonds on the 3,4;3´,4´-positions. Furthermore, the ratio between spx, dhspx and anhydrorhodovibrin was also affected by oxygen, and all the methoxylated carotenoids occurred in the same concentrations. These results are in accordance with the observations that the characteristic spectrum of the cells growing in presence of oxygen does not correspond to solely the spectrum of spx, but is a mixture of these three carotenoids.

The carotenoid mutants were significantly more sensitive to the oxygen concentration than the wild-type. The growth rate and the carotenoid production in stirred bottle showed that the wild-type survives more easily in the presence of oxygen. The wild-type consumes the oxygen first, and then starts to produce carotenoids. In contrast, the carotenoid mutants, which produce carotenoids at low level also in the presence of oxygen, and therefore they are somehow inhibited in growth (Fig. 62B).

Table 13 contains the peak carotenoid concentrations under different oxygen availability. The maximal intracellular carotenoid concentration was measured in SLYC18 in absence of oxygen, whereas in the wild-type at pO_2 = 0.05%, which confirms the higher sensitivity of the carotenoid mutants to oxygen (Table 13).

The biosynthesis of other isoprenoids is found to be synchronized with the carotenoid production indicating that the inducing signal is the same for each pathway.

Strain	pO_2	pathway	$c_{Total\ car.\ peak}$	$c_{end\text{-}peak}$	$t_{car.\ peak}$	Init.car. flux	oscillation
	[%]	-	[µmol/gDW]	[µmol/g]	[h]	[µmol/g*h]	-
S1	0	1	3.6	1.25	24.7	0.15	small
	0	1	3.8	1.6	21	0.13	small
	0.05	1	6	1.9	26.5	0.23	large
	-	1,2,3	3.7	0.72	21	0.18	-
	-/p	1	4.5	1	31.6	0.14	large
ST4	-/p	2,3,4	3.1	2	60	0.05	-
	-	2,3,4	2.2	0.62	30	0.07	-
SLYC18	0	1	7	7	45	0.15	-
	0.6	1	4.17	4.17	22.75	0.18	small
	0.45	1	4.3	4.3	20.7	0.21	-
	0.3	1	2.28	2.28	49	0.05	-
	-	1	3.1	3.1	21	0.15	small
	-/p	1	4.2	4.2	44	0.1	-

Table 13. Carotenoid production in different *R. rubrum* strains under varied oxygen availabilities. 1-normal spx pathway, 2- alternative spx pathway, 3- alternative spheroidene pathway, 4-3,4-didehydrolycopene pathway, p = oxygen pulse

6 Dynamic modelling of carotenoid biosynthesis

The induction of carotenoid biosynthesis shows essentially identical dynamics in all strains. The high resolution time courses of the carotenoid intermediates allowed the characterization the dynamics of the carotenoid biosynthesis under different oxygen availabilites. The observed oscillation in the intracellular carotenoid concentration after an oxygen pulse in the anaerobic bioreactor suggests the UQ pool redox state is a possible regulator for the carotenoid biosynthesis. In order to analyse the regulation inducing the oscillating carotenoid concentration, mathematical investigations of the carotenoid biosynthesis were carried out with different dynamic models.

The model structures were based on the observations that each strain produces different amounts of carotenoid. SLYC18 produces 4 µmol/g, whereas ST4 3.1 µmol/g, and the wild-type carotenoid peak concentration measured was 6 µmol/g (Table 13). Furthermore, the similar end products, spx and thspx reached similar peak concentrations (2µmol/g) in the wild-type and in ST4 (Fig. 68A and Fig. 69A). Lycopene structurally differs significantly from spx and thspx and reaches a higher peak concentration (Fig. 72) than the doubly-methoxylated ones.

Considering these results an endogenous regulation of the carotenoid pathway would be the obvious choice. The similar peak concentration of the structurally similar carotenoids hints at an end-product feedback regulation, which is weaker in the case of lycopene. Therefore, an endogenous regulation following Hill kinetics could be assumed for the carotenoid producing linear reaction sequence.

In addition, according to the literature, two further hypotheses were proposed for the regulation of the carotenoid pathway (Fig. 74):

1. Feedback inhibition of the end product carotenoid on the first reaction of the pathway (Bramley, 2002; Bachmann, 2002).
2. Non-specific inhibition of the total carotenoids via changing the dielectric constant of the photosynthetic membrane (Gruszecki and Strzalka, 2005).
3. Regulation takes place due to an external signal (e.g. UQ pool redox state or regulation of the MEP pathway) affecting the flux on the terpenoid backbone pathway resulting in a pulsed feeding into the carotenoid pathway (Rodri *et al.*, 2002).

Each hypotheses corresponds to a model variant. The ability of the model variants to explain the measurement data allows the compatibility of the hypotheses with the experimental observations to be assessed.

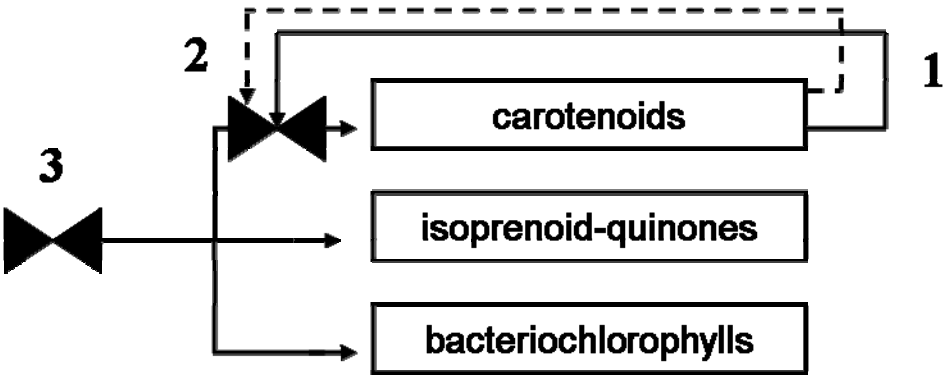

Fig. 74. Potential regulation mechanisms according to the literature (Bramley, 2002; Bachmann, 2002; Gruszecki and Strzalka, 2005; Rodri *et al.*, 2002)

6.1 Introduction of the dynamic carotenoid biosynthesis model

In the case of the wild-type, the model consists of reactions of the "extended normal" spx pathway starting with the reaction of CrtI (Fig. 76). The reactions are described with mass action kinetics as irreversible reactions providing one rate coefficient for each reaction.

The model consists of ordinary differential equations (Fig. 75) which describe the concentration changes of the metabolites. The concentration changes are described as the difference of the producing and consuming reaction as well as dilution. The dilution term is introduced due to bacterial growth.

The first reaction of the carotenoid pathways is the production of phytoene. Since phytoene occurs in traces, its conversion to lycopene must be very fast, therefore the reactions of CrtB and CrtI can be considered as one reaction. The consecutive reactions of CrtI are considered also as one reaction, since neurosporene, the only intermediate measured, occurred only in traces.

$$\frac{dc_{lycopene}}{dt} = k_{CrtI} \cdot k_{input} - k_{CrtC_1} \cdot c_{lycopene} - k_{dil} \cdot c_{lycopene}$$

$$\frac{dc_{rhodopin}}{dt} = k_{CrtC_1} \cdot c_{lycopene} - k_{CrtD_1} \cdot c_{rhodopin} - k_{dil} \cdot c_{rhodopin}$$

$$\frac{dc_{didehydrorhodopin}}{dt} = k_{CrtD_1} \cdot c_{rhodopin} - k_{CrtF_1} \cdot c_{didehydrorhodopin} - k_{dil} \cdot c_{didehydrorhodopin}$$

$$\frac{dc_{anhydrorhodovibrin}}{dt} = k_{CrtF_1} \cdot c_{didehydrorhodopin} - k_{CrtC_2} \cdot c_{anhydrorhodovibrin} - k_{dil} \cdot c_{anhydrorhodovibrin}$$

$$\frac{dc_{rhodovibrin}}{dt} = k_{CrtC_2} \cdot c_{anhydrorhodovibrin} - k_{CrtF_{2a}} \cdot c_{rhodovibrin} - k_{CrtD_2} \cdot c_{rhodovibrin} - k_{dil} \cdot c_{rhodovibrin}$$

$$\frac{dc_{hydroxyspirilloxanthin}}{dt} = k_{CrtD_2} \cdot c_{rhodovibrin} - k_{CrtF_2} \cdot c_{hydroxyspirilloxanthin} - k_{dil} \cdot c_{hydroxyspirilloxanthin}$$

$$\frac{dc_{spirilloxanthin}}{dt} = k_{CrtF_2} \cdot c_{hydroxyspirilloxanthin} - k_{dil} \cdot c_{spirilloxanthin}$$

$$\frac{dc_{dihydrospirilloxanthin}}{dt} = k_{CrtF_{2a}} \cdot c_{rhodovibrin} - k_{CrtD_{2a}} \cdot c_{dihydrospirilloxanthin} - k_{dil} \cdot c_{dihydrospirilloxanthin}$$

Fig. 75. The reaction of the extended spx pathway described with mass action kinetics

Enzyme	Ref	Substrate	Km [(μM)]	Vmax [nmol mg protein -1 h-1]
CrtI	1	phytoene	14.8	5.2
		neurosporene	33.1	0.6
CrtC	2	neurosporene	38.5	2.73
		lycopene	26.9	0.54
		1-hydroxy-neurosporene	36.8	0.78
		spheroidene	7.8	4.92
CrtD	3	1-hydroxy-neurosporene	25	1.35
		1-hydroxy-lycopene	19	0.58
		1,1´-dihydroxy-neurosporene	40	0.69
CrtF	4	1-methoxy-demethyl spheroidene	26.6	-

Table 14. Kinetic parameters of the carotenoid biosynthetic reactions ([1]Stickforth and Sandmann, 2011; [2]Steiger *et al*., 2003, [3]Steiger *et al.*, 2000, [4]Badenhop *et al*., 2003)

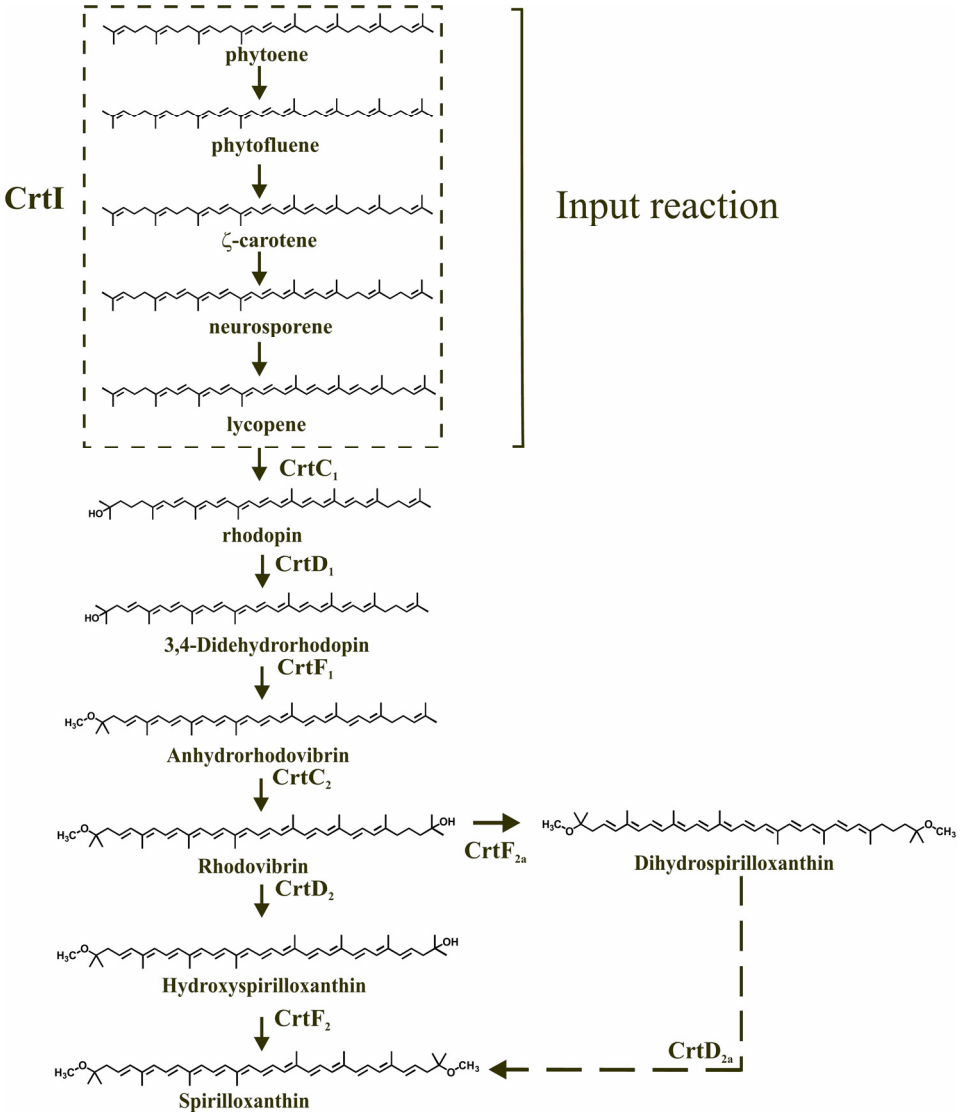

Fig. 76. Reaction path of the "extended normal spx" pathway. The reaction IDs are indicated.

The enzymes have been biochemically characterized in *Rb. sphaeroides* and *Rvi. gelatinosus* (details in chapter 1.3.6). The kinetic parameters of the biosynthetic enzymes are shown in Table 14. Based on the K_m values, a low substrate concentration interval can be defined, where the reaction mechanism can be described with mass action kinetics. *In vivo* the total carotenoid concentration is about 4 µM in the cell and the concentrations of the precursors are even lower. Therefore, the use of the mass action kinetics in the model gives an appropriate approximation.

The data sets contain the concentrations of the intermediate and the end product carotenoids. As initial conditions, all intermediate carotenoid concentrations were set at 0.001µmol/g, since the aerobic inocula contain hardly any carotenoids. The initial time point of the model was set to 12 h time point of the experiments, since the consumption of the repressing oxygen

takes approximately 12 h. Therefore, the initial value of spx corresponds to the value of the 12 fermentation time point.

The many steps in the data generation, such as sampling, extraction and HPLC analysis resulted in a significantly high standard deviation. Since the different carotenoids occur at different concentration levels, the metabolites with higher concentrations are affected less by this error. According to the detection accuracy of each substance, some of the carotenoids can be designated as "accurate" metabolites. These metabolites provide more information than the other ones occurring in traces. During the analysis of the fits, the accurate metabolites are considered first and foremost. The "accurate" metabolites vary among the different strains and are listed in Table 15.

wild-type	total carotenoid, spx, anhydrorhodovibrin, dhspx, lycopene
ST4	total carotenoid, thspx, 3,4-dihydroanhydrorhodovibrin, 3,4-dihydrorhodovibrin, lycopene
SLYC18	lycopene

Table 15. Carotenoids in the different *R. rubrum* strains providing accurate data

In order to identify the reaction parameters, the different model scenarios were fitted on the measured carotenoid time courses. During the fitting procedure the sums of squared error (SSE) is minimized using the Trust region method, which is a gradient-based method with robust convergence properties, therefore it is a standard tool for optimization. The Trust region method searches for a local minimum, which is in our case appropiate, since the initial values can be reasonably defined. According to the concentrations of each carotenoid, we can imply the initial kinetic parameter for the model. The k_{CrtI} value was determined experimentally and can be used as a reference point. The goodness of the fits was ranked by the value of χ^2/N.

This basic model is now extended by implementing the three hypotheses. The resulting model variants are tested against the experimental data.

6.2 Negative feedback regulation with Hill kinetics

A well-known Hill-type equation was used to describe the negative feedback regulation of the end product and the total carotenoid concentration:

$$v_{inhibition} = \frac{1}{\left(\frac{I}{K_{inh}}\right)^{n} + 1}$$

I is the inhibitor concentration and *n* is the Hill coefficient, which determines the steepness of the input function. K_{inh}, the repression coefficient, is the inhibitor concentration of the half-maximal repression.

6.2.1 End-product and total carotenoid product feedback inhibition in wild-type

Applying Hill kinetics, a negative feedback effect of the end product (spx) was assumed. The reaction of CrtI is modified depending on the spx concentration:

$$\frac{dc_{lycopene}}{dt} = k_{CrtI} \cdot \frac{1}{\left(\frac{c_{spx}}{K_{inh}}\right)^{n} + 1} - k_{CrtC_1} \cdot c_{lycopene} - k_{dil} \cdot c_{lycopene}$$

The model was fitted to both the anaerobic and the microaerobic fermentation data of the wild-type.

The model follows the dynamics of the precursors very well, but the input flux (total carotenoid concentration) is underestimated (Fig. 77). The model is not able to describe the dynamics of spx, since the model spx value increases with a significant delay compared to the data spx values. Furthermore, a small oscillation can be seen in the spx concentrations, which cannot be described with the product inhibition model.

The model containing the anaerobic parameter could not describe the microaerophilic time courses. Therefore, all parameters were refitted on the microaerobic data. The new fits could describe the precursor very well including a small delay observed for spx. Furthermore, the model was not able to describe the second carotenoid peak in the spx time course, which leads to the conclusion, that the oscillation is not the result of an inhibition following Hill kinetics. (Fig. 78).

Interestingly, the microaerobic K_{inh} is significantly higher than the anaerobic one (Table 16). The higher K_{inh} values under microaerobic conditions suggests that in the absence of oxygen an additional regulation takes place, resulting in a lower carotenoid concentration. This lower concentration is manifested in a lower K_{inh} in the model.

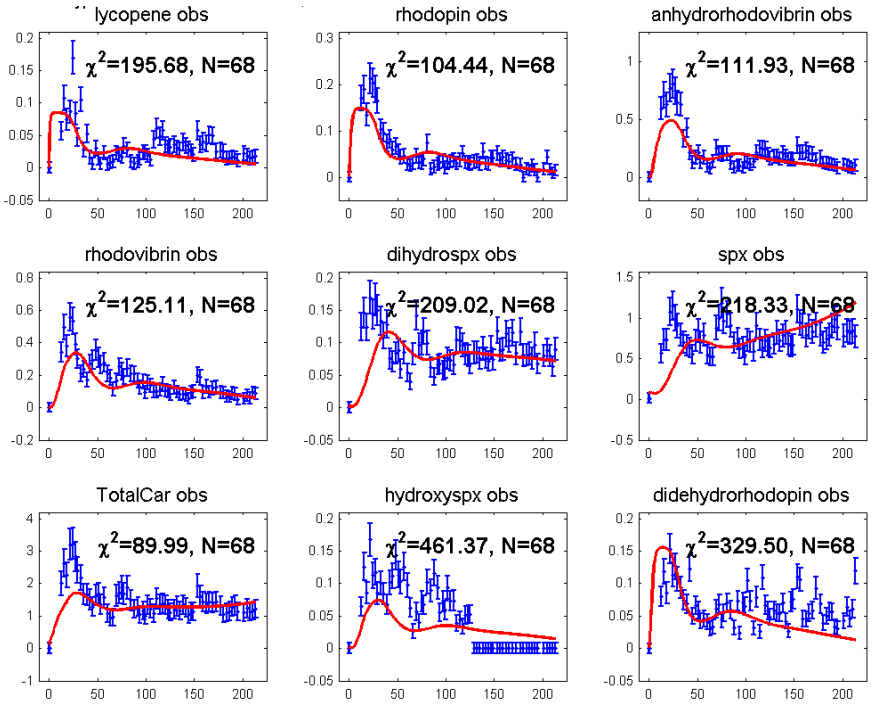

Fig. 77. Spx feedback inhibition following Hill kinetics in the wild-type (χ^2/N= 3.02) growing under anaerobic conditions

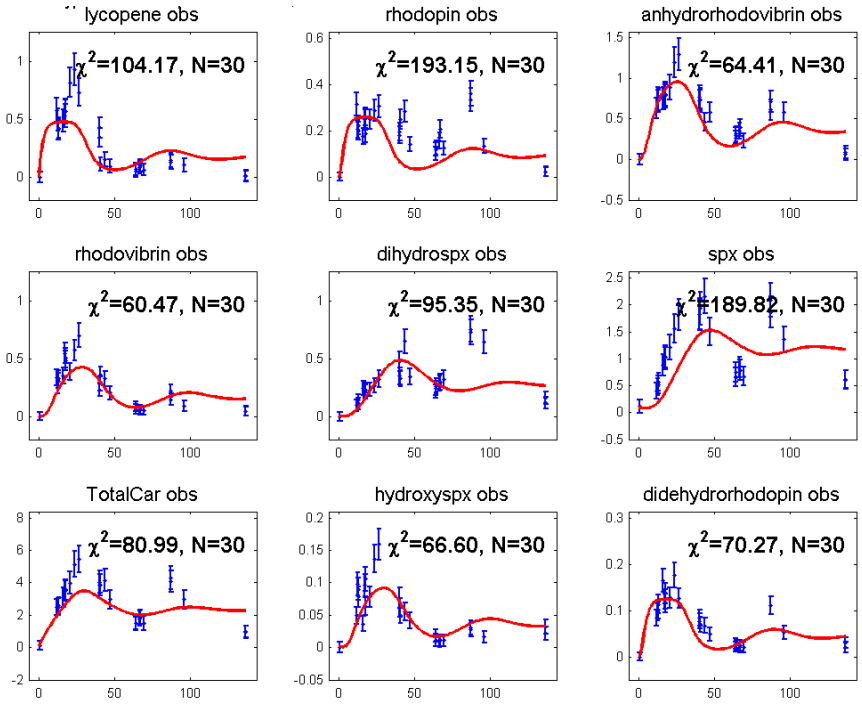

Fig. 78. Spx feedback inhibition following Hill kinetics in the wild-type (χ^2/N= 3.48) growing under microaerobic conditions

enzyme	anaerobic	microaerobic
CrtI	0.111	0.185
$CrtC_1$	1.268	0.375
$CrtD_1$	0.679	0.639
$CrtF_1$	0.607	1.288
$CrtC_2$	0.141	0.136
$CrtF_{2a}$	0.0287	0.104
$CrtD_2$	0.128	0.177
$CrtD_{2a}$	0.025	0.033
$CrtF_2$	0.539	0.782
K_{inh}	**0.531**	**1.158**
n	3.27	6.62

Table 16. Model parameters for the case of spx Hill inhibition

The inhibition of the other end product, dhspx, was also investigated. The feedback inhibition term consisted of two Hill equations (spx and dhspx):

$$\frac{dc_{lycopene}}{dt} = k_{CrtI} \cdot \frac{1}{\left(\frac{c_{spx}}{K_{inh1}}\right)^n + 1} \cdot \frac{1}{\left(\frac{c_{dhspx}}{K_{inh2}}\right)^n + 1} - k_{CrtC_1} \cdot c_{lycopene} - k_{dil} \cdot c_{lycopene}$$

According to the fit of the double- inhibitor model, the inhibition of dhspx does not affect the system, since the K_{inh} value turned out to be extremely high.

Since we cannot exclude that all the carotenoid show inhibitory behavour, the negative feedback inhibition of the total carotenoid was also modelled with Hill kinetics, where the changes of the lycopene concentration can be described as follows:

$$\frac{dc_{lycopene}}{dt} = k_{CrtI} \cdot \frac{1}{\left(\frac{c_{totalcarotenoid}}{K_{inh}}\right)^n + 1} - k_{CrtC_1} \cdot c_{lycopene} - k_{dil} \cdot c_{lycopene}$$

The fits of this model to the anaerobic data are very poor. The dynamics of the "accurate" data are poorly described. The input flux (total carotenoid concentration) is strongly underestimated, and the dynamics of spx could not be described at all (Fig. 79).

The fit of the model assuming spx inhibition on the microaerobic data could describe the first carotenoid induction peak. Therefore, the product inhibition could exist, but it is not the primary regulation for the carotenoid biosynthesis in all conditions.

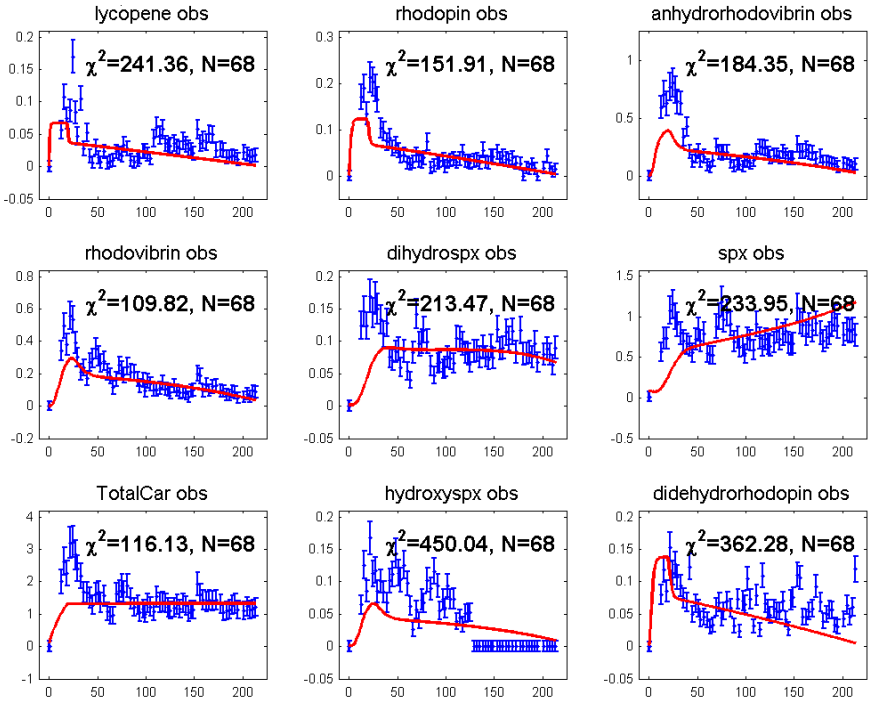

Fig. 79. Total carotenoid feedback inhibition following Hill kinetics in the wild-type (χ^2/N= 3.37) growing under anaerobic conditions

6.2.2 ST4 mutant with alternative spx pathway

Since ST4 has another but structurally similar major carotenoid (thspx) as the wild-type, it is an appropriate system to investigate the inhibitor specificity of the feedback inhibition.

Due to the functional deletion of the gene *crtD*, the mutant ST4 has the alternative spx pathway as main route for carotenoid production starting with lycopene and ending up with thspx. The active carotenoid biosynthetic pathways in ST4 are shown in Fig. 70. The model consisted only of the reactions of the "alternative spx pathway" (black pathway in Fig. 70).

The time courses of both thspx and total carotenoid in ST4 share the same dynamics (Fig. 80 and Fig. 81). Therefore, fitting the model with thspx product inhibition resulted in the same parameters as the model with total carotenoid inhibition with the expection of K_{inh}. In the case of both models, the Hill coefficient is extremely high due to the abrupt inhibition of both the thspx and total carotenoid time courses. The models could describe the dynamics of the accurate metabolites (thspx, total carotenoid, 3,4-dihydroanhydrorhodovibrin, 3,4-dihydrorhodovibrin) well.

In the case of an existing product inhibition following Hill kinetics, the K_{inh} value is dependent on the inhibitor, but the n value is characteristic for a given inhibition mechanism, therefore should show a constant value for different inhibitors. In the case of ST4, the n value of thspx inhibition has found to be significantly higher than that of spx in the wild-type (Table

17). The switch mechanism represented by high *n* value hints at the conclusion that in the case of ST4, the inhibition is induced rather by the total carotenoid concentration.

According to the Hill coefficients, we can conclude that thspx and spx trigger inhibition with different kinetics. This fact makes the hypothesis, that the end products induce negative feedback regulation on CrtI, implausible. However, the high *n* value can arise also from the fact that the production of carotenoid is inhibited in the presence of oxygen in ST4. Therefore, due to the slow carotenoid production, the region corresponding to the decrease of the intracellular carotenoid was not achieved during the experiments.

Strain	**ST4**	**S1**	**ST4**
Inhibitor	**thspx**	**spx**	**TC**
CrtI	**0.06**	**0.185**	**0.059**
$CrtC_1$	2.66	0.375	2.65
$CrtF_1$	0.458		0.418
$CrtF_{1a}$	0.024		0.023
$CrtC_2$	0.298		0.285
$CrtC_{1a}$	0.25		0.294
$CrtF_2$	0.223		0.214
K_{inh}	**1.839**	**1.158**	**2.33**
n	**211**	**6.62**	**328**

Table 17. ST4 and S1 kinetic parameters calculated for the product inhibitory model under microaerobic conditions

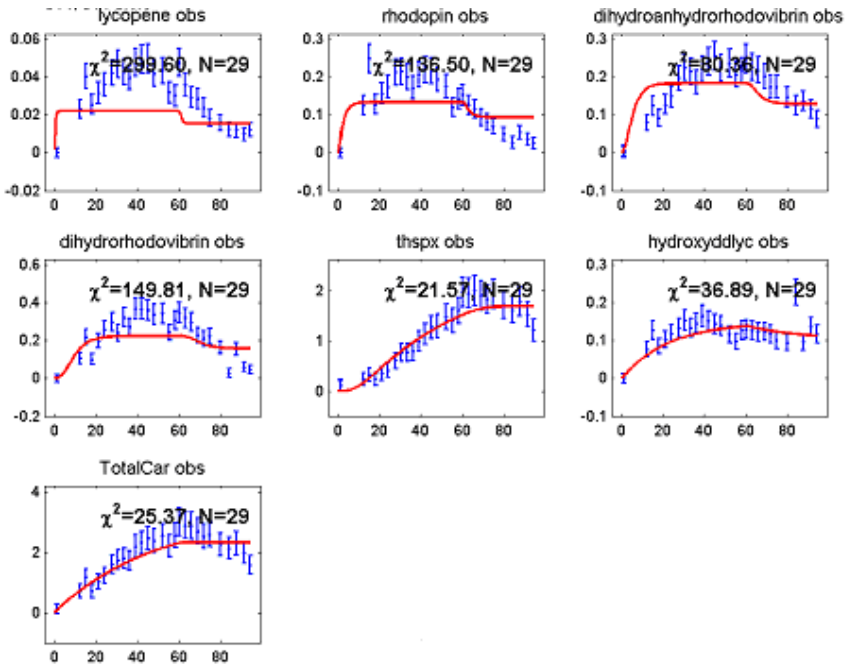

Fig. 80. Total carotenoid feedback inhibition following Hill kinetics in ST4 strain under microaerobic conditions

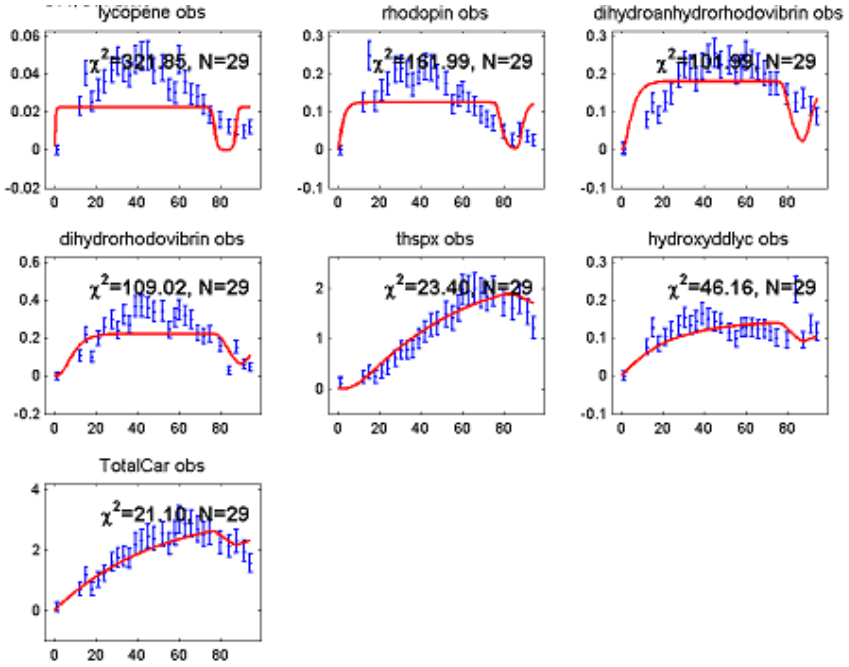

Fig. 81. The feedback inhibition of thspx following Hill kinetics in ST4 under microaerobic conditions

6.3 *Negative feedback regulation with inhibitor protein*

Since the Hill kinetics model could not explain the strong oscillation in the microaerobic data of the wild-type, a second approach of endogenous regulation was used for describing the inhibition. This model assumes an inhibitor protein (P_{inh}), which showes changes in with the concentration carotenoid and triggers an inactivation on PSY (the first carotenogenic enzyme). There is a certain P_{inh} threshold concentration ($c_{high,}$ carotenoid concentration), which inactivates probably the first enzyme of the carotenoid pathway. Due to the bacterial growth, the intracellular carotenoid concentration and the P_{inh} concentration decreases until another threshold (c_{low}) concentration, where the inhibition is released and PSY can be reactivated. (Fig. 82). If the c_{low} and c_{high} is the same value, an extreme case of Hill inhibition occurs.

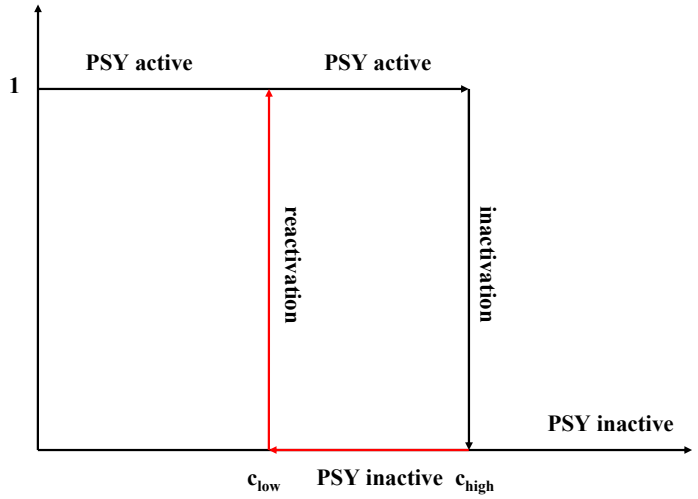

Fig. 82. The activity of PSY dependent on the inhibitor concentration

The changes of the enzyme activity are mathematically described with the following equation, where *e*, is the enzyme activity of PSY and ε is a scaling factor.

$$\frac{de}{dt} = \begin{cases} \frac{1-e}{\varepsilon} & \text{for} \quad P_{inh} < c_{low} \\ \frac{(-e)\cdot(1-e)\cdot(0.5-e)}{\varepsilon} & \text{for} \quad c_{low} < P_{inh} < c_{high} \\ \frac{-e}{\varepsilon} & \text{for} \quad c_{high} < P_{inh} \end{cases}$$

Figure 83. Mathematical equation for describing the hysteresis of the carotenoid biosynthesis depending on the inhibitor level.

The inhibition of both spx and total carotenoids was modelled using the inhibitor protein assumption (Fig. 84 and Fig. 85). The model was fitted on the microaerobic data, providing equally good fits for both inhibitors. The fits are particularly good in the case of the "accurate metabolites": anhydrorhodovibrin, dhspx, spx and total carotenoid. The higher χ^2/N value is caused by the estimated third wave of the oscillation, which could not be recorded, probably due to the stationary phase of the bacteria and the fructose limitation. The deactivating (c_{high}) and reactivating (c_{low}) concentrations and other reaction parameters are listed in Table 18.
The model was also fitted on the anaerobic data (Fig. 86 and Fig. 87). These fits could also describe the accurate metabolites under anaerobic conditions very well. Since the anaerobic c_{low} and c_{high}, turned out to be significantly lower than in microaerobic case, an oxygen dependence of the inhibition can be assumed.

In case of spx inhibition under anaerobic condition, there is no more hysteresis observable. The c_{Low} and c_{high} are practically the same value, which hints for a switching point. This behaviour is an extreme case of Hill inhibition. According to the χ^2/N values, the hysteresis model with total carotenoid inhibition describes the dynamics of the data better than the spx inhibition, since the carotenoid feeding flux is also strongly underestimated in the anaerobic case of spx inhibition (Fig. 87). According to the good fits are achieved with the inhibitor protein regulation, this kind of endogenous regulation seems likely.

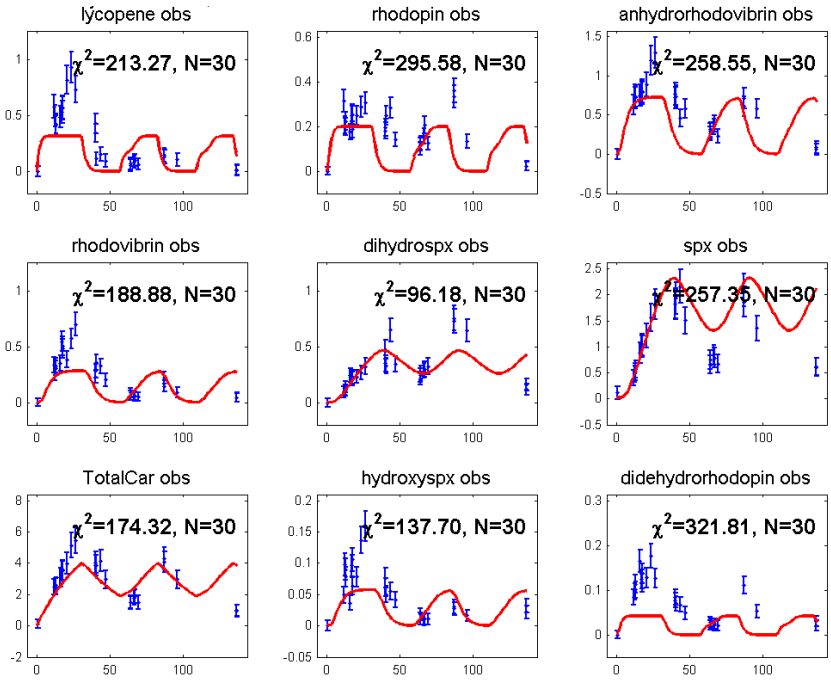

Fig. 84. Negative feedback inhibition via inhibitor protein dependent on total carotenoids shows oscillation under microaerobic conditions (χ^2/N= 7.19)

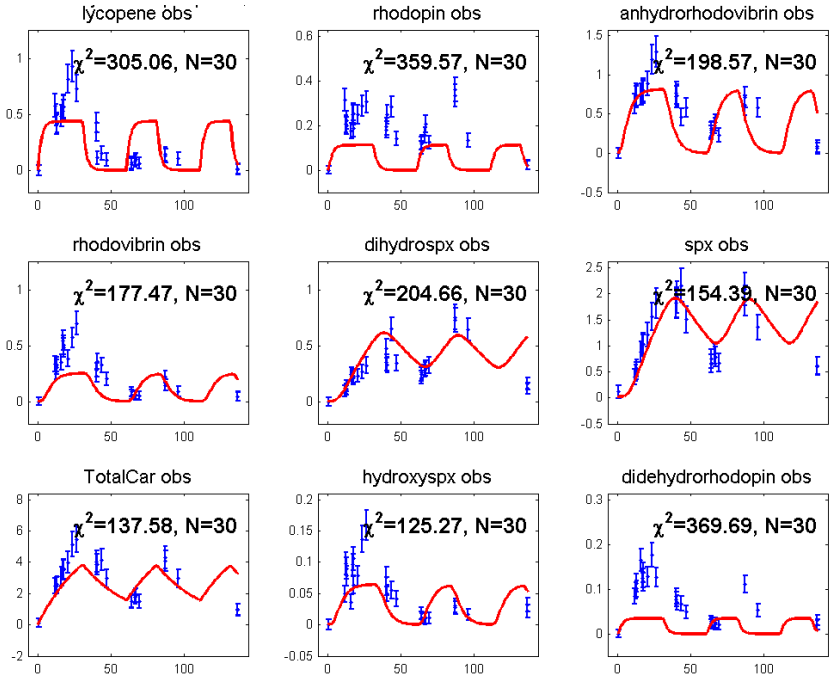

Fig. 85. Negative feedback inhibition via an inhibitor protein dependent on spx shows oscillation under microaerobic conditions (χ2/N= 7.52)

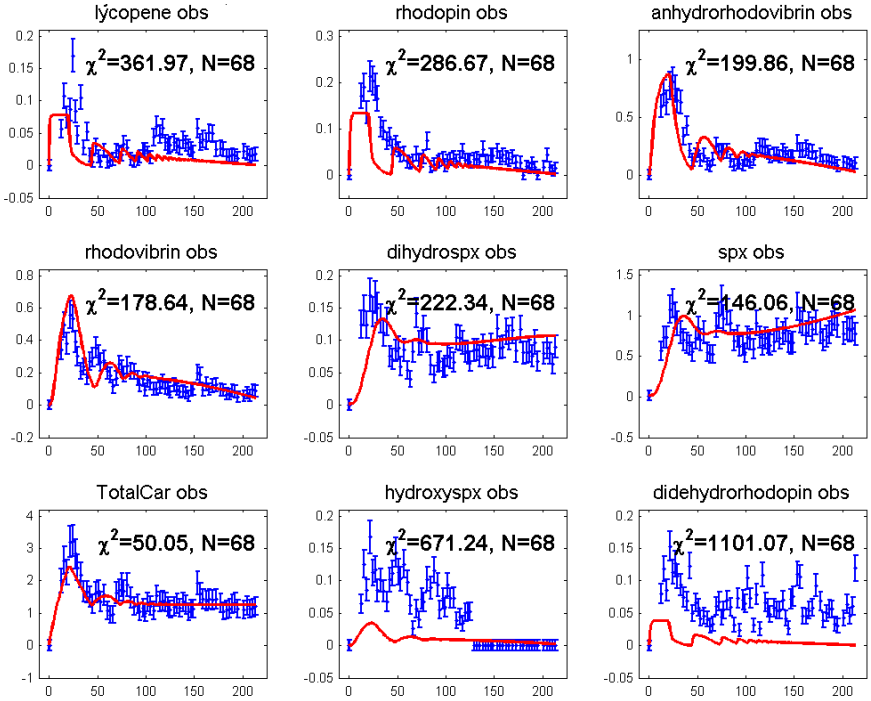

Fig. 86. Negative feedback inhibition via inhibitor protein dependent on the total carotenoid shows oscillation under anaerobic conditions (χ2/N= 5.258)

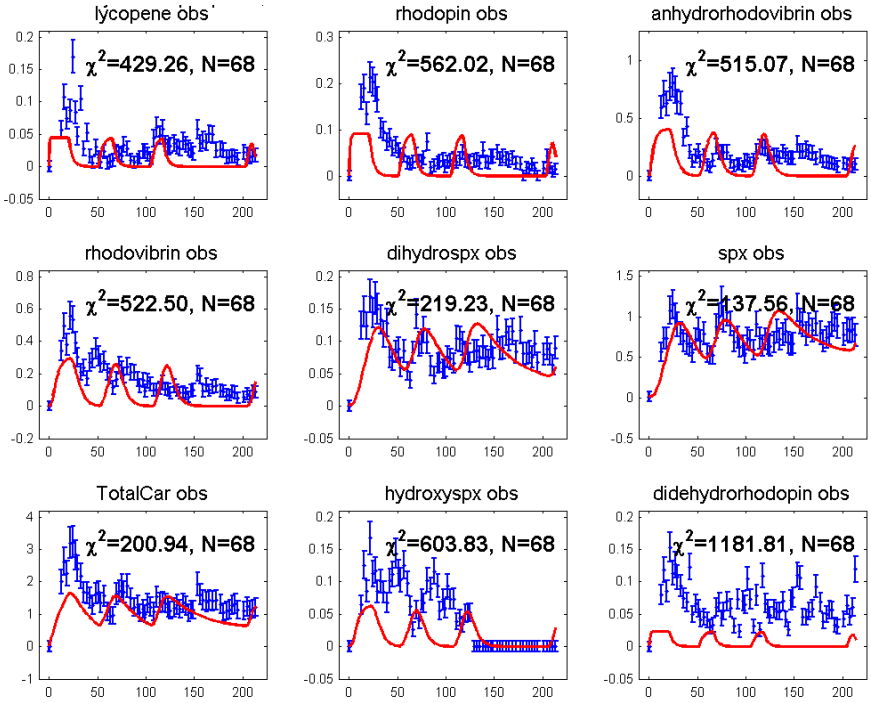

Fig. 87. Negative feedback inhibition via inhibitor protein dependent on spx shows oscillation under anaerobic conditions ($\chi 2/N= 7.14$)

Hysteresis model spx inhibition			**Hysteresis model TC inhibition**		
enzyme	**anaerobic**	**microaerobic**	**enzyme**	**anaerobic**	**microaerobic**
CrtI	0.117	0.191	CrtI	0.178	0.199
CrtC	2.592	0.408	CrtC	2.24	0.598
CrtD	1.234	1.558	CrtD	1.26	0.915
CrtF	4.999	5.041	CrtF	4.366	4.29
CrtC	0.231	0.183	CrtC	0.144	0.22
CrtF2a	0.0329	0.138	CrtF2a	0.015	0.088
CrtD	0.25	0.419	CrtD	0.111	0.442
CrtD2a	0.0049	0.002	CrtD2a	0.004	0.0004
CrtF	1.101	1.622	CrtF	2.094	2.158
car high	**0.597**	**1.605**	car high	**2.377**	**3.967**
car low	**0.591**	**1.2**	car low	**1.259**	**1.897**
ε	3.56	6.067	ε	2.247	0.63

Table 18. Kinetic parameters of the inhibitor protein model

6.4 Regulation of an external signal resulting in pulsing MEP pathway flux

Since all the isoprenoids were oscillating strongly together under both microaerobic and anaerobic conditions, a shared regulation of the terpenoid pathway by an external signal was assumed. In addition, the measured dynamics of the [UQ]/[UQH_2] ratio suggests that the redox state changes of the UQ can be a regulatory signal for the carotenoid biosynthesis. The model uses a pulsing input due to the alternating external signal which was described with an arctan function:

$$k_{input} = \varepsilon \cdot ((1+\frac{1}{2}\tanh(\alpha \cdot (t-0)) - ((1+\frac{1}{2}\tanh(\alpha \cdot (t-t_1)) + (1+\frac{1}{2}\tanh(\alpha \cdot (t-t_2)) - ((1+\frac{1}{2}\tanh(\alpha \cdot (t-t_3))$$

k_{input} feeding flux of the carotenoid production
ε, is the height of the pulse
α, is the slope of the pulse
t, time points

The parameters ε and α are free parameters. The time points are also free parameters but their intervals are defined according to the dataset. In this model, an additional data occurs ("input"), which equals to the slope of the total carotenoid time course if it is positive. If the slope of the total carotenoid time course is negative, input is zero, since carotenoids were not produced.

The model fitted to the microaerobic data of the wild-type could describe the oscillation of the intermediate carotenoids as well as the spx (Fig. 88). The microaerobic data of SLYC18 could also be described using the pulsing input model (Fig. 90).

The fit of the pulsing input model on the anaerobic data results in weak fits but it is still acceptable. It can well describe the dynamics of anhydrorhodovibrin and total carotenoid, but the model has a significant delay in the spx and dhspx concentration compared to the data (Fig. 89).The kinetic parameters of the models are listed in Table 19.

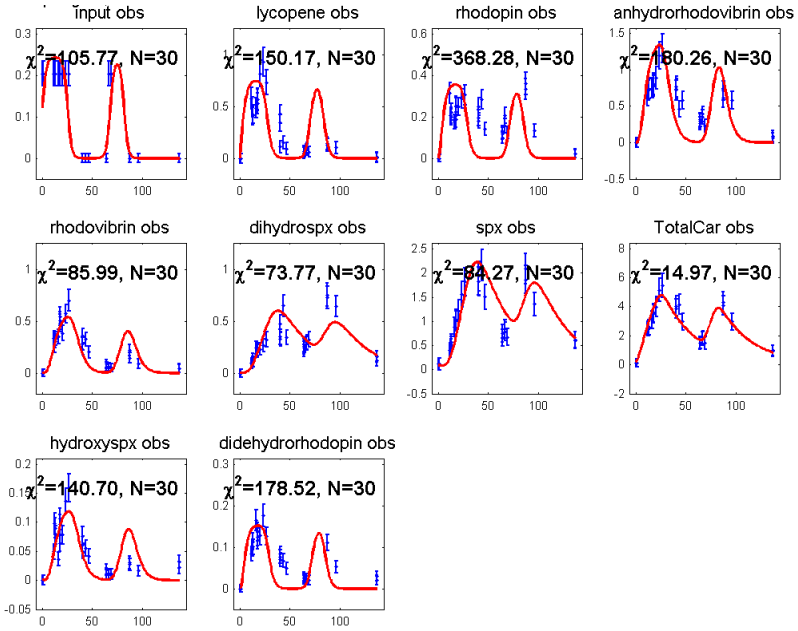

Fig. 88. Applying pulsing input model on microaerobic data obtained from wild-type (χ2/N= 4.609)

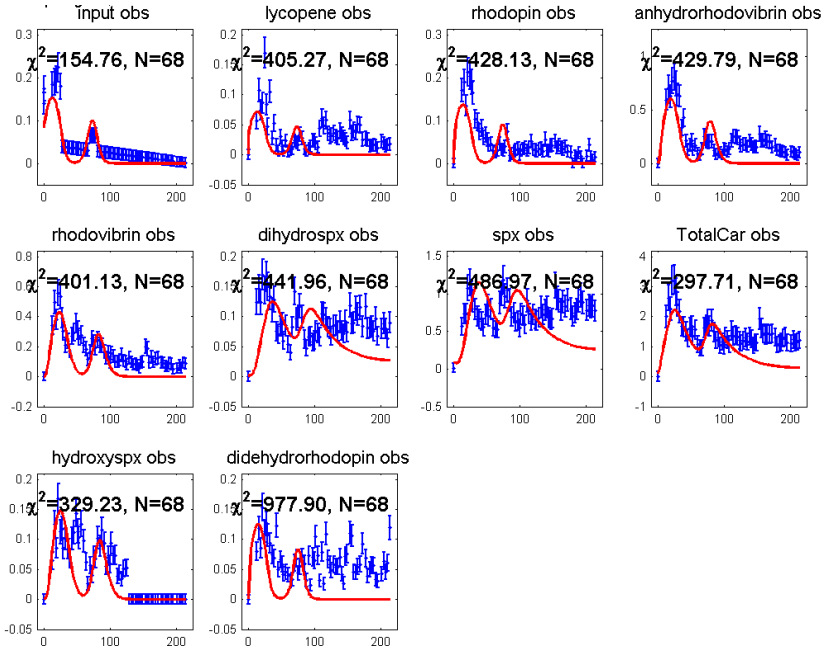

Fig. 89. Applying pulsing input model on anaerobic data obtained from wild-type (χ^2/N= 6.4)

enzyme	anaerobic	microaerobic
CrtI	1.07	1.246
$CrtC_1$	2.269	0.373
$CrtD_1$	1.13	0.751
$CrtF_1$	1.2	1.725
$CrtC_2$	0.195	0.153
$CrtF_{2a}$	0.02	0.072
$CrtD_2$	0.2	0.269
$CrtD_{2a}$	0	0
$CrtF_2$	0.538	1.201
$time_1$	24.999	24.998
$time_2$	67.2	68.19
$time_3$	78.5	81.64
slope	0.12	0.246
height	0.169	0.2444

Table 19. Kinetic parameters of the pulsing input model

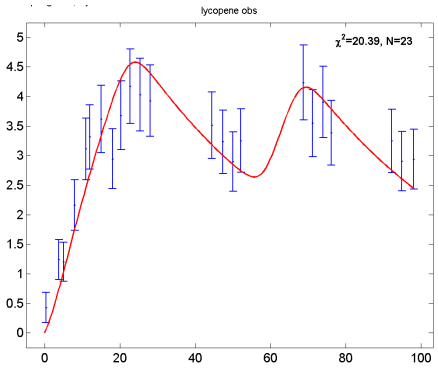

Fig. 90. Applying pulsing input model on anaerobic data obtained from SLYC18

6.5 Discussion

Product inhibition via Hill kinetics The model assuming negative feedback effect following Hill kinetics performed poorly in describing the anaerobic data of the wild-type (Fig. 77) The significant delay in the model spx values compared to the measured spx concentrations makes the model unable to follow the dynamics of the spx data. (Fig. 77) However, in the microaerobic case, where higher carotenoid level occurs, the product inhibition could describe the first induction phase well. Therefore, the product inhibition could exist, but it is not the primary regulation of the pathway. The product inhibition is significant at higher carotenoid concentration, functioning as a safety valve.

Product inhibition via regulator protein In this model, a regulator protein was assumed, which is produced dependent on the carotenoids, triggering inhibition on the carotenogenic enzymes. The model with the regulator protein was made and analyzed only on the carotenoid production but can be easily extended on the isoprenoid production, since all isoprenoids

oscillate together. The model was successfully tested on the wild-type and SLYC18. The parameters c_{high} and c_{low} were significantly dependent on the oxygen availability. The model of an oxygen-dependent carotenoid sensitive regulator could describe the carotenoid time courses very well of the wild-type at both oxygen concentrations (Fig. 84 and Fig. 85). According to the model, it is still unclear as to whether the inhibitor production is dependent on spx or the total carotenoid concentration. Although the χ^2/N is slightly lower in the case of the total carotenoid, than with spx, is it not convincing since the model with spx follow the first 100 hours better than the model with total carotenoid. Consequently, the existence of a regulator protein, whose inhibition power depending on either spx or total carotenoid cannot be excluded.

The model with pulsing input The simultaneous oscillation of the terpenoids let us conclude an existing exogenous regulatory signal. Considering that the external acid concentration and the intracellular PHB concentration also changes if the isoprenoids oscillate, a global signal (e.g. UQ pool redox state) affecting the whole metabolism can be assumed, which resulted also in the oscillation carotenoid concentration. This assumption was tested with a dynamic model where a pulsing input signal of the carotenoid pathway was applied. The model could describe all the datasets in both the wild-type and SLYC18 (Fig. 88and Fig. 89).

Taking the changing acetate and PHB concentrations and the good fits of the pulsing input model into account, it can be concluded that the oscillation of the carotenoids is due to an alternating exogenous signal. However, the end product inhibition also seems likely but it is only significant at higher carotenoid concentrations.

7 Discussion

In this study, the photosynthetic membrane biosynthesis with focus on the carotenoid production and the metabolic changes induced by the aerobic- to-anaerobic/microaerobic transition were investigated in *R. rubrum*. The aerobic inocula in the anaerobic bioreactor using the isoprenoid HPLC-MS analysis allowed us to follow the dynamics of the activation of the anaerobic metabolism including the PM synthesis to be followed. The carotenoid biosynthesis and its dependence upon oxygen were investigated under different oxygen availabilities in the wild-type and in two carotenoid mutants, ST4 (*crtD*$^-$) and SLYC18 (*crtC*$^-$ *crtD*$^-$).

7.1 Metabolic profile under anaerobic conditions

The cells were grown in fructose-succinate medium (Ghosh *et al.*, 1994) under anaerobic conditions in a bioreactor. The detailed study of the growth on fructose-succinate medium under limiting oxygen concentration in absence of light has shown that the semi-aerobic metabolism involves the cooperation of the reductive and oxidative pathways. Furthermore, a highly reduced UQ pool ($[UQH_2]/[UQ] = 1.7$) was observed under these conditions (Grammel *et al.*, 2003), which resulted in a high level of PM biosynthesis (Grammel and Ghosh, 2008). In this study, the growth conditions were significantly different compared to the conditions of Grammel *et al.* (2003). Although different pO_2 values (0-0.6%) were adjusted strong oxygen limitation occurred in all fermentations independent from the pO_2 values. Furthermore, the medium did not contain HCO_3^- and the cells did not produce enough CO_2 under anaerobic conditions, therefore strong CO_2 limitation occurred during all experiments, in addition to the oxygen limitation. These two substrate limitations determine the metabolic pattern observed in the experiments and resulted in extremely long generation times (~60 h). The absence of oxygen immediately induced anaerobic metabolism, which could be seen in the rapid increase of the intracellular acetate concentration and the PM level (A_{880}/A_{660}). The double substrate limitation resulted in large amounts of PHB production, which was not observed in the experiment of Grammel *et al.* (2003). The extremely slow growth and the enhanced PHB production indicate that NADPH cannot be utilized for cell growth (probably due to the low ATP excess), but flow into the PHB biosynthesis, which serves as redox-equivalent sink.

Under these conditions the role of the "pyruvate checkpoint" becomes particularly important. The organic acid excretion, hydrogen and PHB production depend on the availability of acetyl-CoA and pyruvate. The pyruvate decarboxylation via PdH results in high NADH

concentrations, which inhibit PdH. Under the certain conditions, high NADH excess occurs reducing the activity of PdH. Pfor and Pfl produce hydrogen indirectly during the pyruvate decarboxylation step, therefore they may be more preferable enzymes in acetyl-CoA production, than PdH. (Lüderitz and Kleme,1977) The large amount of PHB production indicates that a high excess of acetyl-CoA is produced. Our data support the suggestion that the citramalate pathway may be active under anaerobic conditions. The citramalate cycle arises from pyruvate and acetyl-CoA, forming citramalate. Then, citramalate is converted to propionyl-CoA and glyoxylate (Berg and Ivanovsky, 2007). Glyoxylate enters the reductive TCA pathway with acetyl-CoA, forming malate. Propionate is normally recycled to pyruvate or converted to succinate via the methylmalonyl pathway. Since the cultures were strongly CO_2-limited, the propionyl-CoA conversion to succinate was limited. Thereby, propionyl-CoA was converted to propionate and excreted into the medium. Succinate can also be produced via fumarate reduction using possibly RQH_2 as an electron donor. However, fumarate was observed only at low levels, possibly because this intermediate must rapidly channelled to oxalacetate, which is required in the amino acid biosynthesis.

Tha data of Berg and Ivanovsky (2007) indicate that the ethylmalonyl pathway operates simultaneously with the citramalate pathway. For the two first steps of the ethylmalonyl pathway, which is required for PHB production, only acetate-CoA and NADPH are essential. For the further step, not only NADPH but also CO_2 are required. Therefore, the flux on the ethylmalonyl and methylmalonyl pathways is probably very low due to the strong CO_2 limitation.

SLYC18 could grow twice as fast (G_t=30 h) as the wild-type under CO_2- and oxygen-limited conditions, which occurred in all bioreactor experiments. Furthermore, SLYC18 produced twice as much PHB, than the wild-type. Apart from the PHB production, the maximal [RQ]/[UQ] ratio is 2-fold higher in the lycopene-producing strain (1.7) than in the wild-type (0.9).

The higher PHB level in SLYC18 compared to that of the wild-type indicates a higher excess of NADPH. The processes resulting in enhanced NADPH production in SLYC18 are unknown. SLYC18 only has mutations in two genes of carotenoid biosynthesis (*crtC* and *crtD*), resulting in lycopene production. Since lycopene is more saturated than the normal end-carotenoid, spx, SLYC18 in principle should be less reduced than the wild-type.

The reason for the enhanced RQ level in SLYC18 is also unknown. The carotenoid and isoprenoid-quinones share a common step in their biosynthesis: the methylation uses SAM as cofactor, producing SAH as side product. Already at a 0.2 mM concentration SAH shows

31% inhibition on the isoprenoid biosynthesis (Brajchich *et al.,* 2010). Since SLYC18 has no methylation step due to the lack of the essential hydroxyl group, SAH occurs at lower concentrations, which can affect the RQ biosynthesis. However, SAM is involved in numerous methylation reactions, for example in the biosynthesis of methionine as well as BChl. Therefore the significance of the missing carotenoid methylation on SAM homeostasis is not clear. However, considering the size of the chromatophore vesicles and that RQ is produced together with carotenoids in the chromatophore, the SAM concentration in this small compartment can be affected by the missing methylation step. Nevertheless, the possibility of this interaction cannot be excluded.

How can SLYC18 produce more NADPH than the wild-type? Is the higher RQ level connected to the higher NADPH supply? The most commonly cited reaction for the production of NADPH is the NADH-NADPH TH, which probably is also present in the ICM. Other NADPH sources, such as ICDH are low under anaerobic conditions and G6PdH and 6PGdH are not present in the *R. rubrum* genome (Grammel *et al.,* 2003). Therefore, the NADH TH seems to be the only enzyme capable of catalyzing the NADPH production utilizing the Δp. If this enzyme has such a special role, the knockout of this enzyme should result in large phenotypic changes. However, this was shown not to be the case by two groups (Ghosh and Grammel, data unpublished, Jackson and Obiozo, 2009), since the knockout mutants of NADH TH do not have significant phenotypic changes under either photoautotrophic or chemotrophic conditions. This observation does not support the idea of NADH TH as the major supplier of NADPH.

Grammel and Ghosh (2008) have shown that the NADH/NAD^+ level is approximately constant, when *R. rubrum* is grown in different media, in contrast to the NADPH level, which can be altered significantly. The well-regulated, constant NADH level is important for the cell in order to not become overreduced. Therefore, by converting NADH to NADPH, the latter can be utilized in the production of storage material, which can serve as a redox sink. In *A. suum*, the maintenance of NADH homeostasis by generating NADPH is coupled also to energy generation (Kommunieczki *et al.,* 1993) using RQ under conditions of stress. The large amount of NADPH is utilized in fatty acid production in *A. suum*.

The high level production of PHB using RQ is a similar phenomenon to that of the fatty acid production observed in *A suum.* In *A. suum*, NADH is oxidized by complex I (NADHdH) coupled with proton translocation and the electrons flow to RQ. From RQH_2, they flow to the ETF catalyzed by ETF:RQ oxidoreductase. The reduced ETF gives its electron to the NADH

dependent acyl-reductase enzyme catalyzing reversed ß-oxidation (Ma *et al.*,1993). The reaction sequence is shown in Fig. 91.

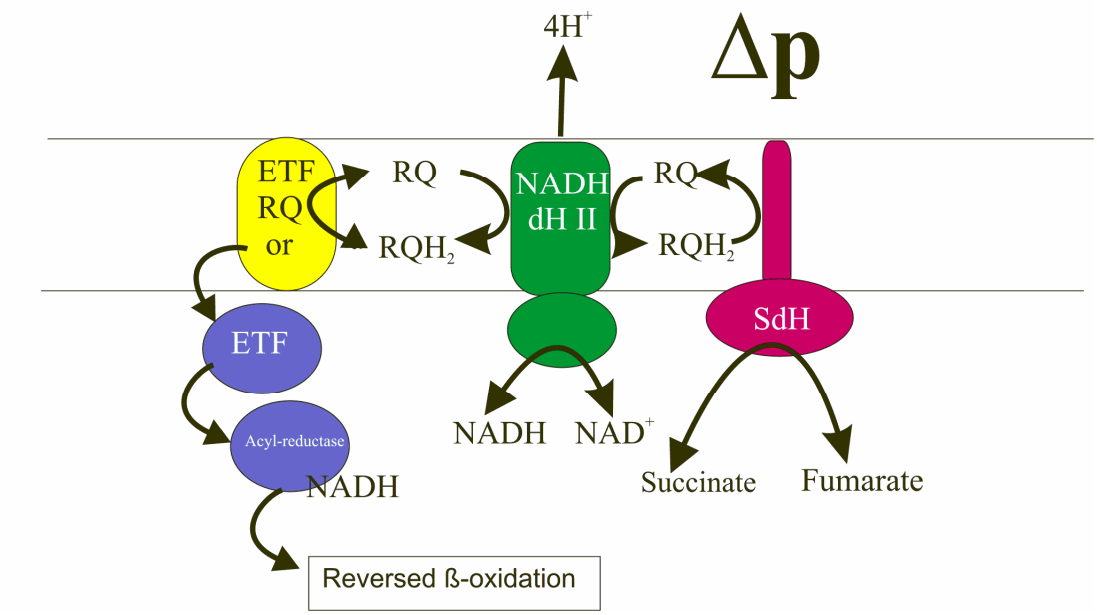

Fig. 91. Reduction of the redox state of the cell coupled to energy generation in *A. suum*

Under anaerobic conditions the excess of NADH is high. Yamamato *et al.* (1970) showed in *R. rubrum* that RQ can accept electrons from NADH via a NADH:RQ oxidoreductase (complex I), but the electron cannot be transferred to the cytochrome bc_1 complex. Therefore, NADH reacts with complex I and the electrons flow to RQ, resulting in the production of RQH_2 while the protons are pumped into the periplasmic space. The electron acceptor of RQH_2 is unknown. The ETF:RQ oxidoreductase was identified in *A. suum* as a membrane-bound protein with an FAD cofactor and 3 iron-sulphur clusters (Ma *et al.,*1993). According to the proposed mechanism in *A. suum*, the RQ occurs in the form of a semiquinone radical intermediate in the iron-sulphur cluster during the reaction (Ma *et al.,* 1993).

SdH is very similar to the ETF reductase determined in *A. suum*: it is a membrane-bound protein with a FAD cofactor and 3 iron-sulphur clusters. The proposed mechanism in *A. suum*, particularly the semiquinone radical intermediate in the iron-sulphur cluster, supports also the idea that SdH could be a good candidate for accepting electrons form RQ. The RQ-dependent fumarate reductase activity, which has been observed in *R. rubrum*, also supports the concept SDH as the electron acceptor for RQH_2.

RQ (-30mV) and UQ (+90mV) (Erabi *et al.,* 1965) have a large difference in their redox potentials. Therefore electron transfer between the two quinones cannot take place (Erabi *et al.,* 1965). If RQ and UQ are in the semiquinone form bound to the enzyme, the redox

potential difference is significantly less, and the reaction between the two quinones cannot be excluded anymore. Therefore, a relief of UQH_2 pool via RQ cannot be excluded.

Furthermore, *R. rubrum* contains genes for 3 NADH dehydrogenases, two of which are closely homologous to NDH1 and NDH2 in *E. coli*. The third set of genes seems to be missing many of the ORFs encoding polypeptides of the polar domain, which might possibly have a hydrophilic domain with an NADPH binding site. Such an NADH3 dehydrogenase would be a good candidate for an RQ-dependent NADPH dehydrogenase which accepts electrons from NADH via RQ and generates NADPH. A membrane-bound NADPH dH has been found in *Desulfobacter postgai* growing on acetate and sulphate, which has been found to be electrically connected to SdH within the membrane, and the electron transfer between these two enzymes, was coupled to proton translocation. The membrane fraction of *D. postgai* was able to reduce $NADP^+$ with succinate (Möhler-Zhinker and Thauer, 1988).

Apart from the NADPH DH, in many organisms the NADPH can be produced also via ferredoxin, using the enzyme NADPH:ferredoxin oxidoreductase. This has been observed in higher plants and cyanobacteria (Bojko *et al*., 2003; Scherer *et al.,* 1988; Bendall and Manasse, 1995). The *R. rubrum* genome contain many potential genes encoding ferredoxins, and also an annotated gene for ferredoxin:NADPH oxidoreductase. Ferredoxin is involved in the electron transfer for the nitrogenase system, which is switched off in our case by the high ammonium concentration in the medium. However, ferredoxin might accept electrons from RQ (via a rhodoquinone:ferredoxin oxidoreductase), and the reduced ferredoxin might be oxidized by the ferredoxin-$NADP^+$ oxidoreductase. It can not be excluded that RQ gives the electrons directly to ferredoxin-$NADP^+$ oxidoreductase producing NADPH in one step.

The 10-fold higher level of hydrogen production in SLYC18 compared to that of the wild-type supports the concept of a reduced ferredoxin, since hydrogen is produced via ferredoxin hydrogenases. Reduced ferredoxin is also produced by one of the anaerobic enzymes, Pfor, which is probably the most significant enzyme among the pyruvate decarboxylation enzymes.

Thus potentially, the electron acceptor of RQH_2 could be SdH, a potential NADH dH, and NADH dH type I, UQH_2, ferredoxin. Considering all the information of the potential enzymes and the experimental observations of this study the following hypothetical processes for RQ-mediated NADPH production can be proposed.

The high concentration of succinate in the presence of RQ induces the reduction of RQ producing fumarate, which is utilized for the conversion to oxaloacetate in order to feed the amino acid biosynthesis. The electron flows to RQ producing RQH_2 with protons from the periplasm utilizing the Δp. RQH_2 is also produced via NADH dH from NADH. The RQH_2 is

oxidized finally by a hypothetical NDH3, producing NADPH, further depleting the Δp. Furthermore, RQH_2 can transfer electrons to a hypothetical RQ:ferredoxin oxidoreductase, producing reduced ferredoxin. Since RQH_2 is not detectable it must be oxidized very quickly. The role of RQ in *A. suum* was to produce NADPH coupled to the generation of Δp. In *R. rubrum*, in this hypothetical pathway, if NADH dH can reduce RQ coupled with proton translocation, NADPH can be produced without consuming Δp.

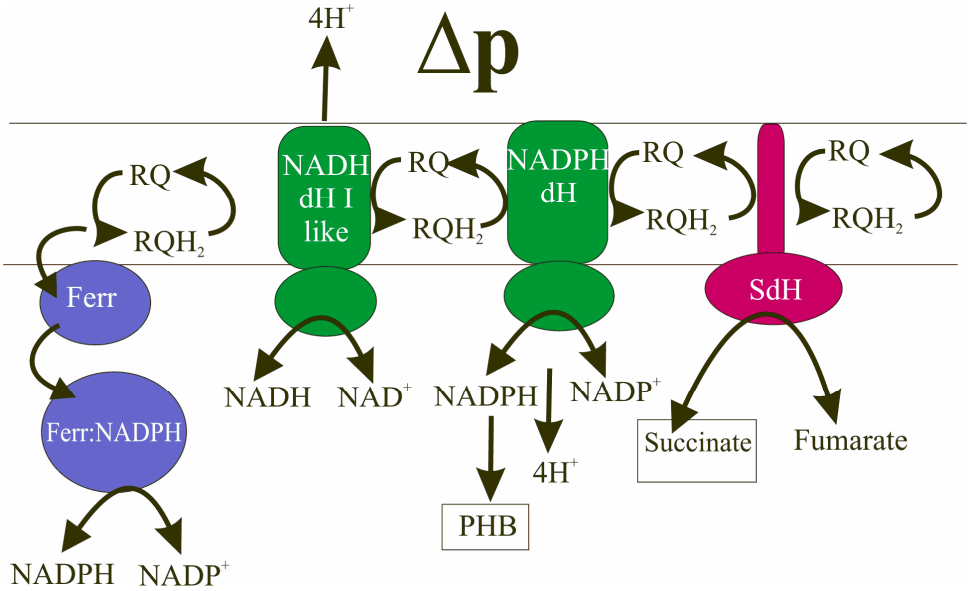

Fig. 92. NADPH production coupled with energy generation in absence of oxygen using low potential RQ

7.2 UQ pool and PM biosynthesis

The aerobic inocula (containing very little amount of PM) were placed into the anaerobic bioreactor. Due to the induction of the photosynthetic genes by the absence of oxygen, the cellular concentration of the PM compounds rapidly increases for up to12 h. At the 24 h time point, the intracellular carotenoid, isoprenoid and BChl*a* content of the cell achieves a maximum concentration, which is always followed by a strong decrease due to the arrested PM production.

The PM production could also be induced by an oxygen pulse. Under anaerobic conditions, the metabolism is very sensitive to oxygen, and after applying an oxygen pulse, the oxidative TCA cycle and the ETC were temporarly activated, inducing changes in the UQ pool redox state. After rapidly consuming the oxygen, the UQ pool becomes reduced again, inducing PM biosynthesis. This oscillation pattern can be seen most significantly in the carotenoid concentration applying oxygen pulse. These observations let us conclude that the induction of the carotenoid genes during the aerobic-to anaerobic transition is partly due to the low pO_2

and the low electron flow through cbb_3. Nevertheless, the $[UQH_2]/[UQ]$ has significant role under non-repressing oxygen concentration.

The reason for the oscillation in the carotenoid time courses has been analyzed with a dynamic mathematical model of the carotenoid biosynthesis. In order to confirm that the oscillation of the PM compounds, especially the carotenoids, is not a result of an endogenous regulation but depends on the UQ pool redox value, different regulatory schemes were tested to describe the carotenoid production time courses. The observations of the similar carotenoid dynamics in the wild-type and the carotenoid mutants under the same oxygen availability suggested the existence of an endogenous mechanism. The most obvious regulation of a linear pathway would be a product feedback inhibition, but the dynamics of a product inhibition following Hill kinetics could not describe the carotenoid oscillation. In the second approach, a regulatory protein was assumed, which is produced proportionally to the carotenoids, inducing inhibition of the carotenogenic enzymes, resulting in an oscillating carotenoid concentration. The model with the regulatory protein was constructed only for the carotenoid production but can be easily extended to the isoprenoid production, since all the production of the isoprenoids. The model was successfully tested on the wild-type and on SLYC18. The model of an oxygen-dependent carotenoid sensitive regulator could describe the carotenoid time courses of the wild-type very well at both oxygen concentrations. (Fig. 84 and Fig. 85) The model could not show unambigously whether the inhibitor is produced proportionally to the end carotenoid or to the total carotenoid concentration. The model could adequately describe the experimental data, but there are some experimental observations conflicting with the assumption of enzyme deactivation. In particular, semi-aerobic growth of *R. rubrum* on M2SF allows the full expression of carotenoids.

Furthermore, the concentration of dhspx is low during the whole fermentation due to its low biosynthetic rate (Fig. 65 B). The constant concentration of dhspx, even if the concentrations of other carotenoids strongly decrease, suggests that the enzyme (CrtF) producing dhspx is active during the whole fermentation. The active CrtF let us deduce, that the other carotenogenic enzymes are active (Fig. 68A).

However, the regulator protein assumption could also imply an endogenous regulation which shuts down the flux into the carotenoid pathway at a threshold carotenoid concentration (c_{high}), and also reactivates it at a certain concentration (c_{low}). The existence of such a negative feedback with the end products on the MEP pathway cannot be excluded.

Since it seems most likely that the input flux varies, the effect of a pulsing input flux on the carotenoid production was investigated. Applying a model with pulsing input signal with

constitutive active enzymes, could describe the dynamics of the carotenoid biosynthesis at all oxygen concentrations (Fig. 88 and Fig. 89). The model could be considered as a confirmation of the observation that the isoprenoids are regulated together via MEP pathway flux. Using this approach, it could be demonstrated that the primary regulation of the pathway is exogenous. Considering the the former metabolic observations, that exogenous signal might be the $[UQH_2]/[UQ]$ ratio. In this study, we have not taken the effect of a potential regulation of BChl into account. This could be studied at later date.

7.3 Dynamics of the reaction of carotenoid biosynthesis

The dynamics of the carotenoid, isoprenoid-quinones and BChl*a* biosynthesis were investigated in three *R. rubrum* strains. The shared dynamics of the pathways competing for the metabolite, GGPP, also suggests a common regulation for the isoprenoid pathways.

The high resolution time courses of each carotenoid allowed us to determine the speed of the conversion rate of each reaction, which was also confirmed a the dynamic model of carotenoid biosynthesis. The occurrence of the intermediates: anhydrorhodovibrin, and rhodovibrin in the wild-type at higher concentrations showed a bottleneck in the carotenogenic reaction path, namely the second reaction of CrtD (Fig 55). The desaturation reaction of rhodovibrin seems to be rate-limiting for the whole pathway. Dhspx arises through methylation via CrtF, which is faster than CrtD in the competition for rhodovibrin. The presence of dhspx and the low concentrations of both CrtD products OH-spx and 3,4-didehydrorhodopin also confirms the positions of the bottleneck reactions. The higher concentration of anhydrorhodovibrin compared to rhodovibrin shows that the methoxylation step of 3,4-didehydrorhodopin is carried out faster than the hydroxylation of anhydrorhodovibrin (Fig. 64). This observation also indicates that the first reactions of the end-modifying carotenogenic enzymes are significantly faster than the second reactions under all conditions (Fig. 64). In *Rb. sphaeroides* the second reaction cannot take place at all resulting in asymmetric carotenoids as spheroidene. *R. rubrum* and *Rvi. gelatinosus* are able to make the second reactions, although in *Rvi. gelatinosus* the spheroidene pathway is still significant. *R. rubrum* has the highest substrate affinity among Rhodospirillaceae for the conversion of carotenoids bearing end groups.

7.3.1 The effect of oxygen on carotenoid biosynthesis

As we have seen, the pO_2 level did not affect the metabolic pattern of the cell, in contrast to the carotenoid production, where significant differences could be observed depending on the

oxygen availability. The presence of oxygen inhibits the conversion of the intermediate carotenoids to spx in the wild-type. In the presence of oxygen the second reactions of all carotenogenic enzymes became slower and anhydrorhodovibrin and dhspx accumulated additionally to spx.

CrtI-product inhibition An alternative spheroidene pathway has been determined in the wild-type after oxygen pulse (Fig. 66). The presence of the alternative spheroidene pathway can be realized via two possible processes. Either CrtI is inhibited by oxygen and catalyzes the conversion of neurosporene to lycopene more slowly, and neurosporene becomes available for the other carotenogenic enzymes or CrtC is very slow and can not convert lycopene to rhodopin, and the presence of lycopene inhibits CrtI. The high lycopene concentration under microaerophilic conditions supports the product inhibition concept.

Inhibition of CrtD by oxygen The metabolites of the alternative spheroidene pathway are similar to the normal spheroidene pathway, only they lack the double bond at the positions: 3,4 and 3´,4´. The absence of the double bonds can be realized either by the partially inactivation of CrtD by oxygen or these substrates are not convertible for CrtD. According to Albrecht *et al.* (1997), CrtD is able to convert chloroxanthin into demethyl-spheroidene. Most likely, CrtD is inhibited by oxygen and due to the reduced activity, the already slow CrtD is fully occupied with its normal substrates, and has no capacity for the metabolites of the other pathways. Furthermore, Davies *et al.* (1970) could observe spheroidene in DPA-inhibited cultures growing under phototrophic conditions. In the experiment of Davies *et al.* (1970) the absence of oxygen allows CrtD to function normally, whereas CrtI was blocked. Therefore we can conclude that the absence of spheroidene in this thesis is a consequence of the oxygen concentration and is consistent with the data of Davies *et al.* (1970). The higher production of dhspx shows also that in the competition for rhodovibrin, CrtF is significantly faster than CrtD under microaerobic conditions. If CrtD is inhibited in the presence of oxygen, CrtF catalyzes the conversion of rhodovibrin more rapidly but also in the methylation of rhodopin opening the alternative spx pathway, which was also observed in the wild-type in the presence of oxygen confirming the oxygen inhibition of CrtD (Fig. 66).

In ST4 the carotenoid composition was also strongly influenced by oxygen. The dynamic model of ST4 showed that predicted kinetic parameter of CrtI is three times lower than in the wild-type under microaerobic conditions. These kinetic circumstances may lead to the unique carotenoid composition. Apart from the alternative spx pathway, two further pathways were identified in the presence of oxygen. The presence of an alternative spheroidene pathway (found also in the wild-type under microaerobic conditions) and a totally new carotenoid

pathway was detected, designated as didehydrolycopene pathway (Fig. 70). The identification of this pathway indicates that CrtI is able to catalyze five desaturase steps in *R. rubrum*, since it is the only desaturase available in ST4.

CrtI-position of the fifth desaturase reaction The position of the fifth desaturase step is ambiguous. The most obvious solution would be that the desaturation of lycopene occurs as in *Rvi. gelatinosus*. However, 3,4-didehydrolycopene could not be detected, even in traces. The other possibility is the desaturation of rhodopin. This idea is supported also by the fact that in ST4, CrtC catalyzed the first hydroxylation faster than in the wild-type under microaerobic conditions. Therefore, lycopene is hardly available for desaturation. Since CrtF is significantly slower than CrtC, rhodopin is also not converted to 3,4-dihydroanhydrorhodovibrin, but is available for further desaturation steps.

Nevertheless, the fifth desaturation step by CrtI, which occurs at the level of rhodopin, must also be possible for lycopene. The reason for the absence of 3,4-didehydrolycopene in SLYC18 is, that lycopene does not accumulate in the Crt-enzyme complex, which kinetically biases a further desaturation, but it is immediately delivered to the LH1 (Wang *et al.*, 2012). This is in contrast to rhodopin, which is an asymmetrical carotenoid, which may hinder the rapid delivery to the LH1. Since rhodopin is available at relative high concentrations, it is desaturated to 1-hydroxy-3,4-didehydrolycopene, thereby opening up the 3,4-didehydrolycopene pathway.

Interestingly, the last possible combinatorial members of the 3,4-didehydrolycopene and the alternative spheroidene pathway are undetectable resulting in carotenoids bearing methoxy and hydroxyl groups as end products. The absence of the doubly-methoxylated carotenoids shows a higher substrate specificity of the CrtF in comparison to CrtC.

Comments to the combinatorial connections Davies *et al.*, (1970) have suggested that the different pathways observed in DPA-inhibited *R. rubrum* cultures can be connected to each other resulting in a combinatorial map of the carotenoid composition. This hypothesis was tested using the example of the desaturation of dhspx to spx. According to the model analysis, this reaction does not seem to take place. This result is consistent with the experiment of Albrecht *et al.* (1997), where CrtD of *Rb. sphaeroides* was unable to convert 1-methoxy-neurosporene into spheroidene due to the presence of the methoxy group. This idea is also supported by the fact, that the metabolite 3,4-dihydrorhodovibin could not detected in the wild-type of *R. rubrum* (Fig. 67B). Probably, 3,4-dihydrorhodovibin is produced at low levels, and either it is desaturated by CrtD to rhodovibrin due to the hydroxyl group at the 3′,4′ end of the molecule, or it is converted to thspx. Furthermore, the existence of 1-

hydroxy-didehydrolycopene shows that the hydroxylated forms can function as connecting point between the different pathways, confirming the combinatorial behaviour of the carotenogenic enzymes.

7.4 Summary and outlook

In this thesis, the metabolism and the PM production of *R. rubrum* was investigated under extreme oxygen and CO_2 limitation, which allowed the identification of a rescue mechanism of the cell under stress conditions. The RQ-dependent NADPH excess of the cell reflected by PHB and the linear regulation occurring in the flux distribution indicates that the cell attempts to get rid of the redox equivalents in every possible pathway. The applied analytical methods were able to yield a large amount of information about the metabolic pathway. However, in order to determine the role of RQ in the production of NADPH, systematic biochemical approaches have to be carried out.

The investigation of the microaerobic carotenoid biosynthesis showed that the cell takes advantage of the combinatorial behaviour of the carotenogenic enzymes and attempts to stabilize the carotenoids by minimizing the number of the double bonds. Physiologically, this strategy may be important as it is well known that the extent of conjugation affects the sensitivity to oxygen.

8 References

Aasen, A. J. and Liaaen-Jensen, S. (1967). Bacterial carotenoids. *Acta Chem. Scand.* **21**: 371–377.

Airs, R. L., Atkinson, J. E. and Keely, B. J. (2001). Development and application of a high resolution liquid chromatographic method for the analysis of complex pigment distributions. *J. Chromatogr. A* **917**: 167–177.

Airs, R. L. and Keely, B. J. (2002). Atmospheric pressure chemical ionisation liquid chromatography/mass spectrometry of bacteriochlorophylls from *Chlorobiaceae*: characteristic fragmentations. *Rapid Commun. Mass Spectrom.* **16**: 453–461.

Airs, R. L. and Keely, B. J. (2003). A high resolution study of the chlorophyll and bacteriochlorophyll pigment distributions in a calcite/gypsum microbial mat. *Org. Geochem.* **34**: 539–551.

Ajikumar, P. K., Xiao, W.-H., Tyo, K. E. J., Wang, Y., Simeon, F., Leonard, E., Mucha, O., Phon, T. H., Pfeifer, B. and Stephanopoulos, G. (2010). Isoprenoid pathway optimization for Taxol precursor overproduction in *Escherichia coli*. *Science* **330**: 70–4.

Albrecht, M., Ruther, A. and Sandmann, G. (1997). Purification and biochemical characterization of a hydroxyneurosporene desaturase involved in the biosynthetic pathway of the carotenoid spheroidene in *Rhodobacter sphaeroides*. *J. Bacteriol.* **179**: 7462–7.

Albrecht, M., Takaichi, S., Steiger, S., Wang, Z. Y. and Sandmann, G. (2000). Novel hydroxycarotenoids with improved antioxidative properties produced by gene combination in *Escherichia coli*. *Nat. Biotechnol.* **18**: 843–6.

Alper, H., Jin, Y.-S., Moxley, J. F. and Stephanopoulos, G. (2005). Identifying gene targets for the metabolic engineering of lycopene biosynthesis in *Escherichia coli*. *Metab. Eng.* **7**: 155–64.

Alper, H., Miyaoku, K. and Stephanopoulos, G. (2006). Characterization of lycopene-overproducing *E. coli* strains in high cell density fermentations. *Appl. Microbiol. Biotechnol.* **72**: 968–74.

Armstrong, G. a, Cook, D. N., Ma, D., Alberti, M., Burke, D. H. and Hearst, J. E. (1993). Regulation of carotenoid and bacteriochlorophyll biosynthesis genes and identification of an evolutionarily conserved gene required for bacteriochlorophyll accumulation. *J. Gen. Microbiol.* **139**: 897–906.

Armstrong, G. A., Alberti, M. and Hearst, J. E. (1990a). Conserved enzymes mediate the early reactions of carotenoid biosynthesis in nonphotosynthetic and photosynthetic prokaryotes. *Proc. Natl. Acad. Sci. U. S. A.* **87**: 9975–9.

Armstrong, G. A., Alberti, M., Leach, F. and Hearst, J. E. (1989). Nucleotide sequence, organization, and nature of the protein products of the carotenoid biosynthesis gene cluster of *Rhodobacter capsulatus*. *Mol. Gen. Genet.* **216**: 254–68.

Armstrong, G. A., Schmidt, A., Sandmann, G. and Hearst, J. E. (1990b). Genetic and biochemical characterization of carotenoid biosynthesis mutants of *Rhodobacter capsulatus*. *J. Biol. Chem.* **265**: 8329–38.

Ausich, R. L. (1997). Commercial opportunities for carotenoid production by biotechnology. *Pure Appl. Chem.* **69**: 2169–2174.

Badenhop, F., Steiger, S., Sandmann, M. and Sandmann, G. (2003). Expression and biochemical characterization of the 1-HO-carotenoid methylase CrtF from *Rhodobacter capsulatus*. *FEMS Microbiol. Lett.* **222**: 237–242.

Bartley, G. E., Schmidhauser, T. J., Yanofsky, C. and Scolnik, P. a (1990). Carotenoid desaturases from *Rhodobacter capsulatus* and *Neurospora crassa* are structurally and functionally conserved and contain domains homologous to flavoprotein disulfide oxidoreductases. *J. Biol. Chem.* **265**: 16020–4.

Bauer, C. E. and Bird, T. H. (1996). Regulatory circuits controlling photosynthesis gene expression. *Cell* **85**: 5–8.

Bauer, C. E. and Marrs, B. L. (1988). *Rhodobacter capsulatus* puf operon encodes a regulatory protein (PufQ) for bacteriochlorophyll biosynthesis. *Proc. Natl. Acad. Sci. U. S. A.* **85**: 7074–8.

Bauer, C. E., Young, D. A. and Marrs, B. L. (1988). Analysis of the *Rhodobacter capsulatus* puf operon. Location of the oxygen-regulated promoter region and the identification of an additional puf-encoded gene. *J. Biol. Chem.* **263**: 4820–7.

Beatty, J. T. and Cohen, S. N. (1983). Hybridization of cloned *Rhodopseudomonas capsulata* photosynthesis genes with DNA from other photosynthetic bacteria. *J. Bacteriol.* **154**: 1440–5.

Bendall, D. S. and Manasse, R. S. (1995). Cyclic photophosphorylation and electron transport. *Biochim. Biophys. Acta - Bioenerg.* **1229**: 23–28.

Biel, a J. and Marrs, B. L. (1983). Transcriptional regulation of several genes for bacteriochlorophyll biosynthesis in *Rhodopseudomonas capsulata* in response to oxygen. *J. Bacteriol.* **156**: 686–94.

Biel, a J. and Marrs, B. L. (1985). Oxygen does not directly regulate carotenoid biosynthesis in *Rhodopseudomonas capsulata*. *J. Bacteriol.* **162**: 1320–1.

Biel, A. J. (2004). Genetic analysis and regulation of bacteriochlorophyll biosynthesis. In R. Blankenship M. Madigan and C. Bauer (eds.), *Anoxygenic Photosynthetic Bacteria SE - 52*, Springer Netherlands, pp.1125–1134.

Bligh, E. G. and Dyer, W. J. (1959). A rapid method of total lipid extraction and purification. *Can. J. Biochem. Physiol.* **37**: 911–7.

Bojko, M., Kruk, J. and Więckowski, S. (2003). Plastoquinones are effectively reduced by ferredoxin:NADP+ oxidoreductase in the presence of sodium cholate micelles. Significance for cyclic electron transport and chlororespiration. *Phytochemistry* **64**: 1055–1060.

Bona-Lovasz, J., Bona, A., Ederer, M, Sawodny, O. and Ghosh, R. (2013). A rapid method for the extraction and analysis of carotenoids and other hydrophobic substances suitable for systems biology studies with photosynthetic bacteria. *Metabolites* **3**: 912-930

Bonam, D., Lehman, L., Roberts, G. P. and Ludden, P. W. (1989). Regulation of carbon monoxide dehydrogenase and hydrogenase in *Rhodospirillum rubrum*: effects of CO and oxygen on synthesis and activity. *J. Bacteriol.* **171**: 3102–7.

de Bont, J. A., Scholten, A. and Hansen, T. A. (1981). DNA-DNA hybridization of *Rhodopseudomonas capsulata*, *Rhodopseudomonas sphaeroides* and *Rhodopseudomonas sulfidophila* strains. *Arch. Microbiol.* **128**: 271–4.

Botella-Pavía, P., Besumbes, O., Phillips, M. a, Carretero-Paulet, L., Boronat, A. and Rodríguez-Concepción, M. (2004). Regulation of carotenoid biosynthesis in plants: evidence for a key role of hydroxymethylbutenyl diphosphate reductase in controlling the supply of plastidial isoprenoid precursors. *Plant J.* **40**: 188–99.

Braatsch, S., Gomelsky, M., Kuphal, S. and Klug, G. (2002). A single flavoprotein, AppA, integrates both redox and light signals in *Rhodobacter sphaeroides*. *Mol. Microbiol.* **45**: 827–36.

Brajcich, B. C., Iarocci, A. L., Johnstone, L. a G., Morgan, R. K., Lonjers, Z. T., Hotchko, M. J., Muhs, J. D., Kieffer, A., Reynolds, B. J., Mandel, S. M., Marbois, B. N., Clarke, C. F. and Shepherd, J. N. (2010). Evidence that ubiquinone is a required intermediate for rhodoquinone biosynthesis in *Rhodospirillum rubrum*. *J. Bacteriol.* **192**: 436–45.

Van Breemen, R. B., Huang, C., Tan, Y., Sander, L. C. and Schilling, A. B. (1996). Liquid Chromatography/Mass Spectrometry of Carotenoids Using Atmospheric Pressure Chemical Ionization. *J. Mass Spectrom.* **31**: 975–981.

Breithaupt, D. E. (2004). Simultaneous HPLC determination of carotenoids used as food coloring additives: applicability of accelerated solvent extraction. *Food Chem.* **86**: 449–456.

Britton, G., Liaaen-Jensen, S. and Pfander, H. (2004). *Carotenoids handbook*, G. Britton S. Liaaen-Jensen and H. Pfander (eds.), Birkhäuser, Basel.

Brostedt, E. and Nordlund, S. (1991). Purification and partial characterization of a pyruvate oxidoreductase from the photosynthetic bacterium *Rhodospirillum rubrum* grown under nitrogen-fixing conditions. *Biochem. J.* **279**: 155–158.

Burke, C. C., Wildung, M. R. and Croteau, R. (1999). Geranyl diphosphate synthase: cloning, expression, and characterization of this prenyltransferase as a heterodimer. *Proc. Natl. Acad. Sci. U. S. A.* **96**: 13062–7.

Burke, D. H., Alberti, M. and Hearst, J. E. (1993). bchFNBH bacteriochlorophyll synthesis genes of *Rhodobacter capsulatus* and identification of the third subunit of light-independent protochlorophyllide reductase in bacteria and plants. *J. Bacteriol.* **175**: 2414–22.

Cabrini, L., Landi, L., Stefanelli, C., Barzanti, V. and Anna Maria, S. (1992). Extraction of lipids and lipophilic antioxidants from fish tissues: A comparison among different methods. *Comp. Biochem. Physiol. Part B Comp. Biochem.* **101**: 383–386.

Callender, H. L., Forrester, J. S., Ivanova, P., Preininger, A., Milne, S. and Brown, H. A. (2007). Quantification of diacylglycerol species from cellular extracts by electrospray ionization mass spectrometry using a linear regression algorithm. *Anal. Chem.* **79**: 263–72.

Careri, M., Elviri, L. and Mangia, A. (1999). Liquid chromatography–electrospray mass spectrometry of β-carotene and xanthophylls. *J. Chromatogr. A* **854**: 233–244.

Carretero-Paulet, L., Ahumada, I., Cunillera, N., Rodríguez-Concepción, M., Ferrer, A., Boronat, A. and Campos, N. (2002). Expression and molecular analysis of the *Arabidopsis* DXR gene encoding 1-deoxy-D-xylulose 5-phosphate reductoisomerase, the first committed enzyme of the 2-C-methyl-D-erythritol 4-phosphate pathway. *Plant Physiol.* **129**: 1581–91.

Castro-Guerrero, N. a, Jasso-Chávez, R. and Moreno-Sánchez, R. (2005). Physiological role of rhodoquinone in *Euglena gracilis* mitochondria. *Biochim. Biophys. Acta* **1710**: 113–21.

Chamovitz, D., Misawa, N., Sandmann, G. and Hirschberg, J. (1992). Molecular cloning and expression in *Escherichia coli* of a cyanobacterial gene coding for phytoene synthase, a carotenoid biosynthesis enzyme. *FEBS Lett.* **296**: 305–10.

Clark, W. G., Davidson, E. and Marrs, B. L. (1984). Variation of levels of mRNA coding for antenna and reaction center polypeptides in *Rhodopseudomonas capsulata* in response to changes in oxygen concentration. *J. Bacteriol.* **157**: 945–8.

Cohen-Bazire, G. and Kunisawa, R. (1963). The fine structure of *Rhodospirillum rubrum*. *J. Cell Biol.* **16**: 401–19.

Cohen-Bazire, G., Sistrom, W. R. and Stanier, R. Y. (1957). Kinetic studies of pigment synthesis by non-sulfur purple bacteria. *J. Cell. Comp. Physiol.* **49**: 25–68.

Collins, M. L. and Niederman, R. A. (1976). Membranes of *Rhodospirillum rubrum*: isolation and physicochemical properties of membranes from aerobically grown cells. *J. Bacteriol.* **126**: 1316–1325.

Collins, M. L. P. and Hughes, C. A. N. (1983). Identity of succinate dehydrogenase in chemotrophically and phototrophically grown *Rhodospirillum rubrum*. *Arch. Microbiol.* **136**: 7–10.

Cordoba, E., Salmi, M. and León, P. (2009). Unravelling the regulatory mechanisms that modulate the MEP pathway in higher plants. *J. Exp. Bot.* **60**: 2933–43.

Cotton, N. P., White, S. a, Peake, S. J., McSweeney, S. and Jackson, J. B. (2001). The crystal structure of an asymmetric complex of the two nucleotide binding components of proton-translocating transhydrogenase. *Structure* **9**: 165–76.

Das, A., Yoon, S.-H., Lee, S.-H., Kim, J.-Y., Oh, D.-K. and Kim, S.-W. (2007). An update on microbial carotenoid production: application of recent metabolic engineering tools. *Appl. Microbiol. Biotechnol.* **77**: 505–12.

Davies, B. H. (1970a). A novel sequence for phytoene dehydrogenation in *Rhodospirillum rubrum*. *Biochem. J.* **116**: 93–9.

Davies, B. H. (1970b). Alternative pathways of spirilloxanthin biosynthesis in *Rhodospirillum rubrum*. *Biochem. J.* **116**: 101–110.

Davis, K. A., Hatefi, Y., Crawford, I. P. and Baltscheffsky, H. (1977). Purification, molecular properties, and amino acid composition of the subunits of *Rhodospirillum rubrum* succinate dehydrogenase. *Arch. Biochem. Biophys.* **180**: 459–64.

Dixon, R. and Kahn, D. (2004). Genetic regulation of biological nitrogen fixation. *Nat. Rev. Microbiol.* **2**: 621–31.

Dubbs, J. M. and Robert Tabita, F. (2004). Regulators of nonsulfur purple phototrophic bacteria and the interactive control of CO2 assimilation, nitrogen fixation, hydrogen metabolism and energy generation. *FEMS Microbiol. Rev.* **28**: 353–376.

Edge, R., McGarvey, D. J. and Truscott, T. G. (1997). The carotenoids as anti-oxidants--a review. *J. Photochem. Photobiol. B.* **41**: 189–200.

Eisenreich, W., Bacher, A., Arigoni, D. and Rohdich, F. (2004). Biosynthesis of isoprenoids via the non-mevalonate pathway. *Cell. Mol. Life Sci.* **61**: 1401–1426.

Elsen, S., Dischert, W., Colbeau, A. and Bauer, C. E. (2000). Expression of uptake hydrogenase and molybdenum nitrogenase in *Rhodobacter capsulatus* is coregulated by the RegB-RegA two-component regulatory system. *J. Bacteriol.* **182**: 2831–7.

Elsen, S., Swem, L. R., Swem, D. L. and Bauer, C. E. (2004). RegB / RegA , a highly conserved redox-responding global two-component regulatory system. *Microbiol. Mol. Biol. Rev.* **68**: 263–279.

Enfissi, E. M. a, Fraser, P. D., Lois, L.-M., Boronat, A., Schuch, W. and Bramley, P. M. (2005). Metabolic engineering of the mevalonate and non-mevalonate isopentenyl diphosphate-forming pathways for the production of health-promoting isoprenoids in tomato. *Plant Biotechnol. J.* **3**: 17–27.

Ensign, S. A. and Ludden, P. W. (1991). Characterization of the CO oxidation/H2 evolution system of *Rhodospirillum rubrum*. Role of a 22-kDa iron-sulfur protein in mediating electron transfer between carbon monoxide dehydrogenase and hydrogenase. *J. Biol. Chem.* **266**: 18395–403.

Eraso, J. M. and Kaplan, S. (2000). From redox flow to gene regulation: role of the PrrC protein of *Rhodobacter sphaeroides*. *Biochemistry* **39**: 2052–2062.

Ernst, H. (2002). Recent advances in industrial carotenoid synthesis. *Pure Appl. Chem.* **74**: 1369–1382.

Estévez, J. M., Cantero, a, Reindl, a, Reichler, S. and León, P. (2001). 1-Deoxy-D-xylulose-5-phosphate synthase, a limiting enzyme for plastidic isoprenoid biosynthesis in plants. *J. Biol. Chem.* **276**: 22901–9.

Eubanks, L. M. and Poulter, C. D. (2003). *Rhodobacter capsulatus* 1-deoxy-D-xylulose 5-phosphate synthase: steady-state kinetics and substrate binding. *Biochemistry* **42**: 1140–9.

Farmer, W. R. and Liao, J. C. (2001). Precursor balancing for metabolic engineering of lycopene production in *Escherichia coli*. *Biotechnol. Prog.* **17**: 57–61.

Ferguson, S. J., Jackson, J. B. and McEwan, A. G. (1987). Anaerobic respiration in the Rhodospirillaceae: characterisation of pathways and evaluation of roles in redox balancing during photosynthesis. *FEMS Microbiol. Lett.* **46**: 117–143.

Fox, J. D., Kerby, R. L., Roberts, G. P. and Ludden, P. W. (1996). Characterization of the CO-induced, CO-tolerant hydrogenase from *Rhodospirillum rubrum* and the gene encoding the large subunit of the enzyme. *J. Bacteriol.* **178**: 1515–24.

Frank, H. A., Chynwat, V., Desamero, R. Z. B., Farhoosh, R., Erickson, J. and Bautista, J. (1997). On the photophysics and photochemical properties of carotenoids and their role as light-harvesting pigments in photosynthesis. *Pure Appl. Chem.* **69**: 2117–2124.

Fraser, P. D., Misawa, N., Linden, H., Yamano, S., Kobayashi, K. and Sandmann, G. (1992). Expression in *Escherichia coli*, purification, and reactivation of the recombinant *Erwinia uredovora* phytoene desaturase. *J. Biol. Chem.* **267**: 19891–5.

Ghosh, R., Bachofen, R. (1989).Die molekulare Struktur der photosynthetischen Memmbranen bei anoxygenen phototropen Bakterien. *Forum Mikrobiol.* **12**: 556-564

Ghosh, R., Hardmeyer, A., Thoenen, I. and Bachofen, R. (1994). Optimization of the Sistrom culture medium for large-scale batch cultivation of *Rhodospirillum rubrum* under semiaerobic conditions with maximal yield of photosynthetic membranes. *Appl. Environ. Microbiol.* **60**: 1698–700.

Gimenez-Gallego, G., Ramírez-Ponce, M. P., Lauzurica, P. and Ramírez, J. M. (1982). Photooxidase system of *Rhodospirillum rubrum* III. The role of rhodoquinone and ubiquinone in the activity of preparations of chromatophores and photoreaction centers. *Eur. J. Biochem.* **121**: 343–7.

Giuliano, G., Pollock, D., Stapp, H. and Scolnik, P. A. (1988). A genetic-physical map of the *Rhodobacter capsulatus* carotenoid biosynthesis gene cluster. *Mol. Gen. Genet.* **213**: 78–83.

Gomelsky, M. and Kaplan, S. (1995a). Genetic evidence that PpsR from *Rhodobacter sphaeroides* 2.4.1 functions as a repressor of puc and bchF expression. *J. Bacteriol.* **177**: 1634–7.

Gomelsky, M. and Kaplan, S. (1995b). appA, a novel gene encoding a trans-acting factor involved in the regulation of photosynthesis gene expression in *Rhodobacter sphaeroides* 2.4.1. *J. Bacteriol.* **177**: 4609–18.

Goodwin, T. W. (1956). The carotenoids of photosynthetic bacteria. II. The carotenoids of a number of non-sulphur purple photosynthetic bacteria (Athiorhodiaceae). *Arch. Mikrobiol.* **24**: 313–22.

Goodwin, T. W., Land, D. G. and Osman, H. G. (1955). Studies in carotenogenesis. 14. Carotenoid synthesis in the photosynthetic bacterium *Rhodopseudomonas spheroides*. *Biochem. J.* **59**: 491–6.

Goodwin, T. W. and Osman, H. G. (1953). Studies in carotenogenesis. 9. General cultural conditions controlling carotenoid (spirilloxanthin) synthesis in the photosynthetic bacterium *Rhodospirillum rubrum*. *Biochem. J.* **53**: 541–6.

Goodwin, T. W. and Osman, H. G. (1954). Studies in carotenogenesis. 10. Spirilloxanthin synthesis by washed cells of *Rhodospirillum rubrum*. *Biochem. J.* **56**: 222–30.

Gorrell, T. E. and Uffen, R. L. (1977). Fermentative metabolism of pyruvate by *Rhodospirillum rubrum* after anaerobic growth in darkness. *J. Bacteriol.* **131**: 533–43.

Grammel, H. and Ghosh, R. (2008). Redox-state dynamics of ubiquinone-10 imply cooperative regulation of photosynthetic membrane expression in *Rhodospirillum rubrum*. *J. Bacteriol.* **190**: 4912–21.

Grammel, H., Gilles, E. and Ghosh, R. (2003). Microaerophilic cooperation of reductive and oxidative pathways allows maximal photosynthetic membrane biosynthesis in *Rhodospirillum rubrum*. *Appl. Environ. Microbiol.* **69**: 6577–6586.

Griffiths, B. Y. M. (1962). Further mutational changes in the photosynthetic pigment system of *Rhodopseudomonas spheroides*. *J. Gen. Microbiol.* **27**: 427–35.

Griffiths, B. Y. M. and Stainer, R. Y. (1956). Some mutational changes in the photosynthetic pigment system of *Rhodopseudomonas spheroides*. *J. Gen. Microbiol.* **14**: 698–715.

Gruszecki, W. I. and Strzałka, K. (2005). Carotenoids as modulators of lipid membrane physical properties. *Biochim. Biophys. Acta* **1740**: 108–15.

Guevara-García, A., San Román, C., Arroyo, A., Cortés, M. E., de la Luz Gutiérrez-Nava, M. and León, P. (2005). Characterization of the Arabidopsis clb6 mutant illustrates the importance of posttranscriptional regulation of the methyl-D-erythritol 4-phosphate pathway. *Plant Cell* **17**: 628–43.

Harada, H. and Misawa, N. (2012). *Microbial Carotenoids from Bacteria and Microalgae*, J.-L. Barredo (ed.), Humana Press, Totowa, NJ.

Harada, J. (2001). Phytoene desaturase, CrtI, of the purple photosynthetic bacterium, *Rubrivivax gelatinosus*, produces both neurosporene and lycopene. *Plant Cell Physiol.* **42**: 1112–1118.

Harker, M. and Bramley, P. M. (1999). Expression of prokaryotic 1-deoxy-D-xylulose-5-phosphatases in *Escherichia coli* increases carotenoid and ubiquinone biosynthesis. *FEBS Lett.* **448**: 115–9.

Hatefi, Y., Davis, K. A., Baltscheffsky, H., Baltscheffsky, M. and Johansson, B. C. (1972). Isolation and properties of succinate dehydrogenase from *Rhodospirillum rubrum*. *Arch. Biochem. Biophys.* **152**: 613–618.

Henderson, R. a. and Jones, C. W. (1997). Physiology of poly-3-hydroxybutyrate (PHB) production by *Alcaligenes eutrophus* growing in continuous culture. *Microbiology* **143**: 2361–2371.

Heo, J., Skjeldal, L., Staples, C. R. and Ludden, P. W. (2002). Carbon monoxide dehydrogenase from *Rhodospirillum rubrum* produces formate. *J. Biol. Inorg. Chem.* **7**: 810–4.

Hiraishi, A. (1988). Fumarate reduction systems in members of the family *Rhodospirillaceae* with different quinone types. *Arch. Microbiol.* **150**: 56–60.

Hiraishi, A. (1999). Isoprenoid quinones as biomarkers of microbial populations in the environment. *J. Biosci. Bioeng.* **88**: 449–60.

Hirayama, O. (1968). Lipids and lipoprotein complex in photosynthetic tissues. *Agric. Biol. Chem.* **32**: 34–41.

Hiseni, A., Arends, I. W. C. E. and Otten, L. G. (2011). Biochemical characterization of the carotenoid 1,2-hydratases (CrtC) from *Rubrivivax gelatinosus* and *Thiocapsa roseopersicina*. *Appl. Microbiol. Biotechnol.* **91**: 1029–36.

Hoffmann, J., Bona-Lovasz, J., Beuttler, H. and Altenbuchner, J. (2012). In vivo and in vitro studies on the carotenoid cleavage oxygenases from *Sphingopyxis alaskensis* RB2256 and *Plesiocystis pacifica* SIR-1 revealed their substrate specificities and non-retinal-forming cleavage activities. *FEBS J.* **279**: 3911–24.

Hoffmeister, M., van der Klei, A., Rotte, C., van Grinsven, K. W. a, van Hellemond, J. J., Henze, K., Tielens, A. G. M. and Martin, W. (2004). *Euglena gracilis* rhodoquinone:ubiquinone ratio and mitochondrial proteome differ under aerobic and anaerobic conditions. *J. Biol. Chem.* **279**: 22422–9.

Inbaraj, B. S., Lu, H., Hung, C. F., Wu, W. B., Lin, C. L. and Chen, B. H. (2008). Determination of carotenoids and their esters in fruits of *Lycium barbarum* Linnaeus by HPLC-DAD-APCI-MS. *J. Pharm. Biomed. Anal.* **47**: 812–818.

Ivanovsky, R., Krasilnikova, E. N. and Berg, I. A. (1997). A proposed citramalate cycle for acetate assimilation in the purple non-sulfur bacterium *Rhodospirillum rubrum*. *FEMS Microbiol. Lett.* **153**: 399–404.

Jackman, L. M. and Liaaen-Jensen, S. (1961). Bacterial carotenoids IX. The constitution of the third member of the P481-group (3,4-dehydro-rhodopin). *Acta Chem. Scand.* **15**: 2058–2060.

Jackman, L. M. and Liaaen-Jensen, S. (1964). Bacterial carotenoids XV on the constitution of the minor carotenoids of *Rhodopseudomonas* 5. The structures of P518(2,2´-diketo-spirilloxanthin), OH-R (OH-spheroidenone), ans OH-Y (OH-spheroidene). *Acta Chem. Scand.* **18**: 1403–1411.

Jackson, J. B. (2003). Proton translocation by transhydrogenase. *FEBS Lett.* **545**: 18–24.

Jackson, J. B., Peake, S. J. and White, S. A. (1999). Structure and mechanism of proton-translocating transhydrogenase. *FEBS Lett.* **464**: 1–8.

Jeeves, M., Smith, K. J., Quirk, P. G., Cotton, N. P. and Jackson, J. B. (2000). Solution structure of the NADP(H)-binding component (dIII) of proton-translocating transhydrogenase from *Rhodospirillum rubrum*. *Biochim. Biophys. Acta* **1459**: 248–57.

Jensen, S. L., Cohen-Bazire, G., Nakayama, T. O. M. and Stanier, R. Y. (1958). The path of carotenoid synthesis in a photosynthetic bacterium. *Biochim. Biophys. Acta* **29**: 477–498.

Joshi, H. M. and Tabita, F. R. (1996). A global two component signal transduction system that integrates the control of photosynthesis, carbon dioxide assimilation, and nitrogen fixation. *Proc. Natl. Acad. Sci. U. S. A.* **93**: 14515–20.

Kachanovsky, D. E., Filler, S., Isaacson, T. and Hirschberg, J. (2012). Epistasis in tomato color mutations involves regulation of phytoene synthase 1 expression by cis-carotenoids. *Proc. Natl. Acad. Sci. U. S. A.* **109**: 19021–6.

Kaiser, P., Geyer, R., Surmann, P. and Fuhrmann, H. (2012). LC-MS method for screening unknown microbial carotenoids and isoprenoid quinones. *J. Microbiol. Methods* **88**: 28–34.

Kaiser, P., Surmann, P., Vallentin, G. and Fuhrmann, H. (2007). A small-scale method for quantitation of carotenoids in bacteria and yeasts. *J. Microbiol. Methods* **70**: 142–9.

Kanemoto, R. H. and Ludden, P. W. (1984). Effect of ammonia, darkness, and phenazine methosulfate on whole-cell nitrogenase activity and Fe protein modification in *Rhodospirillum rubrum*. *J. Bacteriol.* **158**: 713–20.

Kappler, U., Huston, W. M. and McEwan, A. G. (2002). Control of dimethylsulfoxide reductase expression in *Rhodobacter capsulatus*: the role of carbon metabolites and the response regulators DorR and RegA. *Microbiology* **148**: 605–14.

Karlsson, A. Å., Michelsen, P., Larsen, Å. and Odham, G. (1996). Normal-phase liquid chromatography class separation and species determination of phospholipids utilizing electrospray mass spectrometry/tandem mass spectrometry. *Rapid Commun. Mass Spectrom.* **10**: 775–780.

Keister, D. L. and Yike, N. J. (1967). Energy-linked reactions in photosynthetic bacteria. *Arch. Biochem. Biophys.* **121**: 415–422.

Kerby, R. L., Ludden, P. W. and Roberts, G. P. (1995). Carbon monoxide-dependent growth of *Rhodospirillum rubrum*. *J. Bacteriol.* **177**: 2241–4.

Kiley, P. J. and Kaplan, S. (1987). Cloning, DNA sequence, and expression of the *Rhodobacter sphaeroides* light-harvesting B800-850-alpha and B800-850-beta genes. *J. Bacteriol.* **169**: 3268–75.

Kiley, P. J. and Kaplan, S. (1988). Molecular genetics of photosynthetic membrane biosynthesis in *Rhodobacter sphaeroides*. *Microbiol. Rev.* **52**: 50–69.

Kim, Y.-S., Lee, J.-H., Kim, N.-H., Yeom, S.-J., Kim, S.-W. and Oh, D.-K. (2011). Increase of lycopene production by supplementing auxiliary carbon sources in metabolically engineered *Escherichia coli*. *Appl. Microbiol. Biotechnol.* **90**: 489–97.

Komori, M., Ghosh, R., Takaichi, S., Hu, Y., Mizoguchi, T., Koyama, Y. and Kuki, M. (1998). A null lesion in the rhodopin 3,4-desaturase of *Rhodospirillum rubrum* unmasks a cryptic branch of the carotenoid biosynthetic pathway. *Biochemistry* **37**: 8987–94.

Komuniecki, R., McCrury, J., Thissen, J. and Rubin, N. (1989). Electron-transfer flavoprotein from anaerobic *Ascaris suum* mitochondria and its role in NADH-dependent 2-methyl branched-chain enoyl-CoA reduction. *Biochim. Biophys. Acta* **975**: 127–31.

Kovács, A. T., Rákhely, G. and Kovács, K. L. (2005). The PpsR regulator family. *Res. Microbiol.* **156**: 619–25.

Krinsky, N. I. and Yeum, K.-J. (2003). Carotenoid–radical interactions. *Biochem. Biophys. Res. Commun.* **305**: 754–760.

Kröger, A., Winkler, E., Innerhofer, A., Hackenberg, H. and Schägger, H. (1979). The formate dehydrogenase involved in electron transport from formate to fumarate in *Vibrio succinogenes*. *Eur. J. Biochem.* **94**: 465–75.

Kurz, C., Carle, R. and Schieber, A. (2008). HPLC-DAD-MSn characterisation of carotenoids from apricots and pumpkins for the evaluation of fruit product authenticity. *Food Chem.* **110**: 522–530.

Kuzuyama, T. and Seto, H. (2003). Diversity of the biosynthesis of the isoprene units. *Nat. Prod. Rep.* **20**: 171–183.

Lang, H. P., Cogdell, R. J., Takaichi, S. and Hunter, C. N. (1995). Complete DNA sequence, specific Tn5 insertion map, and gene assignment of the carotenoid biosynthesis pathway of *Rhodobacter sphaeroides*. *J. Bacteriol.* **177**: 2064–73.

Lang, J., Gohil, K. and Packer, L. (1986). Simultaneous determination of tocopherols, ubiquinols, and ubiquinones in blood, plasma, tissue homogenates, and subcellular fractions. *Anal. Biochem.* **157**: 106–116.

Lange, B. M., Wildung, M. R., McCaskill, D. and Croteau, R. (1998). A family of transketolases that directs isoprenoid biosynthesis via a mevalonate-independent pathway. *Proc. Natl. Acad. Sci. U. S. A.* **95**: 2100–4.

Lascelles, J. and Szilagyi, J. F. (1965). Phospholipid synthesis by *Rhodopseudomonas spheroides* in relation to the formation of photosynthetic pigments. *J. Gen. Microbiol.* **38**: 55–64.

Liaaen-Jensen, S. and Andrewes, a G. (1972). Microbial carotenoids. *Annu. Rev. Microbiol.* **26**: 225–48.

Liaaen-Jensen, S., Cohen-Bazire, G. and Stainer, R. Y. (1961). Biosynthesis of carotenoids in purple bacteria: a re-evaluation based on considerations of chemical structure. *Nature* **192**: 1168–1172.

Lois, L. M., Campos, N., Putra, S. R., Danielsen, K., Rohmer, M. and Boronat, A. (1998). Cloning and characterization of a gene from *Escherichia coli* encoding a transketolase-like enzyme that catalyzes the synthesis of D-1-deoxyxylulose 5-phosphate, a common precursor

for isoprenoid, thiamin, and pyridoxol biosynthesis. *Proc. Natl. Acad. Sci. U. S. A.* **95**: 2105–10.

Lois, L. M., Rodríguez-Concepción, M., Gallego, F., Campos, N. and Boronat, a (2000). Carotenoid biosynthesis during tomato fruit development: regulatory role of 1-deoxy-D-xylulose 5-phosphate synthase. *Plant J.* **22**: 503–13.

Lonjers, Z. T., Dickson, E. L., Chu, T.-P. T., Kreutz, J. E., Neacsu, F. a, Anders, K. R. and Shepherd, J. N. (2012). Identification of a new gene required for the biosynthesis of rhodoquinone in *Rhodospirillum rubrum*. *J. Bacteriol.* **194**: 965–71.

Lüderitz, R. and Klemme, J. H. (1976). "Isolation and characterization of a membrane-bound pyruvate dehydrogenase complex from the phototrophic bacterium *Rhodospirillum rubrum*." (author's transl) *Z. Naturforsch. C.* **32**: 351–361.

Lytle, C. a, Gan, Y. D., Salone, K. and White, D. C. (2001). Sensitive characterization of microbial ubiquinones from biofilms by electrospray/mass spectrometry. *Environ. Microbiol.* **3**: 265–72.

Ma, Y. C., Funk, M., Dunham, W. R. and Komuniecki, R. (1993). Purification and characterization of electron-transfer flavoprotein: rhodoquinone oxidoreductase from anaerobic mitochondria of the adult parasitic nematode, *Ascaris suum*. *J. Biol. Chem.* **268**: 20360–5.

Mahendra, K., Murthy, Y. L. N., Narasimha Rao, C. V. and Bala Murali Krishna, K. (2011). Determination of ubiquinone Q10 (coenzyme Q10) and its synthesis related impurities by high performance liquid chromatography and mass spectrometry. *Int. J. PharmTech Res.* **3**: 1467–1477.

Maness, P.-C. and Weaver, P. (2001). Evidence for three distinct hydrogenase activities in *Rhodospirillum rubrum*. *Appl. Microbiol. Biotechnol.* **57**: 751–756.

Marrs, B. (1974). Genetic recombination in *Rhodopseudomonas capsulata*. *Proc. Natl. Acad. Sci. U. S. A.* **71**: 971–3.

Masuda, S. and Bauer, C. E. (2002). AppA is a blue light photoreceptor that antirepresses photosynthesis gene expression in *Rhodobacter sphaeroides*. *Cell* **110**: 613–23.

Matthews, P. D. and Wurtzel, E. T. (2000). Metabolic engineering of carotenoid accumulation in *Escherichia coli* by modulation of the isoprenoid precursor pool with expression of deoxyxylulose phosphate synthase. *Appl. Microbiol. Biotechnol.* **53**: 396–400.

Mayne, S. T. (1996). Beta-carotene, carotenoids, and disease prevention in humans. *FASEB J.* **10**: 690–701.

Mercadante, A. Z., Rodriguez-Amaya, D. B. and Britton, G. (1997). HPLC and Mass Spectrometric Analysis of Carotenoids from Mango. *J. Agric. Food Chem.* **45**: 120–123.

Misawa, N., Nakagawa, M., Kobayashi, K., Yamano, S., Izawa, Y., Nakamura, K. and Harashima, K. (1990). Elucidation of the *Erwinia uredovora* carotenoid biosynthetic pathway

by functional analysis of gene products expressed in *Escherichia coli*. *J. Bacteriol.* **172**: 6704–12.

Misawa, N., Truesdale, M. R., Sandmann, G., Fraser, P. D., Bird, C., Schuch, W. and Bramley, P. M. (1994). Expression of a tomato cDNA coding for phytoene synthase in *Escherichia coli*, phytoene formation in vivo and in vitro, and functional analysis of the various truncated gene products. *J. Biochem.* **116**: 980–5.

Mitchell, K. and Fallon, R. J. (1990). The determination of ubiquinone profiles by reversed-phase high-performance thin-layer chromatography as an aid to the speciation of *Legionellaceae*. *J. Gen. Microbiol.* **136**: 2035–2041.

Mizoguchi, T., Harada, J. and Tamiaki, H. (2006). Structural determination of dihydro- and tetrahydrogeranylgeranyl groups at the 17-propionate of bacteriochlorophylls-a. *FEBS Lett.* **580**: 6644–8.

Mizoguchi, T., Isaji, M., Harada, J. and Tamiaki, H. (2008). Identification of 3,4-didehydrorhodopin as major carotenoid in *Rhodopseudomonas* species. *Photochem. Photobiol. Sci.* **7**: 492–7.

Mller-Zinkhan, D. and Thauer, R. K. (1988). Membrane-bound NADPH dehydrogenase- and ferredoxin: NADP oxidoreductase activity involved in electron transport during acetate oxidation to CO2 in *Desulfobacter postgatei*. *Arch. Microbiol.* **150**: 145–154.

Mortensen, a, Skibsted, L. H. and Truscott, T. G. (2001). The interaction of dietary carotenoids with radical species. *Arch. Biochem. Biophys.* **385**: 13–9.

Mortensen, A. (2006). Carotenoids and other pigments as natural colorants. *Pure Appl. Chem.* **78**: 1477–1491.

Mosley, C. S., Suzuki, J. Y. and Bauer, C. E. (1994). Identification and molecular genetic characterization of a sensor kinase responsible for coordinately regulating light harvesting and reaction center gene expression in response to anaerobiosis. *J. Bacteriol.* **176**: 7566–73.

Munk, a C., Copeland, A., Lucas, S., Lapidus, A., Del Rio, T. G., Barry, K., Detter, J. C., Hammon, N., Israni, S., Pitluck, S., Brettin, T., Bruce, D., Han, C., Tapia, R., Gilna, P., Schmutz, J., Larimer, F., Land, M., Kyrpides, N. C., Mavromatis, K., Richardson, P., Rohde, M., Göker, M., Klenk, H.-P., Zhang, Y., Roberts, G. P., Reslewic, S. and Schwartz, D. C. (2011). Complete genome sequence of *Rhodospirillum rubrum* type strain (S1). *Stand. Genomic Sci.* **4**: 293–302.

Muraca, R. F., Whittick, J. S., Daves, G. D., Friis, P. and Folkers, K. (1967). Mass spectra of ubiquinones and ubiquinols. *J. Am. Chem. Soc.* **89**: 1505–1508.

Naylor, G. W., Addlesee, H. A., Charles, L., Gibson, D. and Hunter, N. (1999). The photosynthesis gene cluster of *Rhodobacter sphaeroides*. *Photosynth. Res.* **62**: 121–139.

Neudert, U., Martínez-Férez, I. M., Fraser, P. D. and Sandmann, G. (1998). Expression of an active phytoene synthase from *Erwinia uredovora* and biochemical properties of the enzyme. *Biochim. Biophys. Acta* **1392**: 51–8.

Nickens, D. G. and Bauer, C. E. (1998). Analysis of the puc operon promoter from *Rhodobacter capsulatus*. *J. Bacteriol.* **180**: 4270–7.

Niel, C. B. (1947). Studies on the pigments of the purple bacteria. *Antonie Van Leeuwenhoek* **12**: 156–166.

Van Niel, C. B., Goodwin, T. W. and Sissins, M. E. (1956). Studies in carotenogenesis. 21. The nature of the changes in carotenoid synthesis in *Rhodospirillum rubrum* during growth. *Biochem. J.* **63**: 408–12.

Van Niel, C. B., and Smith, J. H. C. (1935). Studies on the pigments of the purple bacteria I. On spirilloxanthin, a component of the pigment complex of *Spirillum rubrum*. *Arch. Mikrobiol.* **6**: 219–229.

Nishizaki, T., Tsuge, K., Itaya, M., Doi, N. and Yanagawa, H. (2007). Metabolic engineering of carotenoid biosynthesis in *Escherichia coli* by ordered gene assembly in *Bacillus subtilis*. *Appl. Environ. Microbiol.* **73**: 1355–61.

Oelze, J., Golecki, J. R., Kleinig, H. and Weckesser, J. (1975). Characterization of two cell-envelope fractions from chemotrophically grown *Rhodospirillum rubrum*. *Antonie Van Leeuwenhoek* **41**: 273–286.

Oh, J. I. and Kaplan, S. (1999). The cbb3 terminal oxidase of *Rhodobacter sphaeroides* 2.4.1: structural and functional implications for the regulation of spectral complex formation. *Biochemistry* **38**: 2688–96.

Oh, J. I. and Kaplan, S. (2000). Redox signaling: globalization of gene expression. *EMBO J.* **19**: 4237–47.

Ohnuma, S., Nakazawa, T., Hemmi, H., Hallberg, a M., Koyama, T., Ogura, K. and Nishino, T. (1996). Conversion from farnesyl diphosphate synthase to geranylgeranyl diphosphate synthase by random chemical mutagenesis. *J. Biol. Chem.* **271**: 10087–95.

Paiva, S. A. R. and Russell, R. M. (1999). β-Carotene and Other Carotenoids as Antioxidants. *J. Am. Coll. Nutr.* **18**: 426–433.

Pan, J., Lin, S., Allen, J. P., Williams, J. C., Frank, H. a and Woodbury, N. W. (2011). Carotenoid excited-state properties in photosynthetic purple bacterial reaction centers: effects of the protein environment. *J. Phys. Chem. B* **115**: 7058–68.

Pemberton, J. M. and Bowen, a R. (1981). High-frequency chromosome transfer in *Rhodopseudomonas sphaeroides* promoted by broad-host-range plasmid RP1 carrying mercury transposon Tn501. *J. Bacteriol.* **147**: 110–7.

Pemberton, J. M. and Harding, C. M. (1986). Cloning of carotenoid biosynthesis genes from *Rhodopseudomonas sphaeroides*. *Curr. Microbiol.* **14**: 25–29.

Pemberton, J. M. and Harding, C. M. (1987). Expression of *Rhodopseudomonas sphaeroides* carotenoid photopigment genes in phylogenetically related nonphotosynthetic bacteria. *Curr. Microbiol.* **15**: 67–71.

Penfold, R. J. and Pemberton, J. M. (1994). Sequencing, chromosomal inactivation, and functional expression in *Escherichia coli* of ppsR, a gene which represses carotenoid and bacteriochlorophyll synthesis in *Rhodobacter sphaeroides*. *J. Bacteriol.* **176**: 2869–76.

Pinta, V., Ouchane, S., Picaud, M., Takaichi, S., Astier, C. and Reiss-Husson, F. (2003). Characterization of unusual hydroxy- and ketocarotenoids in *Rubrivivax gelatinosus*: involvement of enzyme CrtF or CrtA. *Arch. Microbiol.* **179**: 354–62.

Polgar, A., Van Niel, C. B. and Zechmeiste, L. (1944). Studies on the pigments of the purple bacteria. II. A spectroscopic and stereochemical investigation of spirilloxanthin. *Arch. Biochem. Biophys.* **5**: 243–264.

Polívka, T. and Sundström, V. (2004). Ultrafast dynamics of carotenoid excited states - from solution to natural and artificial systems. *Chem. Rev.* **104**: 2021–71.

Qian, Y. and Tabita, F. R. (1996). A global signal transduction system regulates aerobic and anaerobic CO2 fixation in *Rhodobacter sphaeroides*. *J. Bacteriol.* **178**: 12–8.

Ritter, J. B., Genzel, Y. and Reichl, U. (2006). High-performance anion-exchange chromatography using on-line electrolytic eluent generation for the determination of more than 25 intermediates from energy metabolism of mammalian cells in culture. *J. Chromatogr. B. Analyt. Technol. Biomed. Life Sci.* **843**: 216–26.

Rodriguez-Amaya, D. and Kimura, M. (2004). *HarvestPlus handbook for carotenoid analysis*, International Food Policy Research Institute (IFPRI).

Rodríguez-Concepción, M. and Boronat, A. (2002). Elucidation of the methylerythritol phosphate pathway for isoprenoid biosynthesis in bacteria and plastids. A metabolic milestone achieved through genomics. *Plant Physiol.* **130**: 1079–89.

Rodríguez-Concepción, M., Querol, J., Lois, L. M., Imperial, S. and Boronat, A. (2003). Bioinformatic and molecular analysis of hydroxymethylbutenyl diphosphate synthase (GCPE) gene expression during carotenoid accumulation in ripening tomato fruit. *Planta* **217**: 476–82.

Rodríguez-Villalón, A., Gas, E. and Rodríguez-Concepción, M. (2009). Phytoene synthase activity controls the biosynthesis of carotenoids and the supply of their metabolic precursors in dark-grown *Arabidopsis* seedlings. *Plant J.* **60**: 424–35.

Rohmer, M. (1999). The discovery of a mevalonate-independent pathway for isoprenoid biosynthesis in bacteria, algae and higher plants. *Nat. Prod. Rep.* **16**: 565–74.

Rohmer, M., Knani, M., Simonin, P., Sutter, B. and Sahm, H. (1993). Isoprenoid biosynthesis in bacteria: a novel pathway for the early steps leading to isopentenyl diphosphate. *Biochem. J.* **295 (Pt 2**: 517–24.

Rohmer, M., Seemann, M., Horbach, S., Bringer-Meyer, S. and Sahm, H. (1996). Glyceraldehyde 3-phosphate and pyruvate as precursors of isoprenic units in an alternative non-mevalonate pathway for terpenoid biosynthesis. *J. Am. Chem. Soc.* **118**: 2564–2566.

Ruiz-Jiménez, J., Priego-Capote, F., Mata-Granados, J. M., Quesada, J. M. and Luque de Castro, M. D. (2007). Determination of the ubiquinol-10 and ubiquinone-10 (coenzyme Q10)

in human serum by liquid chromatography tandem mass spectrometry to evaluate the oxidative stress. *J. Chromatogr. A* **1175**: 242–8.

Russell, N. J. and Harwood, J. L. (1979). Changes in the acyl lipid composition of photosynthetic bacteria grown under photosynthetic and non-photosynthetic conditions. *Biochem. J.* **181**: 339–45.

Saegesser, R., Ghosh, R. and Bachofen, R. (1992). Stability of broad host range cloning vectors in the phototrophic bacterium *Rhodospirillum rubrum*. *FEMS Microbiol. Lett.* **95**: 7–11.

Sauret-Güeto, S., Botella-Pavía, P., Flores-Pérez, U., Martínez-García, J. F., San Román, C., León, P., Boronat, A. and Rodríguez-Concepción, M. (2006). Plastid cues posttranscriptionally regulate the accumulation of key enzymes of the methylerythritol phosphate pathway in *Arabidopsis*. *Plant Physiol.* **141**: 75–84.

Scherer, S., Alpes, I., Sadowski, H. and Böger, P. (1988). Ferredoxin-NADP+ oxidoreductase is the respiratory NADPH dehydrogenase of the cyanobacterium *Anabaena variabilis*. *Arch. Biochem. Biophys.* **267**: 228–235.

Schmidt-Dannert, C. (2000). Engineering novel carotenoids in microorganisms. *Curr. Opin. Biotechnol.* **11**: 255–61.

Schnorpfeil, M., Janausch, I. G., Biel, S., Kröger, A. and Unden, G. (2001). Generation of a proton potential by succinate dehydrogenase of *Bacillus subtilis* functioning as a fumarate reductase. *Eur. J. Biochem.* **268**: 3069–74.

Schofield, A. and Paliyath, G. (2005). Modulation of carotenoid biosynthesis during tomato fruit ripening through phytochrome regulation of phytoene synthase activity. *Plant Physiol. Biochem.* **43**: 1052–60.

Schröder, J. and Drews, G. (1968). Quantitative Bestimmung der Fettsäuren von *Rhodospirillum rubrum* und *Rhodopseudomonas capsulata* während der Thylakoidmorphogenese. *Arch. für Mikrobiol.* **64**: 59–70.

Schultz, J. E. and Weaver, P. F. (1982). Fermentation and anaerobic respiration by *Rhodospirillum rubrum* and *Rhodopseudomonas capsulata*. *J. Bacteriol.* **149**: 181–90.

Schwerzmann, R. U. and Bachofen, R. (1989). Carotenoid profiles in pigment-protein complexes of *Rhodospirillum rubrum*. *Plant Cell Physiol.* **30**: 497–504.

Scolnik, P. a and Marrs, B. L. (1987). Genetic research with photosynthetic bacteria. *Annu. Rev. Microbiol.* **41**: 703–26.

Scolnik, P. a, Walker, M. a and Marrs, B. L. (1980). Biosynthesis of carotenoids derived from neurosporene in *Rhodopseudomonas capsulata*. *J. Biol. Chem.* **255**: 2427–32.

Sganga, M. W. and Bauer, C. E. (1992). Regulatory factors controlling photosynthetic reaction center and light-harvesting gene expression in *Rhodobacter capsulatus*. *Cell* **68**: 945–54.

Singh, R. K., Britton, G. and Goodwin, T. W. (1973). Carotenoid biosynthesis in *Rhodopseudomonas spheroides*. S-adenosylmethionine as the methylating agent in the biosynthesis of spheroidene and spheroidenone. *Biochem. J.* **136**: 413–9.

Sippel, C. J., Goewert, R. R., Slachman, F. N. and Olson, R. E. (1983). The regulation of ubiquinone-6 biosynthesis by *Saccharomyces cerevisiae*. *J. Biol. Chem.* **258**: 1057–61.

Sistrom, W. R. (1977). Transfer of chromosomal genes mediated by plasmid r68.45 in *Rhodopseudomonas sphaeroides*. *J. Bacteriol.* **131**: 526–32.

Snozzi, M. and Bachofen, R. (1979). Characterisation of reaction centers and their phospholipids from *Rhodospirillum rubrum*. *Biochim. Biophys. Acta - Bioenerg.* **546**: 236–247.

Sommer, U., Herscovitz, H., Welty, F. K. and Costello, C. E. (2006). LC-MS-based method for the qualitative and quantitative analysis of complex lipid mixtures. *J. Lipid Res.* **47**: 804–14.

Sorensen, D. C. (1982). Newton's method with a model trust region modification. *SIAM J. Numer. Anal.* **19**: 409–426.

Sprenger, G. a, Schörken, U., Wiegert, T., Grolle, S., de Graaf, a a, Taylor, S. V, Begley, T. P., Bringer-Meyer, S. and Sahm, H. (1997). Identification of a thiamin-dependent synthase in *Escherichia coli* required for the formation of the 1-deoxy-D-xylulose 5-phosphate precursor to isoprenoids, thiamin, and pyridoxol. *Proc. Natl. Acad. Sci. U. S. A.* **94**: 12857–62.

Stahl, W. and Sies, H. (2003). Antioxidant activity of carotenoids. *Mol. Aspects Med.* **24**: 345–351.

Steiger, S., Astier, C. and Sandmann, G. (2000). Substrate specificity of the expressed carotenoid 3,4-desaturase from *Rubrivivax gelatinosus* reveals the detailed reaction sequence to spheroidene and spirilloxanthin. *Biochem. J.* **349**: 635–40.

Steiger, S., Mazet, A. and Sandmann, G. (2003). Heterologous expression, purification, and enzymatic characterization of the acyclic carotenoid 1,2-hydratase from *Rubrivivax gelatinosus*. *Arch. Biochem. Biophys.* **414**: 51–58.

Steiger, S., Takaichi, S. and Sandmann, G. (2002). Heterologous production of two unusual acyclic carotenoids, 1,1′-dihydroxy-3,4-didehydrolycopene and 1-hydroxy-3,4,3′,4′-tetradehydrolycopene by combination of the *crt*C and *crt*D genes from *Rhodobacter* and *Rubrivivax*. *J. Biotechnol.* **97**: 51–58.

Stickforth, P. and Sandmann, G. (2011). Structural and kinetics properties of a mutated phytoene desaturase from *Rubrivivax gelatinosus* with modified product specificity. *Arch. Biochem. Biophys.* **505**: 118–122.

Stöggl, W., Huck, C., Wongyai, S., Scherz, H. and Bonn, G. (2005). Simultaneous determination of carotenoids, tocopherols, and γ-oryzanol in crude rice bran oil by liquid chromatography coupled to diode array and mass spectrometric detection employing silica C30 stationary phases. *J. Sep. Sci.* **28**: 1712–1718.

Suh, W. (2012). *Microbial Metabolic Engineering*, Q. Cheng (ed.), Springer New York, New York, NY.

Surpin, M., Larkin, R. M. and Chory, J. (2002). Signal transduction between the chloroplast and the nucleus. *Plant Cell* **14**: 327–339.

Swem, L. R., Elsen, S., Bird, T. H., Swem, D. L., Koch, H. G., Myllykallio, H., Daldal, F. and Bauer, C. E. (2001). The RegB/RegA two-component regulatory system controls synthesis of photosynthesis and respiratory electron transfer components in *Rhodobacter capsulatus*. *J. Mol. Biol.* **309**: 121–38.

Takada, M., Ikenoya, S., Yuzuriha, T. and Katayama, K. (1982). Studies on reduced and oxidized coenzyme Q (ubiquinones). II. The determination of oxidation-reduction levels of coenzyme Q in mitochondria, microsomes and plasma by high-performance liquid chromatography. *Biochim. Biophys. Acta - Bioenerg.* **679**: 308–314.

Takaichi, S. (2008). Distribution and biosynthesis of carotenoids. *The Purple Phototrophic Bacteria*, Springer Netherlands, pp.97–117.

Takaichi, S. (2013). Tetraterpenes: Carotenoids. In K. G. Ramawat and J.-M. Mérillon (eds.), *Natural Products SE - 141*, Springer Berlin Heidelberg, pp.3251–3283 LA – English.

Takaichi, S. and Shimada, K. (1999). Pigment composition of two pigment-protein complexes derived from anaerobically and semi-aerobically grown *Rubrivivax gelatinosus*, and identification of a new keto-carotenoid, 2-ketospirilloxanthin. *Plant Cell Physiol.* **40**: 613–617.

Takamiya, K. I. and Dutton, P. L. (1979). Ubiquinone in *Rhodopseudomonas sphaeroides*. Some thermodynamic properties. *Biochim. Biophys. Acta* **546**: 1–16.

Tang, P. H., Miles, M. V, Miles, L., Quinlan, J., Wong, B., Wenisch, A. and Bove, K. (2004). Measurement of reduced and oxidized coenzyme Q9 and coenzyme Q10 levels in mouse tissues by HPLC with coulometric detection. *Clin. Chim. Acta* **341**: 173–184.

Taylor, R. F. (1984). Bacterial triterpenoids. *Microbiol. Rev.* **48**: 181–98.

Toledo-Ortiz, G., Huq, E. and Rodríguez-Concepción, M. (2010). Direct regulation of phytoene synthase gene expression and carotenoid biosynthesis by phytochrome-interacting factors. *Proc. Natl. Acad. Sci. U. S. A.* **107**: 11626–31.

Tolonen, A., Lehto, T. M., Hannuksela, M. L. and Savolainen, M. J. (2005). A method for determination of phosphatidylethanol from high density lipoproteins by reversed-phase HPLC with TOF-MS detection. *Anal. Biochem.* **341**: 83–88.

Tomisaburo, I. (1975). Polarographic rhodoquinone from studies bound on with chromatophores and *Rhodospirillum rubrum*. **78**: 795–801.

Truscott, T. G. (1990). New trends in photobiology: The photophysics and photochemistry of the carotenoids. *J. Photochem. Photobiol. B Biol.* **6**: 359–371.

Vadali, R. V, Fu, Y., Bennett, G. N. and San, K.-Y. (2005). Enhanced lycopene productivity by manipulation of carbon flow to isopentenyl diphosphate in *Escherichia coli*. *Biotechnol. Prog.* **21**: 1558–61.

Vignais, P. M. and Colbeau, A. (2004). Molecular biology of microbial hydrogenases. *Curr. Issues Mol. Biol.* **6**: 159-188.

Wang, C., Oh, M. K. and Liao, J. C. (2000). Directed evolution of metabolically engineered *Escherichia coli* for carotenoid production. *Biotechnol. Prog.* **16**: 922–6.

Wang, G.-S., Grammel, H., Abou-Aisha, K., Sägesser, R. and Ghosh, R. (2012). High-level production of the industrial product lycopene by the photosynthetic bacterium *Rhodospirillum rubrum*. *Appl. Environ. Microbiol.* **78**: 7205–15.

Weber, R. W. S., Anke, H. and Davoli, P. (2007). Simple method for the extraction and reversed-phase high-performance liquid chromatographic analysis of carotenoid pigments from red yeasts (Basidiomycota, Fungi). *J. Chromatogr. A* **1145**: 118–122.

Welsch, R., Medina, J., Giuliano, G., Beyer, P. and Von Lintig, J. (2003). Structural and functional characterization of the phytoene synthase promoter from *Arabidopsis thaliana*. *Planta* **216**: 523–34.

Willett, J., Smart, J. L. and Bauer, C. E. (2007). RegA control of bacteriochlorophyll and carotenoid synthesis in *Rhodobacter capsulatus*. *J. Bacteriol.* **189**: 7765–73.

Wolfertz, M., Sharkey, T. D., Boland, W. and Kühnemann, F. (2004). Rapid regulation of the methylerythritol 4-phosphate pathway during isoprene synthesis. *Plant Physiol.* **135**: 1939–45.

Wood, B., Nichols, B. W. and James, A. (1965). The lipids and fatty acid metabolism of photosynthetic bacteria. *Biochim. Biophys. Acta - Lipids Lipid Metab.* **106**: 261–273.

Woodall, A. A., Britton, G. and Jackson, M. J. (1997a). Carotenoids and protection of phospholipids in solution or in liposomes against oxidation by peroxyl radicals: relationship between carotenoid structure and protective ability. *Biochim. Biophys. Acta* **1336**: 575–86.

Woodall, A. A., Lee, S. W., Weesie, R. J., Jackson, M. J. and Britton, G. (1997b). Oxidation of carotenoids by free radicals: relationship between structure and reactivity. *Biochim. Biophys. Acta* **1336**: 33–42.

Xiang, S., Usunow, G., Lange, G., Busch, M. and Tong, L. (2006). Crystal structure of 1-deoxy-D-xylulose 5-phosphate synthase, a crucial enzyme for isoprenoids biosynthesis. *J. Biol. Chem.* **282**: 2676–2682.

Yamamoto, N., Hatakeyama, H., Nishikawa, K. and Horio, T. (1970). The function of ubiquinone-10 both in the electron transport system and in the energy conservation system of chromatophores from *Rhodospirillum rubrum*. *J. Biochem.* **67**: 587–98.

Yamano, S., Ishii, T., Nakagawa, M., Ikenaga, H. and Misawa, N. (1994). Metabolic engineering for production of beta-carotene and lycopene in *Saccharomyces cerevisiae*. *Biosci. Biotechnol. Biochem.* **58**: 1112–4.

Yamashita, T., Ino, T., Miyoshi, H., Sakamoto, K., Osanai, A., Nakamaru-Ogiso, E. and Kita, K. (2004). Rhodoquinone reaction site of mitochondrial complex I, in parasitic helminth, *Ascaris suum*. *Biochim. Biophys. Acta* **1608**: 97–103.

Yasushi, K. (1991). New trends in photobiology: Structures and functions of carotenoids in photosynthetic systems. *J. Photochem. Photobiol. B Biol.* **9**: 265–280.

Ye, V. M. and Bhatia, S. K. (2012). Pathway engineering strategies for production of beneficial carotenoids in microbial hosts. *Biotechnol. Lett.* **34**: 1405–14.

Yeliseev, A. a and Kaplan, S. (1997). Anaerobic carotenoid biosynthesis in *Rhodobacter sphaeroides* 2.4.1: H_2O is a source of oxygen for the 1-methoxy group of spheroidene but not for the 2-oxo group of spheroidenone. *FEBS Lett.* **403**: 10–14.

Yen, H. C. and Marrs, B. (1976). Map of genes for carotenoid and bacteriochlorophyll biosynthesis in *Rhodopseudomonas capsulata*. *J. Bacteriol.* **126**: 619–29.

Yoch, D. C. and Arnon, D. I. (1975). Comparison of two ferredoxins from *Rhodospirillum rubrum* as electron carriers for the native nitrogenase. *J. Bacteriol.* **121**: 743–5.

Young, D. a, Bauer, C. E., Williams, J. C. and Marrs, B. L. (1989). Genetic evidence for superoperonal organization of genes for photosynthetic pigments and pigment-binding proteins in *Rhodobacter capsulatus*. *Mol. Gen. Genet.* **218**: 1–12.

Youvan, D. C., Bylina, E. J., Alberti, M., Begusch, H. and Hearst, J. E. (1984). Nucleotide and deduced polypeptide sequences of the photosynthetic reaction-center, B870 antenna, and flanking polypeptides from *R. capsulata*. *Cell* **37**: 949–957.

Youvan, D. C. and Ismail, S. (1985). Light-harvesting II (B800-B850 complex) structural genes from *Rhodopseudomonas capsulata*. *Proc. Natl. Acad. Sci. U. S. A.* **82**: 58–62.

Yuan, L. Z., Rouvière, P. E., Larossa, R. a and Suh, W. (2006). Chromosomal promoter replacement of the isoprenoid pathway for enhancing carotenoid production in *E. coli*. *Metab. Eng.* **8**: 79–90.

Zhu, Y. S., Cook, D. N., Leach, F., Armstrong, G. A., Alberti, M. and Hearst, J. E. (1986). Oxygen-regulated mRNAs for light-harvesting and reaction center complexes and for bacteriochlorophyll and carotenoid biosynthesis in *Rhodobacter capsulatus* during the shift from anaerobic to aerobic growth. *J. Bacteriol.* **168**: 1180–8.

Zhu, Y. S. and Hearst, J. E. (1986). Regulation of expression of genes for light-harvesting antenna proteins LH-I and LH-II; reaction center polypeptides RC-L, RC-M, and RC-H; and enzymes of bacteriochlorophyll and carotenoid biosynthesis in *Rhodobacter capsulatus* by light and oxygen. *Proc. Natl. Acad. Sci. U. S. A.* **83**: 7613–7.

Zsebo, K. M. and Hearst, J. E. (1984). Genetic-physical mapping of a photosynthetic gene cluster from *R. capsulata*. *Cell* **37**: 937–47.

Zsebo, K. M., Wu, F. and Hearst, J. E. (1984). Tn5.7 construction and physical mapping of pRPS404 containing photosynthetic genes from *Rhodopseudomonas capsulata*. *Plasmid* **11**: 182–4.

Zwenger, S. and Basu, C. (2008). Plant terpenoids: applications and future potentials. *Biotechnol. Mol. Biol. Rev.* **3**: 1–7.